UNIVERSITY OF LIVERPOOL

THE ROLE OF HEPARAN SULFATE IN MUSCLE DIFFERENTIATION AND AGEING

Thesis submitted in accordance with the requirements of the University of Liverpool for the degree of Doctor in Philosophy

By
Rachel Ghadiali
February 2017

Acknowledgements

Abstract

Postnatal growth and regeneration of skeletal muscles depend on the activity of satellite cells, resident muscle stem cells defined by their location between the basal lamina and the muscle fibre plasma membrane. In response to injury or disease satellite cells activate, proliferate and eventually differentiate and fuse to one another to form new muscle fibres, or to existing damaged fibres to repair them. The microenvironment surrounding satellite cells, called the satellite cell niche, plays a crucial role in muscle regeneration. Heparan sulfate (HS) is a highly negatively charged, sulfated polysaccharide present on the surface of almost all mammalian cells or residing in the extracellular matrix. HS is usually bound to a core protein termed heparan sulfate proteoglycans (HSPGs). The HS component of the HSPG exhibits a high level of structural variability since it can vary in chain length and notably, in the pattern of sulfation along the length of the HS chain, leading to distinct chemical properties. As a consequence, HS is able to interact with numerous proteins, and thus plays a key role in the regulation of multiple cell processes. A number of HSPGs are expressed in muscle precursors during embryonic development and in satellite cells during postnatal life. However, the changes that muscle HS undergoes during satellite cell differentiation are unknown. In this project, it is shown that the sulfation levels of HS increase during satellite cell-derived myoblast differentiation. Interestingly, a specific increase in 6-*O* sulfation is also observed in HS from ageing muscle, which is shown to lead to promotion of FGF2 signalling and satellite cell proliferation, suggesting a role for HS in age-associated loss of satellite cell quiescence. Addition of chemically modified heparins (referred to as HS mimetics) to differentiating satellite cell derived-myoblast cultures results in differential effects depending on the pattern and level of sulfation: an oversulfated HS mimetic inhibits FGF2 signalling, a known major promoter of myoblast proliferation and inhibitor of differentiation. In contrast, FGF2 signalling is promoted by an *N*-acetylated HS mimetic, which inhibits differentiation and promotes satellite cell-derived myoblast expansion. The effects of a new class of fully synthetic HS mimetics (referred to as HS mimetic clusters), has been investigated on differentiating satellite cell derived-myoblast cultures. Finally, a new HS mimetic cluster has been synthesised and tested for its effects on differentiating satellite cell-derived myoblast cultures. Overall, these HS mimetic clusters have differential effects on myoblast differentiation. Thus, it can be concluded that the HS complement of the satellite cell niche is dynamically regulated during muscle differentiation and ageing, and that such changes might account for some of the phenotypes and signalling events that are associated with these processes. Furthermore, a novel class of HS mimetic clusters may offer promising therapeutic candidates for HS-mediated signalling events in muscle ageing and disease.

Table of Contents

List of Figures

List of Tables

List of Abbreviations

BMP	bone morphogenetic protein
BODIPY	4,4-Difluoro-5,7-Dimethyl-4-Bora-3a,4a-Diaza-s- Indacene-3-Propionic Acid
BrdU	5-bromo-2'-deoxyuridine
cDNA	complementary deoxyribonucleaic acid
DAPI	4,6-diamidino-2-phenylindole
DEAE	diethylaminoethyl cellulose
Den T	target dendrimer
ECM	extracellular matrix
EDL	extensor digitorum longus
EGF	epidermal growth factor
Erk1/2	extracellular signal–regulated kinase 1/2
ESC	embryonic stem cell
FACS	fluorescence activated cell sorting
FGF	fibroblast growth factor
FGFR	fibroblast growth factor receptor
GAG	glycosaminoglycan
GalN	galactosamine
GCE	C-5 epimerase
GlcA	glucuronic acid
GlcN	glucosamine
GlcNAc	N-acetylglucosamine
HBGF	heparin binding growth factor
HGF	hepatocyte growth factor
HPLC	high performance liquid chromatography
HPSE	heparanase
HS	heparan sulfate
HS2ST	2-O-sulfotransferase
HS3ST	3-O-sulfotransferase
HS6ST	6-O-sulfotransferase
HSPG	heparan sulfate proteoglycans
IdoA	iduronic acid
IGF	insulin growth factor
MAPK	mitogen activate protein kinase
MRF	myogenic regulatory factor
mRNA	messenger ribonucleic acid
MTT	thiazolyl blue tetrazolium bromide
Myf5	myogenic factor 5

MyHC	myosin heavy chain
MyoG	myogenin
NDST	*N*-deacetylase/ *N*-sulfotransferase
NMR	nuclear magnetic resonance
Pax7	paired box transcription factor 7
PBS	phosphate-buffered saline
P0	passage 0
PP1	pre-plating 1
PP2	pre-plating 2
qPCR	quantitative polymerase chain reaction
RGTA	regenerating agent
RNA	ribonucleic acid
RT	room temperature
RT-PCR	real-time polymerase chain reaction
SAX	strong anion exchange
SC	satellite cell
SEM	standard error of the mean
Ser	serine
siRNA	small interfering ribonucleic acid
SULF1	sulfatase 1
SULF2	sulfatase 2
TA	tibialis anterior
Tcf4	transcription factor 7-like 2
TDLA	TaqMan® Low-Density Array
TGF-β	transforming growth factor- β
UA	uronic acid

Chapter 1

1   Introduction

1.1   The Big Picture

Skeletal muscle wasting is a significant problem within the ageing population. During ageing skeletal muscle becomes weaker, smaller and muscle regeneration becomes impaired. Overall, loss of muscle leads to frailty, lack of independence and increased risk of mortality. A similar process also occurs in muscle wasting diseases such as muscular dystrophy, characterised by progressive skeletal muscle degeneration, loss of muscle mass, muscle weakness and extensive fibrosis. Considerable research is focused on understanding the mechanisms involved in skeletal muscle degeneration and regeneration, however, information is still lacking regarding the components of the extracellular matrix that play critical roles in skeletal muscle maintenance. This thesis aims to better understand the dynamic expression of heparan sulfate, with differing sugar sequences, a major component of the muscle stem cell niche, in an attempt to increase knowledge of how muscle growth and regeneration are controlled and the molecular mechanisms that are involved. The results presented in this thesis have the potential to open up promising new therapeutic avenues for the treatment of muscle wasting in ageing and in muscle degenerative diseases.

1.2   Introduction Outline

This introduction is presented in four parts;

1. *Skeletal Muscle, Myogenesis and Muscle Ageing*: I will introduce skeletal muscle anatomy and biology, and the molecular mechanisms that are involved in muscle growth and regeneration.

2. *Heparan Sulfate Proteoglycans (HSPGs):* I will introduce HSPGs, with a focus on the heparan sulfate (HS) component discussing its biosynthesis, structural importance and biological roles.

3. *Heparan Sulfate and Heparan Sulfate Proteoglycans in Myogenesis:* I will discuss the involvement of HSPGs in myogenesis and will review the current literature.

4. *Structural Analysis of Heparan Sulfate:* I will review the current methods for analysing the structure of HS and methods for determining structure-function relationships as well as the use of HS mimetics to interfere with HS-regulated biological processes.

1.3   Skeletal Muscle and Myogenesis

1.3.1   *Structure of Skeletal Muscle*

Skeletal muscle, also known as striated muscle, is anchored to the bone by tendons and functions under conscious control to move the skeleton, control breathing and maintain posture. Skeletal muscle consists of bundles of muscle fibres, known as myofibres, which are elongated, nearly cylindrical, multinucleated cells (**Figure 1.1**). In healthy myofibres the nuclei are located at the periphery of the cell under the plasma membrane termed the sarcolemma. Each myofibre is packed with myofibrils, which extend the length of the cell. The myofibrils are further subdivided into alternating light bands termed I bands and dark bands, termed the A bands. A segment containing one half of an I band and one half of an A band is termed a sarcomere, which is the structural and functional unit of skeletal muscle. Each sarcomere contains *thick filaments* composed of myosin II protein and *thin filaments* containing actin protein. It is the interaction between actin filaments and myosin that allows the contraction of muscle cells. Myosin acts as the 'motor', the actin filaments are the tracks along which myosin moves and adenine triphosphate (ATP) is the fuel that powers movement. The endomysium, the connective tissue that surrounds the individual muscle fibres, includes the basal lamina produced by the myofibre and extracellular matrix produced by surrounding fibroblasts. The endomysium provides the chemical environment for the exchange of ions required for myofibre excitation.
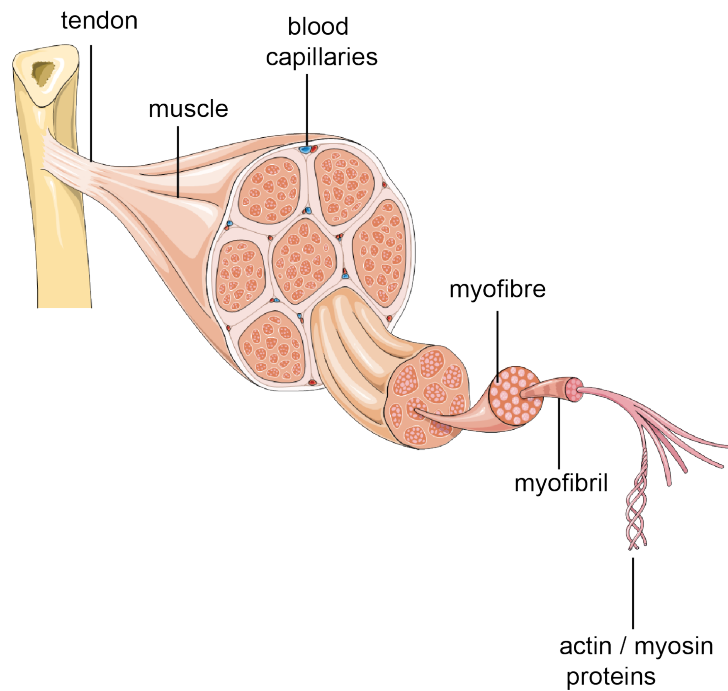
Figure 1.1 The Structure of Skeletel Muscle.

Simplified view of the relationship of the anatomic structure of skeletal muscle consisting of bundles of myofibres. Each myofibre is packed with myofibrils, which comprise dark A bands and light I bands. These form the structural and functional unit of skeletal muscle; the sarcomere. Each sarcormere conatins thick filaments, made up of myosin, and thin filaments, made up of actin. It is the interaction between actin and myosin that allows for muscle contraction. (Image adapted from optistem.org)

1.3.2   The Muscle Stem Cell: Satellite Cells

Skeletal muscle satellite cells are myogenic stem cells responsible for muscle development, growth and regeneration, defined anatomically by their location between the basal lamina and the sarcolemma of terminally differentiated myofibres (Mauro, 1961) (**Figure 1.2**). Satellite cells represent less than 2% of the nuclear content of myofibres and are present in a quiescent state (G_0 of the cell cycle) in adult muscle (Allbrook et al., 1971).
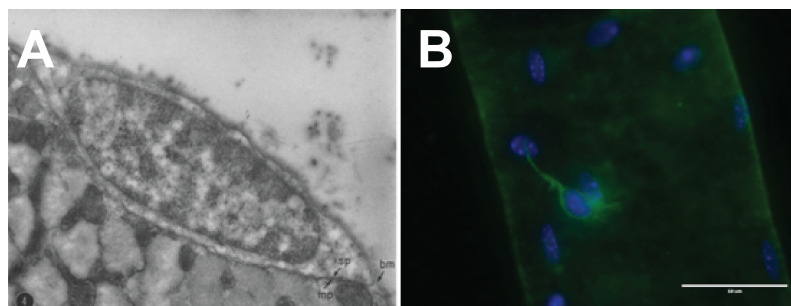
Figure 1.2 The Satellite Cell.

A) Electron micrography showing a satellite cell between the basal lamina and sarcolemma first discovered in 1961 in frog muscle (Mauro, 1961). B) A myofibre where myonuclei are stained with DAPI. The satellite cell is in green detected with an anti-syndecan-3 antibody where the scale bar = 50 μm (Pisconti, unpublished)**.**

1.3.3   Myogenesis

Quiescent satellite cells are the only cell type expressing the paired box transcription factor, Pax7. In skeletal muscle *Pax7*^{+} satellite cells are indispensable for muscle regeneration (Lepper et al., 2011; Murphy et al., 2011; Sambasivan et al., 2011). Satellite cells become activated in response to a stress such as injury or exercise, enter the cell cycle and convert into muscle progenitor cells known as myoblasts (**Figure 1.3**) (Reznik, 1969). Myoblasts then undergo terminal differentiation, withdrawing from the cell cycle, and fusion either with one another to form multinucleated myotubes, or with damaged myofibres (Morgan and Partridge, 2003; Reznik, 1969). A proportion of satellite cells self-renew, generating an identical, undifferentiated cell that can return to a quiescent state in order to maintain full muscle regenerative capacity (Charge and Rudnicki, 2004). A wide variety of signalling molecules in the microenvironment surrounding the satellite cell, known as the satellite cell niche, control satellite cell fate regulation and thus the process of skeletal muscle growth and regeneration (Bentzinger et al., 2012).

1.3.4   Molecular Regulation of Myogenesis

Many signalling pathways are involved in the regulation of skeletal muscle growth and regeneration, which are governed by the satellite cell itself or the satellite cell niche. These pathways affect the expression of the myogenic regulatory factors (MRFs), a family of transcription factors that are exclusively expressed in myogenic cells and activate the expression of muscle specific genes (Londhe and Davie, 2011). The MRFs consist of the basic helix-loop-helix transcription factors MyoD (Davis et al., 1987), Myf-5 (Braun et al., 1989), myogenin (Edmondson and Olson, 1990) and MRF4 (Rhodes and Konieczny, 1989). The expression of the MRFs changes depending on the stage of myogenesis reflecting distinct roles of the MRFs in the regulation of satellite cell commitment and differentiation (Sabourin and Rudnicki, 2000). Quiescent satellite cells express Paired box 7 (Pax7) at the mRNA and the protein level and Myf5 and MyoD mRNAs, which are not translated (Crist et al., 2012; Hausburg et al., 2015; Montarras et al., 2013). Upon activation, Myf5 is translated and MyoD expression is induced, thus activated satellite cells co-express Pax7 with MyoD and Myf5 (Cooper et al., 1999; Zammit et al., 2004). The majority of satellite cells proliferate, down-regulate Pax7 and up-regulate Myf5 and MyoD which then in turn drive myogenic differentiation. After one or more rounds of proliferation, the majority of myoblasts will withdraw from the cell cycle indicating commitment to terminal differentiation by the expression of myogenin (Edmondson and Olson, 1990) and MRF4 (**Figure 1.3**).
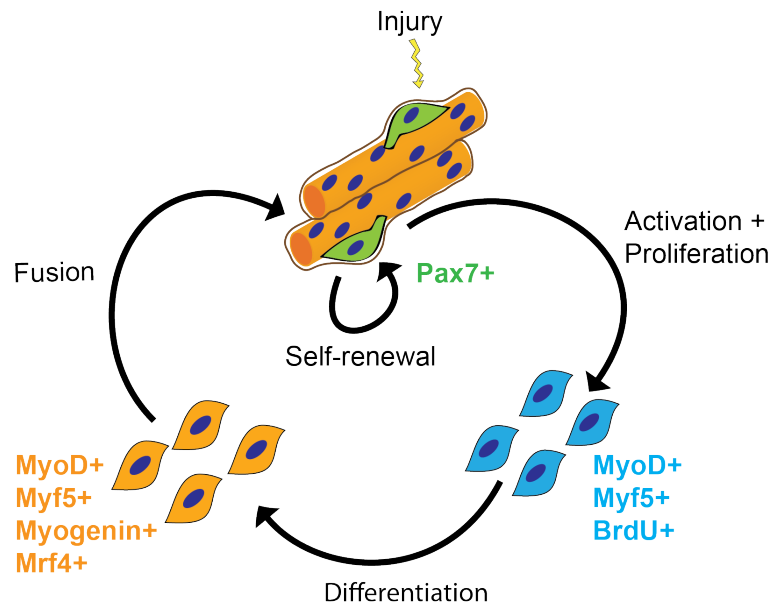
Figure 1.3 Scheme of Satellite Cell Myogenesis.

Satellite cells become activated in response to a stress such as injury, enter the cell cycle and convert into myoblasts (Reznik, 1969) expressing MyoD, Myf5 and replicating DNA (detectable via BrdU incorporation). Myoblasts undergo terminal differentiation, withdrawing from the cell cycle and fusing either with one another to form multinucleated myotubes, or with damaged myofibres (Morgan and Partridge, 2003; Reznik, 1969) expressing, MyoD, Myf5, myogenin and Mrf4. A proportion of SCs self-renew returning to a quiescent state, expressing Pax7, in order to maintain full muscle regenerative capacity (Charge and Rudnicki, 2004).

1.3.5   The Satellite Cell Niche: The Extracellular Matrix

The extracellular matrix (ECM) surrounding each individual myofibre is a basement membrane consisting of two layers: the basal lamina and the reticular lamina. Satellite cells reside between the basal lamina and the myofibre sarcolemma, and therefore interact with basal lamina components. Thus, the ECM plays a crucial role in satellite cell regulation, as it directs a plethora of signalling pathways involved in cell migration, myotube formation and muscle regeneration (Barberi et al., 2013; Conboy and Rando, 2002; Le Grand et al., 2009; Urciuolo et al., 2013). Another major role of the ECM is to provide structural integrity to the satellite cell niche. The ECM is made up of collagens, which are the major structural proteins secreted primarily by muscle fibroblasts (Shea et al., 2010; Zou et al., 2008), laminins, fibronectin and glycosaminoglycans (GAGs) (Sanes, 2003). GAGs are long, unbranched polysaccharides consisting of repeating disaccharide units of an amino sugar and an uronic acid sugar, which are usually bound to a core protein to form proteoglycans, the properties of which will be discussed in detail in section 2 of the Introduction.

1.3.5.1   Extracellular Matrix Composition

Satellite cells bind directly to the basal lamina through their integrin receptors (Ervasti and Campbell, 1993; von der Mark et al., 1991) to collagen type IV and laminin, which are cross-linked by the ECM glycoprotein nidogen forming the primary constituents of the basal lamina (**Figure 1.4**) (Ervasti, 2003; Sanes, 2003). This matrix complex is then able to bind to collagen type VI and many proteoglycans such as perlecan and decorin. Collagen type VI integrates the basal lamina with the reticular lamina composed predominantly of collagen types I and III and fibronectin (Rao et al., 1985). The myofibre sarcolemma is also linked to the basal lamina through the dystroglycan complex, which binds the actin cytoskeleton in the myofibre through dystrophin and to laminin in the basal lamina. The dystroglycan complex stabilizes the sarcolemma during contraction-induced stress and thus forms the basis for basement membrane architecture (Grounds et al., 2005).
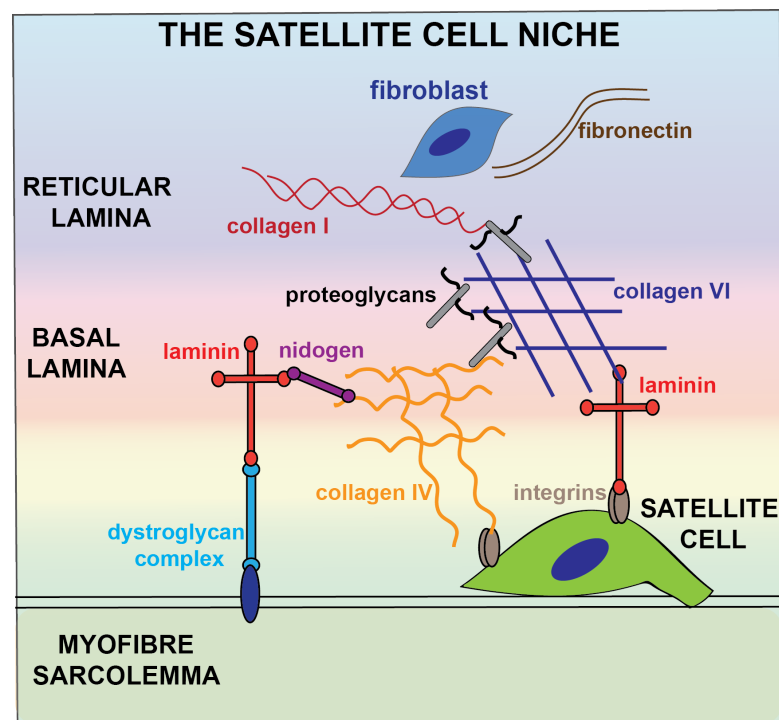
Figure 1.4 Schematic Diagram of the Satellite Cell Niche

Satellite cells reside between the myofibre sarcoelmma and the basal lamina where they are able to interact with ECM components of the satellite niche through their integrins. Through their integrins, satellite cells are able to interact with collagen type IV and laminins, which are crosslinked with the glycoprotein nidogen. The matrix formed is then able to interact with colllagen type VI and various proteolglycans. Collagen type VI of the basal lamina is also able to interact with the reticular lamina via primarily with collagen type I and fibronectin. The myofibre sarcolemma also interacts with the basal lamina through the dystroglycan complex.

1.3.5.2   Extracellular Matrix Remodelling

As well as providing structural integrity, proteoglycans, such as perlecan, which reside in the basal lamina, are able to bind and sequester growth factors and thus serve a significant signalling role in the satellite cell niche during muscle growth and regeneration as reviewed in (Yin et al., 2013). Myogenesis and muscle regeneration post-injury are associated with significant remodelling of the basal lamina, reflecting the differing requirements for growth factor signalling (Kovanen, 2002).

1.3.6   Growth Factor Signalling in Myogenesis

A wide variety of signalling molecules in the satellite cell niche inhibit or stimulate the expression of the MRFs and thus control satellite cell fate (Bentzinger et al., 2012; Olguín and Pisconti, 2012). Some of the key extrinsic regulatory factors that are involved in the regulation of myogenesis are: fibroblast growth factors (FGFs), insulin-like growth factors (IGFs), hepatocyte growth factor (HGF) and transforming growth factor-*β* (TGF-*β*). FGF, and HGF activate myoblast proliferation and are potent inhibitors of myogenic differentiation and thus repress MRF activity (Clegg et al., 1987; Evinger-Hodges et al., 1982; Schabort et al., 2009; Sheehan and Allen, 1999; Tatsumi and Allen, 2004). IGF on the other hand promotes both proliferation and subsequently differentiation (Jennische and Hansson, 1987).

1.3.6.1   FGF signalling

One of the most well studied growth factor families that regulate self-renewal, proliferation and differentiation of multiple cell types, including the regulation of satellite cell fate, are the fibroblast growth factors (FGFs) (Coutu and Galipeau, 2011; Hannon et al., 1996; Lanner et al., 2010; Olwin et al., 1994). The FGFs are a family of 22 structurally related members, which signal via a family of 4 transmembrane tyrosine kinase high affinity receptors (FGFR1, FGFR2, FGFR3 and FGFR4), (Eswarakumar et al., 2005). FGF signalling is also reliant on the presence of heparan sulfate, a structurally complex glycosaminoglycan (GAG) that acts as a low affinity co-receptor. The structural importance of HS and its regulatory properties in FGF signalling will be discussed in detail in section 2 of the Introduction.

1.3.6.2   FGF Signalling in Myogenesis

FGF signalling plays an important role in skeletal muscle development (Clegg et al., 1987; Olwin et al., 1994; Seed and Hauschka, 1988) mostly by controlling muscle differentiation (Clegg et al., 1987). Previous studies have demonstrated that distinct FGF pathways are involved in the regulation of myogenesis (Kudla et al., 1998), which cannot be recapitulated

by stimulation of other growth factor receptors (Hannon et al., 1996; Lim and Hauschka, 1984; Linkhart et al., 1980). Specifically, FGF signalling activates mitogen-activated protein kinase (MAPK) pathways (Campbell et al., 1995; Milasincic et al., 1996; Mourey et al., 1996). Proliferating MM14 myoblasts, a satellite cell-derived cell line, express FGF1, FGF2, FGF6 and FGF7 mRNA (Clegg et al., 1987; Fedorov et al., 1998; Hannon et al., 1996; Kudla et al., 1998). Myofibre cultures exposed to FGF2 have a twofold increase in the number of proliferating myoblasts by 48 hours in culture (Yablonka-Reuveni and Rivera, 1997). *In vivo* FGF2 is believed to enhance myogenic proliferation by facilitating the recruitment of additional satellite cells from the quiescent state thus effectively being an activating factor (Yablonka-Reuveni et al., 1999). FGFR1 is the only FGF receptor detected in MM14 myoblasts (Kudla et al., 1998; Templeton and Hauschka, 1992). Genetic ablation of FGFR1 results in significantly reduced satellite cell mitogenic response to FGF2 in isolated fibres suggesting an important role for FGFR1 in FGF2 signalling (Yablonka-Reuveni et al., 2015). However, FGFR1 ablation does not supress subsequent myogenic differentiation or have significant effects on muscle regeneration (Yablonka-Reuveni et al., 2015).

1.3.7   Skeletal Muscle Ageing

Ageing is often associated with sarcopenia, defined as the loss of muscle mass, strength and function during ageing in the absence of a specific disease (Morley et al., 2001). In the development of sarcopenia, the loss of muscle mass appears to be irrecoverable (Roubenoff, 2001). Since satellite cells are responsible for muscle regeneration and maintenance, it is reasonable to speculate that there is a decline in the number of satellite cells and/or that they become dysfunctional during ageing leading to reduced regenerative potential.

1.3.7.1   Satellite Cell Decline During Ageing

There have been several reports supporting the hypothesis that the number of satellite cells declines during ageing (Brack et al., 2005; Collins et al., 2007; Dedkov et al., 2003; Gibson and Schultz, 1983; Neal et al., 2012; Shefer et al., 2006). Although, in some cases the significant decline in satellite cell numbers only becomes apparent in geriatric (>26 months) mice (Brack and Rando, 2007; García-Prat et al., 2013). However, other studies have shown contradictory findings, suggesting that there are no significant differences in the number of satellite cells between young and aged muscle (Nnodim, 2000; Schäfer et al., 2005). Furthermore, the ablation of satellite cells in young mice does not cause sarcopenia with ageing, suggesting that the development of sarcopenia is not dependent on the number of satellite cells in the absence of injury (Fry et al., 2015). However, it has previously been demonstrated that there is a subpopulation of satellite cells that maintains a healthy

phenotype during ageing, and these cells are primarily responsible for muscle regeneration in aged mice (Collins et al., 2007). Thus, it is possible that in the ablation model (Fry et al., 2015), the number of satellite cells is not entirely eliminated and a progeny of healthy satellite cells remain, thereby providing the basis for extensive self-renewal and regenerative capacity. The number of satellite cells, does however, become a limiting factor for regenerative capacity after injury (Boldrin et al., 2012; Chakkalakal et al., 2012; Neal et al., 2012). Furthermore, satellite cell depletion in young mice leads with ageing to ECM accumulation as measured by an increase in collagens and specifically an increase in the level of *N*-acetyl-glucosamine residues (Fry et al., 2015).

1.3.7.2   Intrinsic Defects in Satellite Cells During Ageing

There have been many studies suggesting that satellite cells become dysfunctional during ageing, as they display a reduction in their ability to self-renew and thus lose their regenerative capacity (Bernet et al., 2014; Chakkalakal et al., 2012; Conboy et al., 2003; Cosgrove et al., 2014; Day et al., 2010; Sousa-Victor et al., 2014a). So far, evidence suggests that loss of satellite cell regenerative capacity in ageing is due to both intrinsic impairment and changes in molecular signalling that occur in the satellite cell niche.

Through the transplantation of aged satellite cells and young satellite cells in equivalent *in vivo* models, it has been demonstrated that the age-dependent dysfunction of satellite cells is in part due to intrinsic defects including both defects in self-renewal and defects in satellite cell contribution to myofibre formation (Bernet et al., 2014; Chakkalakal et al., 2012; Cosgrove et al., 2014; Price et al., 2014; Sousa-Victor et al., 2014b). These intrinsic defects arise from a combination of altered activation of signal transductions, such as: altered p38α/β mitogen-activated protein kinase (MAPK) signalling (Bernet et al., 2014) and FGFR-Sprouty1 signalling (Chakkalakal et al., 2012). However, it has been demonstrated that a small portion of satellite cells maintain the regenerative capacity of young satellite cells, and are capable of robust regeneration after engraftment into an 'injury setting,' indicating that a progeny of satellite cells does not become intrinsically defective during ageing (Collins et al., 2007).

1.3.7.3   Extrinsic Influences on Satellite cell Function During Ageing

In contrast to findings that intrinsic defects persist in engraftment studies, there is evidence from experiments of parabiosis that the extracellular environment significantly contributes to satellite cell function. Indeed the myogenic potential of aged satellite cells is restored through exposure to a young environment via parabiosis (Conboy et al., 2005). The discrepancies in

findings are likely to be due to differences in the procedures used to assess satellite cell engraftment, such as the recipient mouse age, which might strongly influence regenerative capacity as reviewed in (Brack and Muñoz-Cánoves, 2016). Moreover, more recent studies have implied that, although older cells maintain regenerative capacity when transplanted into a young environment, they nonetheless delay the onset of regeneration upon engraftment (Shavlakadze et al., 2010; Smythe et al., 2008). These results suggest that a combination of both the intrinsic defects and considerable extrinsic influences on satellite cell regenerative capacity is likely to be responsible for muscle regeneration impairment during ageing. In support of this hypothesis, satellite cells from aged and young muscle have similar proliferative rates *ex vivo*, indicating that the aged muscle environment plays a crucial role in satellite cell fate (Alsharidah et al., 2013; George et al., 2010; Verdijk et al., 2014).

Additionally, the levels of local and systemic inflammatory cytokines and growth factors significantly change with ageing (Chakkalakal et al., 2012). Myofibres are progressively replaced by fibrotic (Brack et al., 2007) and adipose tissue leading to an increase in the levels of TGF-*β* in the satellite cell niche (Carlson et al., 2008; Zacks and Sheff, 1982). Systemic attenuation of TGF-*β* signalling leads to muscle regeneration improvement in older mice (Yousef et al., 2015). Furthermore, it has been reported that the FGF signalling is increased in the satellite cell niche during ageing leading to an increase in satellite cell activation and proliferation which eventually leads to satellite cell exhaustion (Chakkalakal et al., 2012). Consistently, reducing FGF activity through inhibition of FGFR1 signalling diminishes satellite cell depletion in ageing muscle (Chakkalakal et al., 2012) as fewer satellite cells are stimulated to break quiescence.

Overall, the data strongly support the contention that ageing is associated with changes both within satellite cells and their niche leading to quiescent satellite cell depletion and reduced regenerative capacity. However, it is still in question which factors are dominant in contributing to the ageing phenotype. Understanding the sources of dysregulated cytokine and growth factor signalling during ageing may identify new therapeutic targets in muscle for the treatment of defective regeneration and sarcopenia.

1.4   Heparan Sulfate

Heparan sulfate proteoglycans are biomolecules composed by a core protein harbouring covalently linked complex carbohydrate chains of the HS class (Sarrazin et al., 2011).

1.4.1   *Carbohydrates*

Carbohydrates are a large class of biomolecules, which includes monosaccharides and their derivatives, oligosaccharides and polysaccharides. Generation of a polysaccharide chain starts with two monosaccharides being linked together by the glycosylation reaction, leading to either: 1) equatorial bond formation, where the bond makes a small angle compared with the plane of the ring or 2) axial bond formation, where the bond makes an angle of about 90° with the plane of the ring (**Figure 1.5**). The glycosidic bond involves at least one anomeric carbon (carbon 1), which are stereocentres of the monosaccharide. The resulting disaccharide contains a free anomeric carbon, which can be involved in further glycosylation reactions increasing the length of the polysaccharide chain. The anomeric end of sugar, which is involved in the glycosylation reaction, is termed the 'reducing end.' The non-anomeric side of the polysaccharide is termed the 'non-reducing end'. Polysaccharides contain large numbers of hydroxyl groups, which can be further functionalised (**Figure 1.5**).
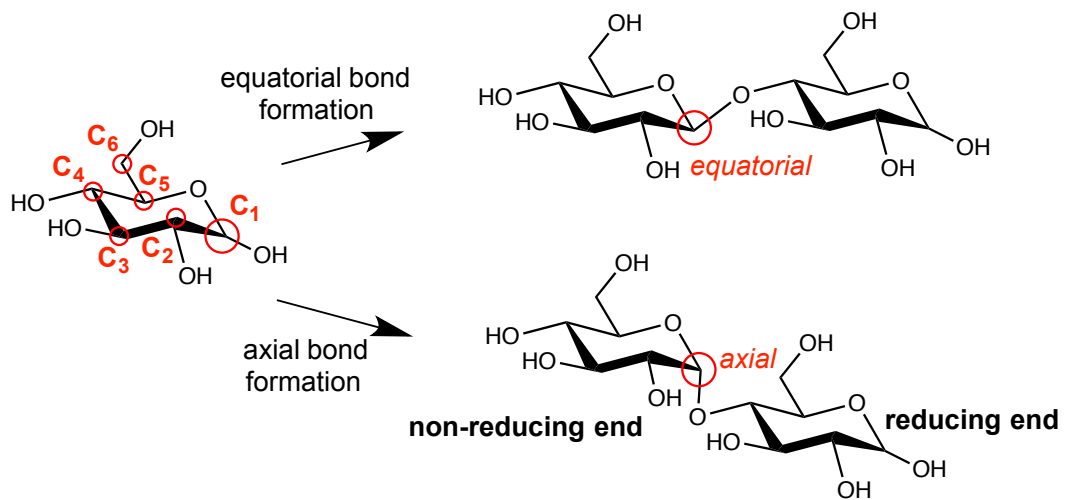
Figure 1.5 Scheme showing the glycosylation reaction.

A general scheme showing the glycosylation reaction linking two monosaccharides of glucose together at the anomeric carbon (carbon 1) and carbon 4 to form a) equatorial glycosidic linkage and c) axial glycosidic linkages between the disaccharide maltose.

1.4.2   *Glycosaminoglycans*

HS is a member of the glycosaminoglycan (GAG) family, consisting of large linear polysaccharides with a repeating disaccharide unit of; a) an amino sugar, N-acetyl glucosamine (GlcN) for HS and b) an uronic acid residue, either iduronic acid (IdoA) or glucuronic acid (GlcA) (**Figure 1.6**). The GAG is defined by the specific disaccharide unit and the stereochemistry of the *O*-glycosidic linkage (**Table 1.1**). The structural complexity of the GAG chains is determined by the fact that they contain large numbers of hydroxyl groups, which are differentially functionalized with sulfate groups, giving rise to a highly negatively charged macromolecule capable of multiple electrostatic and other interactions.

The position and level of sulfation varies depending on the GAG species and its origin. The position of sulfation is identified by the carbon that the sulfate group is attached to on the monosaccharide ring, starting from the anomeric carbon, carbon 1, as depicted in **Figure 1.4**.

HS is present on the cell surfaces of nearly all mammalian cells, and is characterized by a linear chain of 10-200 disaccharide units of *N*-acetyl-*D*-glucosamine (GlcNAc) linked to *D*-glucuronic acid (GlcA) with an average molecular weight of 25-100kDa. It has the most variable structure in the GAG family and, as a consequence, HS has the highest potential for functional diversity within the GAG family (Turnbull et al., 2001). Indeed, the different biological roles played by HS depend mostly on its structural composition, which arise from the different levels and patterns of sulfation and is termed the "heparanome" (Turnbull et al., 2001). Structural analyses of HS indicate cell and tissue-specific HS compositions, highlighting the importance of specific structure-function activities (Lawrence et al., 2008; Ledin et al., 2004; Maccarana et al., 1996).
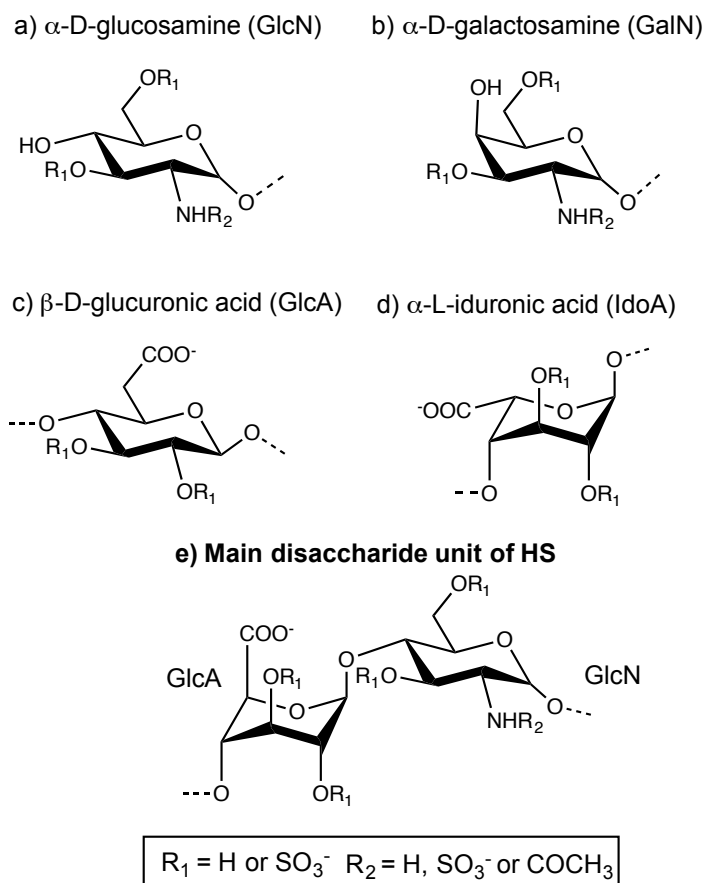
Figure 1.6 Main monosaccharide units of the GAG family.

The two amino sugars: a) glucosamine (GlcN) and b) galactosamine (GalN). The two uronic acids: c) glucuronic acid (GlcA) and d) iduronic acid (IdoA). e) The main disaccharide unit of HS. The monosaccharides contain differing functional groups along the chain (R$_1$, R$_2$ and R$_3$ substitutions as indicated).

Table 1.1 GAG chains with corresponding major disaccharide units.

 The GAG chains with the corresponding main disaccharide unit and main glycosidic linkage between the disaccharide units throughout the GAG chain.

GAG chain	Major Disaccharide	Glycosidic Linkage
heparan sulfate	D-GlcNAc - D-GlcA	β(1—4) and α(1—4)
heparin	D-GlcNAc - L-IdoA	β(1—4)
chondroitin sulfate	D-GalNAc - D-GlcA	β(1—4)
dermatan sulfate	D-GalNAc - L-IdoA	β(1—3)
keratan sulfate	D-Gal- D-GlcNAc	β(1—4)

1.4.3   Heparan Sulfate Biosynthesis

1.4.3.1   Conventional HS Biosynthetic pathway

HS is synthesized in a dynamic manner with extensive structural modifications throughout and thus HS should be considered a heterogeneous family of structurally related molecules each with distinct functional properties. Families of HS biosynthetic enzymes are responsible for HS synthesis, which occurs in the Golgi apparatus following a non-templated scheme. The action of each enzyme does not go to completion throughout the entire HS chain (Turnbull et al., 2001) resulting in a high degree of structural diversity (**Figure 1.7**). Although the biosynthetic pathway remains a topic of controversy, the conventional pathway is perceived to follow a standard order, in which the HS biosynthetic enzymes function consecutively and irreversibly (Lander and Selleck, 2000; Lindahl et al., 1989; Perrimon and Bernfield, 2000; Selleck, 2000). HS synthesis starts with the formation of a tetrasaccharide linker region, attaching the HS chain to the protein core via a serine (Ser) residue, consisting of xylose-galactose-galactose-glucuronic acid (Esko and Zhang, 1996; Zhang et al., 1995). Xylosyl-transferase-1 (XylT1) catalyses the addition of the xylose to the serine residue of the protein core (Zhang et al., 1995). Two galactosyltransferases (GalT1 and GalT2) catalyse the addition of two galactose residues on to the xylose residue respectively followed by the addition of a glucuronic acid residue by glucuronic acid transferase 1 (GlcAT1). Polymerization of the chain is then initiated by exostosin-like-3 (EXTL3), which catalyses the addition of a glucosamine on to the glucuronic acid residue of the tetrasaccharide linkage region (Kim et al., 2001). Polymerization continues through the action of HS polymerases, the exostosin glycosyltransferases, EXT1 and EXT2 (Lind et al., 1998), which add (in an alternating pattern) glucuronic acid and glucosamine to the non-reducing end of the growing HS chain. Structural modification of the HS chains occurs concomitantly with chain elongation. The conventional route starts with the activity of the bifunctional enzymes N-

deacetylase-N-sulfotransferases (NDSTs), which catalyse the removal of an N-acetyl group and the addition of a sulfate group, producing *N*-sulfated domains along the HS chain (Aikawa and Esko, 1999). Subsequently, C-5 epimerization of a small proportion of D-glucuronic acid residues to L-iduronic acid occurs through the activity of C-5 epimerase (GCE) (Li et al., 1997). Further modifications include: firstly, 2-*O*-sulfation of uronic acid by 2-*O*-sulfotransferase (HS2ST) (Kobayashi et al., 1997). Secondly, 6-*O*-sulfation by the 6-*O*-sulfotransferases (HS6STs) occurs on *N*-acetylated and *N*-sulfated glucosamine residues (Habuchi et al., 2000). Thirdly, but rarely, 3-*O*-sulfation can occur on glucosamine residues catalysed by the 3-*O*-sulfotransferases (HS3STs) (Shworak et al., 1999). These structural modifications lead to regions containing a high level of sulfation, termed S-domains, and regions containing a low level of sulfation or non-sulfated domains, termed NA-domains. Intermediate domains (NA/NS) are also present flanking the NS domains.

1.4.3.2   HS Post-Synthetic Modification

Structural modifications of HS can occur also after the chains have been deposited on the cell surface or in the extracellular matrix, by two sets of enzymes: a) the 6-*O*-endosulfatases (Sulf1 and Sulf2) and b) heparanase (HPSE). Firstly, the 6-*O*-endosulfatases, which are extracelluarly targeted, catalyse the removal of 6-*O*-sulfate groups from glucosamine (Habuchi et al., 2003). Evidence suggests that both SULFs are able to act on both heavily sulfated domains of HS and also less-sulfated domains (Ai et al., 2006). Secondly, heparanase, an endo-β glucuronidase, cleaves HS within the chains yielding HS fragments of 10-20 disaccharide units and modifying the activity of the HS chains (Gong et al., 2003). Although evidence suggests that there is a preference for a trisaccharide sequence containing N-sulfation and 6-*O*-sulfation, the precise structure of HS substrate required for heparanase activity is still under investigation (Okada et al., 2002; Peterson and Liu, 2010; Wu et al., 2016).
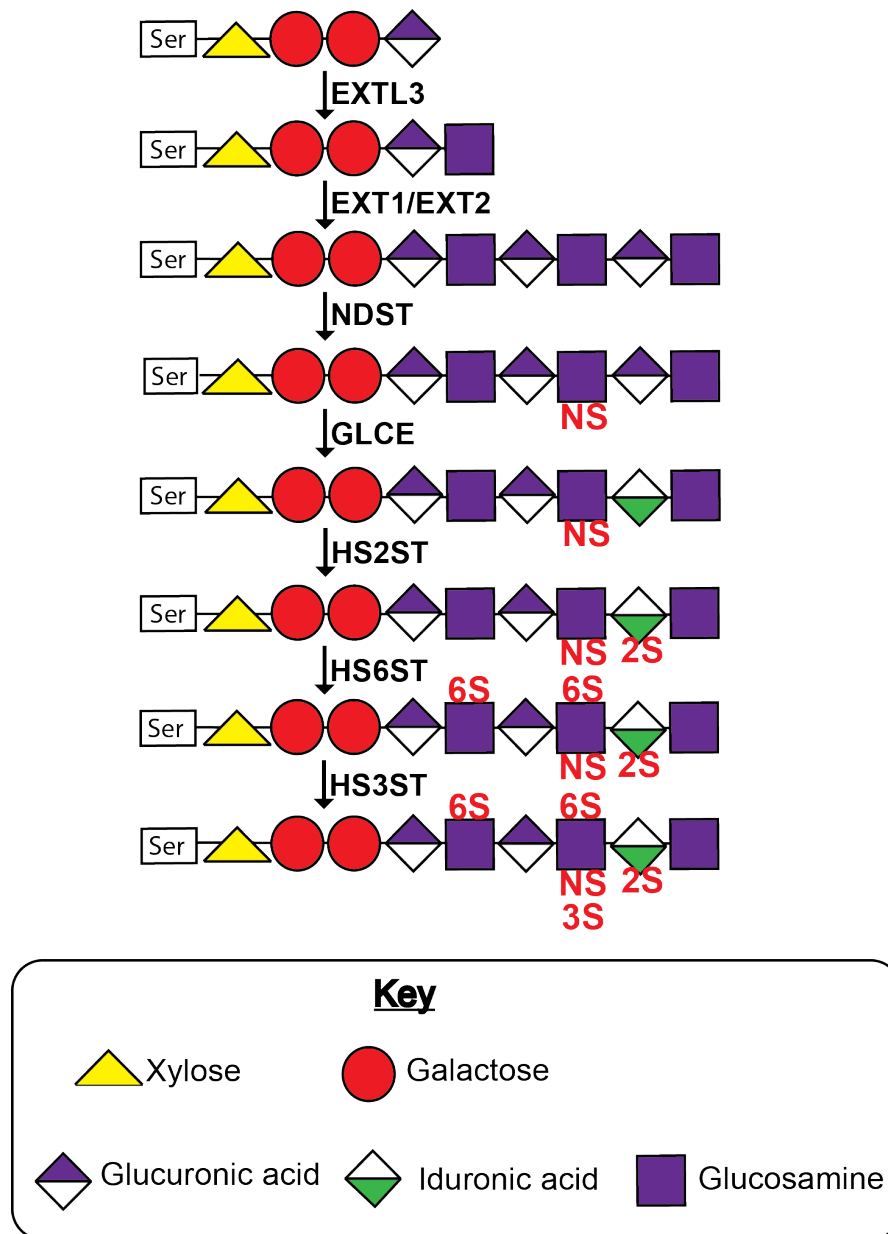
Figure 1.7 Schematic showing conventional view of the HS biosynthetic pathway.

Schematic of HS biosynthetic pathways showing the activity of the HS biosynthetic enzymes depicted following a standard order. HS synthesis takes place in the Golgi apparatus following formation of the tetrasaccharide linker on the core protein of xylose-galactose-galactose-glucuronic acid. Chain elongation is initiated with EXTL3 which catalyses the addition of a glucosamine, followed by EXT1/2 which catalyse the addition of glucosamine and glucuronic acid units alternatively. This occurs concomitantly with chain modification starting with the NDSTS, which are dual action enzymes, catalysing the removal of an acetyl group from the amino sugar and the addition of an sulfate group. Chain modification continues with the 2-O-sulfotransferases, catalysing the addition of a sulfate group of the uronic acid residue and the 6-O- and 3-O-sulfotransferases catalysing the addition of sulfate groups on the amino sugar. These structural modifications lead to regions along the chain of high sulfation, termed S-domains interspersed with regions of lower sulfation, termed NA-domains. Intermediate domains (NA/NS) are also present flanking the NS domains.

1.4.3.3   Biosynthetic Ambiguity

With the exception of C5-epimerase and HS 2-*O*-sulfotransferase, the HS biosynthetic enzymes, represent a multi-isomer family of enzymes. Despite sharing a high degree of structural similarity, each family of enzymes displays differences in substrate affinities and activity (Aikawa and Esko, 1999; Habuchi et al., 2000; Liu et al., 1999). This presumably gives rise to high levels of structural diversity of HS, depending on which isoforms are expressed and their level of expression. Despite significant advances in the characterization of the biosynthetic process, the precise pathway remains a subject of debate. Following the conventional pathway, there are restrictions in the order of activity of the HS biosynthetic enzymes and therefore restrictions in the structural output of HS. In reality, some of the basic disaccharide structural units that are found naturally in HS are not accounted for by the restrictive order of the conventional biosynthetic pathway (Rudd and Yates, 2012). In contrast, a biosynthetic pathway of a highly symmetrical tree structure provides an explanation for the biosynthesis of all possible structural disaccharide units of HS (Rudd and Yates, 2012). According to this alternative biosynthetic pathway and experimental evidence, epimerisation can occur both before and after *N*-sulfation leading to a major branch consisting of the most common disaccharides and a minor route, consisting of the more rare disaccharide structural units. It also suggests that some of the biosynthetic enzymes can operate as complexes, adding further complexity to the structural composition of the chain depending on the composition of the enzyme complex and thus its activity (Pinhal et al., 2001; Victor et al., 2009). Despite many advances in the understanding of the HS biosynthetic machinery, the precise mechanisms regulating HS biosynthesis, remain poorly understood.

1.4.4   Heparan Sulfate Proteoglycans

HS chains are usually covalently bound to a core protein via a serine residue to form heparan sulfate proteoglycans (HSPGs). There are three subfamilies of HSPGs:

   (I)   transmembrane HSPGs: the 4 syndecans, betaglycan and CD44
   (II)   glycophosphatidylinositol (GPI)-linked HSPGs: the 6 gyplicans
   (III)   extracellular matrix HSPGs: perlecan, agrin, type XVIII collagen and the 3 testicans.

The length and number of HS chains attached may also vary between different protein cores (Turnbull et al., 2001). Furthermore, it has been shown that domains on the protein core other that the GAG binding site may also have regulatory functions for HS biosynthesis (Chen and Lander, 2001; Shworak et al., 1994) affecting the structural composition of the HS chain bound.

1.4.5   The Biological Role of HS

The complexity of the HS biosynthetic pathway leads to an exceptionally structurally diverse macromolecule, which is able to interact with a plethora of proteins such as plasma proteins, cell surface proteins, enzymes and growth factors termed the HS "interactome". There is increasing evidence suggesting that the structure of HS is critical for correct protein interaction and thus plays an important role in regulating biological function (Bernfield et al., 1999; Gao et al., 2016; Hileman et al., 1998; Lindahl et al., 1998; Takemura and Nakato, 2017; Thacker et al., 2016; Zhao et al., 2015). Thus far, 100s of HS binding proteins have been identified (Meneghetti et al., 2015; Ori et al., 2008, 2011). As a consequence, HSPGs play multiple roles in cells and tissues, specifically in: a) cell adhesion, which depends on the heparin binding domain of matrix proteins such as fibronectin and the laminins (Bernfield et al., 1999; Oh and Couchman, 2004; Saoncella et al., 1999; Woods et al., 2000); b) cell migration, which involves the recruitment of growth factors via interactions with HS (Arrington and Yost, 2009; Mitsi et al., 2006; Smith et al., 2009); and c) co-receptor signalling, which can facilitate the formation of ligand-receptor complexes (Rapraeger et al., 1991; Yayon et al., 1991). **Figure 1.8** highlights some of the key biological functions in which HSPGs participate. Since HS is involved in multiple cellular processes, HS is crucial in the regulation of many biological processes such as in development and stem cell differentiation, and in disease pathogenesis (such as in cancer (Knelson et al., 2014), Alzehimer's disease (Scholefield et al., 2003; Zhang et al., 2014), and HIV and influenza infection (Connell and Lortat-Jacob, 2013; Patel et al., 1993)). In an attempt to better understand the role of HS in regulation of biological processes, several studies involving mutations in the core proteins or the HS biosynthetic enzymes have highlighted the critical role played by HPSGs as regulators of multiple biological functions (Sarrazin et al., 2011). In addition, mouse mutants for the HS biosynthetic enzymes display more severe phenotypic effects than proteoglycan mutants, with many of the knockouts studied to date being embryonically or perinatally lethal, highlighting the importance of the HS structural composition as reviewed in Sarrazin et al., 2011.
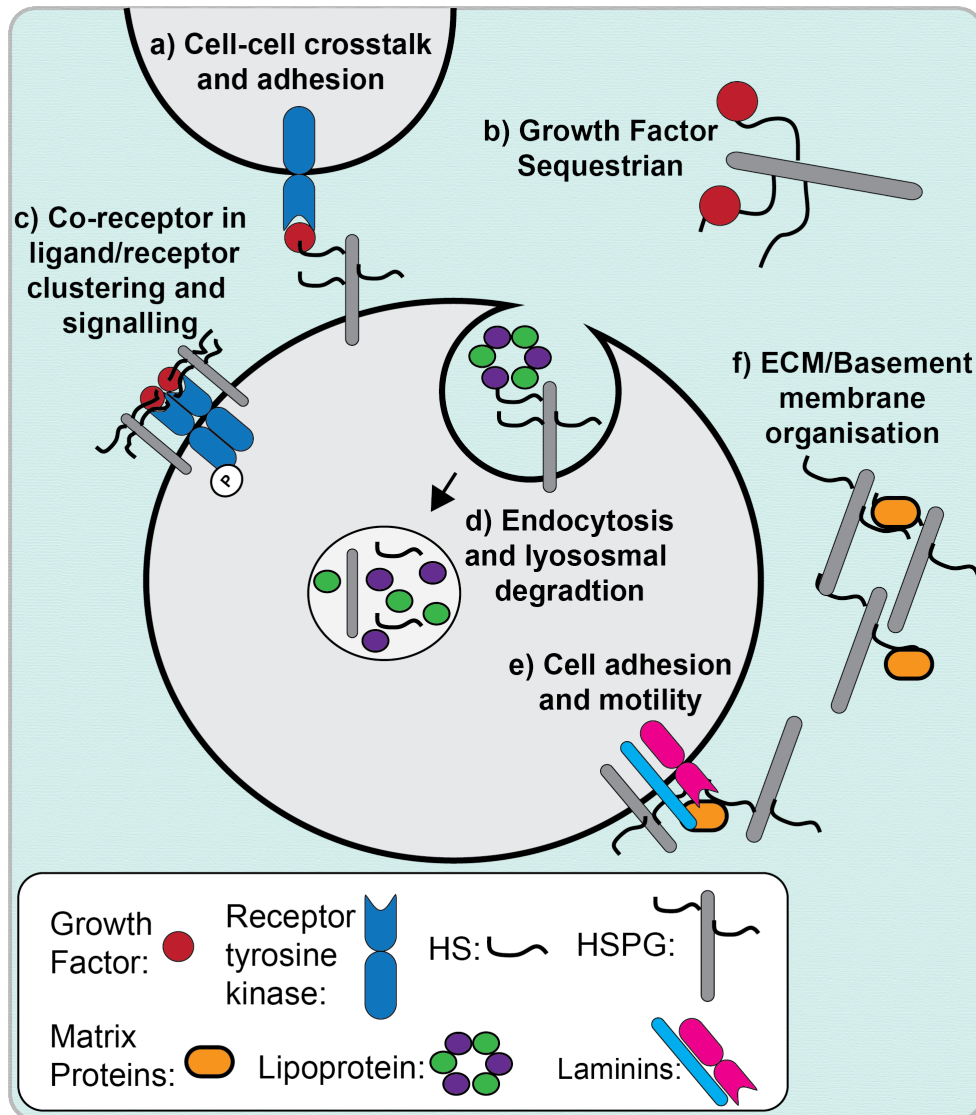
Figure 1.8 HSPGS participate in key biological functions.

Owing to the high structural complexity of HS determined by; the length of chain, number of chains, pattern/level of sulfation, localisation or the protein core to which it is attached, HS/HSPGs are involved in the regulation of multiple biological processes. Some of the key processes which HS is involved in are depicted in the diagram; a) cell-cell cross talk and cell adhesion b) growth factor sequestering in the ECM c) as a co-receptor in ligand/receptor clustering and signalling on the cell surface d) endocytosis and lysosaml degradation e) Cell adhesion and motility based on their interaction with laminins, integrins and matrix proteins f) the structrual role the play in ECM and basement membrane organisation. (Adapted from (Bishop et al., 2007))

1.4.6   HS Structural Specificity

Although it is clear that the structure of HS is crucial in numerous biological functions, in the vast majority of cases strong levels of a specific structural sequence of HS are not required for its biological activity (Mulloy, 2005). The most well investigated case, in which a specific sulfation pattern is vital for biological activity, is the interaction of heparin with antithrombin III (Björk and Olson, 1997; Jin et al., 1997; Olson et al., 1992). Each of the sulfate groups present on a specific pentasaccharide sequence in heparin is critical for binding to antithrombin and its anticoagulant activity. In the majority of cases however, there is some redundancy in HS sequences that support binding and activity, whereby an intermediate level of specificity of HS is required. In these cases, if a minimal specific motif of sulfate substitution is present, different substitutions can be present in the same binding site (Mulloy, 2005). Thus, this feature of HS allows for complex differential affinities between proteins (Ashikari-Hada et al., 2004). Primarily, intermediate levels of HS structural specificity are involved with binding to morphogens and growth factors and thus accommodate for multi-dynamic signalling.

1.4.7   Heparin Binding Growth Factors

As mentioned previously, a key function HS has is to bind and interact with growth factors. HS binding to growth factors can have either a positive or a negative downstream effect on signalling. HS can sequester growth factors away from their receptors and, as a consequence, protect them against proteolysis or prevent them from signalling (Gospodarowicz and Cheng, 1986; Vlodavsky et al., 1991; Vlodavsky et al., 1996). Then, selective degradation of HSPGs, can liberate growth factors thus playing an important role in regulating growth factor release in the extracellular environment and establishing growth factor gradients (Bernfield et al., 1999; Manon-Jensen et al., 2010). However, HS can also serve as a cell-surface receptor by facilitating ligand-receptor interactions, lowering their activation threshold or modulating the extent of signalling (Rapraeger et al., 1991; Yayon et al., 1991) (**Figure 1.9**). Growth factors, which contain a heparin-binding domain are termed heparin binding growth factors (HBGFs) (Olwin, 1989). These include several fibroblast growth factors (FGFs), bone morphogenetic proteins (BMPs), epidermal growth factor (EGF), vascular endothelial growth factor (VEGF), hepatocyte growth factor (HGF), insulin-like growth factor (IGF) and platelet derived growth factor (PDGF) (reviewed by (Ori et al., 2008; Zhang, 2010).
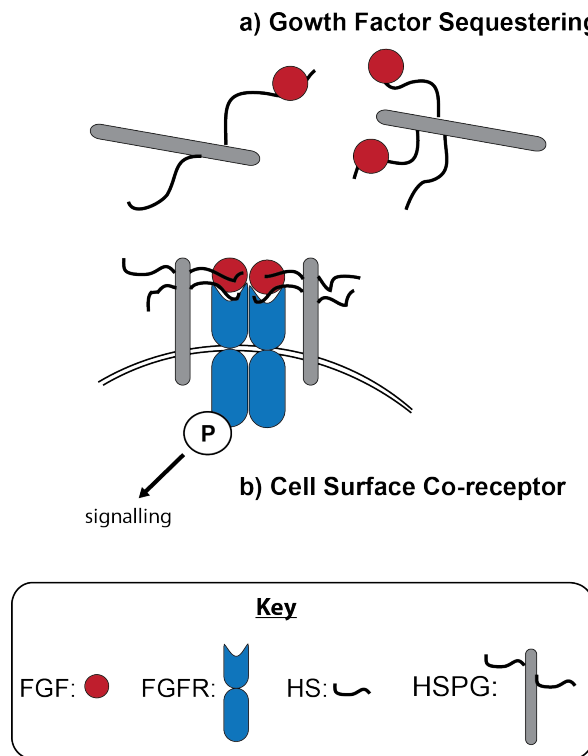
Figure 1.9 Role of HS and Heparin Binding Growth factors.

a) HS in the extracellular matrix is able to interact with heparin-binding growth factors (e.g. FGF) sequestering growth factors away from the cell surface and reducing signalling and/or protecting them from proteolysis and thus permiting growth factor signallling. b) HS present on the cell surface can act as a co-recepor prompting ligand-receptor clustering and promoting growth factor signalling.

1.4.8   Heparan Sulfate as a co-receptor for FGF2 signalling

Cell surface HSPGs facilitate the formation of FGF2 and FGF receptor complexes by acting as a high affinity co-receptor (Burgess and Maciag, 1989; Rapraeger et al., 1991; Yayon et al., 1991). The HS-FGF-FGFR interaction has been shown to signal through the mitogen-activated protein kinase/extracellular regulated signalling kinase (MAPK/ERK) pathway (Chua et al., 2004; Delehedde et al., 2000). The HS-FGF-FGFR interaction is the most extensively studied of the heparin-binding growth factors where FGFR1 activation and downstream signal transduction is dependent on the formation of a ternary complex determined by its crystal structure (Schlessinger et al., 2000). Distinct structural sequences, the position and level of HS sulfation are crucial for FGF ligand and receptor binding (Brickman et al., 1998a; Brickman et al., 1998b; Guimond and Turnbull, 1999; Lundin et al., 2000) and thus the formation of the ternary complex (Jastrebova et al., 2006). Specifically, evidence suggests that HS 2-O-sulfation is required for the binding to FGF2 (Turnbull et al., 1992), whereas 6-*O*-sulfation is important for binding to FGF receptor and the subsequent formation of the ternary complex (**Figure 1.10**) (Guimond et al., 1993; Pye et al., 1998). 6-O-desulfation of HS reduces the formation of the ternary complex specifically via inhibition of the FGFR1 and FGF2 interaction and thus inhibition of FGF signalling (Wang et al., 2004).

However, it must be noted that even analogous non-GAG structures are able to promote FGF2 signalling and exhibit inhibitory activity (Rudd et al., 2010).
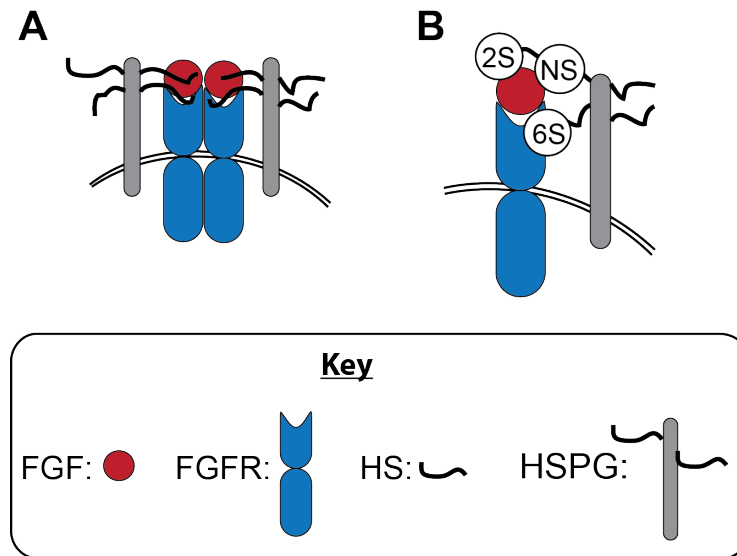
Figure 1.10 Heparan Sulfate as a co-receptor in FGF signalling.

Diagram depicts the mechanisms by which HS serves as a co-receptor in FGF2 signalling, for example. **A** depicts the formation of the ternary complex of HS-FGF2-FGFR1 (2:2:2) on the cell surface permitting signalling to take place. **B** depicts the key sulfation positions of HS important for the formation of the ternary complex. 2-*O*, and *N*-sulfation is important for interacting with FGF2 wherease 6-*O*-sulfation is important for interacting with the FGFR.

1.4.9   *Heparan Sulfate in Stem Cell Differentiation*

Many groups have demonstrated that specific GAGs, including HS, regulates stem cell differentiation through their ability to interact with multiple proteins (Dombrowski et al., 2009; Lanner et al., 2010; Smith et al., 2011) and that the structure of HS changes during embryonic stem cell (ESC) differentiation into different lineages (Baldwin et al., 2008; Johnson et al., 2007). For example, HS from ESCs undergoing differentiation shows increasing sulfation (Johnson, 2007; Nairn et al 2007; Hirano 2012) and specifically, an increase in N- 2- and 6-*O*-sulfation. To study the effects of HS structure on stem cell regulation, mouse ESCs harbouring mutations in the HS biosynthetic enzymes have been used (Jakobsson et al., 2006). Mouse ESCs lacking NDST1/2 are unresponsive to VEGF and subsequently their differentiation into blood capillary structures is blocked (Jakobsson et al., 2006). Similarly, ESCs lacking NDST1/2 are unable to differentiate into different lineages in response to FGF4 (Kraushaar et al., 2010; Lanner et al., 2010), and more recent findings show genetic targeting of NDST2, inhibits ESC adipogenic and neural differentiation (Forsberg et al., 2012). These findings highlight the importance of the structural composition of the heparanome of the stem cell niche and its role in regulating differentiation.

1.4.10 Heparan Sulfate in Ageing

Ageing is associated with progressive changes in stem cell number and function, and altered expression levels of growth factors leading to age-related stem cell dysregulation and reduced tissue regenerative capacity (Baumann, 2012; Oh et al., 2014). Since HS is involved in the regulation of growth factor signalling, it is not surprising that the structure and amount of HS is also altered in several tissues during ageing. Firstly, it has been demonstrated that HS on the cell surface of human diploid fibroblasts accumulates during *in vitro* ageing (Aizawa et al., 1980). Secondly, the structure of human aorta HS is gradually modulated during ageing, specifically showing an increase in 6-*O*-sulfation and thus enhanced binding to platelet-derived growth factor (PDGF) (Feyzi et al., 1998). HS binding to FGF2 is also increased but to a lesser extent (Feyzi et al., 1998). Furthermore, human osteoblast HS structure changes during ageing (Grzesik et al., 2002). Additionally, studies in the rat myocardium found an age-dependent increase in GAG levels and specifically an increase in the amount of HS (Huynh et al., 2012a). Furthermore, during ageing in the myocardium, there is an increase in the level of HS 6-*O*-sulfation (Huynh et al., 2012a). The aged HS also shows an increase in the potentiating effect of VEGF and decreased capacities to potentiate FGF2-dependent mitogenic activity (Huynh et al., 2012a). Finally, recent studies have found an age-dependent decrease in the amount of HS in Bruch's membrane of the eye. This is accompanied by a decrease in HS sulfation in the aged Bruch's membrane and an increase in heparanase leading to altered binding capacities in the ageing HS (Keenan et al., 2014). These studies highlight the importance of HS during ageing, suggesting that the change in structure of HS is specific to the tissue of origin leading to different biological consequences.

1.5 Heparan Sulfate and Heparan Sulfate Proteoglycans in Myogenesis

1.5.1 Heparan Sulfate Proteoglycans in Myogenesis

During skeletal muscle development, regeneration and degeneration, HSPGs are dynamically expressed and differentially located suggesting different functional roles for HS during myogenesis (Brandan and Gutierrez, 2013; Jenniskens et al., 2002; Liu et al., 2002). However, the HS composition during myogenesis has remained largely unexplored.

1.5.1.1 Heparan Sulfate Proteoglycans in Muscle Development

It has been demonstrated that HSPGs play an essential role during muscle development due to their ability to regulate important signalling pathways (Asundi et al., 1997; Lin, 2004; Poulain and Yost, 2015). During human skeletal muscle formation, syndecan-1 is

upregulated at week 13 of gestation whereas perlecan is undetectable (Sogos et al., 1998). In the development of mouse limb muscles, syndecan-1 and glypican-1 are detectable at day 10.5, while syndecan-3, syndecan-4 and perlecan are up regulated from day 12.5 (Olguin and Brandan, 2001). Syndecan-2, however, is undetectable in muscle cells during mouse embryonic development (David et al., 1993). In turkey pectoral muscle development, syndecan-1 and glypican-1 are also up regulated between days 18 and 20, respectively (Liu et al., 2004). Finally, HS 6-*O*-sulfation specifically has been found to be essential for muscle development in zebrafish (Bink et al., 2003). Morpholino-mediated functional knockdowns of HS6ST, led to a specific inhibition of 6-O-sulfation and impaired muscle growth during development (Bink et al., 2003). Morphant zebra-fish displayed disrupted somitic muscle development and later defects in muscle differentiation, which eventually led to severe muscle degeneration (Bink et al., 2003).

1.5.1.2   *Heparan Sulfate Proteoglycans in Muscle Differentiation and Regeneration*

Certain aspects of the process of muscle regeneration recapitulate the process of muscle development and therefore it is not surprising that the expression levels and localisation of several HSPGs change during muscle regeneration. Amongst the HSPGs, syndecans seem to have significant importance in satellite cell regulation. All four syndecans are down regulated during skeletal muscle differentiation (Fuentealba et al., 1999; Gutierrez et al., 2006; Larraín et al., 1997b). Syndecan-3 and syndecan-4 expression is restricted to satellite cells and thus serve as useful markers (Cornelison et al., 2001). Both syndecan-1 and 3 are important in the regulation of FGF2 activity (Fuentealba et al., 1999; Larraín et al., 1998) with syndecan-1 likely promoting FGF2 signalling and syndecan-3 inhibiting FGF2 signalling which is upregulated at the onset of differentiation (Cornelison et al., 2001; Cornelison et al., 2004). With the exception of syndecan-3, syndecans are down regulated during myogenesis and thus allow differentiation to take place due to reduced sensitivity to FGF2 (Fuentealba et al., 1999; Larraín et al., 1998; Larraín et al., 1997b). *In vivo* syndecan-4 knockout (*Sdc4$^{-/-}$*) satellite cells fail to regenerate damaged muscle with low levels of activation, proliferation, myotube fusion and differentiation (Cornelison et al., 2004). In contrast, syndecan-3 knockout (*Sdc3$^{-/-}$*) mice successfully regenerate damaged muscle with satellite cells exhibiting impaired quiescence maintenance and self-renewal, and slower proliferation than wild type cells (Pisconti et al., 2010). In addition, *Sdc3-/-* regenerating muscle shows an increase in the number of myonuclei and myofibre size indicating enhanced myoblast fusion (Pisconti et al., 2010). Perlecan, a component of the basal lamina which surrounds myofibres, is also downregulated during terminal muscle differentiation (Larraín et al., 1997a). Unlike the syndecans and perlecan, which are downregulated during myogenesis, glypican expression remains constant throughout myogenesis (Jen et al., 2009). Interestingly, glypican-1 is the only HSPG localized in lipid raft domains in myoblasts

sequestering FGF2 away from its receptor and thus decreasing FGF2 signalling (Brandan et al., 1996; Gutiérrez and Brandan, 2010). Glypican deficient mice exhibit increased FGF2 signalling, reduced myogenin and muscle myosin expression, and decreased myoblast fusion (Brandan et al., 1996; Gutiérrez and Brandan, 2010).

1.5.2   Heparan Sulfate Biosynthetic Enzyme Regulation in Myogenesis

Studies focusing on the role of the HS biosynthetic enzymes in myogenic regulation provide a useful indication of the importance of HS structure during myogenesis. The role of the heparan sulfate 6-O-sulfatases (Sulfs), in skeletal muscle has been described. Sulf 1 and 2 affect several extracellular signals involved in skeletal muscle regeneration (Gill et al., 2010; Langsdorf et al., 2007). Since Sulfs modify sulfated HS moieties after HS biosynthesis by removing 6-O-sulfate groups from tri-sulfated IdoA2S-GlcNS6S and di-sulfated UA-GlcNS6S, the removal the 6-O-sulfate group on HS disrupts the FGF2 ternary complex, repressing FGF signalling (Tran et al., 2012). As myogenic differentiation is inhibited by FGF signalling, *Sulf* double mutant mice exhibit delayed myogenic differentiation and prolonged Pax7 expression upon muscle injury (Langsdorf et al., 2007). More recent studies suggest that the heparanome composition is important for maintaining satellite cell quiescence, since satellite cells activated *in vivo* in response to injury, led to the majority of biosynthetic enzymes being significantly downregulated (Pisconti et al., 2012). This is with exception of EXTL2 and HS3ST3b1, a 3-O-sulfotransferase, which are up-regulated during satellite cell activation (Pisconti et al., 2012).

1.5.3   Heparan Sulfate in Myogenesis

With regards to the specific structure of HS itself, epitope analysis via phage display technology has demonstrated that different specific HS epitopes exist in skeletal muscle, and their abundance changes in developing muscle *in vitro* and *in vivo* (Jenniskens et al., 2002; Jenniskens et al., 2000). This suggests a role for specific structural moieties of the HS chains in regulating skeletal muscle growth and regeneration. Total sulfated GAG amounts (including HS and chondroitin sulfate) have been found to increase in the C2.7 myoblast cell line (derived from the C2 mouse myoblast cell line) when myoblasts are differentiated to myotubes (Barbosa et al., 2003). Leading on from this, it was discovered that the amount of HS specifically increases during differentiation of the C2.7 myoblast cell line (Barbosa et al., 2005).

1.5.3.1   Structure of Heparan Sulfate in Muscle Regeneration

It has been well reported that GAG levels increase in several tissues during regeneration (DiMicco et al., 2004; Ghatak et al., 2015; Papakonstantinou and Karakiulakis, 2009). During

muscle regeneration, total sulfated GAG content increases compared to intact muscle and this increase is enhanced in the presence of TGF-*β* (Barbosa et al., 2003; Zimowska et al., 2009). Furthermore, when male rats are subjected to ischaemic-injury the expression levels of HS biosynthetic enzymes change significantly, correlating with structural changes in HS and CS (Chevalier et al., 2015). Specifically, HS from muscle post ischaemic-injury has increased chain length, increased sulfation and different sulfation patterns compared to HS from intact muscle (Chevalier et al., 2015). Moreover, HS from regenerating muscle post ischaemic injury display differential binding affinities towards FGF2 and IL8 depending on the stage of regeneration (Chevalier et al., 2015). Total GAG content from regenerating muscle from day 8-post injury potentiates FGF2 mitogenic activity with an increasing effect up to 21 days post injury (Chevalier et al., 2015).

1.5.3.2   Structure of Heparan Sulfate in Muscular Dystrophy

Muscular dystrophy is a family of genetic disorders characterised by progressive skeletal muscle degeneration (Emery, 2002). A feature of the disease is extensive fibrosis due to an accumulation of ECM around muscle fibres leading to a hostile environment and compromised satellite cell function (Morgan and Zammit, 2010). Myoblasts from dystrophic (*mdx*) mice have been shown to synthesise 10 times the normal amount of sulfated GAGs, both HS and chondroitin sulfate (Crisona et al., 1998), correlating with the increase in ECM. Further investigations into the role of sulfated GAGs in Duchenne muscular dystrophy (DMD) demonstrated an increase and differential localisation of three HSPGs: gylpican-1, perlecan and syndecan-3 (Alvarez et al., 2002). In dystrophic (mdx) mice, syndecan-3 loss leads to improved muscle regeneration, with decreased muscle fibrosis and enhanced muscle function, shown by the ability of the mice to run longer when tested for endurance training performance (Pisconti et al., 2016). With regards to structural changes in sulfated GAGs, a modification of the sulfation pattern of chondroitin sulfate and dermatan sulfate in DMD muscles has been described, whereas the structure of HS appears comparable to wild type muscle (Negroni et al., 2014) despite there being significant changes in the structure of HS during post-ischaemic injury (Chevalier et al., 2015).

1.6   Structural Analysis of Heparan Sulfate

Since the structure of HS is critical in multiple biological processes, efficient and accurate methods are crucial for determining the structure of HS. Unlike DNA and protein synthesis, HS biosynthesis is not template driven, and the mechanisms of regulation are poorly understood. Therefore, it is not possible to determine structural sequences of HS chains based on expression levels of HS biosynthetic enzymes alone.

1.6.1   *Heparan Sulfate Antibodies*

One method for determining HS distribution in tissues and cells is by using antibodies that recognise specific HS epitopes. The first monoclonal HS-specific antibodies, 10E4 and 3G10, were developed in 1992 (David et al., 1992). 3G10 recognises the epitope produced after HSPGs have been treated with an HS degrading enzyme, heparinase III, thereby removing the HS chain from the protein core, providing a quantitative method of detection of HS chains present on a protein core (David et al., 1992). 10E4 on the other hand, recognises mainly N-sulfated domains on the HS chain (David et al., 1992). Later JM403 (van den Born et al., 2005) and NAH46 (Suzuki et al., 2008) antibodies were developed which recognise N-unsubstituted glucosamine residues and disaccharide residues containing N-acetyl glucosamine respectively. Thus, these antibodies are useful for the localization of specific HS epitopes in tissues. However, they still remain relatively limited compared to antibodies available for other GAG species and do not provide information on fine structural entities of HS.

1.6.2   *Heparan Sulfate Phage Display Antibodies*

An alternative technique for detecting different structural entities of HS involves the use of HS-specific single chain variable fragment antibodies that have been generated by phage display technology (van Kuppevelt et al., 1998). However, it must be considered that when cations bind to polysaccharides, both to HS analogues and HS on a cell surface, phage display antibody binding is often altered (Solari et al., 2015). This suggests that phage display antibodies do not bind to single specific structural sequences on the polysaccharide chain but that their binding depends rather on the overall conformation, the charge distribution and the flexibility of the HS chain (Thompson et al., 2009). Although phage display antibodies may be useful for determining general differences in the structure of HS, it must be considered that this is an overall interaction of the antibody to the polysaccharide and the surrounding environment, and therefore is not a sufficient technique alone for deciphering HS sequences. Furthermore, the epitopes for the antibodies are often insufficiently defined, and low abundance HS epitopes may not be detected.

1.6.3   *Heparan Sulfate Isolation*

For a more inherently accurate method of HS structural analysis, HS can be structurally analysed post isolation from tissues or cells. HS can be extracted from tissues or cells because of the high anionic nature of the sulfated HS chain, which binds to positively charged species via strong electrostatic attractions. Various enzymes can be employed to depolymerise HS chains from their protein core, bound DNA or from other GAG chains that are isolated in the process (Guimond et al., 2009a).

1.6.4   HS Quantification

One of the most common methods for HS quantification is the 1,9-dimethylmethylene Blue (DMMB) assay (Farndale et al., 1986; Farndale et al., 1982). DMMB is a cationic dye that can bind sulfated GAGs. The blue of the dye shifts to a violet tone when the dye binds to the polyanionic sulfate groups of the HS chain (Templeton, 1988). The HS-dye complex can then be isolated and the optical density measured for HS quantification. This measures the amount of sulfated HS isolated but does not account for non-sulfated HS species. Therefore the results may be skewed if the proportion of non-sulfated HS varies between samples. An alternative method for HS quantification is by exploiting the double bond, formed post heparinase digestion. Bacterially derived enzymes heparinase I, II and III digest the HS into its constituent disaccharide units (Ernst et al. 1995) resulting in a double bond per disaccharide (**Figure 1.10**). The double bond absorbs UV light strongly and thus can be used for HS quantification for sulfated and non-sulfated regions. Other quantification methods that do not include heparinase are destructive and also require larger quantities of HS.

1.6.5   Analytical Techniques for Heparan Sulfate Structural Analysis

Nuclear magnetic resonance (NMR) spectroscopy can be used to determine the structure of heparin as an intact polymer, without the requirement of cleaving the chain providing information on the monosaccharide composition, sulfation states and the uronic acid neighbouring linkages (Mulloy and Johnson, 1987; Rudd et al., 2011; Yates et al., 1996). However, NMR requires milligrams of material, and often it is difficult to isolate enough HS material from cells or tissues for NMR analysis as a single species (Venkataraman et al., 1999). Mass spectrometry on the other hand, requires much less material for structural analysis but is limited in the information it can provide from intact HS chains, as sulfate groups are often lost during fragmentation especially with matrix-assisted laser desorption/ionisation mass spectrometry (MALDI-MS) (Venkataraman et al., 1999). Recently, mass spectrometry has allowed for more detailed analysis, including identification of the epimeric forms of the uronic acid residues (Leary et al., 2015; Miller et al., 2016b). More commonly, initial HS structural analysis is achieved via HS degradation into its constituent disaccharide units, followed by separation using SAX-HPLC in reference to authentic HS standards. This method requires little material and allows for the detection of specific disaccharide units and their relative abundance.

1.6.6   Heparan Sulfation Depolymerisation

1.6.6.1   Nitrous Acid Depolymerisation

The most common form of chemical degradation of HS into its constituent disaccharide units is the use of nitrous acid oxidative depolymerisation, resulting in the selective cleavage of the acid sensitive *N*-sulfated residues leading to 2,5-anyhdromannose terminal units (**Figure 1.10**). *N*-acetylated domains are preserved and O-sulfated domains remain unmodified (Turnbull, 2001). The benefit of using this method is that the uronic acid is maintained in its authentic epimeric state and the method is overall relatively cheap. A downside to this method is that since nitrous acid degradation reacts at N-sulfated domains, N-acetylated domains will not be depolymerized and thus important structural information may be lost (Turnbull, 2001). This may be overcome by sulfating N-acetylated domains prior to depolymerisation. Furthermore, the non-reducing end of the sugar, which is converted into anhydromannose, is modified leading to further loss of information. Finally, the disaccharides produced from nitrous acid degradation lack a chromophore and so further labelling at the reducing end of the sugar is required for detection (Shriver et al., 2012).

1.6.6.2   Heparinase Depolymerisation

An alternative approach for HS depolymerisation is the use of HS degrading enzymes. As mentioned briefly, bacterially derived enzymes heparinase I, II and III digest HS into its constituent disaccharide units (Ernst et al. 1995) at pH 7 (**Figure 1.11**). Each enzyme has a distinct substrate specificity, some of which are overlapping and thus results in complete (or near complete) HS depolymerisation (Desai et al., 1993; Linhardt et al., 1988; Linhardt et al., 1990; Nader et al., 1999). Cleavage of the HS chain results in the formation of a Δ 4,5 double bond on the uronic acid, which absorbs UV light strongly at 232 nm (with a molar extinction coefficient of 5500 $M^{-1}cm^{-1}$) and thus represents a method for disaccharide detection. However, one downside of enzymatic degradation is that the uronic acid identity is lost in the formation of the double bond, as both GlcA and IdoA degrade to a common structure. The reducing end of the sugar, which is highly reactive, is left unmodified, and thus an available site for labelling with chromophores for alternative methods of detection with increased sensitivity.
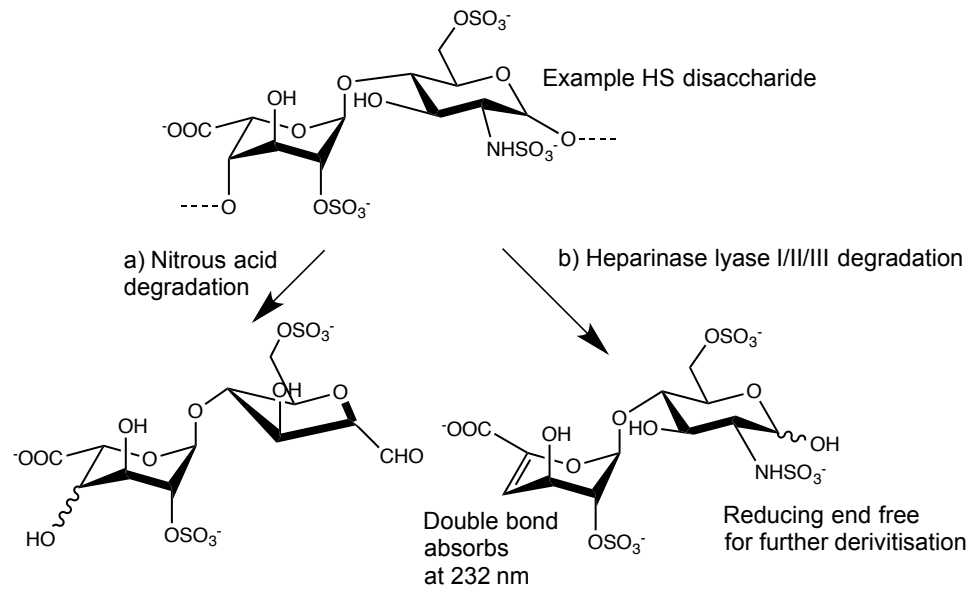
Figure 1.11 Nitrous acid and heparinase depolymerisation.

a) Nitrous acid depolymerisation results in oligosaccharides with 2,5-anyhdromannose terminal units. b) Heparinase I/II/II enzymes lead to HS depolymerisation resulting in disaccharides with a Δ 4,5 double bond on the uronic acid at the non-reducing end.

1.6.7   Remodelling Endogenous Heparan Sulfate

The methods described above are useful for determining the structure of HS from a pure sample, however, further studies exploring the functional role of the HS analysed can be difficult due to the high structural complexity, the dynamic turnover and low abundance of HS. An alternative approach for studying structure-function relationships of HS is to use exogenous HS of well-defined structures. In this way the biological effect of specific structures can be investigated. Naturally occurring HS, which is highly heterogeneous, can be separated based on fragment size and charge to produce better-defined structures with less variability for testing (Powell et al., 2010). However, HS is produced in minute quantities and as a consequence, it is often difficult to obtain enough material for structural determination and bioassays.

Alternatively, many groups have investigated the complex chemical synthesis of HS oligosaccharides and recent advances have been made (Arungundram et al., 2009; Schwörer et al., 2013). However, despite several modifications and improvements, the synthesis of HS remains a multi-step and costly process. A new chemoenzymatic approach as emerged using recombinant HS biosynthetic enzymes combined with unnatural uridine diphosphate monosaccharide donors (Liu and Linhardt, 2014; Liu et al., 2010; Xu et al., 2012). Although, chemoenzymatic approaches provide a general method for preparing different HS sequences, the target selection is restricted by the substrate specificities of the enzymes and thus synthetic selectivity remains a challenge (Xu et al,. 2012).

1.7   HS Mimetics

1.7.1   Chemically Modified Natural Products

To combat the difficulties of chemical synthesis of HS, a common method for developing HS mimetics is to chemically modify naturally occurring non-GAG polysaccharides by introducing functional sulfated groups along the chain to mimic the biological function of HS or other GAG species (Christman et al., 2008; Ikeda et al., 2011; Lee et al., 2010; Meddahi et al., 1996a; Roy et al., 2014; Ziebell et al., 2001).

1.7.2   Chemically Modified Heparin

Heparin, a more highly sulfated, close structural analogue of HS, can also be used for producing HS mimetics and studying structure-function relationships. However, it should be noted that the uronic acid residue of heparin is predominantly L-iduronic acid rather than the majority of glucuronic acid in HS. Additionally, heparin is more highly sulfated than HS and therefore less structurally diverse. Nonetheless heparin shows a broad molecular weight distribution, giving rise to a highly heterogeneous mixture of oligosaccharides. Heparin is produced by mast cells, it is more abundant than HS and thus commercially available at relatively low cost. Heparin can then be chemically modified, by selective de-sulfation at different positions (N-, 2-O- and 6-O-sulfation), producing more well-defined and simpler polysaccharides than parent heparin. The modified heparins can then be further separated based on fragment size after cleavage, allowing for more specific structural studies in which structural modifications are correlated to changes in activity or binding (Yates et al., 1996).

1.7.3   Glycomimetics in Muscle Regeneration

As discussed earlier, HS is implicated in skeletal muscle disease and muscle repair (Alvarez et al., 2002; Chevalier et al., 2015; Crisona et al., 1998). For this reason, evidence suggests that controlling the GAG composition of the ECM might represent a promising therapeutic approach to enhance muscle regeneration. One hypothesis postulates that GAG mimetics are resistant to enzymatic degradation and thus reside in the ECM longer than naturally occurring HS, permitting further growth factor regulation and subsequently, promoting muscle regeneration (Meddahi et al., 2002b; Meddahi et al., 1996b). Thus far, experiments involving GAG mimetics in muscle regeneration have largely focused around the use of so-called regenerating agents (RGTAs). These are matrix-based therapies, synthesised from natural dextran derivatives to contain defined amounts of various modifications (carboxymethyl, benzylamide and sulfonate groups). RGTAs serve to recreate the ECM microenvironment lost in degeneration and are able to interact with and protect several heparin-binding growth factors from proteolysis (Meddahi et al., 2002b; Meddahi et al.,

1995), preserving the natural endogenous cytokine signalling of the ECM. RGTAs successfully stimulate tissue repair when applied at a site of injury in several tissues (Blanquaert et al., 1995; Meddahi et al., 2002a; Meddahi et al., 1996a) including skeletal muscle (Aamiri et al., 1995; Gautron et al., 1995; Yamauchi et al., 2000). In EDL muscle of mice, RGTA protects muscle fibres from degeneration and preserves a differentiated state of fibres in ischaemic muscle (Desgranges et al., 1999). Further experiments have shown that RGTAs promote satellite cell proliferation and fusion *in vitro* (Papy-Garcia et al., 2002; Zimowska et al., 2005; Zimowska et al., 2001) and also change the GAG species during myogenesis of the C2.7 myoblast cell line (Barbosa et al., 2005). Thus they provide a good proof-of-concept for the activity of GAGs and GAG mimetics in muscle function.

1.7.4   Chemical Synthesis of HS mimetics

RGTAs have shown to be promising in the development of matrix-based therapies for tissue regeneration. Since they are based on dextran, which is a polysaccharide consisting of glucose residues, structural specificity can be a limitation. Furthermore, RGTAs are able to interact with numerous growth factors(Meddahi et al., 1996b), and if added in excess at a site of injury, in which all heparin-binding sites are occupied, heparin-binding growth factors can compete for sites on the matrix bound RGTAs. In this case, it might be beneficial to use a more highly selective compound, with fewer off-target effects.

1.8   Overall Project Aims

The central aim of this project was to investigate the structure-function relationship of HS in myogenesis. Although it has been previously demonstrated that HSPGs are dynamically regulated during myogenesis, in the majority of cases the focus was on the protein core, leaving the structural composition of the HS component largely unexplored. There has been no investigation to our knowledge, into the HS structural composition of primary myoblasts, nor investigations into the effects of ageing on the HS structural component of skeletal muscle. Alongside the main aim of this project, was the plan to investigate the use of chemically modified and fully synthetic HS mimetics as potential indications for therapeutic intervention to enhance muscle regeneration in ageing or in disease.

Thus, the aims of this project were to:

1) Determine the structure of HS during myogenic differentiation and assess the affects on signalling in the satellite cell niche
2) Determine the structure of HS during ageing in skeletal muscle
3) Investigate the structural importance of HS on myogenesis with the use of chemically modified HS mimetics

4) Investigate the effects of fully synthetic HS mimetics on myogenesis and potential use as novel therapeutic agents

Chapter 2

2   Materials and Methods

2.1   Mice

Young (11-13 weeks) and old (1 year and 2 years) C57Bl/6J female mice were obtained from Charles River, housed in a pathogen-free facility at the University of Liverpool, UK and used in accordance with the Animals (Scientific Procedures) Act 1986 and the EU Directive 2010/63/EU and after local ethical review and approval by Liverpool University's Animal Welfare and Ethical Review Body (AWERB).

2.1.1   *Skeletal Muscle Dissection*

Mice were euthanized by cervical dislocation. Before dissection, the mouse was sprayed with 70% ethanol. The skin was lifted on the back and a small incision was made with scissors. The incision was extended and the skin was retracted to the ankle to expose the hindlimb muscles. Forceps were used to remove the fascia coating the exterior muscles. The tibialis anterior (TA), extensor digitorum longus (EDL), gastrocnemius and soleus muscles were detached from the tibia and fibula. The quadriceps, hamstrings and remaining muscle were detached from the femur. Visible fat and hair were removed. For heparan sulfate extraction or RNA extraction, the individual muscles were placed in a cryovial and snap frozen in liquid nitrogen before being stored at -80 °C. For satellite cell-derived myoblast isolation, all muscles were collected in ice-cold F12-C + 0.4 mM $CaCl_2$ in a 50 ml falcon tube.

2.2   Cell Culture

2.2.1   Cell Culture Materials

2.2.1.1   Primary Myoblast Media

Primary myoblasts were isolated from the hindlimb muscles of 3-month-old female mice.

Primary Myoblast Growth Medium: F12 + 0.4 mM $CaCl_2$ (F12C)+ 15% horse serum + 1% penicillin/streptomycin + 2 mM glutamine (supplemented with 2 nM FGF2)

Primary Myoblast Differentiation Medium: F12 + 0.4 mM CaCl2 + 3% horse serum + 1% penicillin/streptomycin + 2 mM glutamine

2.2.1.2   C2C12 Myoblast Medium

C2C12 myoblasts are a subclone (produced by Blau, et al) of the mouse myoblast cell line established by D. Yaffe and O. Saxel(Yaffe and Saxel, 1977).

C2C12 Myoblast Growth Medium: Dulbecco's Modified Eagle Medium (DMEM), Gibco + 10% foetal bovine serum (FBS, Gibco) + 1% penicillin/streptomycin + 2 mM glutamine

C2C12 Myoblast Differentiation Medium: Dulbecco's Modified Eagle Medium (DMEM), Gibco + 2% horse serum, + 1% penicillin/streptomycin + 2 mM glutamine

2.2.1.3   BaF3 Cell Medium

BaF3 cells are interleukin-3 dependent mouse pro B lymphocytes established from peripheral blood.

BaF3 Cell Growth Medium: RPMI-1640 supplemented + 10% FCS + 100 Units/ml penicillin G + 100 µg/ml streptomycin sulfate (all from ThermoFisher, UK) and 1 ng/ml murine interleukin-3 (R&D Systems, UK)

2.2.2   Cell Culture Methods

2.2.2.1   Isolation of Satellite Cell Derived Myoblasts: Differential Plating Protocol

Muscles were dissected from mouse hindlimbs as described above, transferred to a Petri dish and minced with scissors for approximately 5 minutes until the muscles were reduced to a homogeneous slurry. Minced muscles were then transferred to a 50 ml conical tube containing 15 ml of 400 units/mg collagenase type I (Worthington Biochemical Corporation) + F12C (F12 + 0.4 mM $CaCl_2$) for 1.5 hour at 37°C with agitation every 15 minutes. The homogenate was spun down by centrifugation at 30 x g for 4 minutes. The supernatant was

collected and diluted with double the volume of growth media medium (F12C+ 15% horse serum + 1% penicillin/streptomycin + 2 mM glutamine). A pellet was obtained after centrifugation at 500 x g for 10 minutes. The pellet was resuspended in growth medium and filtered through a 40 µM cell strainer (BD Falcon®). The filtrate was spun down by centrifugation at 500 x g for 10 minutes. The pellet was resuspended in medium and plated on two gelatin-coated 10 cm plates per mouse for pre-plating 1 (PP1) under a humidified atmosphere of 5% CO_2 for two hours. The plates were then washed gently with their own medium and collected for re-plating on to two new gelatin-coated 10 cm plates for one hour; this was pre-plating 2 (PP2). PP2 were again washed gently with their own medium and collected for final plating (PO) on two gelatin-coated 10 cm plates per mouse. FGF2 was added at a final concentration of 2nM and satellite cell-derived myoblasts were expanded in growth medium (F12 + 0.4 mM $CaCl_2$ + 15% horse serum + 1% penicillin/streptomycin + 2 mM glutamine + 2 nM FGF2) under a humidified atmosphere of 5% CO_2 for two days. Recombinant FGF2 was prepared in house and kindly donated by Dr Dave Fernig, University of Liverpool.

2.2.2.2   Pre-plating Method Validation

In order to validate primary myoblast separation from contaminating fibroblast through the pre-plating technique, fresh growth medium (primary myoblast growth medium + 2nM FGF2) was added to PP1 and PP2 adhered cells and expanded for 2 days. After 2 days of expansion cells from PP1, PP2 and PO were fixed with 4% paraformaldehyde prepared in phosphate buffered saline (PBS) for 10 minutes at room temperature and then washed 3 times with PBS. Fixed cells were stored in PBS at 4°C until immunostaining was performed.

2.2.2.3   Preparation of Gelatin-Coated Culture Dishes

0.6 % (w/v) gelatin solution was boiled for 2 minutes prior to addition on to either;
a) 12 multi-well culture dishes and incubated at RT for 30 minutes. The excess gelatin was removed before being air-dried for a further 30 minutes at RT.
b) 10 cm culture dish in which the gelatin was spread with a sterilised glass spreader and air-dried at RT for 30 minutes.

2.2.2.4   Routine Culture of Primary Myoblasts

Primary myoblasts were obtained as described above from 11-13 week old female mice (Charles River) and plated on gelatin-coated 10 cm plates. Satellite cell-derived myoblasts were expanded in growth medium (F12C + 15% horse serum + 1% penicillin/streptomycin +

2 mM glutamine + 2 nM FGF2) under a humidified atmosphere of 5% CO_2 at 37°C for two days then either used as proliferating cells or passaged, using 40 units/ml of collagenase I in F12C, onto 12 multi-well culture dishes at a density of 800 cells/cm^2. Primary myoblasts could then be expanded for a further day in growth medium and then fixed as proliferating cells or be induced to differentiate by replacing the growth medium with differentiation medium (F12C + 3% horse serum + 1% penicillin/streptomycin + 2 mM glutamine). Primary myoblasts were differentiated for 3 days for differentiation assays.

2.2.2.5   Routine Culture of C2C12 Myoblast Cell Line

C2C12 myoblasts at passage number 3 were kindly donated by Prof Bradley Olwin (University of Colorado, USA) and grown in growth medium (Dulbecco's Modified Eagle Medium, Gibco) + 10% foetal bovine serum (FBS, Gibco) + 1% penicillin/streptomycin + 2 mM glutamine) under a humidified atmosphere of 5% CO_2 at 37°C. Cells were maintained at 40-70% confluence on uncoated plastic dishes for proliferating cells. Confluent cultures were switched to differentiation medium (Dulbecco's Modified Eagle Medium, Gibco + 2% horse serum, + 1% penicillin/streptomycin + 2 mM glutamine) and differentiated for 5 days for biological assays.

2.2.2.6   Routine Culture of BaF3 Cells

Murine BaF3 lymphocytes stably expressing murine FGFR1IIIc were a gift from Professor David Ornitz (Washington University, St. Louis, USA). They were grown in RPMI-1640 supplemented + 10% FCS + 100 Units/ml penicillin G + 100 µg/ml streptomycin sulfate (all from ThermoFisher, UK) with 1 ng/ml murine interleukin-3 (R&D Systems, UK) under a humidified atmosphere of 5% CO_2 at 37°C. Cells were maintained in suspension 10^5 to 10^6 cells/ml in uncoated plastic flasks.

2.3 Immunochemistry

2.3.1   General Fixation of cells

For general fixation of cells, medium was removed with aspiration and 4% paraformaldehyde (PFA, Sigma Aldrich) prepared in PBS, was added to the cells. Cells were incubated at RT for 5 minutes, before removing PFA and washing cells three times in PBS (5 minutes each). Cells were stored for a maximum of 2 days at 4 °C until immunostaining.

2.3.2   Fixation of cells for 5-bromo-2'-deoxyuridin Detection

For proliferation assays, 10 µM BrdU 5-bromo-2'-deoxyuridin (BrdU, Sigma Aldrich) was added to cells for 2 hours prior to fixation. For immunostaining of BrdU, cells were fixed with ice-cold 20% methanol and incubated for 10 minutes at -20°C, before removing methanol and washing cells three times in PBS (5 minutes each). Cells were stored for a maximum of 2 days at 4 °C until immunostaining.

2.3.3   Immunostaining of Cells

2.3.3.1   General Antibody Immunostaining

For detection of Tcf4, Myf5, myosin heavy chain (MyHC), myogenin (MyoG) and Pax7, fixed cells were permeabilized with PBS + 0.2% TritonX100 for 20 minutes at RT and then blocked with 3% bovine serum albumin (BSA, Sigma Aldrich) for 1 hour before incubation with primary antibodies over night in PBS + 1% BSA at 4 °C. Primary antibodies used were: mouse anti-MyHC (Developmental Studies Hybridoma Bank at Iowa University, MF20 clone) at 1:200, mouse monoclonal anti-Pax7 (Developmental Studies Hybridoma Bank at Iowa University) at 1:100, rabbit anti-Tcf4 (Cell Signalling), 1:200, rabbit anti-Myf5 (Santa Cruz) 1:500, rabbit anti-MyoG and rabbit anti-GFP (Thermo Fisher Scientific), 1:200. Cells were then washed 3 times with PBS + 0.2% TritonX100 and incubated for 1 hour at RT with PBS + 1% BSA + secondary antibodies conjugated with AlexaFluor 488, 555 or 647 (Invitrogen), at 1:500 followed by incubation with 2 µg/mL DAPI (Life Technologies) in PBS for 5 minutes at RT. Cells were then washed 3 times with PBS + 0.2% TritonX100 then stored at 4 °C in PBS until imaging.

2.3.3.2   BrdU Immunostaining

For detection of BrdU fixed cells were permeabilized with PBS + 0.2% TritonX100 + 1% BSA for 10 minutes at RT. Cells were quickly washed with 3N HCl and then DNA was denatured with 3N HCl for 20 minutes at RT. Cells were quickly washed with 0.1 M sodium-borate, pH 8.5 and then incubated in 0.1 M sodium-borate, pH 8.5 for 10 minutes at RT. Cells were washed 3 times with PBS and then blocked with PBS + 3% BSA for 30 minutes at RT before incubation with primary antibody rat anti-BrdU (Serotec) at 1:100 over night in PBS + 1% BSA at 4 °C. In some cases where stated, rabbit anti-GFP (Thermo Fisher Scientific), 1:200 or mouse anti-MyHC (Developmental Studies Hybridoma Bank at Iowa University, MF20 clone) at 1:200 were included in the incubation. Cells were then washed 3 times with PBS + 0.2% TritonX100 and incubated for 1 hour at RT with PBS + 1% BSA + secondary antibodies conjugated with AlexaFluor 555 (Invitrogen) at 1:500 followed by incubation with 2 µg/mL DAPI (Life Technologies) in PBS for 5 minutes at RT. Cells were then washed 3 times

with PBS + 0.2% TritonX100 then stored at 4 °C in PBS until imaging.

2.4   Microscopy, Image Processing and Quantification

2.4.1   Microscopy and Image Processing

Fixed cells were imaged on an epifluorescence microscope (EVOS-FL, Life Technologies), 10 X objectives were used for all images unless otherwise stated. Images were composed using Photoshop 7.0 (Adobe Systems). Background was linearly reduced using contrast and brightness adjustments, and all modifications were applied to the whole image.

2.4.2   Manual Quantification of Immunostaining

Quantification of immunostaining was achieved by manually counting cells with positive immunofluorescence. Conducted for 10 random images per dish, repeated over at least three technical replicates. All experiments were conducted at least three independent times.

2.4.3   Automated Quantification of Immunostaining

In some cases, images were analysed using a bespoke macro written for Fiji (available at [http://fiji.sc]). Assistance in analysis was provided by the Liverpool Centre for Cell Imaging, University of Liverpool. Bespoke macros were written to calculate:

a) The Differentiation Index;

$$\left(\frac{MyHC\ positive\ nuclei}{total\ nuclei}\right) \times 100$$

b) The Fusion Index;

$$\left(\frac{MyHC\ positive\ cells\ with\ at\ least\ two\ nuclei}{total\ nuclei\ in\ all\ MyHC\ positive\ cells}\right) \times 100$$

c) The number of proliferating cells;

$$\left(\frac{BrdU\ positive\ nuclei}{total\ nuclei}\right) \times 100$$

2.5   Heparan Sulfate Compositional Analysis

2.5.1   Heparan Sulfate Proteoglycan Extraction

2.5.1.1   Heparan Sulfate Proteoglycan Extraction from Cells

Proliferating or differentiating primary myoblasts or C2C12 myoblasts, were washed twice with ice-cold PBS and solubilized in 1 ml TUT buffer (8 M urea, 1 % Triton X100, 10 mM Trizma Base, 0.1 mM Na_2SO_4, pH 8.0), per 10 cm^2 culture dish followed by sonication to disrupt DNA. Samples were stored at 4 °C for a maximum of 2 days.

2.5.1.2   Heparan Sulfate Proteoglycan Extraction from Muscle

Quadricep, gastrocnemius or tibialis anterior muscles were homogenized with a blade homogenizer and solubilized in 1 ml of TUT buffer (8 M urea, 1 % Triton X100, 10 mM Trizma Base, 0.1 mM Na_2SO_4, pH 8.0), then cleared by centrifugation at 13,000 x g for 10 minutes, followed by sonication to disrupt DNA. Samples were stored at 4 °C for a maximum 2 days.

2.5.2   Heparan Sulfate Disaccharide Preparation

2.5.2.1   DEAE Partial Purification of HSPGs

Cell or muscle homogenates were added to diethylaminoethyl (DEAE) Sephacel beads (GE healthcare) and incubated over night at 4°C with gentle mixing. The DEAE beads were washed with 10 volumes of PBS, pH 7.4 followed by 10 volumes of PBS + 0.3 M NaCl, pH 7.4 and then eluted with 10 volumes of PBS + 2 M NaCl, pH 7.4. Eluted fractions were desalted on HiTrap Desalting Columns (GE healthcare) and freeze-dried.

2.5.2.2   Heparinase Depolymerisation

Freeze-dried samples were resuspended in 100 mM sodium acetate, 0.1 mM calcium acetate, pH 7.0 and digestion by sequential addition at 37 °C of 2.5 mU of heparinase I (2 hours, 37 °C) followed by 2.5 mU of heparinase III (2 hours, 37 °C) and finally with 2.5 mU of heparinase II (2 hours, 37 °C). All three enzymes were then added together at 2.5 mU each (16 hour, 37 °C), to ensure full depolymerisation of HS. The cleavage specificities for the heparinase enzymes are shown in **Table 2.1**. The enzymes and core proteins were removed using Pierce C18 Spin Columns (Life Technologies) and the salt removed using Pierce

Graphite Spin Columns (Life Technologies). The samples were then freeze-dried before labelling.

Table 2.1 Cleavage specificity of the HS chain required for the corresponding heparinase enzymes.

Treatment of HS with the three heparinase enzymes at 37 °C leads to complete depolymerisation of the chain into its constituent disaccharide units.

Enzyme	Sequence Specificity
Heparinase I	-GlcNS(±6S)-α (1-4) IdoA(2S)-
Heparinase II	-GlcNR(±6S)-α (1-4) GlcA/IdoA-
Heparinase III	-GlcNR(±6S)-α (1-4) GlcA-

2.5.2.3   BODIPY Labelling for Fluorescence Detection

Freeze-dried samples were resuspended in BODIPY hydrazide (5 mg/ml in methanol). Methanol was removed by centrifugation under vacuum, and samples were resuspended in dimethyl sulfoxide (DMSO): acetic acid (17:3 v/v) prior to incubation for 4 h at room temperature in the dark. Samples were snap frozen and freeze dried. Excess free BODIPY tag was removed by thin layer chromatography (TLC plates, Sigma Aldrich). Bound labelled disaccharides were eluted from the silica scrapings with deionized water (3 x 4 ml) and then freeze-dried. 800 µl of saturated ethanol solution (sodium acetate in molecular biology grade ethanol) was added to lyophilised samples, incubated on ice for 15 minutes and then centrifuged at 13000 x g for 5 minutes. The supernatant was collected and dried by centrifugation under vacuum.

2.5.2.4   Strong Anion Exchange-High Liquid Performance Chromatography (SAX-HPLC)

The fluorescently labelled disaccharides were resuspended in H_2O (700 µl) prior to loading onto a Propac PA-1 column and eluted using a linear gradient of 0 – 1 M sodium chloride (prepared in 150 mM NaOH) over 30 minutes at a flow rate of 1 ml/minute on a Shimadzu HPLC system. Peaks were detected using inline fluorescence detection at excitation wavelength of 488 nm and an emission wavelength of 520 nm using a Shimadzu RF-551 detector. The column was reconditioned by washing with 2 M NaCl (in 300 mM NaOH) before equilibrating in 150 mM NaOH. Disaccharides were identified with reference to authentic heparin unsaturated disaccharide standards (**Table 2.2**) (Dextra Labs). Previously calculated correction factors were applied to quantify the observed disaccharides (**Table 2.2**) (Skidmore et al., 2010).

Table 2.2 BODIPY Labelled HS Disaccharide Standards.

HS disaccharides purchased from Sigma with the corresponding structure prior to BODIPY labelling. The typical elution times by SAX-HPLC correspond to the BODIPY labelled disaccharides. Correction factors were used in the calculation of peak area based on the labelling efficiency of each standard disaccharide.

Sigma Ref	Standard structure	Elution time	Correction Factor
IV-A	Δ-UA-GlcNAc	12.784	1.3
IV-S	Δ-UA-GlcNS	18.594	1.7
II-A	Δ-UA-GlcNAc(6S)	21.257	1.2
III-A	Δ-UA(2S)-GlcNAc	23.906	1.2
II-S	Δ-UA-GlcNS(6S)	27.661	1.0
III-S	Δ-UA(2S)-GlcNS	31.138	1.1
I-A	Δ-UA(2S)-GlcNAc(6S)	37.507	1.4
I-S	Δ-UA(2S)-GlcNS(6S)	46.079	1.1

2.6   Heparan Sulfate Activity Assays

2.6.1   *Isolation of HS for activity assays*

Muscle or C2C12 myoblast homogenates (from HSPG extraction using TUT buffer) were added to diethylaminoethyl (DEAE) Sephacel beads (GE healthcare) and incubated over-night at 4°C on gentle mixing. The DEAE beads were washed with 10 volumes of PBS, pH 7.4 followed by 10 volumes of PBS + 0.3 M NaCl, pH 7.4 and then eluted with 10 volumes of PBS + 2 M NaCl, pH 7.4. Eluted fractions were desalted on HiTrap Desalting Columns (GE healthcare) and freeze-dried. Freeze-dried samples were re-suspended in 1:5 volume of 10x DNase solution (200 mM Tris-acetate pH 8.0, 30 mM $MgCl_2$, 50 mM $CaCl_2$ with 1 µg/ml DNase was added for 4 hours, 37 °C. 1:5 volume of 5x RNase solution was then added (50mM Tris pH 8.0, 25 mMEDTA, 40 mM Na-Acetate) with 0.5 mg/ml RNase was added for 1 hour, 37 °C. 1:5 volume of 5x Chondroitin ABC lyase (cABCase) solution (500 mM Tris-acetate pH 8.0) with 1.25U cABCase was added for 4 hours 37 °C. A 1:5 volume of 5x Neuraminidase buffer (250 mM Tris Acetate pH 7.5) with 2.5 mU of neuraminidase was added for 4 hours, 37 °C. 1:5 volume of 5x keratanase buffer (250 mM Tris Acetate, pH 7.5) with 100 mU keratanse was added for 4 hours, 37 °C. A 1:5 volume of 5X Pronase solution (500 mM Tris-acetate, 50mM Calcium acetate pH 8.0) with 10 mg/ml Pronase was added for 16 hours, 37 °C. The samples were then added to (DEAE) Sephacel beads to remove the enzymes. The isolated HS chains were eluted from the beads as described previously.

Samples were freeze-dried and re-suspended in 100 µl filtered milliQ water. 5 µl was taken through for heparinase digestion (described above) for HS quantification. After the enzymes were removed the freeze-dried samples were re-suspended in 20 µl of miliQ water for quantification on the nano-drop measuring the absorbance of the $C_4=C_5$ bond at 232 nm.

2.6.2   BaF3 cell Assays

For assays, BaF3 cells were plated at 10^5 cells/ml in 96-well, flat-bottomed Costar tissue culture plates (Corning, USA) in 100 µl growth medium without interleukin-3 supplemented with FGF2 (R&D Systems, UK) and heparan sulfate at the indicated concentrations. Cells were incubated for 72 hours at 37°C, 5% CO_2. Thiazolyl blue tetrazolium bromide (MTT) (Sigma, UK) was then added to a final concentration of 250 µg/ml and the cells were incubated a further 4 hours at 37°C, 5% CO_2. The assay was stopped with the addition of 50 µl 10% SDS, 0.01N HCl and the plates were incubated 4 hours to overnight at 37°C to dissolve the formazan products. Plates were read at 570 nm using a Thermo multiskan EX plate reader (ThermoFisher, UK).

2.7   Knockdown of HS6STs

C2C12 myoblasts were seeded in a 12-well plate at a density of 5000 cells/cm^2. Cells were cultured in growth medium for 24 hours after which the medium was replaced with Optimem (Gibco). 250 ng/ml pClover (Addgene) was co transfected with 20 nM of each HS6ST siRNA using with Lipofectamine®2000 (Thermo FisherScientific) according to manufactures instructions. siRNA sequences were obtained from Sigma Aldrich (HS6ST1, SASI_Mm01_00066864; HS6ST2, SASI_Mm02_00292422; HS6ST1, SASI_Mm01_00105592; universal negative control. Following knockdown:

1) To assess the extent of knockdown by quantitative real time PCR (qPCR) using RNA purified from siRNA-treated cells 24 hours post transfection was performed.
2) To assess proliferation of siRNA-treated cells, 22 hours post transfection a BrdU proliferation assay was performed on myoblasts in the 12-well plates
3) To assess differentiation of siRNA-treated cells, 24 hours post transfection myoblasts in the 12-well plates were fixed and immunostained to detect myogenin.

2.8   Real Time Polymerase Chain Reaction

2.8.1   RNA Isolation

2.8.1.1   RNA Isolation from C2C12 Myoblasts

RNA was isolated using a Qiagen RNeasy Mini Kit (Qiagen) following manufacturer's instructions. RNA quality and integrity were checked using a Nanodrop®1000 (Thermo Fisher Scientific).

2.8.1.2   RNA Isolation from Skeletal Muscle

Whole TA muscle, which had been snap frozen in liquid nitrogen and stored at -80°C, was ground by pestle and mortar in liquid nitrogen to a fine powder. The powdered muscle was added to 1 ml of cold Invitrogen™TRIzol™ (Thermo Fisher Scientific). 200 µl of chloroform was added and the mixture was then vortexed until a homogenous mixture was obtained. The homogenate was centrifuged at 12,000 x g for 20 minutes. After centrifugation, the top, aqueous, clear layer was carefully collected and transferred into a new eppendorf tube. 500 µl of ice-cold isopropanol was added and then thoroughly vortexed. The mixture was incubated for 30 minutes at RT before centrifugation at 12,000 x g for 20 minutes. The supernatant was carefully removed to expose a clear pellet. 200 µl of 80% ethanol was added and was immediately centrifuged for at 12,000 x g for 20 minutes. The supernatant was removed carefully avoiding the pellet. The pellet was air-dried before being resuspended in 20 µl of RNase-free water and stored at -80°C. RNA quality and concentration were checked using a Nanodrop®1000 (Thermo Fisher Scientific).

2.8.2   cDNA Synthesis

2.8.2.1   cDNA Synthesis for Manual RT-PCR

Following RNA extraction from C2C12 myoblasts, cDNA was synthesised from a maximum of 5 µg of RNA using the Tetro cDNA Synthesis Kit (Bioline).

2.8.2.2   cDNA Synthesis for Automated RT-PCR

Following RNA extraction from whole muscle RNA was taken to Oxford on dry ice. cDNA was synthesised using the Applied Biosystems™ High-Capacity cDNA Reverse Transcription Kit (Thermo Fisher Scientific) carried out by Dr Anastasios Chanalaris in Dr Linda Troeberg's laboratory (Kennedy Institute of Rheumatology, University of Oxford).

2.8.2.3   Manual RT-PCR

Gene expression was quantified by qPCR using the LightCycler 460 SYBR Green I Master kit (Roche) with 5 µl cDNA corresponding to 20 ng total RNA in a 20 µl final volume and 0.4 µM of each primer. Experiments were performed in duplicate for each sample in a 96-well plate (Roche). The PCR programme contained: 95°C for 5 minutes followed by 45 cycles at 95°C for 12 seconds, at the annealing temperature of 57°C for 10 seconds, and the extension at 72°C for 10 seconds. Amplification specificity was assessed using a melting curve following the manufacturer's instructions. Primers were designed using the NCBI Primer-BLAST software to have a melting temperature of 60°C and an amplicon size between 100-200 base pairs (**Table 2.3**). Primers were purchased from Eurofins Genomics. Results were analysed with the LightCycler software (Roche) using the second derivative maximum method to set the threshold cycle (C_T). The relative quantitative analysis was carried out using the comparative C_T method ($2^{-\Delta\Delta CT}$) method such that expression levels of all three HS6STs were first normalised to the reference gene glyceraldehyde 3-phosphate dehydrogenase (GAPDH) and then the normalised HS6ST/GAPDH values obtained from cells transfected with HS6ST siRNAs where expressed as percentage of the HS6ST/GAPDH values obtained from cells transfected with control (scrambled) siRNA.

Table 2.3 Sequences of Primers used in Manual RT-PCR

Gene	Forward Primer	Reverse Primer	Size
GAPDH	CCCCTTCATTGACCTCAACTAC	TCCACGACATACTCAGCACC	182
HS6ST1	CGTTCGCCCAGAAAGTTCTAC	CACACATGTGCAAGGAGGTC	118
HS6ST2	CCCTTGGCCAGCGTCG	GCACACGTATTGGACGA	102
HS6ST2	GGCAAGAAGGAGACCTGGCT	GTAGAAATTCCTGGTGTGGCTGTG	150

2.8.2.4   Taqman® Low Density Array Microfluidic cards

Taqman® Low Density Array (TLDA) microfluidic cards were used to study the transcript expression levels of the HS biosynthetic enzymes in the tibialis anterior muscles of 3 month and 2 year-old mice. TLDA experiments were carried out by Dr Anastasios Chanalaris in Dr Linda Troeberg's laboratory (Kennedy Institute of Rheumatology, University of Oxford). TLDA microfluidic cards were custom designed to contain pre-selected Taqman gene probes and carry out 384 real time PCR reactions simultaneously. A total of 8 samples were run on one card (four from 3 month old muscle and four from 2 year old muscle). For each sample 48 HS-related genes were analysed, including the endogenous control, GAPDH. Cards were

prepared with a total reaction mixture for each sample of 100 µl containing 50 µl 2X Universal PCR mix (Applied Biosystems, USA) and 50 µl cDNA template (200 ng starting RNA) in nuclease-free water. Prior to loading, the reaction mixture of each sample was vortexed and briefly centrifuged. Once loaded the card was centrifuged twice (1 minute at 12,000 rpm) and sealed with the microfluidic card sealer. The cards were run on the 7900HT ABI thermocycler (Applied Biosystems, USA). The thermocycling conditions were as follows: held at 50°C for 2 minutes, denatured at 94.5°C for 10 minutes, followed by 40 cycles of denaturing at 97°C for 30 seconds, and lastly annealing/extending for 1 minute at 60°C.

2.9   Treatment With Modified Heparins

Chemically modified heparins were prepared and kindly donated by Dr Ed Yates, University of Liverpool (Yates et al., 1996).

2.9.1   *Differentiation Assay*

Primary satellite-cell derived myoblasts were induced to differentiate in the presence/absence of modified heparins for 3 days prior to fixation with 4% PFA was prepared in PBS for 10 minutes at room temperature and then washed 3 times with PBS. Fixed cells were stored in PBS at 4°C until immunostaining was performed.

2.9.2   *Proliferation Assay in High Serum*

Primary satellite-cell derived myoblasts were grown under proliferating conditions in the presence/absence of modified heparins for 24 hours prior to a BrdU assay.

2.9.3   *Proliferation Assay in the Absence of Serum*

Primary satellite-cell derived myoblasts were serum-starved for 12 h to induce cell cycle exit followed by treatment with FGF2 with or without the modified heparin over night. To assess proliferation of treated cells in the absence of serum, a BrdU assay was then performed on myoblasts in the 12-well plates.

2.9.4   *Western Blotting*

Whole cell extracts were obtained by incubating C2C12 cells in modified RIPA buffer (50 mM Tris-HCl, pH 7.4, 1% NP-40, 0.25% sodium-deoxycholate, 150 mM NaCl, and 1 mM ethylenediaminetetraacetic acid (EDTA)) supplemented with a protease inhibitor cocktail

(Complete, Roche) and phosphatase inhibitors (2 mM Na_3VO_4 and 2 mM NaF) for 30 minutes on ice, then cleared by centrifugation at 13,000 x g for 10 minutes at 4°C. Protein was quantified with a bicinchoninic acid (BCA)-based kit (Pierce) according to the manufacturer's instructions. Total protein content (10–30 µg) was separated on a 10% SDS-PAGE gels and transferred onto nitrocellulose membranes (Hybond, GE Healthcare) for Western blotting. Primary antibodies were incubated overnight at 4 °C in PBS + 5% BSA and were: rabbit anti-p44/42 MAPK (Erk1/2, *Cell Signalling Technology*) used at 1:1,000, rabbit anti-Phospho-p44/42 MAPK (Erk1/2, Thr202/Tyr204, *Cell Signalling Technology*) used at 1:1,000. Anti–rabbit horseradish peroxidase (HRP)-conjugated secondary antibodies (*Santa Cruz Biotechnology*) were used at 1:10,000 in PBS + 5% BSA for 1 hour at room temperature, and HRP activity was visualized using the ECL Plus system (*BioRad*). Images were quantified using the "Analyze Gel" function of *ImageJ*.

2.10 Statistical Analysis

All statistical analyses were carried out using Microsoft Exel or GraphPad Prism. Each experiment consisted of at least three technical replicates, where statistical significance was determined using an unpaired Student's t-test or a one-way ANOVA. Data were plotted as the mean ± standard error of the mean (SEM) for normally distributed data. Data were deemed statistically significant when $p < 0.05$.

Chapter 3

3   The Structure of HS Changes During Myogenic Differentiation

3.1   General Introduction

3.1.1   *Myogenic Cultures*

To study myogenesis *in vitro,* satellite cell derived-myoblasts can be isolated from skeletal muscle and expanded *ex vivo*. Isolation requires satellite cells to be liberated from their niche, by manual muscle mincing followed by enzymatic digestion to break-up connective tissue and the myofibres to which the satellite cells adhere. Several murine myoblast cell lines have been developed from isolated myoblasts whose behaviour corresponds to that of progenitor lineage. C2C12 myoblasts, the most commonly used myoblast cell line (Blau et al., 1983b), are a sub-clone of C2 myoblasts (Yaffe and Saxel, 1977), which differentiate spontaneously after serum withdrawal (Blau et al., 1983a). The C2C12 myoblast cell line requires standard culture conditions with no extra growth factor supplements, is highly robust and thus can be readily expanded at low cost. An alternative cell line is the MM14 myoblast cell line, which is less widely used than the C2C12 myoblast cell line but retain more similar morphological and molecular characteristics of primary satellite cells (Linkhart et al., 1980). Furthermore a conditionally immortal satellite cell-derived cell-line, H2K 2B4 has been generated, which display no tumorogenic tendency *in vivo* unlike the C2C12 myoblast cell line (Morgan et al., 1994). Although myoblast cell lines provide consistency and convenience for studying biochemical and molecular mechanisms of myogenesis *in vitro*, they lack some critical features of satellite cells. For example, primary satellite cells display significantly differential adhesion and motility on extracellular matrix substrates than both C2C12 and MM14 myoblasts (Siegel et al., 2009). Primary satellite cell-derived myoblast cultures are therefore a better representation of an *in vivo* system (Cornelison, 2008), effectively mimicking most of the molecular mechanisms involved in satellite cell self-renewal, proliferation and differentiation. Thus, efficient purification protocols are essential for isolating

satellite cell-derived myoblasts dissociated from whole skeletal muscle. A method based on fluorescence-activated cell sorting (FACS) has been recently developed for purifying satellite cell derived myoblasts, by using antibodies directed against specific satellite cell surface antigens (Liu et al., 2015; Pasut et al., 2012). However, antibodies and FACS are highly expensive and laser exposure can induce cell death during the purification process, leading to loss of material (Mollet et al., 2007). Alternatively, satellite cells can be separated from fibroblasts and myofibril debris by a series of pre-plating steps based on differences in adhesion characteristics (Goetsch et al., 2015; Qu-Petersen et al., 2002; Rando and Blau, 1994; Richler and Yaffe, 1970). Since fibroblasts are more adhesive than quiescent and early activated satellite cells, they adhere to the dish in the first series of pre-plating steps, while satellite cell-derived myoblasts remain in suspension and after pre-plating can be collected for culturing and expansion.

3.1.2   HS Structural Analysis During Muscle Differentiation

As discussed previously, many heparin-binding growth factors are involved in the regulation of myogenesis, and depend heavily on the structure of HS. Currently, however, there is little information available with regards to the structural composition of HS during myogenesis. There has been one study, which reported an increase in the amount of HS during differentiation of the C2.7 myoblast cell line (Barbosa et al., 2005). Modest changes in the structural composition of HS were also implicated based on antibody expression and the expression levels of a small proportion of HS biosynthetic enzymes (Barbosa et al., 2005). However, these techniques do not reveal more subtle structural changes in HS, such as differences in the abundance of specific HS disaccharide units. Furthermore, studies *in vivo* suggest that structural changes in HS do affect myogenic regulation. Firstly, mutant mice lacking the two extracellular sulfatases that remove the sulfate group in 6-*O* position, mSulf1 and mSulf2, exhibit delayed myogenic differentiation (Langsdorf et al., 2007; Tran et al., 2012). Secondly, structural changes in HS have been reported in regenerating muscles post ischaemic-injury (Chevalier et al., 2015), suggesting that the structure of HS has a role in regulating satellite cell homeostasis. Given this, it would be important to further investigate the structural composition of HS during myogenesis in primary cultures of satellite cell-derived myoblasts in an attempt to better understand the structure-function relationships of HS during myogenesis.

3.1.3   HS Structural Analysis Background

Efficient protocols are crucial for purifying and analysing HS from tissues and cells. HS purification involves the initial release of HS by the homogenisation of cells or tissues in a manner that leads to disruption of cell membranes. Although HS is a highly stable macromolecule in most physiological conditions, caution must be taken with the method of extraction, since extreme conditions, such as low pH and high temperatures, can lead to *N*-

desulfation and other modifications (Drummond et al., 2001; Inoue and Nagasawa, 1976; Yates et al., 1996). More commonly, methods for HS extraction from cells and tissues involve the use of detergent for cell membrane disruption. Following on from HS extraction, an efficient approach for the rapid isolation of proteoglycans has been developed (Guimond et al., 2009a), which involves little loss of material and is readily scalable. Since HS is highly negatively charged, ion exchange is used for HS partial purification. HS binds to gel matrix beads derivatised with a positively charged molecule, such as diethylaminoethanol (DEAE) and is released from the matrix with an increasing salt gradient. Contaminating macromolecules can also be removed at this step by single-pot sequential enzymatic digests and a second ion exchange and desalting procedure for preparing highly purified HS suitable for bioassays. For structural analysis, due to the structural complexity, depolymerisation of the HS chain for subsequent disaccharide compositional analysis is commonly used. HS disaccharide units harbour different levels and positions of sulfation and consequently, will bind with different affinities to a strong anion exchange (SAX) column, allowing for separation and detection by high performance liquid chromatography (HPLC). The heparinase enzymes are lyases that, acting together, catalyse complete depolymerisation of the HS chain into its constituent disaccharide units, harbouring a 4,5 unsaturated bond at the newly introduced non-reducing end allowing for its detection at 232 nm; ε = 5500 $M^{-1}cm^{-1}$. HS disaccharide abundance can be determined by reference to the elution times of a set of commercially available HS disaccharides. Additionally, the introduction of the unsaturated bond allows for HS quantification via absorption at 232 nm. This is more advantageous than other methods of HS quantification, which often require complete disruption of HS, such as the cationic dye 1,9-dimtehylmethylene blue (DMMB), which covalently binds to sulfated GAGs and thus the HS cannot be used for further structural analysis.

However, since it is difficult to isolate HS in sufficient quantities from primary cells and tissues, UV absorption is often not sensitive enough for individual disaccharide detection and therefore an alternative method of detection is important. The reducing end of the disaccharide allows for labelling with a fluorescent tag. The fluorophore 4,4-difluoro-5,7-dimethyl-4-bora-3a,4a-diaza-*s*-indacene-3-propionic acid, hydrazide (BODIPY) (**Figure 3.1**), has been found to produce improved yields and sensitivity compared to other more widely used fluorescent tags (Skidmore et al., 2006; Skidmore et al., 2010), permitting structural analyses of HS approximately 1000-fold higher sensitivity than UV detection (Lohse and Linhardt, 1992) and 10-100-fold higher sensitivity than previous fluorescence detection methods (Deakin and Lyon, 2008; Kinoshita and Sugahara, 1999; Kitagawa et al., 1995; Toyoda et al., 1997). Owing to its higher reactivity, BODIPY labelling also requires less harsh chemical conditions, which can often be problematic when dealing with the acid sensitive *N*-sulfate groups of HS. Furthermore, unlike many other fluorescent labels, which are charged, BODIPY is a neutral compound and therefore does not interact strongly with anion exchange columns. The resulting labelled HS disaccharides can then be passed over

a SAX-HPLC column eluted with a salt gradient and detected at λ_{exc} = 488 nm and λ_{emm} = 520 nm.
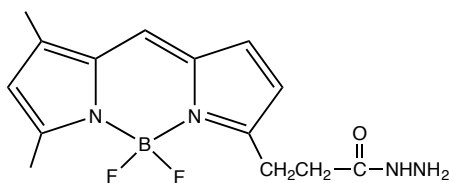
Figure 3.1 Structure of BODIPY fluorophore.

Structure of the BODIPY fluorescent tag used for derivatisation of the HS disaccharide at the reducing end of the disaccharide after HS digestion with heparinase I/II/III.

3.2   General Hypothesis

Given that HS controls many signalling pathways that are involved in the regulation of myogenesis, it was hypothesized that the structural composition of HS changes during satellite cell differentiation and thus is a contributory factor for regulating the balance between proliferation and differentiation.

In this chapter it will be shown that:

1. Pure populations of myoblasts can be isolated from murine skeletal muscle using a quick and economical differential plating protocol
2. The level of sulfation of the primary myoblast heparanome increases with differentiation
3. The level of sulfation of the C2C12 myoblast heparanome increases with differentiation
4. HS from proliferating myoblasts but not that from differentiating myoblasts promote FGF2 signalling

3.3   Results

3.3.1   Isolating Satellite cell-derived Myoblasts

3.3.1.1   Differential Adhesion Protocol for the Isolation of Satellite Cell-Derived Myoblasts

Since HS controls many of the protein functions that are involved in the regulation of myogenesis (as reviewed in Turnbull et al, 2001;Bishop et al, 2007), it was hypothesized that the structure of HS changes during muscle progenitor differentiation, and thus may be a contributory factor that regulates the balance between myoblast proliferation and

differentiation. To explore this hypothesis, primary myoblast cultures were initially used for HS extraction, since primary myoblasts are generally more representative of an *in vivo* system than myoblast cell lines. For satellite cell-derived myoblast purification, a differential plating protocol was employed based on an adapted version of the method previously described by Rando and Blau (Rando and Blau, 1994) (**Figure 3.2**). Myoblasts were derived from the hind-limb muscles of 3 month-old female mice following the protocol outlined in **Figure 3.2**. Firstly, muscles were minced into a fine slurry and cells were then enzymatically dissociated with collagenase type I. The slurry was filtered before centrifugation to pellet cells, resuspended and plated onto gelatin-coated plates, which was referred to as pre-plating 1 (PP1). After two hours of incubation, the supernatant containing non-adherent cells was transferred to a second pre-plating, again onto gelatin-coated plates, which was referred to as pre-plating 2 (PP2). After a further one hour incubation on PP2, the supernatant containing non-adherent cells was transferred to a final plating onto gelatin-coated plates, labelled as passage 0 (P0). Adherent cells from PP1 and PP2 were also supplied with fresh medium. To ensure fibroblasts were successfully removed in the initial pre-platings (PP1 and PP2) that the final plating (P0) was enriched for myoblasts, 48 hours post isolation, cells were fixed and immunostained to detect transcription like-7 2 factor (Tcf4), a fibroblast marker (Mathew et al., 2011), myogenic regulatory factor, Myf5 and paired box transcription factor, Pax7.
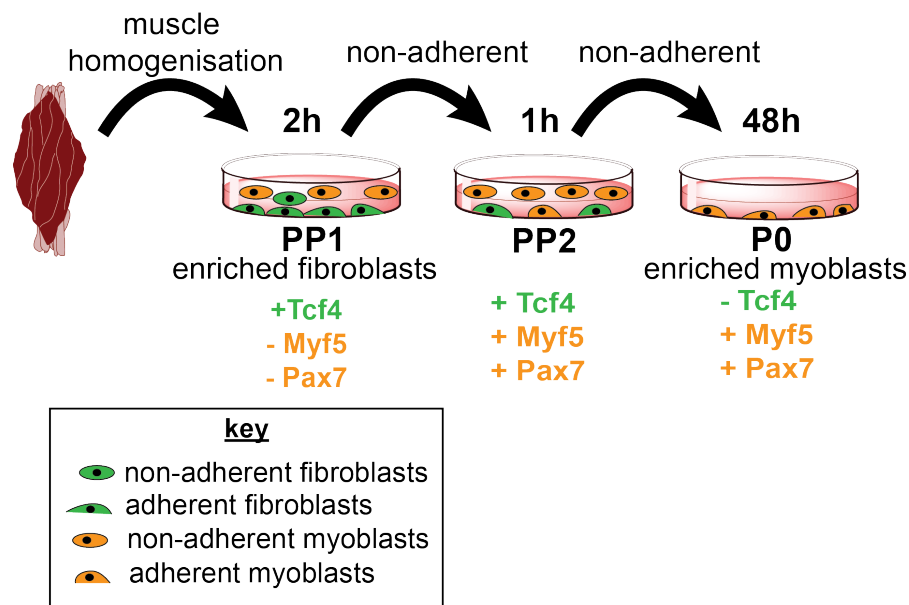
Figure 3.2 Schematic showing differential plating protocol for myoblast isolation.

The hindlimb muscles of 3 month-old female mice were minced and incubated at 37°C with collagenese type I for 1 h to release cells. Myoblasts were isolated through a series of two pre-plating steps: PP1 and PP2. The differential plating protocol is based on the shorter adhesion time of fibroblasts compared to myoblasts. After 2 h on PP1, the supernatant containing non-adherent cells was transferred to PP2. Then, after 1 h on PP2, the supernatant containing non-adherent cells was transferred to passage 0 (P0). Adhered cells were cultured for a further 48 h before fixing and immunostaining to detect the fibroblast marker, Tcf4 and myogenic markers; MyoD, Myf5 and Pax7. Cells were supplemented with FGF2 daily and grown on plates coated with gelatin.

3.3.1.2   Myoblast Enrichment Validation

After 48 hours in culture, the majority of cell populations present in PP1 and PP2 displayed distinct fibroblast-like morphological features (**Figure 3.3**), exhibiting diverse, elongated shapes. The majority of cells present at passage 0 (P0) were more homogeneous in shape, smaller and rounder, which is highly characteristic of satellite cell-derived primary myoblasts plated on gelatin (Motohashi et al., 2014). Cells present in PP1 stained positively for Tcf4 but did not co-express Pax7 or Myf5 (**Figure 3.4** + **Figure 3.5**). At PP2, cells labelled positively for Tcf4 or Myf5. Cells present at PP2 did not express Pax7. At P0 only 1.49 (± 0.97) % of cells stained positively for Tcf4. Lastly, at P0, 48 hours after isolation, 80.9 (± 4.4) % of cells stained positively for Pax7 and 85.9 (3.1) % cells stained positively for Myf5. Thus this provided a clear indication that PP1 consisted of predominantly fibroblasts and P0 consisted predominantly of myoblasts, with few contaminating fibroblasts.
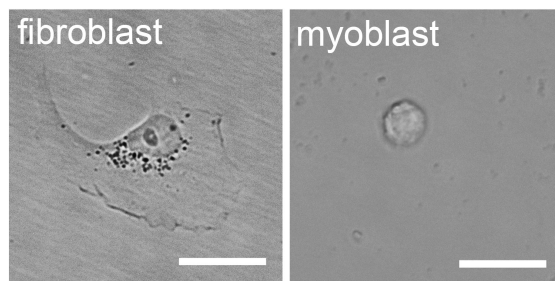
Figure 3.3 Morphological validation of fibroblasts and myoblasts.

Firstly, a representative image of adhered fibroblast at PP1, showing elongated shape with large nuclei (left image). Representative image of adhered myoblast at P0, which are rounder and smaller (right image). Images taken at 40 X magnification. Scale bar = 20 µm
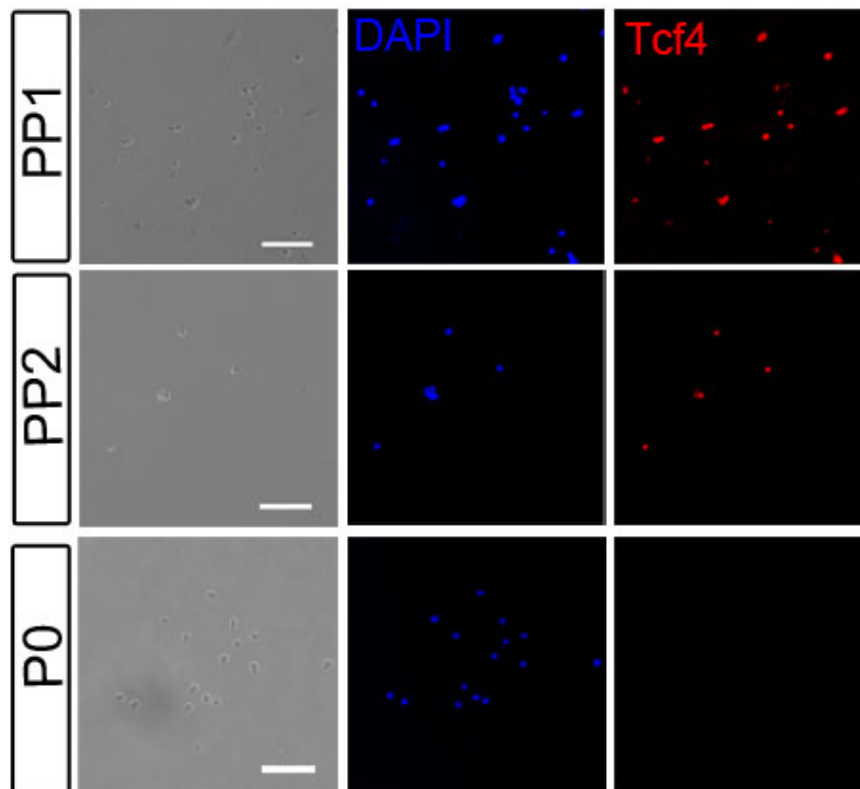
Figure 3.4

Representative images of cell populations from PP1, PP2 and P0 immuno-labelled with anti-Tcf4 (red) antibody. Cells were fixed and immunostained 48 h after the initial isolation. Nuclei are detected with the DNA stain DAPI (blue). A minimum of 5 random fields were taken to calculate the percentage of Tcf4+. Scale bar = 100 µm across all images.
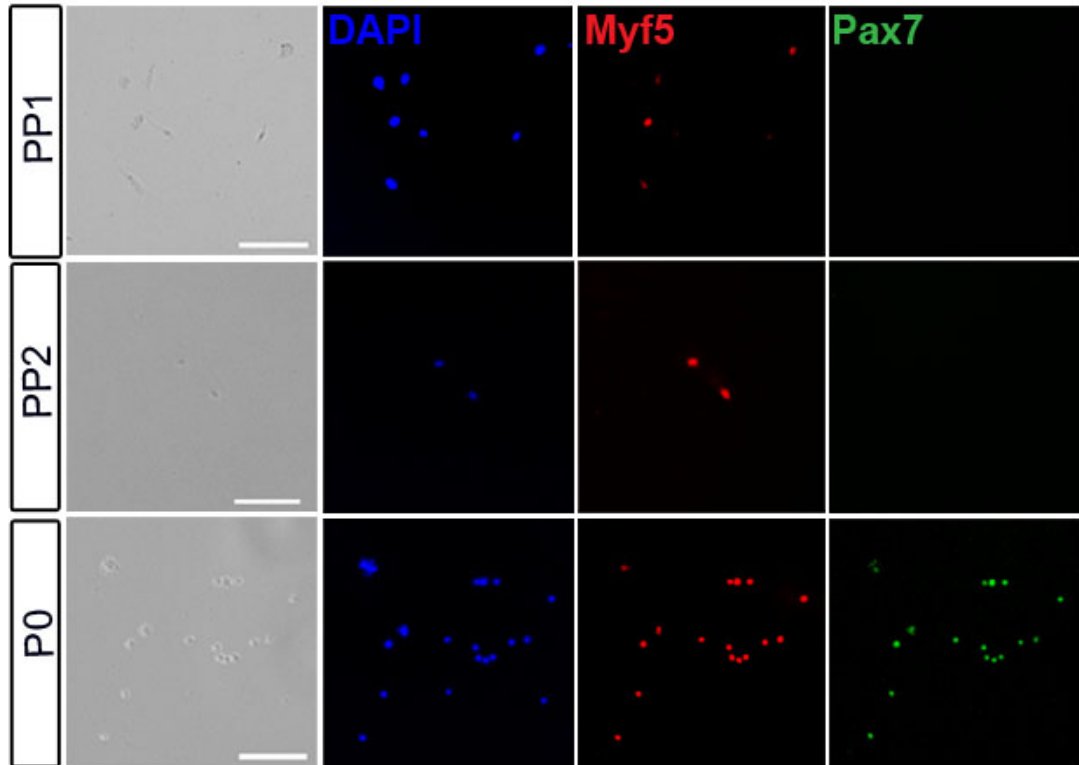
Figure 3.5 Representative images of cell populations from PP1, PP2 and P0 immuno-labelled with anti-Myf5 (red) and anti-Pax7 (green) antibodies.
Cells were fixed and immunostained 48 h after the initial isolation. Nuclei are detected with the nuclear stain DAPI (blue). A minimum of 5 random fields was taken to calculate the percentage of Myf5+ and Pax7+ over the total number of DAPI+ cells. Scale bar = 100 μm across all images.

3.3.2   The Structure of HS from Satellite Cell-Derived Myoblasts

3.3.2.1   Proliferating and Differentiating Satellite Cell-Derived Myoblasts

After purifying satellite cell-derived myoblasts in culture, HS was extracted from proliferating myoblasts 48 hours after plating of Passage 0. HS was extracted from differentiating myoblasts, which had been induced to differentiate with reduced serum medium for a further 72 hours. Incorporation of the cell cycle marker 5-Bromo-2′-deoxyuridine (BrdU) was used as an indication of myoblasts proliferating, in particular of cells in S-phase of the cell cycle, (**Figure 3.6**) and thus is nearly absent in differentiating myoblast cultures (**Figure 3.6**). Myosin heavy chain (MyHC), a muscle myosin protein, is found only in differentiating myoblasts and thus was used as a marker of myoblast differentiation (**Figure 3.6**). To further investigate the level of myoblast proliferation 3 days after culture in low serum-medium, Ki-67, a nuclear protein involved in cell cycle regulation (Gerdes et al., 1983), was used as a marker of myoblast proliferation since it is found only in proliferating cells and is absent from quiescent and differentiating cells, which are both in G_0 phase of the cell cycle. In

differentiating myoblast cultures only 0.29 (± 0.2) % of cells stained positively for Ki-67 strongly indicating that nearly all cells in these cultures had left the cell cycle (**Figure 3.7**). It has been shown that upon serum deprivation, a sub-population of both satellite cell-derived myoblasts and C2C12 myoblasts exits the cell cycle but does not differentiate. These cells, named 'reserve cells', do not express differentiation markers, express Pax7 and enter a temporary G0 phase, thus effectively representing an *in vitro* model of satellite cell self-renewal (Yoshida et al., 1998). Under the conditions of the experiments shown here, since only a negligible percentage of non-differentiated cells expressed proliferation markers after 3 days in low serum medium, we concluded that nearly all the non-differentiated cells that expressed Pax7 were *bona fide* reserve cells.
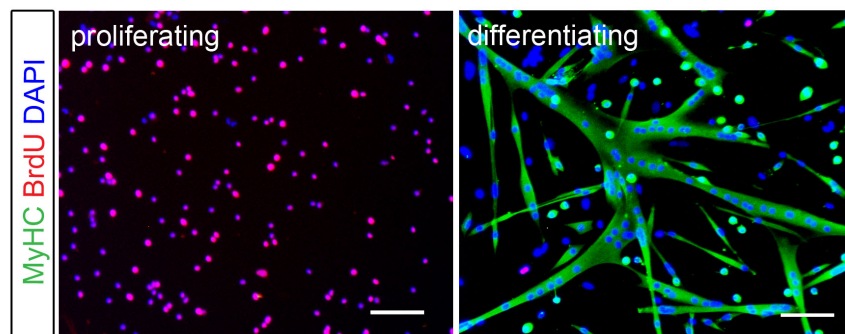
Figure 3.6 Representative images of proliferating and differentiating satellite cell-derived myoblasts. Satellite cell-derived myoblasts were isolated from the hind-limb muscles of 3 month old female mice. Proliferating myoblasts were grown in culture for 72 h post isolation with growth medium supplemented with 2 nM FGF2. Differentiating myoblasts were differentiated for another 72 h in culture with differetiating medium. Proliferation was detected via BrdU incorporation and immunostaining (red) whilst differentiation is detected via myosin heavy chain (MyHC, green) immunostaining. Nuclei were detected with the DNA stain DAPI (blue). Scale bar = 100 µm (Ghadiali et al., 2016).
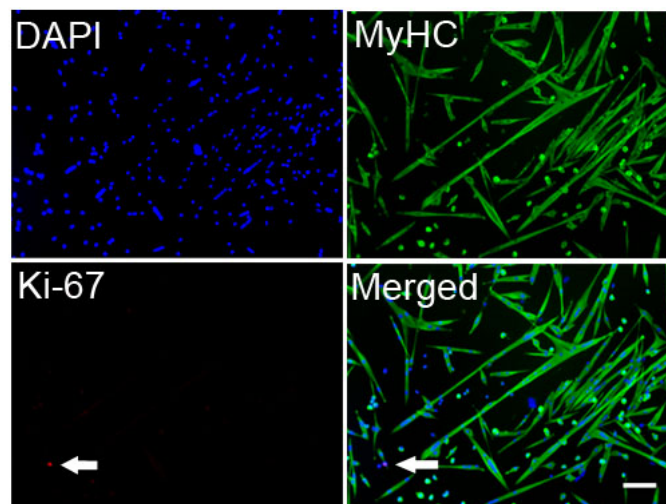
Figure 3.7 Representative images of the number of Ki-67 positive cells in differentiating conditions. Satellite cell-derived myoblasts were isolated from the hind-limb muscles of 3 month old female mice. Differentiating myoblasts were differentiated for 72 h in culture with differetiating medium. Myoblasts were fixed with 4% PFA before immunostaining. Proliferating myoblasts were detected via Ki-67 immunostaining (red) whilst differentiation was detected via myosin heavy chain (MyHC, green) immunostaining. Nuclei were detected with the DNA stain DAPI (blue). Scale bar = 100 µm.

3.3.2.2   HS Extraction from Proliferating and Differentiating Satellite Cell-Derived Myoblasts

For HS extraction, proliferating and differentiating satellite cell-derived myoblasts were homogenised to extract HS with a strong homogenisation buffer. The homogenate was applied to DEAE beads to partly purify HS, desalted and then the HS was digested into its constituent disaccharide units with heparinase I, II and III. The resulting disaccharides were labelled with the fluorophore BODIPY, separated and detected by strong anion exchange high performance liquid chromatography (SAX-HPLC) relative to a set of 8 commercially available HS disaccharide standards. **Figure 3.8** shows the main steps involved in the process of HS extraction and disaccharide compositional analysis.
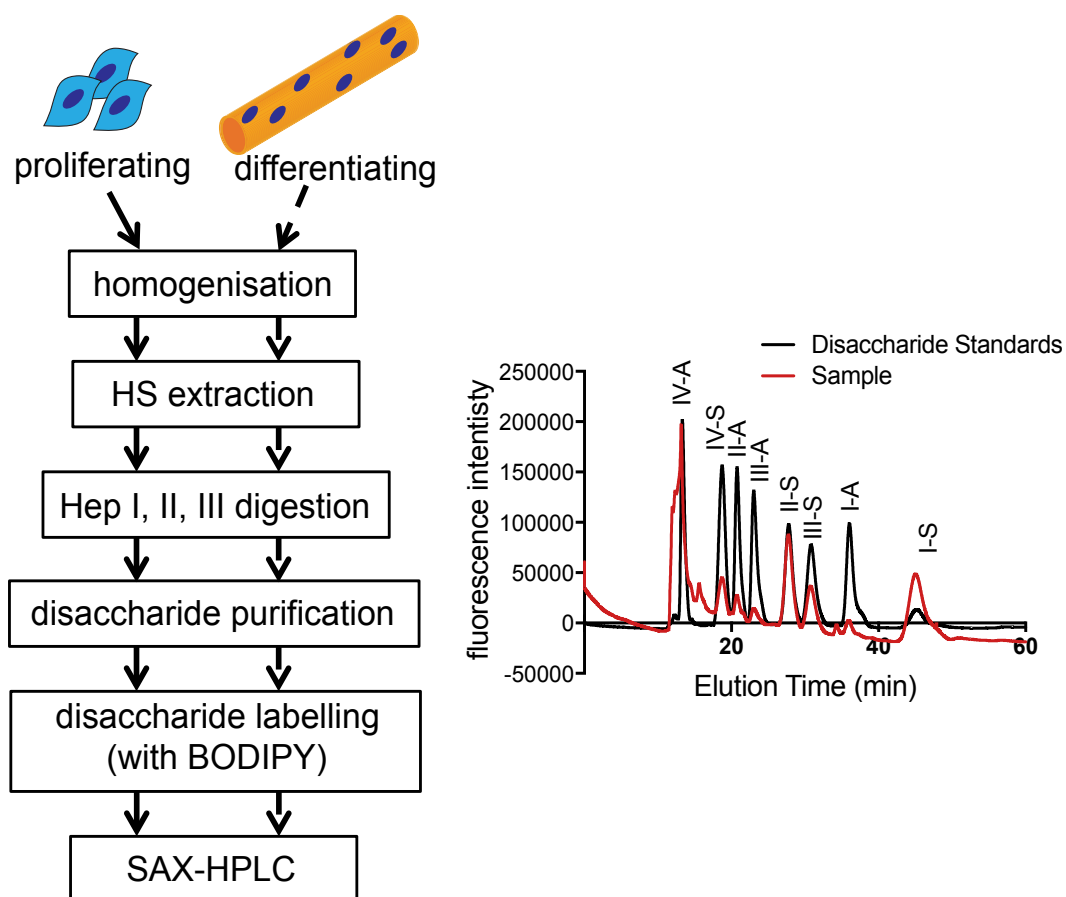
Figure 3.8 Main steps involved in the process of HS extraction and disaccharide compositional analysis.

Cells were homogenised with TUT buffer (8 M urea, 1 % Triton X100, 10 mM Trizma Base, 0.1 mM Na_2SO_4, pH 8.0) to release the HS from a) proliferating satellite cell-derived myoblasts which had been grown in culture for 72 h post isolation and b) differentiating satellite cell-derived myoblasts which had been differentiated in culture for a further 72 h. HS chains were isolated using DEAE beads and eluted with a high salt gradient. HS was digested into its constituent disaccharides, with heparinase I, II and III enzymes. Disaccharides were purified and labelled with the fluorescent tag BODIPY at the reducing end of the disaccharides. Disaccharides (in red) were profiled via SAX-HPLC relative to a set of 8 HS authentic disaccharides (in black).

HS disaccharides from proliferating and differentiating myoblasts were identified relative to the elution times of a set of commercially available, 8 most common authentic HS disaccharides (**Figure 3.9** and **Table 3.1**), which were also derivatised with the BODIPY fluorophore. The most highly sulfated disaccharides, and thus the most negatively charged, interact most strongly with the SAX column and therefore had the highest elution times. The fluorescence intensity was measured by the λ_{exc} = 488 nm and λ_{emm} = 520 nm of the BODIPY fluorophore. The peak areas of the individual disaccharides were then used to calculate their abundance relative to the total peak area of the 8 disaccharides.
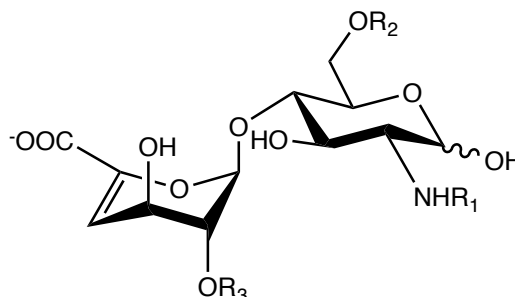
Figure 3.9 Common HS disaccharide units derived by heparinase digestion.

The general HS disaccharide unit post heparinase digestion. The 8 most common disaccharide structural units are displayed in **Table 3.1** where R_1 = $COCH_3$ or SO_3^- and R_2, R_3 = H or SO_3^-. Disaccharides are labelled with BODIPY for fluorescence detection.

Table 3.1 HS disaccharide reference standards structure and elution times.

The structure of the 8 commonly occurring HS disaccharides (in reference to **Figure 3.8**) derived from heparinase digestion before derivitisation with BODIPY and the elution times of the commercially available (Sigma) HS disaccharide standards from SAX-HPLC post derivitisation with BODIPY. Elution times were used to identify HS disaccharides. On the general disaccharide structural unit shown in **Figure 3.9**: R_1 corresponds to position N (Pos. N), R_2 corresponds to position 6 (Pos. 6) and R_3 corresponds to position 2 (Pos. 2).

Sigma Ref	Standard structure	Elution time	(Pos. N) R_1	(Pos. 6) R_2	(Pos. 2) R_3
IV-A	Δ-UA-GlcNAc	12.784	$COCH_3$	H	H
IV-S	Δ-UA-GlcNS	18.594	SO_3^-	H	H
II-A	Δ-UA-GlcNAc(6S)	21.257	$COCH_3$	SO_3^-	H
III-A	Δ-UA(2S)-GlcNAc	23.906	$COCH_3$	H	SO_3^-
II-S	Δ-UA-GlcNS(6S)	27.661	SO_3^-	SO_3^-	H
III-S	Δ-UA(2S)-GlcNS	31.138	SO_3^-	H	SO_3^-
I-A	Δ-UA(2S)-GlcNAc(6S)	37.507	$COCH_3$	SO_3^-	SO_3^-
I-S	Δ-UA(2S)-GlcNS(6S)	46.079	SO_3^-	SO_3^-	SO_3^-

3.3.2.3   The Level of Sulfation of the Muscle Stem Cell Heparanome Increases with Differentiation

Since the level of sulfation in HS has been reported to increase in embryonic stem cell differentiation (Hirano et al., 2012; Johnson et al., 2007; Nairn et al., 2007), it was hypothesised that the level of sulfation of HS may change during myogenic differentiation of muscle stem cells. To investigate this, the proportion of unsulfated disaccharides (Δ-UA-GlcNAc) and sulfated disaccharides (the seven remaining sulfated disaccharides) was calculated as a percentage of the total disaccharide content. In proliferating myoblasts there was an equal distribution between unsulfated and sulfated disaccharides (**Figure 3.10**). In differentiating myoblasts however, there was a higher proportion of sulfated disaccharides compared to non-sulfated disaccharides (**Figure 3.10**).
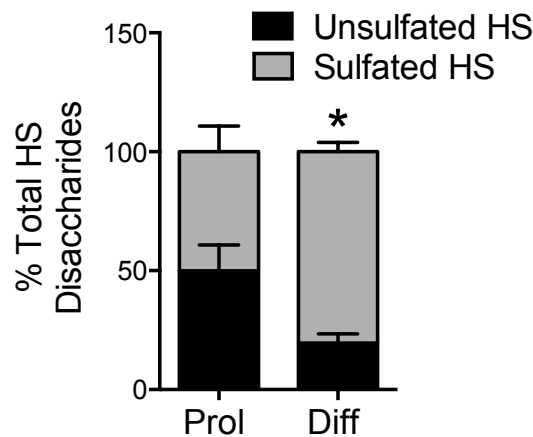
Figure 3.10 HS is more sulfated in differentiating myoblast cultures compared to proliferating myoblast cultures. HS was extracted and anlaysed via the process shown in Figure 3.8. The relative proportion of each disaccharide was calculated as the percentage peak area of the total peak of the 8 HS disaccharide units. The percentage of non-sulfated disaccharides (Δ-UA-GlcNAc, unsulfated, black bars) and sulfated (sum of all remaining disaccharides which are sulfated, grey bars) disaccharides is plotted as averages of four independent experiments ± S.E.M. * = $p < 0.05$ (Pro; N=4, Diff; N=4) (Ghadiali et al., 2016).

3.3.2.4   Specific Changes in the Disaccharide Composition During Satellite Cell-Derived Myoblast Differentiation

To investigate the increase in HS sulfation during differentiation, the relative abundance of mono-sulfated, di-sulfated and tri-sulfated disaccharides was quantified. There was a statistically significant increase in the abundance of mono-sulfated disaccharides in differentiating myoblasts compared to proliferating myoblasts (**Figure 3.11**). This was accompanied by a marked decrease in the abundance of non-sulfated disaccharides and a slight decrease in tri-sulfated disaccharides in differentiating myoblast cultures although these did not reach statistical significance (**Figure 3.11**). Specifically, there was an increase

in the two mono-sulfated disaccharides: Δ-UA-GlcNAc(6S) and Δ-UA(2S)-GlcNAc in differentiating myoblasts (**Figure 3.12**). There was also a decrease in the abundance of the non-sulfated disaccharide Δ-UA-GlcNAc although this did not reach statistical significance (**Figure 3.12**).
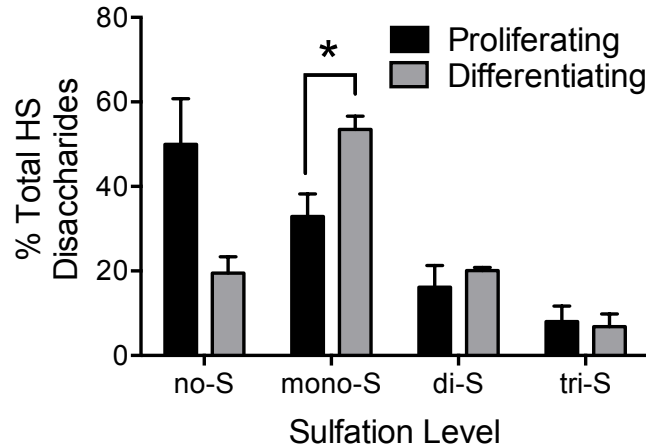
Figure 3.11 The proportion of mono-sulfated disaccharides in differentiating satellite cell-derived myoblast cultures is increased compared to proliferating satellite cell-derived myoblast cultures. HS was extracted and anlaysed via the process shown in Figure 3.8. The relative proportion of each disaccharide was calculated as the percetage peak ratio of the 8 HS disaccharide units. The percentage of non-sulfated Δ-UA-GlcNAc disaccharides (no-S) and the sum of the percentages of all mono-sulfated (mono-S), di-sulfated (di-S) and tri-sulfated (tri-S) disaccharides in proliferating (black) and differentiating (grey) cells was calculated. Plots show averages of four independent experiments ± S.E.M. * = $p < 0.05$ (Pro; N=4, Diff; N=4).
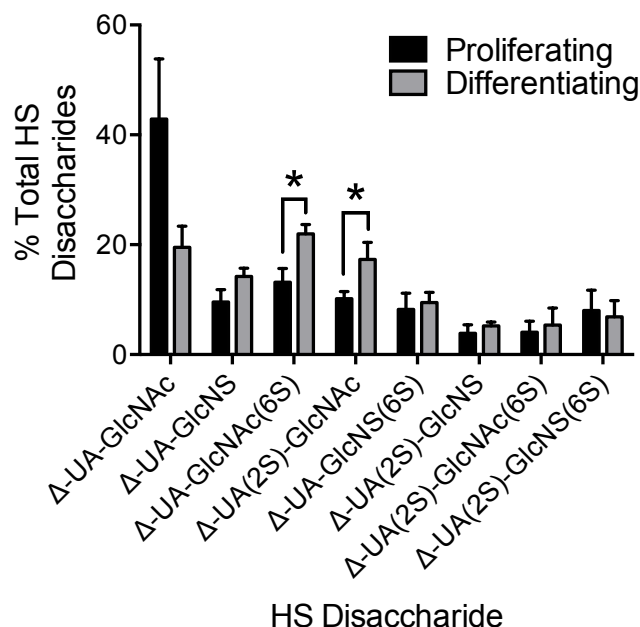
Figure 3.12 HS has increased levels of specific mono-sulfated disaccharides in differentiating compared to proliferating satellite cell-derived myblasts. HS was extracted and anlaysed for proliferating (black) and differentiating (grey) satellite cell-derived myoblasts. The peak ratios of the individual HS disaccharides are plotted as the averages of four independent experiments ± S.E.M. * = $p < 0.05$. (Pro; N=4, Diff; N=4) (Ghadiali et al., 2016).

3.3.2.5   Average Level of Sulfation at Specific Positions of the Primary Myoblast Heparanome Remains Unchanged During Differentiation

After observing that the overall level of sulfation is altered during myogenic differentiation, it was reasoned that the pattern of sulfation might also change, since the position of sulfation of HS is an important factor in determining its bioactivity. The three positions of the disaccharide unit, which are differentially functionalised in the 8 most common HS disaccharides are at position N, position 6-O and position 2-O. Thus, to assess the overall position of HS sulfation, the proportion of HS disaccharides containing 2-*O*-sulfation, 6-*O*-sulfation and *N*-sulfation was calculated. There were no statistically significant differences between the global positions of sulfation in HS from proliferating satellite cell-derived myoblasts compared with HS from differentiating myoblasts (**Figure 3.13**). There was a slight decrease in the level of 6-*O*- and 2-*O*-sulfation, and a slight increase in *N*-sulfation although these did not reach statistical significance.
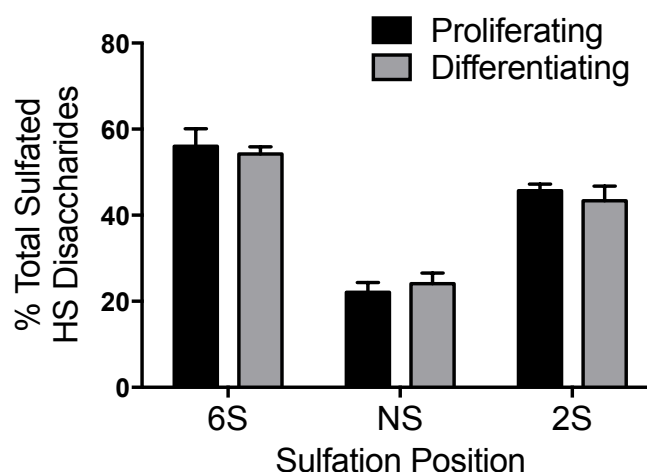
Figure 3.13 Average level of sulfation at specific positions is not altered between HS from proliferating and differentiating satellite cell-derived myoblasts. Analysis of the abundance of disaccharides containing specific sulfate groups: 6-O-sulfation, N-sulfation and 2-O-sulfation reveals no statistically significant differences in proliferating (black) and differentiating (grey) satellite cell-derived myoblasts. The abundance of specific sulfate groups are plotted as the averages of four independent experiments ± S.E.M. * = p < 0.05 (Pro; N=4, Diff; N=4) (Ghadiali et al., 2016).

3.3.3   The heparanome of the Myoblast C2C12 Cell Line Changes During Myogenic Differentiation

Since the structure of HS changes during differentiation of primary myoblasts and FGF2 is a potent inhibitor of myogenic differentiation, it was hypothesised that the HS from proliferating myoblasts would promote FGF2 signalling more than the HS from differentiating myoblasts. Thus we sought to test the effect on FGF2 signalling exerted by HS extracted from proliferating or differentiating cells. Since the quantities of HS necessary for cell biology experiments are large and difficult to obtain from primary cells, it is more advantageous to

use cell lines, which are more readily expandable compared to primary cultures. Thus, before investigating the effect of HS from proliferating and differentiating cells on FGF2 activity, we characterised the HS present in proliferating and differentiating C2C12 myoblasts to verify that it was comparable to that of primary myoblasts.

3.3.3.1   *Differentiating C2C12 Myoblasts Show an Increase in the Level of HS Sulfation*

HS was isolated from proliferating C2C12 myoblasts or from C2C12 myoblasts that were induced to differentiate for five days by serum reduction. Overall, the structural changes in HS observed in differentiating C2C12 myoblasts followed a similar trend compared to the changes observed in satellite cell-derived myoblast cultures. Importantly, a statistically significant increase in the proportion of sulfated disaccharides in differentiating C2C12 myoblasts compared to proliferating myoblasts was observed (**Figure 3.14**).
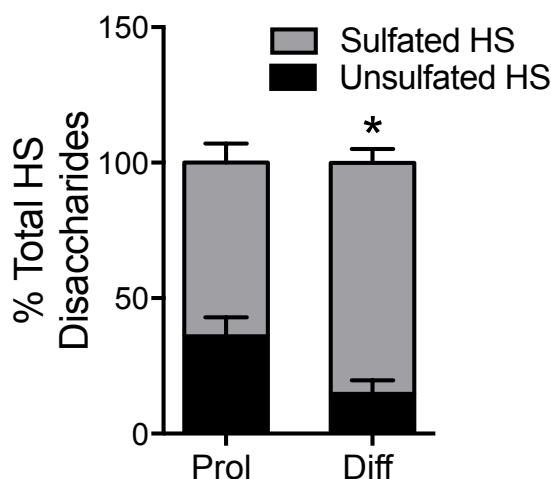
Figure 3.14 HS is more sulfated in differentiating C2C12 myoblast cultures compared to proliferating cultures. HS was extracted from proliferating and differentiatin C2C12 myoblasts and anlaysed via the process shown in Figure 3.8. The relative proportion of each disaccharide was calculated as the percentage peak area of the total peak area of the 8 HS disaccharide units. The percentage of non-sulfated disaccharides (Δ-UA-GlcNAc, unsulfated, black bars) and sulfated (sum of all sulfated, grey bars) disaccharides are plotted as the average of 4 independent experiments. ± S.E.M.   * = $p < 0.05$ (Pro; N=4, Diff; N=4).

3.3.3.2   *Specific Changes in Disaccharide Composition Are Observed During C2C12 Myoblast Differentiation*

As in the case of primary satellite cell-derived myoblasts, the increase in sulfation associated with differentiation was primarily due to an increase in the proportions of mono-sulfated disaccharides and a decrease in the proportion of the unsulfated disaccharide, although the latter did not reach statistical significance in C2C12 myoblast cultures (**Figure 3.10**). However, C2C12 myoblasts also showed a statistically significant decrease in the proportion

of tri-sulfated disaccharides in differentiating cells compared to proliferating cells (**Figure 3.15**). The increase in the abundance of mono-sulfated disaccharides during myogenic differentiation was due to a statistically significant increase in: Δ-UA-GlcNAc(6S), Δ-UA(2S)-GlcNAc and Δ-UA-GlcNS (**Figure 3.16**). In addition to these, there was also a significantly higher proportion of the di-sulfated disaccharide Δ-UA(2S)-GlcNS in differentiating C2C12 myoblasts compared to proliferating C2C12 myoblasts. The tri-sulfated disaccharide Δ-UA(2S)-GlcNS(6S) was also significantly reduced in differentiating C2C12 myoblasts.
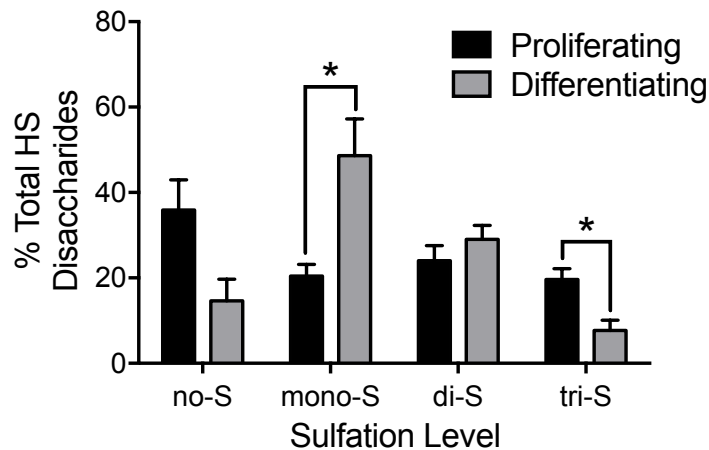
Figure 3.15 Mono-sulfated disaccharides are increased and non-sulfated and tri-sulfated disaccharides are decreased in differentiating C2C12 myoblasts compared to proliferating C2C12 myoblasts. The percentage of non-sulfated Δ-UA-GlcNAc disaccharides (no-S) and the sum of the percentages of all mono-sulfated (mono-S), di-sulfated (di-S) and tri-sulfated (tri-S) disaccharides in proliferating (black) and differentiating (grey) C2C12 myoblasts are plotted as averages of four independent experiments $\pm$ S.E.M. * = $p < 0.05$ (Pro; N=4, Diff; N=4).
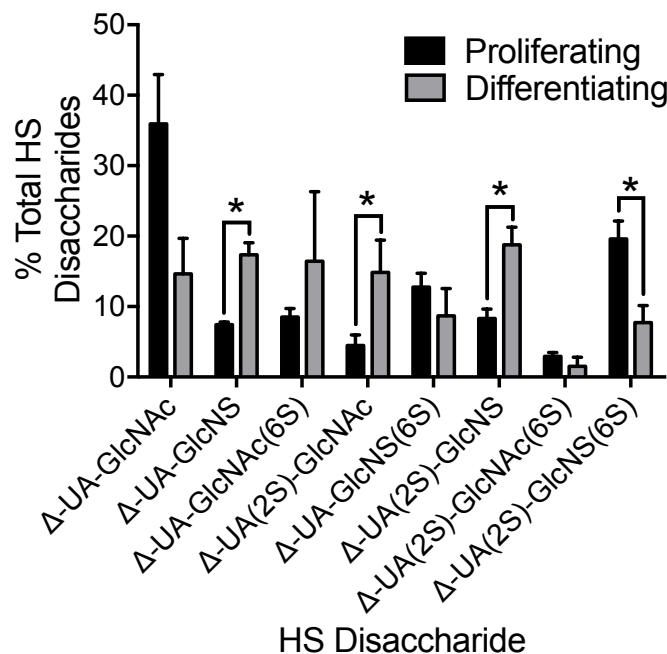
Figure 3.16 Specific HS disaccharide levels are different between proliferating and differentiating C2C12 myoblasts. HS was extracted and anlaysed via the process shown in Figure 3.8 from proliferating (black) and differentiating (grey) C2C12 myoblasts. HS disaccharide peak ratios are plotted as averages of four independent experiments $\pm$ S.E.M. * = $p < 0.05$

3.3.3.3   The Average Position of Sulfation of the C2C12 Myoblast Heparanome Remains Unchanged During Differentiation

Since the overall position of sulfation remained unchanged during primary myoblast differentiation (**Figure 3.13**), it was hypothesised that there would be no significant changes in the level of 6-*O*-sulfation, *N*-sulfation and 2-*O*-sulfation during differentiation of the C2C12 myoblast cell line. As predicted, there were no statistically significant changes in the global position of sulfation in differentiating C2C12 myoblasts compared to proliferating C2C12 myoblasts (**Figure 3.17**). There appeared to be a modest decrease in 6-*O*-sulfation in differentiating myoblasts accompanied by a modest increase in N-sulfation and 2-O-sulfation but these did not reach statistical significance.
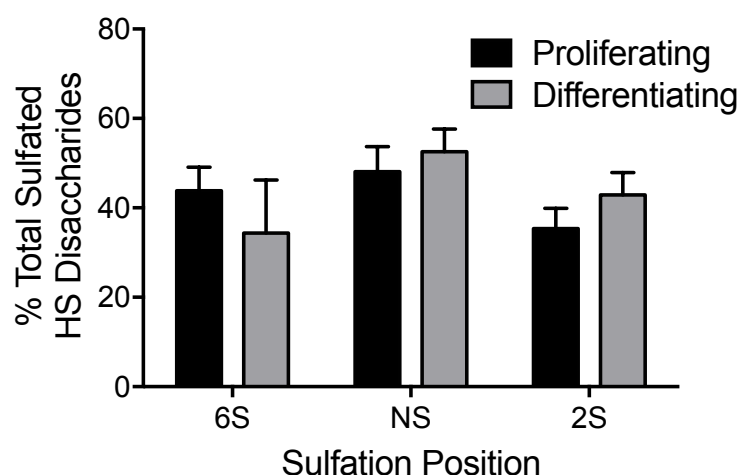
Figure 3.17 Average levels of sulfation at specific positions in HS are not changed bewteen proliferating and differentiating C2C12 myoblasts. Analysis of the abundance of specific sulfate groups: 6-O-sulfation, N-sulfation and 2-O-sulfation reveals no statistically significant differences in proliferating (black) and differentiating (grey) C2C12 myoblasts. The abundance of specific sulfate groups are plotted as the averages of four independent experiments $\pm$ S.E.M. * = p < 0.05 (Pro; N=4, Diff; N=4).

3.3.4   HS from proliferating C2C12 myoblasts is more effective at promoting FGF2 mitogenic activity than HS from differentiating C2C12 myoblasts

After determining that the level of HS sulfation increases in differentiating C2C12 myoblasts in similar way to that observed during primary myoblast differentiation, it was reasoned that the C2C12 myoblast cell line could be used as a proxy for studying the effects of myogenic differentiation on HS-mediated regulation of FGF2 mitogenic activity as a measure of FGF2 signalling. Since FGF2 signalling is a potent inhibitor of myogenic differentiation and requires HS as a co-receptor, it was hypothesised that the HS from proliferating myoblasts would promote FGF2 signalling more than the HS from differentiating myoblasts. One way of investigating the effects of HS on FGF2 mitogenic activity is to use a BaF3 mitogenic cell assay. BaF3 lymphoid cell cultures produce no endogenous HS and thus require an exogenous source of HS and FGF in order to promote FGF signalling for survival and

proliferation (Guimond and Turnbull, 1999; Ornitz et al., 1996). Since FGF receptor 1 (FGFR1) is the main FGF receptor expressed in myoblasts, and the receptor for FGF2, BaF3 cells stably transfected with FGFR1 were utilised for studying the effects of HS extracted from proliferating and differentiating cells on FGF2 mitogenic activity. HS from proliferating and differentiating C2C12 myoblasts was isolated and, subsequently put through a series of enzymatic digests to remove protein, DNA and other GAG impurities and thus produce a highly pure HS species. A proportion of the fully purified HS was digested with heparinases I, II and III for quantification via absorption at 232 nm of the double bond. BaF3 cells were then treated with FGF2 and the purified, non-digested HS at various concentrations for 72 hours and the extent of cell proliferation analysed with an MTT assay. BaF3 cells treated with HS from proliferating myoblasts showed a dose-dependent increase in FGF2-induced mitogenic activity compared to cells treated with FGF2 alone (**Figure 3.18**), with a dose of 10 µg/ml producing a statistically significant difference. In contrast, BaF3 cells treated with HS from differentiating myoblasts showed no increase in FGF2-induced mitogenic activity at any dose compared to cells treated with FGF2 alone (**Figure 3.18**). Indeed, the FGF2 mitogenic activity in BaF3 cells treated with HS from differentiating myoblasts was significantly lower than that in cells treated with HS from proliferating myoblasts at 10 µg/ml HS (**Figure 3.18**).
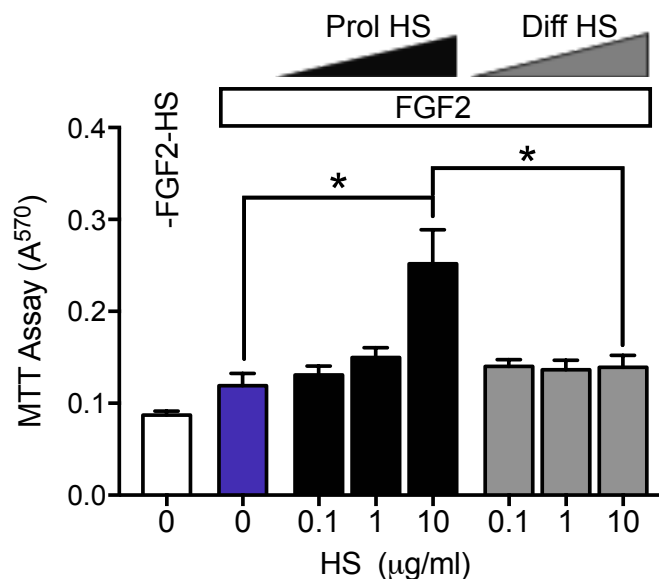
Figure 3.18 FGF2 mitogenic activity is promoted by HS extracted from proliferating myoblasts but not by HS extracted from differentiating myoblasts. BaF3 cell assay where the mitogenic activity of FGF2 on BaF3 cells was measured in response to FGF2 alone or in the presence of FGF2 and HS extracted from the proliferating (black) and differentiating (grey) C2C12 myoblasts. Data from 3 independent experiments with 3 technical replicates each were analysed and plotted as averages ± S.E.M. * = $p < 0.05$ (Pro; N=3, n =3 Diff; N=3, n=3).

3.4   Discussion

The work described in this chapter has demonstrated that: (1) the structure of HS changes during myogenic differentiation; (2) HS from proliferating and differentiating cells, which have different structures, also have different functional properties. To explore the hypothesis that the structural composition of HS changes during myogenic differentiation, HS was initially analysed from primary satellite cell-derived myoblasts, which better reflect the *in vivo* situation than any myogenic cell line. In addition, we also characterised the structural composition of C2C12 myoblasts, which we later used in bioassays that require amounts of starting material that are difficult to obtain from primary cells. Indeed C2C12 myoblasts are commonly used in biochemical assays, since they are financially more favourable, they bypass ethical concerns associated with the use of animal tissue, are more robust and have a higher expansion capacity than primary myoblasts, and thus yields higher amounts of material. In order to isolate pure populations of satellite cell-derived myoblasts, a differential plating protocol was employed based on an adapted protocol previously developed by Rando and Blau (Rando and Blau, 1994). By assessing a combination of fibrogenic and myogenic cell markers, and marked morphological differences, fibroblasts and myoblasts were readily distinguished. Overall, the procedure led to little loss of myoblasts in pre-plating cultures and produced highly pure cultures of myoblasts at passage 0, with few contaminating fibroblasts. Overall, this procedure is cost- and time-effective, with the whole isolation process being completed in one day.

After successfully obtaining pure populations of satellite cell-derived myoblasts, HS was extracted and analysed from proliferating and differentiating myoblasts. Previously, general trends have been observed during embryonic stem cell differentiation (ESC), displaying an overall increase in the amount of HS and level of sulfation, irrespective of the ESC lineage fate (Hirano et al., 2012; Johnson et al., 2007; Nairn et al., 2007). The findings from this chapter reveal that satellite cells are an additional stem cell type displaying an increase in HS sulfation during differentiation. The same phenomenon was observed in C2C12 myoblast differentiation; taken together these results are consistent with the idea that the level of HS sulfation is an important factor in the satellite cell niche supporting myogenic differentiation.

Although the overall positions of sulfation were not significantly altered during differentiation in both primary myoblasts and C2C12 myoblasts, it is possible that the increase in specific disaccharides leads to changes in specific sequences and/or alterations in conformation of HS chains, which might support reduced activation and even inhibition of pro-proliferative factors, such as FGF2, and thus permitting myogenic differentiation. For example it has been demonstrated that two isomeric heparin oligosaccharides with differences in just one position of sulfation (either 6-*O*-sulfation of glucosamine or 2-*O*-sulfation of the uronic acid), exhibit significantly   different   binding   affinities   to   the   oligomeric   chemokine   Monocyte

Chemoattractant Protein-1 (MCP-1)/CCL2 (Miller et al., 2016a). It has also well established that 2-*O*-sulfation on iduronic acid has a significant effect on the conformation of the ring, whereas glucuronic acid remains rigid regardless of 2-*O*-sulfation (de Paz et al., 2001; Ferro et al., 1990; Hsieh et al., 2014). This is a reflection of the conformational flexibility of iduronic acid, which can equilibrate between two forms: the $^2S_0$ (skew boat) and $^1C_4$ (chair) conformers, whereas the glucuronic acid residue remains rigid in the $^4C_1$ conformer (Ferro et al., 1990; Sattelle et al., 2010). In turn, the conformation can have significant effects on the spatial orientation of the sulfate groups and thus the chemical environment (Canales et al., 2005; Faham et al., 1996).

Interestingly, during differentiation there is a significant increase in the proportion of ΔUA(2S)-GlcNAc in both satellite cell-derived myoblasts and C2C12 myoblasts tested. In HS, the uronic acid residue is made up of approximately 20 % iduronic acid residues (Höök et al., 1974). Therefore, depending on the uronic acid epimer present in the HS disaccharide unit, the increase in 2-*O*-sulfation on the uronic acid residue may lead to significant conformational changes reflecting differences in binding affinities and biological activity. For example, the binding of antithrombin to the heparin pentasaccharide, the IdoA2S residue is crucial since when IdoA2S is replaced with GlcA2S, binding is not permitted (Hsieh et al., 2014). However, for the HS structural analysis shown here, the HS has been depolymerised with heparinase enzymes in order to allow for disaccharide compositional analysis, and as a consequence, iduronic acid and glucuronic acid both appear as a common delta-uronic acid structure and thus are non-distinguishable. Therefore, in the future, it could be beneficial to determine the epimeric form of the uronic acid residues of the HS extracted from myoblasts. To do this, nitrous acid could be employed to depolymerise HS, as this process leaves the uronic acid residues intact (Conrad, 2001; Turnbull, 2001). It might then be possible to determine if there is a specific increase in ΔIdoA(2S)-GlcNAc specifically, which may provide more insight into the altered structures and possibly conformations of HS produced in differentiating myoblasts, and whether this reflects differences in the biological functions exhibited.

Furthermore, we demonstrated a significant increase in the proportion of ΔUA-GlcNAc(6S). Although it has been reported that there are no significant changes in conformation due to 6-*O*-sulfation alone, the chemical environment of the neighbouring residues is affected by 6-*O*-sulfation (Hsieh et al., 2014) which in turn may reflect differences in biological function. Interestingly, the most significant changes were noted for the mono-sulfated disaccharides ΔUA(2S)-GlcNAc and ΔUA-GlcNAc(6S), which are disaccharides most commonly found in the transition zones of HS (between N-acetylated regions and the more highly sulfated NS-domains). It is interesting to speculate that these regions may be particularly important for regulation of the activity of HS during myogenesis. Overall, these findings suggest that alterations in specific HS disaccharides during myogenic differentiation may present regions

along the HS chains with altered sequences and different conformations and chemical environments, reflecting the ability to modulate distinct biological functions.

Since there are many heparin-binding growth factors that are involved in the regulation of myogenesis which are dependent on the structure of HS, it was hypothesised that the change in structure of HS during myogenic differentiation would alter growth factor signalling. Since FGF2 is a potent inhibitor of myogenic differentiation (Olwin et al., 1994; Rapraeger et al., 1991; Yablonka-Reuveni and Rivera, 1997), it was hypothesised that altered HS sulfation present in differentiating primary and C2C12 myoblasts would act as a repressor of FGF2 signalling or, at least, would not promote FGF2 signalling to the same degree as the HS present on proliferating myoblasts. Indeed, HS from differentiating myoblasts was less able to promote FGF2 mitogenic activity than HS from proliferating myoblasts. This lends strength to the hypothesis that the HS component of the extracellular matrix is a contributory factor evolved to repress FGF2 signalling during myogenic differentiation.

One way in which more highly sulfated HS from differentiating myoblasts could be ineffective at promoting FGF2 signalling is that highly sulfated HS binds more strongly to FGF2 (Gospodarowicz and Cheng, 1986) thus sequestering FGF2 away from its receptor, since it has previously been demonstrated that HS with different patterns and levels of sulfation bind FGF2 with different strengths (Uniewicz et al., 2010). This could be reminiscent of the role of the HSPG, glypican-1 during myogenesis, which sequesters away FGF2 *in vivo* thus permitting myogenic differentiation (Gutiérrez and Brandan, 2010). Further studies must be undertaken to explore this hypothesis. However, it must be noted that there are also some significant differences in the heparanome of satellite cell-derived myoblasts and the C2C12 myoblast cell line. Therefore, caution must be taken when studying HS signalling pathways in the C2C12 cell line, which could potentially exclude critical features of the satellite cell heparanome. Further investigations could be undertaken to determine whether the differences in structure of HS also correspond to significant differences in biological activity in both satellite cell-derived myoblast cultures and the C2C12 myoblast cell line.

Earlier investigations into the GAG composition during myogenesis have indicated that the structure of HS does not change significantly during differentiation of the C2.7 myoblast cell line (Barbosa et al., 2005). However, structural analysis was carried out with HS antibodies, which recognise HS sub-domains only, and a small number of the HS biosynthetic enzymes; EXT1/2, NDST1, GCE, HS2ST and HS6ST1 (Barbosa et al., 2005). Therefore, more specific or subtle changes in HS structure, such as changes in specific disaccharide abundance, overall levels and positions of sulfation may have been undetectable using these methods. Furthermore, the study used the C2.7 myoblast cell line, which may be less representative of the situation *in vivo* and indeed, there have been other studies *in vivo* which have detected

significant changes in the expression levels of the HS biosynthetic enzymes during differentiation (Langsdorf et al., 2007; Pisconti et al., 2012). It has been demonstrated that there is a significant down-regulation in the extracellular sulfatases, Sulf1 and Sulf2 during satellite cell activation and differentiation *in vivo* (Olguín and Pisconti, 2012; Pisconti et al., 2012). In contrast to this finding, mice lacking both Sulf1 and Sulf2 delayed myogenic differentiation *in vivo* upon muscle injury. However, in the HS compositional analysis of *Sulf1/2*[-/-] satellite cell-derived myoblast cultures, only one out of the three 6-*O*-sulfated disaccharides analysed was increased; the tri-sulfated disaccharide IdoA2S-GlcNS6S (Langsdorf et al., 2007), suggesting that expression level analysis of the HS biosynthetic enzymes do not directly reflect the final HS structure in a simplistic manner. Indeed, complex changes in 6-*O*-sulfation but also N- and 2-*O*-sulfation were also observed in mSulf1^{-/-} and Sulf2^{-/-} mice brain, suggesting feedback mechanisms and compensation effects when changes in sulfation are induced (Kalus et al., 2015). Therefore, we believe that the observations from this chapter provide strong evidence that the structural composition of HS does indeed change during myogenic differentiation and in turn has an important role in regulating myogenesis.

Chapter 4

4 The Structure of HS Changes During Ageing in Skeletal Muscle

4.1 General Introduction

4.1.1 Structural Changes in HS During Ageing

In the previous chapter, it was demonstrated that the structure of HS is altered during myogenic differentiation and that HS from differentiating myoblasts has a reduced capacity to promote FGF2 induced mitogenic activity compared to HS from proliferating myoblasts. In aged satellite cells many MAPK signalling pathways, which are heavily affected by HS, are altered (Bernet et al., 2014; Cosgrove et al., 2014). These include FGF2 signalling (Chakkalakal et al., 2012). Yet the muscle heparanome during ageing has not been investigated. However, age-related changes in HS have been reported in several other tissues (Aizawa et al., 1980; Feyzi et al., 1998; Huynh et al., 2012a; Huynh et al., 2012b). In some cases, structural changes in HS have been linked to differences in their abilities to potentiate growth factors (Feyzi et al., 1998; Huynh et al., 2012a; Huynh et al., 2012b). The age-related changes in HS are tissue-specific, suggesting that the altered structure might have specific effects on growth factor signalling during ageing. Since FGF2 signalling is altered in ageing satellite cells, it is possible that an altered heparanome may contribute to altered FGF2 signalling. Understanding the composition of the heparanome of skeletal muscle during ageing would provide new insights into HS-mediated signalling events involved in the ageing process. Indeed, changes in HS could be a contributory factor to the loss of satellite cell number and/or function observed during ageing.

4.1.2 HS Biosynthetic Enzyme Regulation

The structure of HS is determined largely during biosynthesis by HS biosynthetic enzymes and then by post synthetic structural modifications by the sulfatases (SULFS). The biochemical role of each biosynthetic enzyme is well determined. Transcript expression

analysis acts as a useful complement with HS compositional analysis, providing insights into HS regulation and synthesis. Gene expression profiling studies using real-time reverse transcription PCR (RT-PCR) are generally rapid and reproducible. However, the HS biosynthetic enzymes are made up of over 20 genes, and thus gene expression profiling for all the enzymes would be highly labour-intensive. A more time-effective solution is to use TaqMan® Low-Density Arrays (TLDA) microfluidic cards (*applied biosystems*). TLDA microfluidic cards act as a medium-throughput technique for real-time RT-PCR as it is possible to simultaneously assay the RNA expression levels of up to 384 pre-selected genes at a time. Furthermore, only a small amount of RNA is required for screening multiple genes, which is highly beneficial when using small muscle biopsies.

For a more in-depth analysis of structure-function relationships of HS, the expression of specific HS biosynthetic enzymes can be selectively silenced *in vivo* or *in vitro* using RNA interference (RNAi) technology (Fire et al., 1998). Commercially available synthetic small interfering RNA (siRNA) can be used to silence HS biosynthetic genes and in turn alter the structure of the endogenous HS in a selective manner. Biological assays can then be employed to analyse the effects of changes in HS biosynthetic gene expression and altered HS structure.

4.2   General Hypothesis

Since: 1) Age-associated changes in HS-regulated signalling pathways, such as FGF2 signalling, have been reported and 2) the structure and amount of HS changes in several tissues during ageing, it was hypothesised that changes in the structure of muscle HS occur with ageing and may affect satellite cell homeostasis and/or fate.

In this chapter it is shown that:

1. The muscle heparanome is altered with ageing. Particularly, there is an increase in 6-*O*-sulfation during ageing.
2. The altered heparanome of ageing muscle is associated with changes in FGF2 mitogenic activity
3. A decrease in 6-*O*-sulfation is associated with reduced myoblast proliferation and increased differentiation

4.3   Results

4.3.1   *The Structure of HS During Ageing in Skeletal Muscle*

4.3.1.1   *The Amount of Muscle HS Does Not Significantly Change During Ageing*

HS was quantified from the gastrocnemius muscles of 3 month and 2 year-old mice relative to the wet weight of the muscle. Overall, there was a slight trend for a reduction in the amount of HS in aged muscle (2 year-old muscle) compared to young muscle (3 month-old muscle). However, this difference did not reach statistical significance (p=0.63) (**Figure 4.1**).
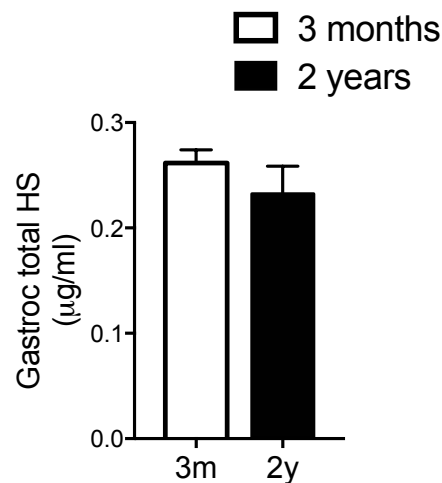
Figure 4.1 The level of is similar in 3 month and 2 year old mouse muscle. HS was extracted from the gastrocnemius muscles (3 month, n = 3, 2 year n = 4) of 3 month and 2 year-old mice. A proportion of the HS was digested into its constituent disacchardies with heparinase I, II and III enzymes. HS was quantified by measuring the absorbance at 230 nm of the double bond. The amount of HS was normalised to the total wet weight of the muscle. The averages ± S.E.M of n = 3 (3 months) and n = 4 (2 years) biological replicates were plotted.

4.3.1.2   *The Level of HS Sulfation Remains Unchanged During Ageing in Muscle*

To explore the hypothesis that the structural composition of HS changes during ageing in muscle, HS was extracted and characterised from the quadriceps of 3 month, 1 year and 2 year-old female mice. Firstly, the relative abundance of unsulfated and sulfated disaccharides was calculated. Overall, there was no change in the proportions of unsulfated and sulfated disaccharides during ageing (**Figure 4.2**). Furthermore, there was no statistically significant change in the abundance of the specific disaccharides during ageing (**Figure 4.3**).
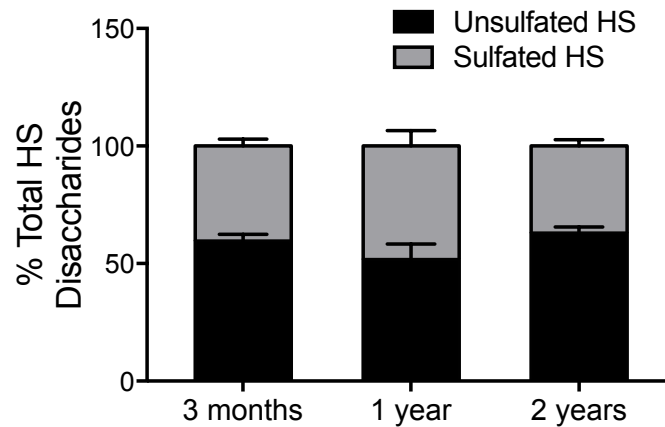
Figure 4.2 HS sulfation levels are similar in 3 month, 1 year and 2 year-old mouse quadricep muscles. HS was extracted using TUT lysis buffer and a blade homogeniser. HS was then profiled as in schematic 1. HS has the same proportion of sulfated and non-sulfated HS in 3 month, 1 year, and 2 year-old muscles. The percentage of non-sulfated disaccharides (Δ-UA-GlcNAc, unsulfated, black bars) and sulfated (sum of all sulfated, grey bars) disaccharides is plotted as the average of at least 4 independent experiments. ± S.E.M. (n = 4 in 3 months and 1 year age groups and n = 5 in 2 years age group) * = $p < 0.05$ (Ghadiali et al., 2016).
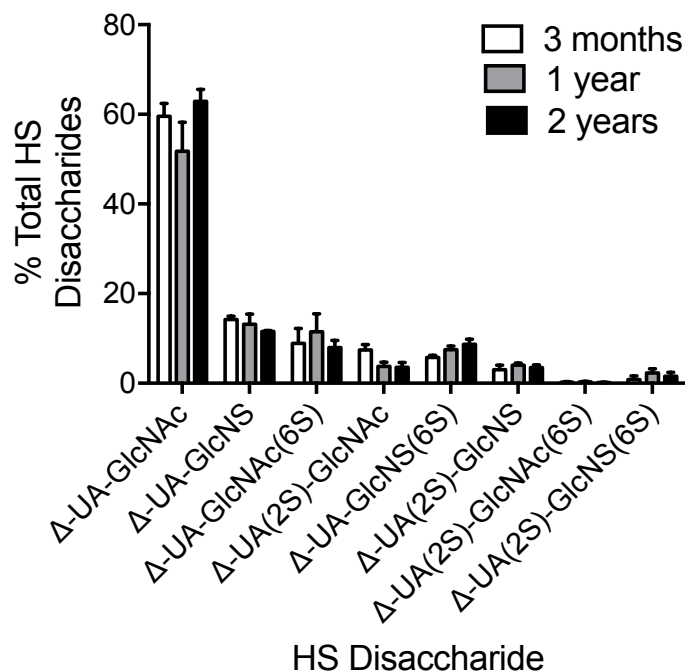
Figure 4.3 HS disaccharide compositions are similar in 3 month, 1 year and 2 year old mouse muscle. HS disaccharide peak ratio analysis in 3 month (black), 1 year (grey) and 2 year old (dark grey) muscle are plotted as averages of at least 4 independent experiments. ± S.E.M. (n = 4 in 3 months and 1 year age groups and n = 5 in 2 years age group) * = $p < 0.05$ (Ghadiali et al., 2016)

4.3.1.3   HS 6-O-Sulfation Increases in Skeletal Muscle During Ageing

Although the abundance of individual disaccharides does not significantly change, when the relative abundance of disaccharides containing 2-O-sulfation, 6-O-sulfation and N-sulfation in the muscles during ageing was calculated, a statistically significant increase in the abundance of sulfated HS disaccharides containing 6-*O*-sulfation was found in the quadriceps of old mice (1 year and 2 year-old mice) compared to young mice (3 month-old mice) (**Figure 4.4**). There was also a trend towards a reduction in 2-*O*-sulfation in the HS from old mice compared to young mice, although this did not reach statistical significance. (3 months compared to 1 year; *p*=0.27 and 3 months compared to 2 years; *p*=0.20)
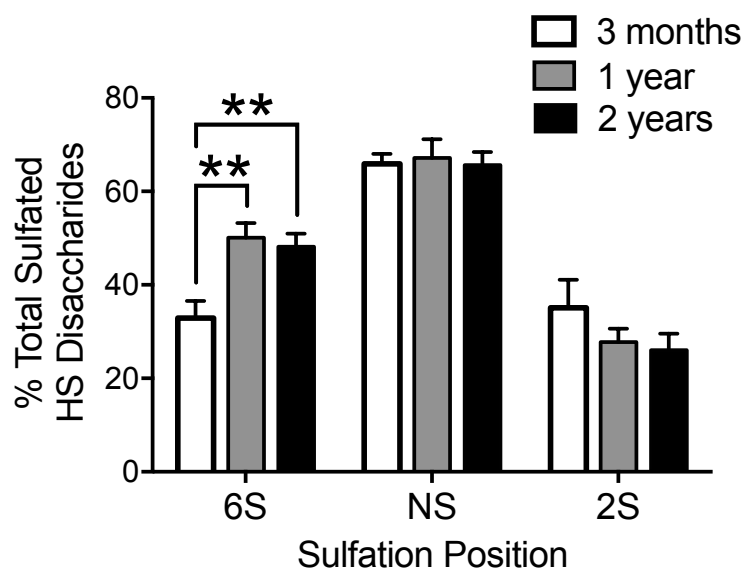
Figure 4.4 HS 6-O-sulfation is increased in quadriceps muscle from aged mice. Analysis of the abundance of specific sulfate groups (6-O-sulfation, N-sulfation and 2-O-sulfation) reveals a statistically significant increase in 6-O-sulfation from 3 month (black) muscle compared to 1 year (grey) and 2 year (dark grey) old muscle. The percentages of disaccharides are plotted as averages of at least 4 independent experiments. ± S.E.M. (n = 4 in 3 months and 1 year age groups and n = 5 in 2 years age group) ** = p < 0.01 (Ghadiali et al., 2016)

These findings on 6-*O*-sulfation were not specific to the muscle type analysed as similar results were obtained when the tibialis anterior (TA) muscles of young and old mice were examined. HS was extracted from the TA muscle of 3 month and 2 year-old mice for HS compositional analysis. A trend towards an increase in the levels of HS 6-*O*-sulfation in TA muscles of 2 year-old mice compared to TA muscles 3 month-old mice was observed, although this result did not reach statistical significance (*p*=0.26) (**Figure 4.5**). Intriguingly, although in quadriceps muscle the increase in 6-*O*-sulfation was accompanied by a modest decrease in 2-*O*-sulfation, in TA muscles the increase in 6-*O*-sulfation was accompanied by a marked, though not statistically significant, decrease in *N*-sulfation *(p*=0.059). This suggests that different muscles might age in different ways, which could lead to different effects on the resident satellite cell population.
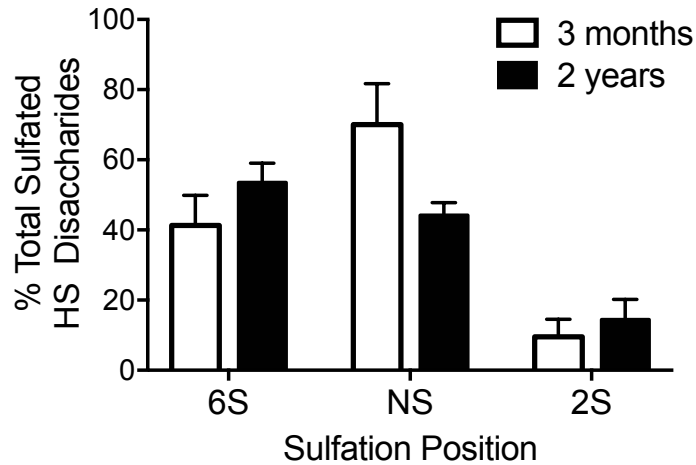
Figure 4.5 HS 6-O-sulfation shows a trend for increasing in aged TA muscle. Analysis of the abundance of specific sulfate groups: 6-O-sulfation, N-sulfation and 2-O-sulfation from 3 month (black) TA muscle compared to 1 year (grey) and 2 year (dark grey) old TA muscle. The percentages of disaccharides are plotted as averages of at least 4 independent experiments. ± S.E.M.

4.3.2   HS 6-O-Sulfation Modulates Mitogenic Activity

4.3.2.1   HS from Ageing Muscle Promotes FGF2 Induced Mitogenic Activity

Since HS 6-O-sulfation is proportionally increased in aged muscle without leading to an increase in the overall sulfation levels and since 6-O-sulfation is heavily implicated in FGF2 signalling (Pye et al., 1998), it was hypothesised that the HS from old (2 year-old) mouse muscle may promote FGF2 signalling more than HS from young (3 month-old) muscle. To test this hypothesis, the BaF3 assay was employed and the effect of HS from the quadricep muscles of 3 month and 2 year-old mice on FGF2 mitogenic activity via FGFR1 was measured (**Figure 4.6**). HS from 3 month-old muscles inhibited FGF2 signalling compared to the FGF2 alone and this effect was statistically significant with 10 µg/ml treatment. In contrast, FGF2 mitogenic activity in BAF3 cells treated with HS from 2 year-old muscle was increased in a dose-dependent manner, and this effect was statistically significant at 10 µg/ml compared to cells treated with FGF2 alone.
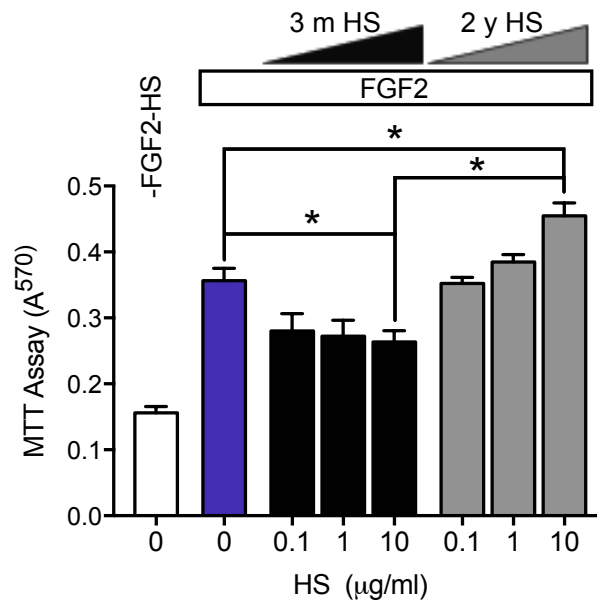
Figure 4.6 HS from aged muscle enhances FGF2 mitogenic activity. Murine BaF3 lymphocytes were stably transfected with FGFR1IIIc to assess the mitogenic activity of FGF2 on BaF3 cells measured in plain growth medium (white bar), and in response to either FGF2 alone (blue bar) or FGF2 and HS extracted from either 3 month (black bars) or 2 year-old (grey bars) muscle. Data from 3 independent experiments with 3 technical replicates were analysed and plotted as averages ± S.E.M. * = *p* < 0.05. 2 of the 3 independent experiments were conducted by Dr Scott Guimond (Ghadiali et al., 2016).

4.3.2.2   Reduction in Myoblast HS 6-O-sulfation Reduces Proliferation

Since the increase in HS 6-*O*-sulfation in aged muscle was also associated with increased mitogenic activity of FGF2, it was hypothesised that HS 6-*O*-sulfation supports myoblast proliferation and that a reduction in myoblast HS 6-*O*-sulfation would reduce myoblast proliferation. Mice express three 6-*O*-sulfotransferases (HS6ST1, HS6ST2 and HS6ST3) which catalyse the transfer of a sulfate group to the 6 position of the glucosamine residue in HS. RNAi technology was utilised to transiently knockdown all three HS6STs simultaneously in C2C12 myoblasts, to reduce endogenous HS 6-*O*-sulfation. Myoblasts were co-transfected with a GFP plasmid to aid detection of cells that had been successfully transfected (**Figure 4.7**). The day after transfection gene knockdown was confirmed via RT-PCR (**Appendix 1**). Proliferation was then measured using a BrdU incorporation assay. Only cells that were GFP positive were scored to ensure that only cells that had been successfully transfected were analysed. A significant reduction in myoblast proliferation (BrdU+GFP+ cells) by approximately 50% was found in the knockdown cells compared to the negative control (**Figure 4.8**). Therefore, these data strongly support the hypothesis that a reduction in endogenous HS 6-O-sulfation leads to a reduction in myoblast proliferation, confirming that the three 6-O-sulfotransferases have a positive regulatory role in myoblast proliferation, possibly via promotion of FGF2 signalling.
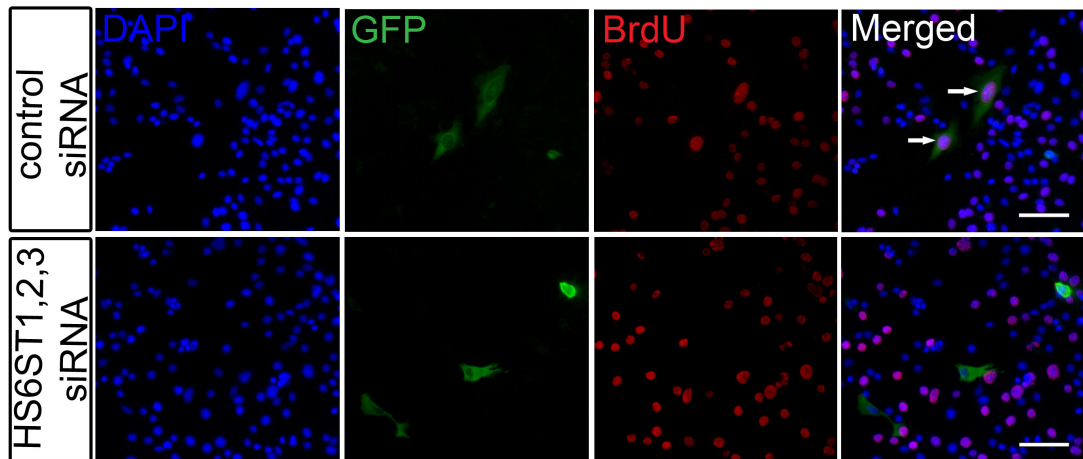
Figure 4.7 Representative images showing a reduction in HS 6-O-sulfation leads to a reduction in proliferation in C2C12 myoblasts. Representative images of GFP (pClover) and siRNA simultaneously to the three HS6STs or control scrambled siRNA were transfected into C2C12 myoblasts and 24 h later 10 µM BrdU was added to the culture medium 2 h prior to fixation and immunostaining to detect GFP (green) and BrdU (red). Nuclei were detected with the nuclear stain DAPI (blue). The proportion of BrdU+GFP+ myoblasts are increased in control cells indicated by white arrows. Ten images across two technical replicates for three independent experiments were taken. Scale bar = 100 µm.
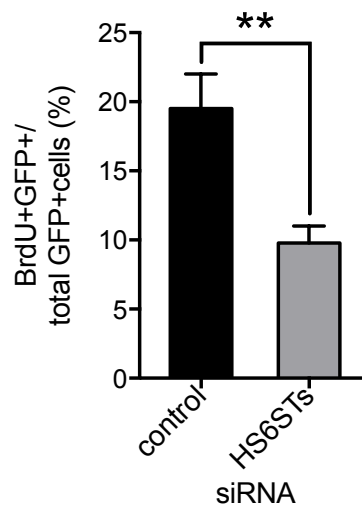
Figure 4.8 A reduction in HS 6-O-sulfation leads to a decrease in proliferation in C2C12 myoblasts. GFP (pClover) and siRNA simultaneously to all three HS6STs or universal control siRNA were transfected into C2C12 myoblasts and 24 h later 10 µM BrdU was added to the culture medium 2 h prior to fixation and immunostaining to detect GFP and BrdU. The percentage of BrdU+/GFP+ cells was calculated over the total number of GFP+ cells was caluated. Simultaneous knockdown of all three HS6STs produces a significant decrease in C2C12 myoblast proliferation. The averages of ten images across two technical replicates for three independent experiments ± S.E.M. are plotted.** = p < 0.01 (Ghadiali et al., 2016)

4.3.2.3   Reduction in Myoblast HS 6-O-Sulfation Promotes Myoblast Differentiation

Myoblast proliferation and differentiation are mutually exclusive events. Since proliferation was reduced in myoblasts, which had been subjected to simultaneous knock down of all three HS6ST enzymes, it was hypothesised that myogenic differentiation would increase. In order to investigate the extent of differentiation, the myogenic regulatory factor myogenin, which is expressed in terminally differentiated myoblasts, was measured in C2C12 myoblasts 24 hours post transfection (**Figure 4.9**). There was a significant increase in myoblast differentiation (MyoG+/GFP+ cells) by approximately 50%, in the knockdown cells compared with the negative control (**Figure 4.10**). This further supports the hypothesis that a reduction in myoblast HS 6-*O*-sulfation, has both anti-proliferative and pro-differentiative effects.
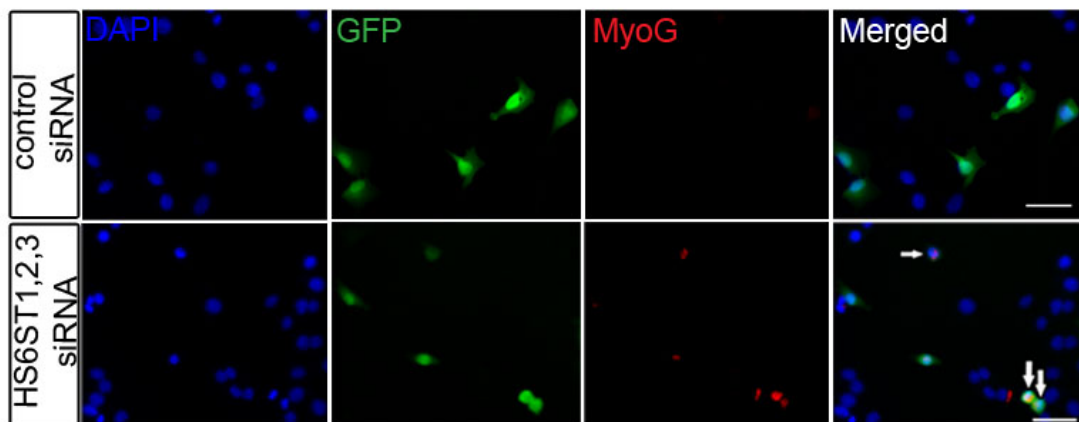
Figure 4.9. Representative images showing a reduction in HS 6-O-sulfation leads to an increase in myogenin expression in the C2C12 myoblast cell line. Representative images of GFP (pClover) and siRNA simultaneously to the three HS6STs or universal control siRNA were transfected into C2C12 myoblasts and 24 h later cells were fixed and immunostained for detection of GFP (green) and myogenin (MyoG, red). Simultaneous knockdown of all three HS6STs produces a significant increase in C2C12 myoblast differentiation. Nuclei were detected with the nuclear stain DAPI (blue). The proportion of Myogenin+ GFP+ cells was increased in myoblasts transfected with HS6ST1,2,3 indicated by the white arrows. Ten images across two technical replicates for three independent experiments were taken. Scale bar = 100 µm
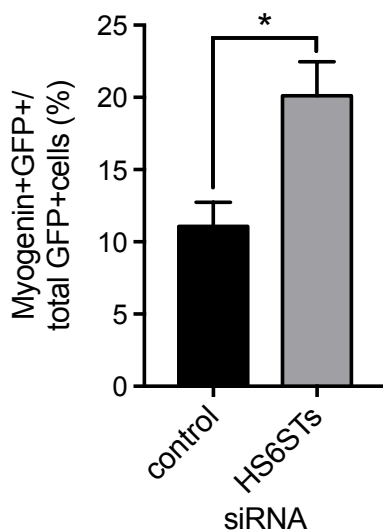
Figure 4.10 A reduction in HS 6-*O*-sulfation leads to an increase in myogenin expression in the C2C12 myoblast cell line. GFP (pClover) and siRNA simultaneously to the three HS6STs or universal control siRNA were transfected into C2C12 myoblasts and 24 h later cells were fixed and immunostained for detection detect of GFP and myogenin. Simultaneous knockdown of all three HS6STs produces a significant increase in C2C12 myoblast differentiation. The averages of ten images across two technical replicates for three independent experiments ± S.E.M. plotted * = p < 0.05.

4.3.3   HS Biosynthetic Regulation

Since the structure of HS is altered during ageing in muscle, it was hypothesised that the expression levels of the HS biosynthetic enzymes might be differentially regulated during ageing in muscle. To test this hypothesis, RNA was extracted from the TA muscles of 3 month and 2 year-old mice. Taqman Low Density Array (TLDA) microfluidic cards were custom designed to contain 25 HS biosynthetic enzyme gene probes, including endogenous controls, for simultaneous real time PCR reactions. Out of the 25 HS biosynthetic enzymes analysed, 21 were expressed in both 3 month and 2 year-old muscles. To study the relative expression levels of the HS enzymes between young and old muscle, gene expression was calculated relative to the endogenous control GAPDH, which displayed the lowest variability of the endogenous controls present on the TLDA microfluidic card. For the majority of genes, there were no statistically significant differences in the transcript levels between the 3-month and 2 year-old muscle (**Figure 4.12**). This might have been a consequence of the high biological variability and small sample size. However, two HS enzymes that did show statistically significant differences between young and old muscle were: 1) heparan sulfate 3-*O*-sulfotransferase 5 (HS3ST5), which displayed a significantly higher expression level in the 2 year-old muscle compared to the 3 month-old muscle and 2) heparan sulfate 6-*O*-sulfotransferase 1 (HS6ST1), which displayed a significantly lower expression level in the 2 year-old muscle (**Figure 4.11**).
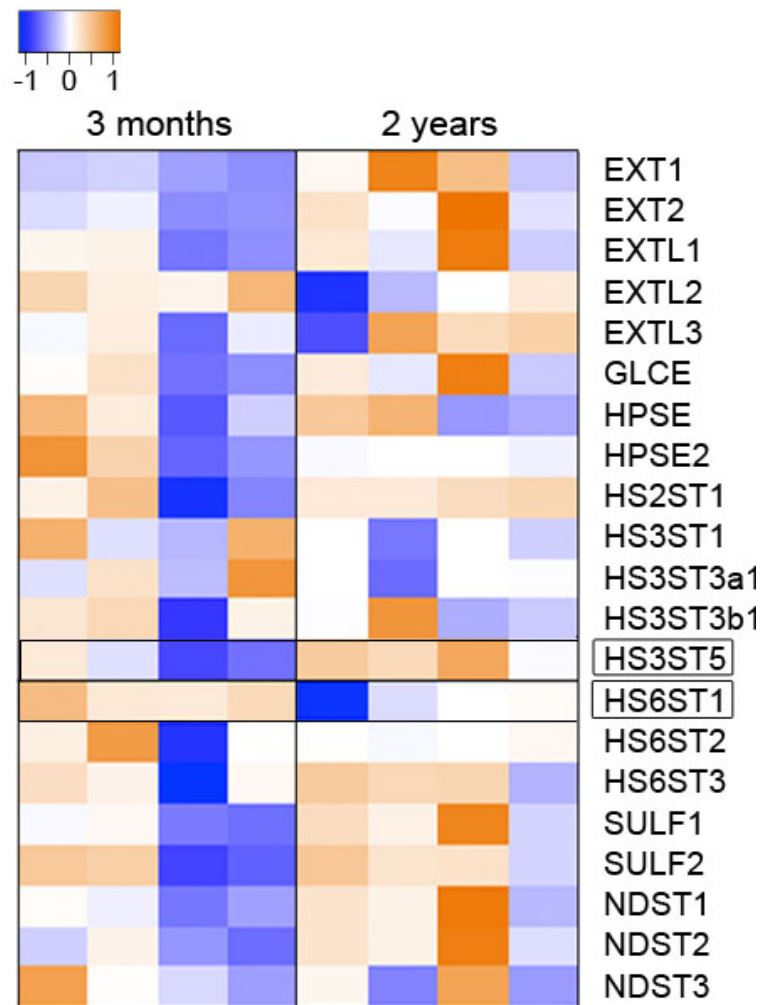
Figure 4.12 Heatmap of 21 HS biosynthetic enzyme transcript levels in 3 month and 2 year-old muscle. Complementary DNA (cDNA) was generated from RNA extracted from the TA muscle of 3 month (left, n=4) and 2 year-old muscle (right, n=4). TDLA microfluidic cards were custom designed to contain HS biosynthetic gene probes to carry out 384 real time PCR reactions simultaneously and a total of 8 samples were run in one card. The log of the $\Delta\Delta^{CT}$ values relative to GAPDH expression levels are plotted using R Studio, where blue is low expression and orange is high expression. The two genes that are significantly different between young and old muscle are highlighted with black boxes.
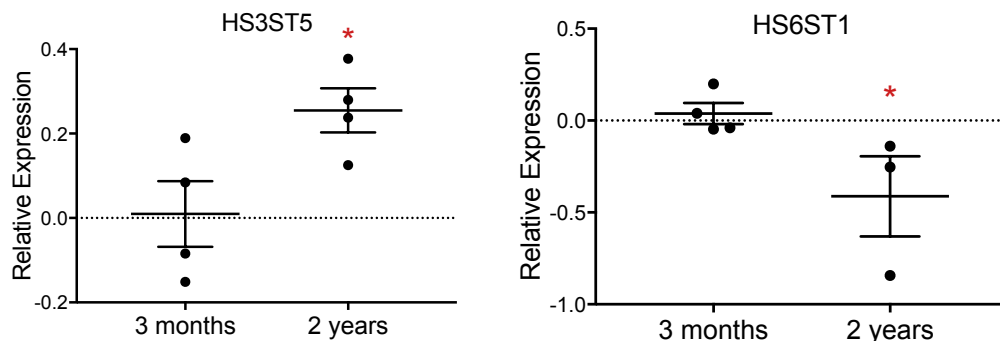
Figure 4.11 1D scatter plots of the relative expression levels of HS biosynthetic enzymes. The individual transcript expression levels (log $\Delta\Delta CT$) relative to GAPDH are plotted on 1D scatter plots. In 2 year-old muscles there is a significantly higher HS3ST5 transcript level and a significant downregulation of HS6ST1 compared to 3 month-old muscle where * = p<0.05.

90

4.4   Discussion

There have been several reports showing age-related changes in the heparanome in different tissues (Aizawa et al., 1980; Huynh et al., 2012a; Keenan et al., 2014) and in this chapter, it has been shown for the first time that skeletal muscle is another tissue in which the heparanome is altered during ageing. Although no significant differences in the abundance of specific HS disaccharides were found, there was an overall increase in the levels of HS 6-*O*-sulfation in the muscles of 1 year and 2 year-old mice compared to 3 month-old mice. Interestingly, 1 year-old mice display no signs of sarcopenia (Brack et al., 2005) suggesting that changes at the molecular level are already occurring in the muscle before any macroscopic changes at the tissue or functional level are detected. Furthermore, HS was extracted from the TA muscles of 3 month and 2 year-old mice. Unfortunately, the HS chromatographs from the majority of the HS samples were poorly resolved and thus difficult to analyse. This could have been due to a contaminant in the samples or simply a lack of material leading to poor resolution. However, a trend towards an increase in 6-*O*-sulfation of the ageing TA muscle was still observed. There also appeared to be a marked reduction in the level of *N*-sulfation although this did not reach statistical significance. This may be indicative of differences in the structural composition of HS during ageing depending on the muscle type. However, further experiments including more replicates and different muscle types are required to explore this hypothesis.

Owing to the fibrosis that occurs during ageing in muscle (Brack et al., 2007; Fry et al., 2015; Paliwal et al., 2012), it was difficult to obtain pure cultures of myoblasts using the differential plating protocol, leading to a heterogeneous mixture of predominantly fibroblasts and thus, it was not possible to analyse the structure of HS from satellite cell-derived myoblasts from aged muscle. Therefore, it cannot be ruled out that the change in structure of HS in aged muscle is a consequence of the increased numbers of fibroblasts. To better understand the altered heparanome in ageing muscle, satellite cell-derived myoblasts and fibroblasts isolated from aged muscle, could be purified using fluorescence-activated cell sorting (FACS) to obtain pure cultures for HS compositional analysis. This would provide an indication of the cell type responsible for the structural changes in HS in aged muscle.

In an attempt to elucidate the function of the HS from ageing muscle, and since 6-O-sulfation is important in FGF2 signalling and FGF2 signalling is increased in ageing muscle (Chakkalakal et al., 2012), it was hypothesised that the HS from aged muscle with an increase in 6-O-sulfation might further promote FGF2 signalling compared to HS from young muscle. HS from 2 year-old muscles promoted FGF2 mitogenic activity in BaF3 cells while HS from 3 month-old muscles inhibited it. This result strongly supports two important points: (1) that the altered heparanome in ageing muscle may be a contributory factor to loss of satellite cell quiescence by promoting FGF2 signalling. This spontaneous breaking of

quiescence would then lead to satellite cell depletion (Chakkalakal et al., 2012) and consequently muscle fibrosis (Fry et al., 2015). (2) That the muscle heparanome in young mice is normally inhibitory of FGF2 signalling, thus effectively contributing to maintenance of satellite cell quiescence. Future investigations might involve culturing myoblasts *ex vivo* in the presence of HS from either young or old muscle to investigate the effects of an old HS extracellular environment on the phenotype of myoblasts.

Next, we sought to better characterise the role of HS 6-*O*-sulfation in myogenesis by knocking down the three 6-O-sulfotransferases in C2C12 myoblast to reduce endogenous HS 6-*O*-sulfation. Myoblasts that had been transfected with HS6ST1, 2 and 3 siRNA exhibited a significant reduction in proliferation and a significant increase in differentiation compared to myoblasts transfected with scrambled siRNA. Since FGF2 promotes myoblast proliferation and is a potent inhibitor of differentiation, this study suggests that the reduction in myoblast HS 6-*O*-sulfation represses FGF2 signalling and thus: (1) reinforces previous findings that 6-*O*-sulfation is important for FGF2 signalling (Guimond et al., 1993; Pye et al., 1998), (2) supports our hypothesis that a difference in HS 6-*O* sulfation between young and old muscle is responsible for the different effect of young and old muscle HS on FGF2 mitogenic activity and possibly on the overall control of satellite cell quiescence. Earlier evidence suggests that FGF2 binding to HS does not require 6-O-sulfation (Ashikari-Hada et al., 2004; Kreuger et al., 1999; Kreuger et al., 2001; Maccarana et al., 1993; Turnbull et al., 1992) but rather, is important in the formation of the HS:FGF:FGFR ternary complex and thus for FGF2 signalling to take place (Allen and Rapraeger, 2003; Powell et al., 2002). Interestingly, although the presence or absence of 6-*O*-sulfation has significant biological effects, altered 6-*O*-sulfation actually has the smallest impact on HS conformation compared to changes in 2-*O*-sulfation and *N*-sulfation on the other hand (Rudd and Yates, 2010). This suggests that HS biological activity is reliant on the patterns of sulfation and distribution of charge for biological activity as well as conformations of the iduronate rings. As mentioned previously, 6-*O*-sulfation can have a significant effect on the chemical environment of neighbouring residues (Hsieh et al., 2014) and this may also contribute to the altered biological function. Future work could investigate the binding affinities of HS from young and old muscle to FGF2/FGFR1 and its role in the formation of the ternary complex (FGF2-HS-FGFR1), which is crucial for signalling to take place (Schlessinger et al., 2000).

It should also be noted that the altered structure of HS present in ageing muscle might affect different FGF signalling pathways that are involved in the regulation of myogenesis. Several members of the FGF family are expressed in mouse muscle during injury-induced regeneration, which display different requirements for the optimal HS sequence for binding and signalling (Guimond and Turnbull, 1999; Powell et al., 2002). In consideration of the scope of this project, FGF2 signalling was selected as a priority for investigation because: 1) FGF2 signalling is a potent inhibitor of myoblast differentiation, 2) FGF2 signalling is

increased in ageing muscle (Chakkalakal et al., 2012) and 3) HS 6-O-sulfation is crucial for FGF2 signalling (Allen and Rapraeger, 2003; Powell et al., 2002). However, the results obtained here provide scope for future research into how other FGFs, or indeed other heparin-binding growth factors, are affected by the structural changes in HS during ageing.

To further investigate the age-related regulation of the muscle heparanome, transcript expression analysis of the HS biosynthetic enzymes was performed on 3 month and 2 year-old TA muscles. Although, the biochemical role of the biosynthetic enzymes is well determined, how HS biosynthesis is regulated and how the fine structure of HS is produced is largely unknown (Kreuger and Kjellén, 2012). Since HS synthesis is non-template driven, and a number of the enzymes consist of a multiple family of isoforms with differing levels of expression and activity, the expression levels alone may not reflect the resulting structure of HS. Thus we sought to test whether analysis of HS biosynthetic and remodelling enzyme gene expression could provide a useful complement to HS compositional analysis. Since aged muscle displayed a significant increase in the levels of HS 6-O-sulfation, it was hypothesised that this was due to either an increase in the expression levels of the HS6STs, the enzymes responsible for the addition of 6-O-sulfate group, and/or a decrease in the expression levels of the SULFs, the enzymes that are responsible for the removal of 6-O-sulfate groups. Two out of the 21 HS biosynthetic genes expressed, HS6ST1 and HS3ST5, were significantly different between the 3-month and 2-year old mice.

Firstly, HS6ST1 was downregulated in the 2 year-old muscles compared to the 3 month-old muscles, which was expected to lead to a reduction in 6-O-sulfation rather than the observed increase in 6-O-sulfation. Moreover, the expression levels of HS6ST2, HS6ST3, Sulf1 and Sulf2 were not significantly altered during ageing, with only a modest trend for an increase in the expression levels of HS6ST3 in the ageing muscle. These data indicate that the gene expression levels alone do not reflect enzyme activity and subsequently the level of 6-O-sulfation. Indeed, it has previously been demonstrated that each HS6ST isoform exhibits characteristic substrate preferences (Bink et al., 2003; Habuchi et al., 2000). For example, HS6ST2 preferentially catalyses 6-O-sulfation of IdoA(2S)-GlcNS to IdoA(2S)-GlcNS(6S), but unfortunately from the compositional analysis, it is not possible to distinguish IdoA from GlcA. Furthermore, the HS 6-O-endosulfatses (Sulf1 and Sulf 2), which catalyse the removal of sulfate groups of glucosamine from HS, are also crucial regulators of HS 6-O-sulfation. From the expression level analysis, there are no significant differences in Sulf1 or Sulf2 expression levels. However, as in the case of the HS6STs, Sulf1 and Sulf2 recognise distinct structural features and enzymatic activities (Ai et al., 2006) and thus expression levels do not solely reflect catalytic activity and fractional effects. Therefore, to further assess the origin of the increase in 6-O-sulfation observed in ageing muscle, it would be useful to investigate protein levels and enzymatic activity of the three HS6STs and the two Sulfs.

The second enzyme that was significantly altered during ageing in muscle was HS3ST5, a 3-O-sulfotransferase, which catalyses the addition of sulfate groups at the 3-O- position of the glucosamine residue in HS. HS3ST5 was upregulated in 2 year-old muscles compared to the 3 month-old muscles. From the HS disaccharide compositional analysis that was performed in this study, only the 8 most abundant HS disaccharide units could be identified with the HS standards used, which do not include disaccharides containing 3-*O*-sulfation. Therefore, we were unable to determine the presence or abundance of disaccharides containing 3-*O*-sulfation from the HS compositional analysis. Thus, it is possible that the level of 3-*O*-sulfation is increased in HS during ageing in muscle. Intriguingly, the HS3STs make up the largest gene family among all the sulfotransferases (Liu and Pedersen, 2007) yet 3-*O*-sulfation is relatively rare, with few modifications along the chain or absent entirely (Thacker et al., 2014). However, it has been demonstrated previously that HS3ST5 is expressed in human skeletal muscle (Xia et al., 2002) suggesting that 3-*O*-sulfation may play an important role in skeletal muscle although there have been no *Hs3st5* mutants reported to date. Furthermore, HS3ST3b1 is significantly up-regulated during satellite cell activation which might support the hypothesis that 3-*O*-sulfation is associated with satellite cells breaking quiescence in ageing muscle (Pisconti et al., 2012). However, little information on the role of 3-*O*-sulfation in protein binding is currently available. To date six proteins have been identified, including the well-recognised HS binding protein antithrombin, that are affected by 3-*O*-sulfation (Thacker et al., 2014). Interestingly, there is indirect evidence that 3-*O*-sulfation might have a role in FGF1 and FGF2 binding to FGFR1 (McKeehan et al., 1999; Ye et al., 2001) and more recently it has been shown that 3-*O*-sulfation controls the FGFR2b-dependent signalling during organogenesis (Patel et al., 2014). Thus, it is possible to postulate that an increase in 3-*O*-sulfation during ageing in muscle may contribute to increased FGF2 signalling, supporting our finding that HS from ageing muscle is more effective at promoting FGF2 signalling than HS from younger muscle. Furthermore, in mouse embryonic stem cells, overexpression of HS3ST5 induces differentiation (Hirano et al., 2012), suggesting that altered 3-*O*-sulfation has a significant effect on the signalling properties of HS. However, it must be noted that the data on HS biosynthetic enzyme expression shown here are only preliminary, with only a few samples for each age group being analysed. Therefore, to investigate this further, transcript expression analyses with more replicates is required. Additional investigations would also be necessary to allow for the characterisation of HS 3-*O*-sulfation. This would require the production of defined HS disaccharides standards for 3-*O*-sulfation, that could be identified after heparinase digestion, or the use of nitrous acid depolymerisation which has been used to identify disaccharides with 3-*O*-sulfate groups (Turnbull, 2001).

As mentioned above, the majority of enzymes from the same family have different substrate affinities, such as a difference in affinity for glucuronic acid over iduronic acid (Hsieh et al., 2016). Since the compositional analysis does not account for differences in abundance of

iduronic acid or glucuronic acid, further investigations may involve nitrous acid degradation of HS to retain the epimeric form of the uronic acid residue. Furthermore, other regulatory enzymes may alter HS enzyme catalytic activity and thus, cannot be excluded from our data. For example, the cofactor, 3'-phosphoadenosine-5'-phosphosulfate (PAPS) is crucial for HS sulfotransferase activity (Kurima et al., 1998), which may be differentially regulated during ageing in muscle and thus affecting the activity of the HS sulfotransferases.

Chapter 5

5 Effect of Semi-Synthetic Heparan Sulfate Mimetics on Myogenesis

5.1 General Introduction

In the previous chapters it was shown that the structural composition of HS is altered during myogenic differentiation and ageing in skeletal muscle, and these changes are associated with changes in HS-dependent FGF2 mitogenic activity. In the case of myogenic differentiation, a more highly sulfated HS species is associated with reduced FGF2 induced mitogenic activity. In the case of muscle ageing, on the other hand, increased levels of 6-O-sulfation are associated with an increased ability to promote FGF2 mitogenic activity, possibly leading to breaking of satellite cell quiescence and eventually loss of satellite cell numbers. From these findings it is evident that the biological function of HS is dependent on a combination of the overall charge density and the patterns of sulfation. To further investigate the structure-function relationships of HS, "HS mimetic" polysaccharides can be used to model in a systematic way an altered extracellular heparanome. Thus far, sulfated dextran derivatives, known as Regenerating Reagents (RGTAs), have been used to investigate the effects of altering the ECM during myogenesis. Firstly, it has been demonstrated that satellite cell-derived myoblasts treated with RGTAs exhibit a significant increase in proliferation by increasing the potency of FGF2 and scatter factor/hepatocyte growth factor (HGF) (Papy-Garcia et al., 2002). It was also shown that RGTAs lead to the production of an altered HS species during differentiation of the C2.7 myoblast cell line (Barbosa et al., 2005). These investigations provide an important indication of the mechanisms by which RGTAs affect myogenesis. However, since RGTAs are produced by derivatisation of dextran, which is made of branched chains of glucose monosaccharides, structural diversity becomes a limitation for structure-function investigations.

Another method for generating HS mimetics, which are simpler, more readily available and low cost, is by chemically modifying heparin, a highly sulfated type of HS, to resemble naturally occurring HS species (Yates et al., 1996). Since heparin is readily available, it is

possible to produce modified heparins in large quantities. The structure of the HS species obtained via this method can then be determined with nuclear magnetic resonance (NMR) spectroscopy (Rudd et al., 2011; Yates et al., 1996) and compositional analysis (Patey et al., 2006). The majority of methods for the production of chemically modified heparins involve the chemical de-sulfation from one or more positions, usually to completion, creating simplified structures. This approach leads to a library of chemically modified heparins, each consisting of one of the 8 most common disaccharide units found in naturally occurring HS, containing discrete, specific, structural entities. Thus far, modified heparins produced in this way, have proven useful for determining the importance of HS sulfation in different biological scenarios. For example, modified heparins have allowed for the elucidation of the importance of specific structural entities of HS such as; in the inhibition of Alzheimer's protease BACE-1 (Patey et al., 2006), in the FGF/FGFR tyrosine kinase signalling system (Guimond et al., 2006) and in the binding of FGF1 and FGF2 (Uniewicz et al., 2010). Furthermore, chemically modified heparins have been used to identify the importance of HS sulfation in boundary formation by glial cells (Higginson et al., 2012).

5.2 General Hypothesis

In this chapter it is shown that:

1. HS mimetics harbouring different degrees and patterns of sulfation differentially affect expansion, differentiation, fusion and Pax7 expression of satellite cell-derived myoblast cell fate decisions
2. HS mimetics have differential effects on FGF2-induced myoblast proliferation through Erk1/2 activation

5.2.1 Modified Heparins: HS mimetics

To model in a systematic way changes in the structure of HS in the satellite cell niche which may affect myogenic differentiation, a library of chemically modified heparins was produced by Dr Edwin Yates and kindly donated to us. These will be referred to as HS mimetics throughout (**Figure 5.1** and **Table 5.1**). Heparin was chemically modified to produce a library of 8 diversely sulfated HS mimetics, containing different levels and positions of sulfation. 7 HS mimetics contain reduced levels of sulfation compared to native heparin, mimicking various structures of HS found normally in tissues: HS with sulfation in two positions (HS mimetic 2, HS mimetic 3 and HS mimetic 4), HS with sulfation in one position (HS mimetic 5, HS mimetic 6 and HS mimetic 7) and completely de-sulfated HS (HS mimetic 8). A more highly sulfated HS mimetic was also produced, with sulfation in more than the three most common positions (oversulfated heparin, HS mimetic 1) in which additional 3-O-sulfate groups are present on glucosamine and uronic acid rings. The structural unit and

corresponding HS mimetic label are summarised in **Figure 5.1** and **Table 5.1.**
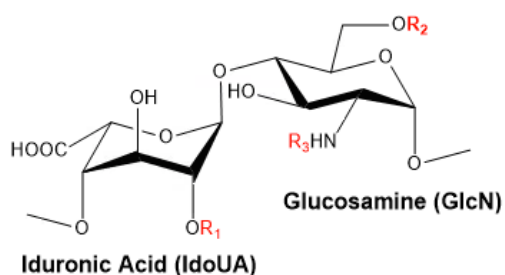
Figure 5.1 Structural disaccharide units of the HS mimetics. Figure of general structural disaccharide unit of the HS mimetics which are differentially functionalised indicated by the R group. Corresponding functional groups for specific HS mimetics are displayed in **Table 5.1**.

Table 5.1 HS mimetics obtained by chemical modification of heparin. The structural composition of the HS mimetics with corresponding nomenclature and functionalised R groups. R groups are indicated on the disaccharide unit in **Figure 5.1**.

Modified Heparin HS mimetic	Fig Annotation	R_1	R_2	R_3	Additional Modification
Heparin	hep	SO_3^-	SO_3^-	SO_3^-	
Oversulfated Heparin	HS mim 1	SO_3^-	SO_3^-	SO_3^-	+ SO_3^- at C3 of GlcN and C3 of IdoA
N-Acetylated Heparin	HS mim 2	SO_3^-	SO_3^-	$COCH_3$	
2 de-Sulfated-N-Sulfated Heparin	HS mim 3	H	SO_3^-	SO_3^-	
6 de-Sulfated-N-Sulfated Heparin	HS mim 4	SO_3^-	H	SO_3^-	
2 de-Sulfated-N-Acetylated Heparin	HS mim 5	H	SO_3^-	$COCH_3$	
6 de-Sulfated-N-Acetylated Heparin	HS mim 6	SO_3^-	H	$COCH_3$	
2,6 de-Sulfated-N-Sulfated Heparin	HS mim 7	H	H	SO_3^-	
2,6 de-Sulfated-N-Acetylated Heparin	HS mim 8	H	H	$COCH_3$	

5.2.2 HS mimetics differentially affect differentiation

Satellite cell-derived myoblasts were isolated using the differential plating protocol as described in Chapter 3. Satellite cell-derived myoblasts were treated with heparin and HS mimetics at 10 ng/ml, 100 ng/ml or 1 µg/ml concomitant with induction of myogenic differentiation by serum reduction for 72 hours. To measure the effect of the HS mimetics on myogenic differentiation, the percentage of nuclei contained in cells staining positive for myosin heavy chain (MyHC) over the total number of nuclei (DAPI positive cells) was calculated, which is defined as the differentiation index (DI) (**Figure 5.2**). It was found that the effect of different HS mimetics on myoblast differentiation was structure-specific and concentration-dependent with the lowest doses tested often leading to non-significant differences compared to absence of treatment (**Figure 5.3**). At the highest concentration of 1 µg/ml, almost all of the HS mimetics showed a significant reduction in differentiation with the exception of mimetic 1 (oversulfated heparin), which showed little effect on differentiation. Furthermore, myoblasts treated with HS mimetic 1, 3, 5, 6, 7 and 8 at 10 ng/ml displayed a significant increase in differentiation compared to myoblasts treated with heparin at the same

concentration. However, at 1 µg/ml, HS mimetic 1 was the only HS mimetic to significantly increase differentiation compared to myoblasts treated with heparin at 1 µg/ml.
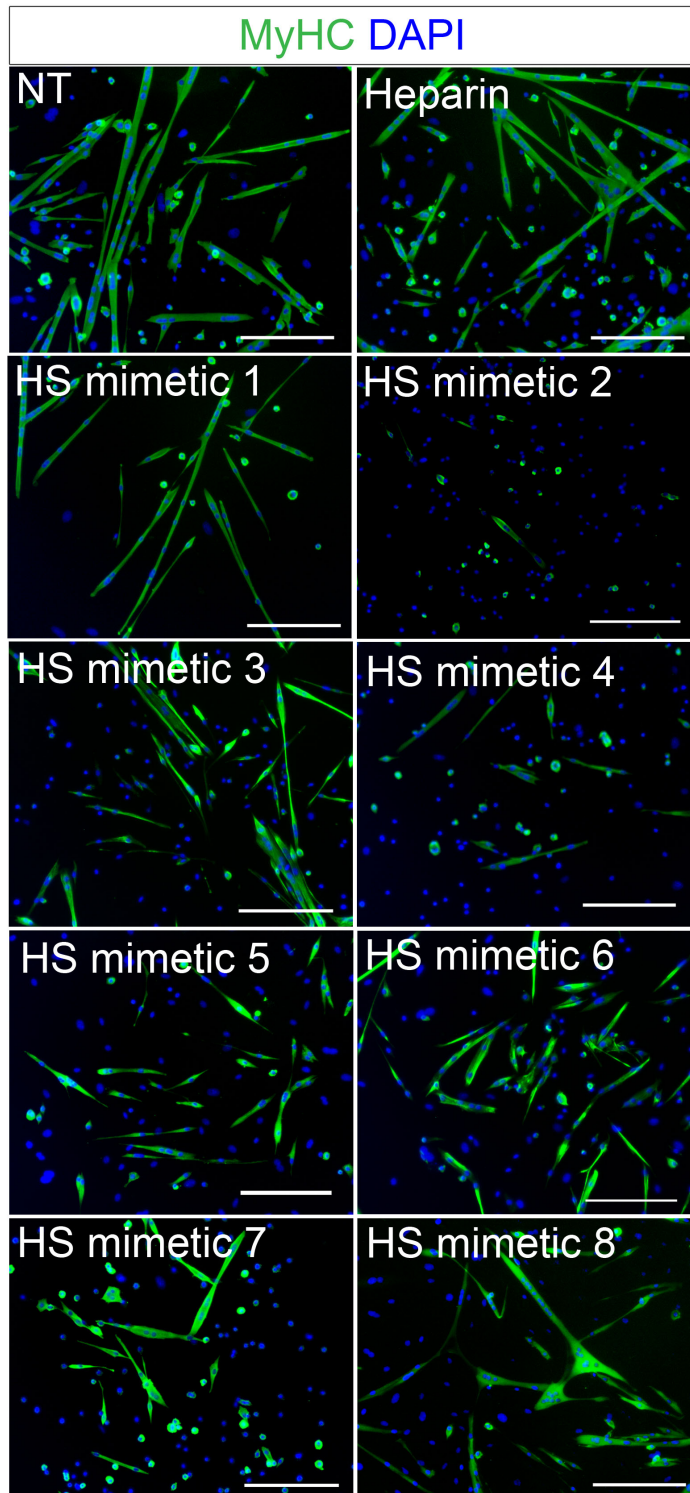
Figure 5.2 Representative images showing the effects of HS mimetics on myoblast differentiation. Primary SC-derived myoblasts were cultured for 48 h and then induced to differentiate for an additional 72 h. Differentiated cells, both mono- and multi-nucleated, were identified via immuno-staining to detect myosin heavy chain (MyHC, green). Nuclei were detected with the nuclear stain DAPI (blue). Ten images were taken across two technical replicates for three independent experiments for each condition shown. Scale bar = 100 µm across all images
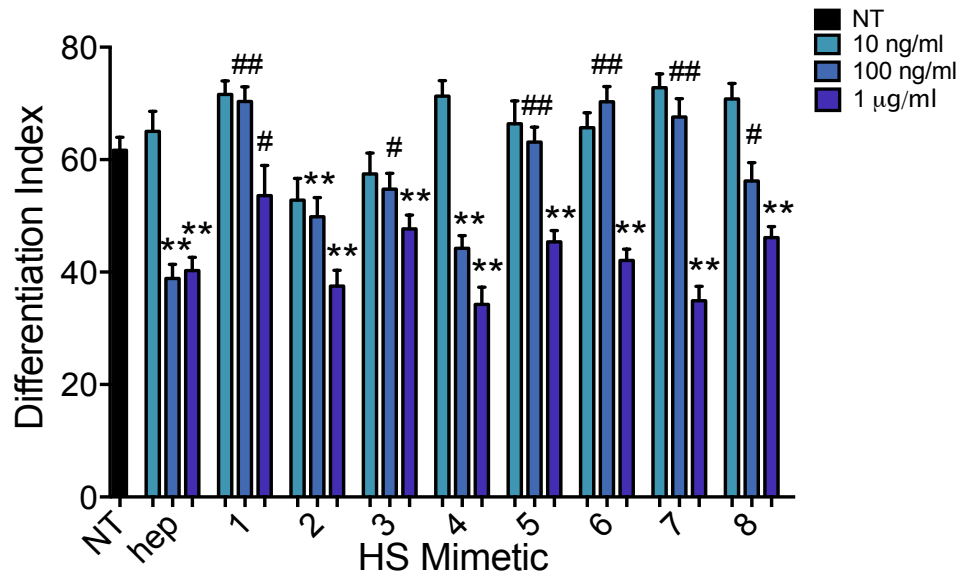
Figure 5.3 HS mimetics differentially effect myoblast differentiation. Primary SC-derived myoblasts were cultured for 2 days in growth medium and then induced to differentiate for a further 3 days. For each condition shown, the differentiation index was calculated as the percentage of nuclei in MyHC+ cells (both mono- and multi-nucleated) over the total number of nuclei (DAPI+). The average of ten images across two technical replicates for three independent experiments ± S.E.M. was calculated and plotted. Asterisks are p-values for each condition compared to non-treated (NT) cells. ** = $p < 0.01$; * = < b 0.05. ** = $p < 0.01$; * = < b 0.05. Hash signs are p-values for each condition compared to heparin-treated cells. ## = $p < 0.01$; # = $p < 0.05$ (Ghadiali et al., 2016).

5.2.3   HS Mimetics Differentially Affect Myoblast Cell Numbers

In myoblasts, differentiation and proliferation are mutually exclusive and thus, it was hypothesised that the addition of less sulfated HS mimetics in low serum conditions increased pro-proliferative and/or anti-differentiative signals, delaying differentiation and promoting cell expansion. To measure this, the average nuclei count (DAPI positive cells) was calculated. The HS mimetics that decreased differentiation the most (HS mimetic 2, HS mimetic 3 and HS mimetic 4), also showed the greatest effect on increasing cell numbers at the highest concentration tested (1 µg/ml) (**Figure 5.4**). HS mimetic 2 was the only HS mimetic to increase cell numbers at the lower concentrations tested (10 and 100 ng/ml). Furthermore, HS mimetic 2 displayed similar effects on myoblast expansion compared to heparin at all concentrations tested. In contrast, myoblasts treated with oversulfated HS (HS mimetic 1), which did not reduce differentiation even at the highest concentration of 1 µg/ml, showed significantly reduced cell numbers yet there was no notable cell death or detached cells. In contrast, HS mimetics tested in high serum conditions on primary myoblasts, had no significant effects on proliferation (**Appendix 2**).
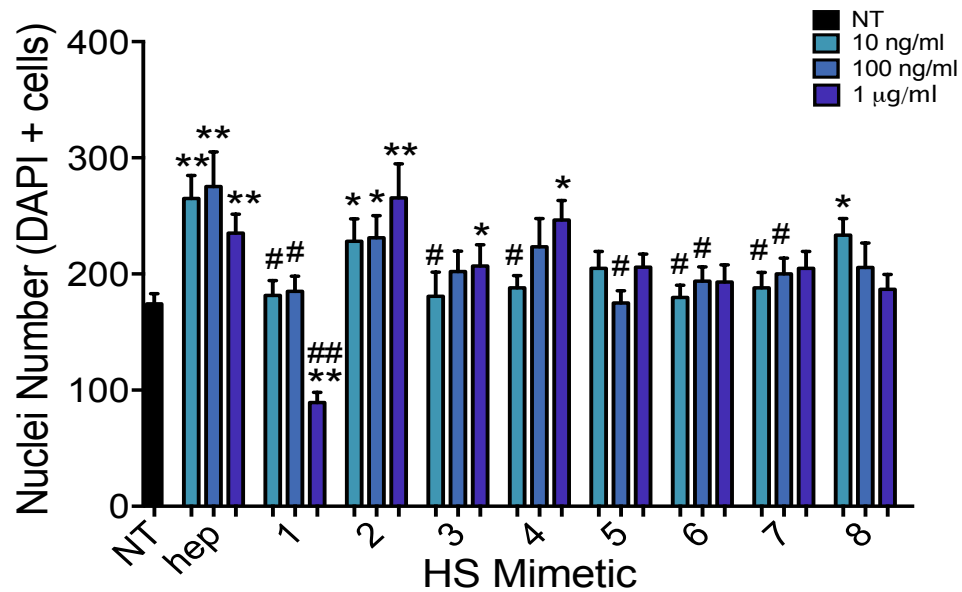
Figure 5.4 HS mimetics differentially affect myoblast cell number. Primary SC-derived myoblasts were cultured for 2 days in growth medium and then induced to differentiate for a further 3 days. For each condition shown, the total number of nuclei was measured and the average of ten images across two technical replicates for three independent experiments ± S.E.M. plotted. Asterisks are p-values for each condition compared to non-treated (NT) cells. ** = $p < 0.01$; * = < b 0.05. Hash signs are p-values for each condition compared to heparin-treated cells. ## = $p < 0.01$; # = $p < 0.05$ (Ghadiali et al., 2016).

5.2.4 HS Mimetics Differentially Affect Cell Fusion

The effects of the HS mimetics on myoblast fusion were then investigated. Fusion is the process by which differentiated myoblasts fuse together to form myotubes. The extent of fusion is defined as the fusion index (FI), which is calculated by dividing the number of differentiated cells over the number of nuclei contained in multinuclear MyHC positive cells. In general fusion followed a similar pattern to differentiation with fusion decreasing at increasing concentrations of HS mimetics (**Figure 5.5**).

5.2.5 HS mimetics differentially affect Pax7 expression

As shown in chapter 3, after three days in low serum nearly all myoblasts in primary satellite cell-derived myoblast cultures have either differentiated or entered a quiescent state, with the percentage of proliferating cells being negligible. Whereas differentiated myoblasts express myosin heavy chain (MyHC), non-differentiated quiescent cells express the transcription factor Paired Box 7 (Pax7) and are *bona fide* reserve cells. To test whether the changes in the extracellular heparanome affected the level of non-differentiated cells, the numbers of Pax7+ *bona fide* reserve cells was quantified in myoblast cultures that had been induced to differentiate and treated with the highest concentration (1 µg/ml) of HS mimetics previously tested for differentiation and cell expansion (**Figure 5.6**).
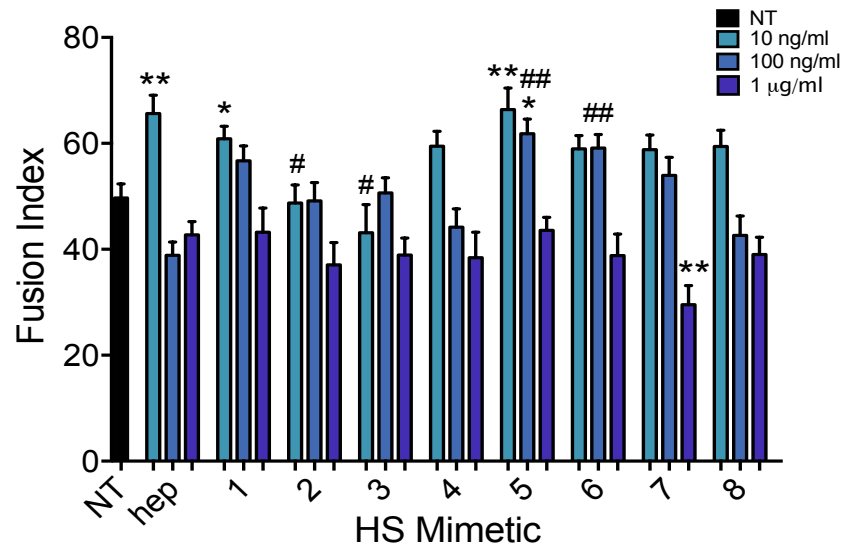
Figure 5.5 HS mimetics differentially affect myoblast cell fusion. Primary SC-derived myoblasts were cultured for 2 days and then induced to differentiate for a further 3 days. For each condition shown, the fusion index was calculated as the percentage of nuclei in multinucleated MyHC+ cells (multinucleated) over the total number of nuclei in MyHC+ (mono-nucleated and multinucleated) cells. The average of ten images across two technical replicates for three independent experiments ± S.E.M. was calculated and plotted. Asterisks are p-values for each condition compared to non-treated (NT) cells. ** = p < 0.01; * = < b 0.05. Hash signs are p-values for each condition compared to heparin-treated cells. ## = p < 0.01; # = p < 0.05 (Ghadiali et al., 2016).

At this concentration, with exception of HS mimetic 1 (oversulfated heparin), all of the HS mimetics produced a reduction in satellite cell-derived myoblast differentiation, however, the effects on the number of Pax7+ cells were more variable (**Figure 5.7**). Myoblasts treated with HS mimetics 2, 3 4 and 7 showed a significantly higher proportion of cells expressing Pax7 compared to non-treated cells and cells treated with heparin. However, cells treated with HS mimetic 1 and 6 presented a modest reduction in cells expressing Pax7 although these results did not reach statistical significance. Cells treated with HS mimetic 5 and 8 showed similar numbers of cells expressing Pax7 compared to non-treated cells despite displaying statistically significant differences in the level of differentiation (**Figure 5.8**). Overall this suggests that the HS mimetics are working by different mechanisms on myoblast cell fate decision.
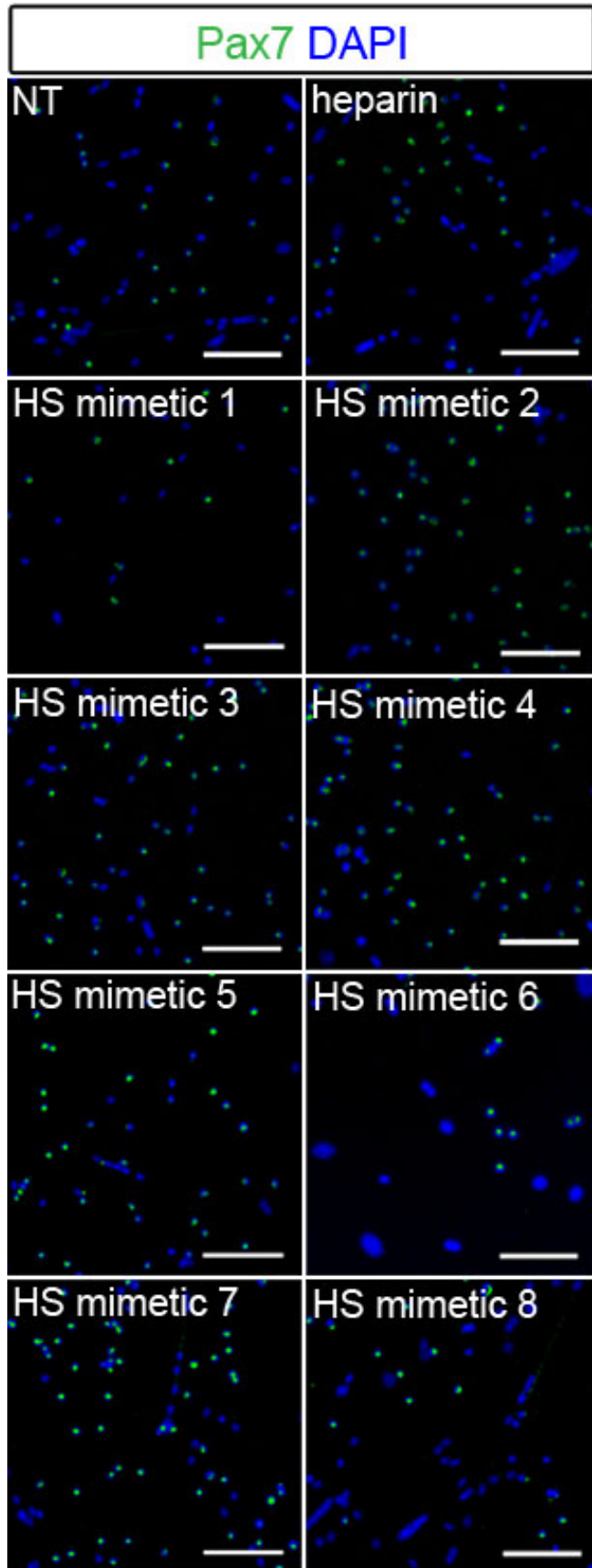
Figure 5.6 Representative images showing that HS mimetics differentially affect the numbers of Pax 7+ cells. Primary satellite cell-derived myoblasts were cultured for 48 h in growth medium and then induced to differentiate for an additional 72 h. Immunostaining for Pax7 (green) and nuclei are detected with the nuclear stain DAPI (blue). Ten images were taken across two technical replicates for three independent experiments for each condition shown. Scale bar = 100 μm across all images**.**
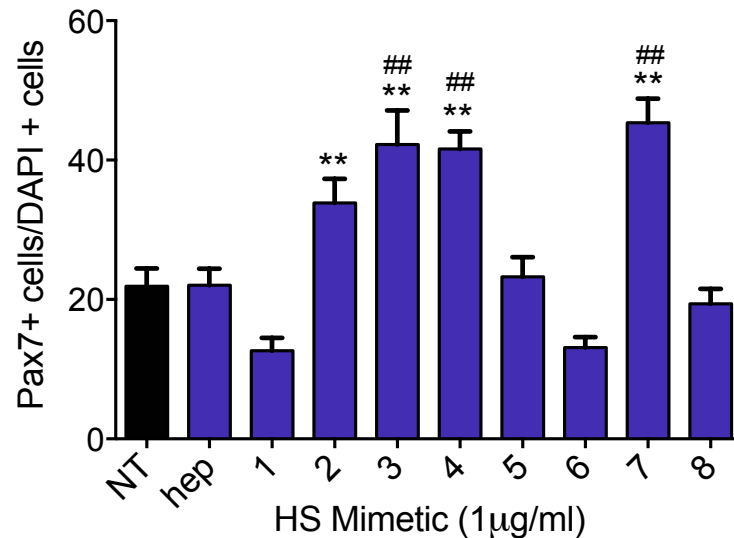
Figure 5.7 HS mimetics differentially affect Pax7 expression. Primary satellite cell-derived myoblasts were cultured for 2 days in growth medium and then induced to differentiate for a further 3 days. For each condition shown, the percentage of Pax7+ nuclei over the total number of nuclei was calculated and plotted as the average of ten images across two technical replicates for three independent experiments ± S.E.M. Asterisks are p-values for each condition compared to non-treated (NT) cells. ** = p < 0.01; * = < b 0.05. Hash signs are p-values for each condition compared to heparin-treated cells. ## = p < 0.01; # = p < 0.05 (Ghadiali et al., 2016).
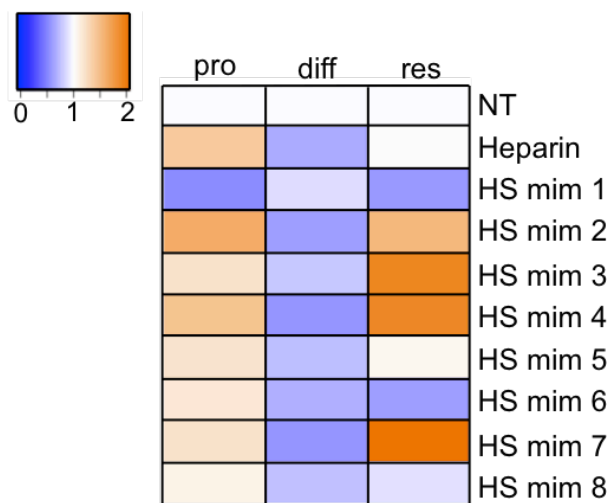
Figure 5.8 Summary of the effect produced by HS mimetics on primary satellite cell-derived myoblasts. Key: pro = proliferation, diff = differentiation, res = reserve cell generation where the mean values are plotted for each condition for 1 µg/ml normalised to non-treated (NT) cells.

5.2.6   FGF2 signalling via Erk1/2 are differentially affected by different HS structures in myoblasts

FGF2 promotes myoblast proliferation and is a potent inhibitor of myogenic differentiation. Since FGF2 depends on the presence of HS to signal and is sensitive to the level and pattern of HS sulfation (Guimond and Turnbull, 1999), it was hypothesised that the differences in myogenic activity observed in myoblasts treated with structurally different HS mimetics could be due to differences in their abilities to interact with and promote FGF2 signalling. In order to explore this hypothesis, the effects of two HS mimetics on FGF2-induced Erk1/2 activation, were tested, since it is well established that FGF2 induces ErK1/2

activation leading to an up-regulation of phospho-Erk1/2, which is critical for myoblast proliferation (Rao et al., 1985). Since HS mimetic 1 (oversulfated heparin) was the only HS mimetic to significantly reduce cell numbers and had no statistically significant effects on myoblast differentiation, it was hypothesised that mimetic 1 could inhibit FGF2 signalling and thus lead to reduced myoblast proliferation. HS mimetic 2 on the other hand was the HS mimetic which had the strongest effect on increasing cell number and reducing differentiation, therefore it was hypothesised that HS mimetic 2 might enhance FGF2 signalling and thus leads to increased myoblast proliferation. In order to measure the levels of ErK1/2 activation in response to FGF2 and/or various HS structures, the C2C12 myoblast cell line was utilised. Myoblasts were serum-starved for 6 hours before being treated with mimetic 1 with or without FGF2. Myoblasts treated with FGF2 alone increased Erk1/2 activation at 15 minutes post stimulation (**Figure 5.9**). Myoblasts treated with FGF2 and mimetic 1 on the other hand showed a reduction in Erk1/2 activation suggesting that mimetic 1 inhibits FGF2 induced Erk1/2 activation. Interestingly, myoblasts treated with HS mimetic 1 alone showed a decrease in Erk1/2 activation below basal levels 15 minutes post stimulation.
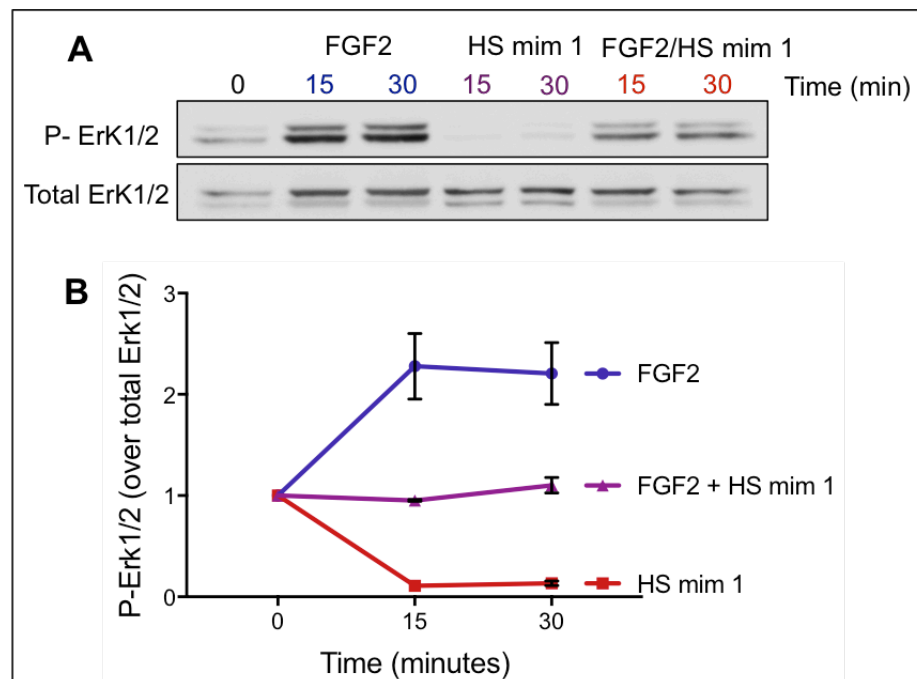
Figure 5.9 FGF2 signalling via Erk1/2 is reduced by HS mimetic 1 A) C2C12 myoblasts were serum-starved for 6 h (lane 1) then stimulated with either 2 nM FGF2 alone (lanes 2, 3) or HS mimetic 1 alone (lanes 4, 5) or FGF2 + HS mimetic 1 (1 µg/ml) together (lanes 6, 7) for the indicated amounts of time. At the end of the stimulus cells were immediately lysed and analysed via Western blotting to detect phosphorylated Erk1/2 (P-Erk1/2) and total Erk1/2. One representative of three independent experiments is shown. **B**) Quantification of phospho-Erk1/2 band intensity normalised to total Erk1/2 intensity. Moreover, all time points were then normalised to time zero (end of serum starvation) and the averages of three independent experiments plotted ± S.E.M., except for the condition "FGF2 alone at 15 and 30 minutes" which were averaged across 6 independent experiments (Ghadiali et al., 2016).

HS mimetic 2 on the other hand, showed the opposite effect. Although HS mimetic 2 alone did not appear to have any significant effect on the levels of Erk1/2 activation, HS mimetic 2 and FGF2 appeared to increase Erk1/2 activation levels compared to FGF2 alone (**Figure 5.10**). Activation also appeared to be sustained for a longer period of time to (60 minutes) compared to myoblasts treated with FGF2 alone. This suggests that HS mimetic 2 may inhibit differentiation by both increasing and prolonging FGF2 signalling.
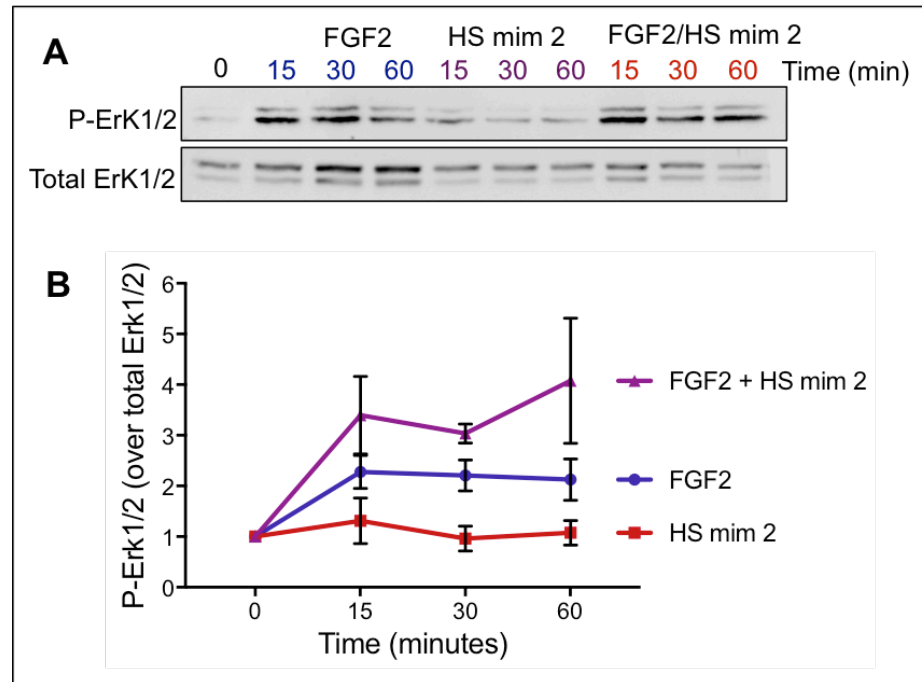
Figure 5.10 FGF2 signalling via Erk1/2 is increased by HS mimetic 2 A) C2C12 myoblasts were serum-starved for 6 h (lane 1) then stimulated with either 2 nM FGF2 alone (lanes 2, 3, 4) or HS mimetic 2 (1 µg/ml) alone (lanes 5, 6, 7) or FGF2 + HS mimetic 2 (lanes 8, 9, 10) for the indicated amounts of time. At the end of the stimulus cells were immediately lysed and analysed via Western blotting to detect phosphorylated Erk1/2 (P-Erk1/2) and total Erk1/2. One representative of three independent experiments is shown. **B**) Quantification of phospho-Erk1/2 band intensity normalised to total Erk1/2 band intensity, moreover all time points were then normalised to time zero (end of serum starvation) and the averages of three independent experiments plotted ± S.E.M., except for the condition "FGF2 alone at 15 and 30 min" which were averaged across 6 independent experiments (Ghadiali et al., 2016).

5.2.7 *FGF2 mitogenic activity on myoblasts is differentially affected by different HS structures in myoblasts*

To investigate if the increase in FGF2-induced Erk1/2 activation also led to increased mitogenic activity on the myoblasts, satellite cell-derived myoblasts were grown overnight in serum free medium with or without HS mimetic 1 or 2 and FGF2. BrdU incorporation was used as a measure of mitogenic activity (**Figure 5.11**). Myoblasts treated with FGF2 and HS mimetic 1 showed a statistically significant reduction in the proportion of BrdU positive cells compared to myoblasts treated with FGF2 alone (**Figure 5.12**). On the other hand, myoblasts treated with FGF2 and HS mimetic 2 showed an increase in the proportion of

BrdU positive cells compared to myoblasts treated with FGF2 alone, although this result did not reach significance. These results suggest that whilst HS mimetic 2 promotes FGF2-induced proliferation of satellite cell-derived myoblasts, mimetic 1 inhibits FGF2-induced proliferation. This is consistent with the result that HS mimetic 1 reduces FGF2-induced Erk1/2 activation, which is upstream of myoblast proliferation pathways.
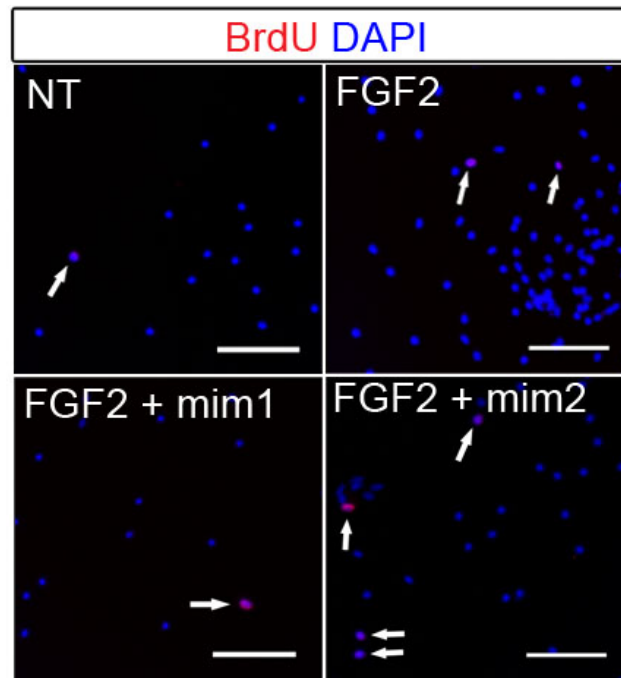
Figure 5.11 Representative images showing that HS mimetics differentially affect myoblast proliferation. Primary satellite cell-derived myoblasts were expanded for two days in growth medium then serum-starved for 12 hours to induce cell cycle exit followed by treatment with either vehicle (NT), FGF2, FGF2 + HS mimetic 1 or FGF2 + HS mimetic 2 overnight. 10 µM BrdU was then added to the culture medium 2 h prior to fixation and immunostaining to detect BrdU (red). Nuclei are detected with DAPI (blue). Ten images were taken across two technical replicates for three independent experiments for each condition shown. White arrows indicate BrdU postive nuclei. Scale bar = 100 µm across all images.
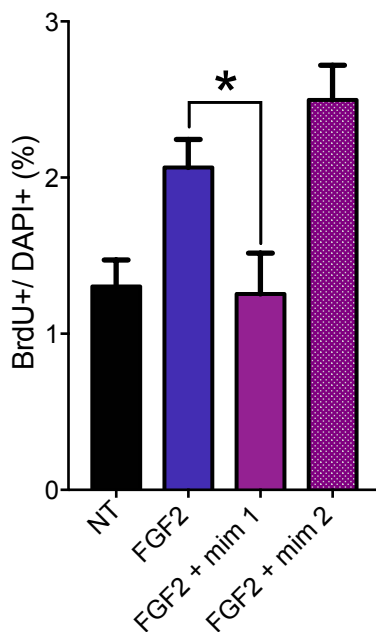
Figure 5.12 HS mimetics differentially affect proliferation of serum-deprived myoblasts. Primary satellite cell-derived myoblasts were cultured for 2 days in growth medium and then serum-starved for 12 h to induce cell cycle exit followed by treatment with either vehicle (NT), FGF2, FGF2 + HS mimetic 1 or FGF2 + HS mimetic 2 overnight. Cells were then treated with BrdU for 2 hours before fixing and immunostaining. For each condition shown, the percentage of BrdU+ nuclei over the total number of nuclei was calculated and plotted as the average of ten images across two technical replicates for three independent experiments ± S.E.M (Ghadiali et al., 2016).

5.3   Discussion

In this chapter, heparin and a small library of chemically modified heparin derivatives with different levels and patterns of sulfation (HS mimetics), were tested on satellite cell-derived myoblasts for their effects on proliferation, differentiation and self-renewal. The process of myogenesis is regulated by several heparin-binding growth factors; whilst some growth factors promote cell proliferation; such as FGF (Clegg et al., 1987; Schabort et al., 2009; Sheehan and Allen, 1999), others promote myogenic differentiation such as IGF (Jennische and Hansson, 1987). Since growth factor signalling is heavily affected by the sulfation pattern of HS and the structure of HS changes during myogenesis, it was hypothesised that HS mimetics displaying various structures might differentially affect myogenesis, further elucidating structure-function properties of HS during myogenesis. To investigate this hypothesis, satellite cell-derived myoblasts were treated with HS mimetics at differing concentrations concomitant with induction to differentiation. Consistent with the hypothesis, different effects on myoblast cell number, differentiation, fusion and self-renewal were observed between HS mimetic treatments. In general, the effects of the HS mimetics on the different stages of myogenesis were structure-specific and concentration-dependent.

The majority of the HS mimetics, at the highest concentration tested (1 μg/ml), produced a significant reduction in myoblast differentiation. Oversulfated heparin (HS mimetic 1), was the only mimetic that did not reduce myoblast differentiation and produced a significant reduction in myoblast cell number. Since there was no noticeable cell detachment or cell death in myoblasts treated with HS mimetic 1, it is likely that the reduction in cell number was due to cell cycle arrest. Since on the first day in low serum, myoblasts are still dividing, it is possible that HS mimetic 1 induces cell cycle arrest more rapidly than serum reduction alone or serum reduction and other HS mimetics. This is likely due to the strong inhibitory effect of HS mimetic 1 on FGF2 induced proliferation, leading to reduced cell numbers. Indeed, myoblasts treated with FGF2 and HS mimetic 1 together, did not produce an increase in Erk1/2 phosphorylation and showed a significant reduction in the number of cells re-entering the cell cycle. These observations together suggest that HS mimetic 1 leads to a reduction in myoblast proliferation by blocking FGF2 signalling. This lends strength to our previous findings that the more highly sulfated HS species produced during myogenic differentiation is associated with reduced FGF2 induced mitogenic activity. However, it cannot be ruled out that oversulfated heparin may affect other signalling pathways, which could also contribute to the reduction in myoblast proliferation and this requires further investigation. Mimetic 2, on the other hand, which had the largest effect on increasing cell number, was found to increase FGF2/Erk1/2 signalling pathway, prolonged FGF2 induced Erk1/2 phosphorylation and produced a significant increase in the number of cells re-entering the cell cycle. This suggests that HS mimetic 2 increases myoblast proliferation in low serum by promoting FGF2 signalling.

When myoblasts are maintained under differentiating conditions *ex vivo*, a proportion of myoblasts exits the cell cycle and remains in an un-differentiated state and express Pax7. *In vitro* quiescent cells are called "reserve cells" which are Pax7+ Ki-67- negative and represent an *ex vivo* model of satellite cell self-renewal (Yoshida et al., 1998). Since after three days in differentiating conditions the number of proliferating (Ki-67+) cells are negligible (**Figure 3.7**), it was reasoned that the level of Pax7 expression was an appropriate predictor of the level of reserve-cell generation with the effects of the HS mimetics on cell numbers being limited to the cells still completing the cell cycle in the hours following serum withdrawal. Interestingly, despite all HS mimetics, with the exception of HS mimetic 1, producing a reduction in myoblast differentiation, the effects on the number of Pax7+ *bona fide* cells were more variable. Notably, at 1 μg/ml, on HS mimetics 2 and 4 promoted cell expansion, which alone would justify an increase in the proportion of undifferentiated cells. In contrast, HS mimetics 3 and 7 did not affect cell expansion and reduced differentiation, thus suggesting that HS mimetics 3 and 7 might have a direct effect on promoting reserve cell generation. Further characterisation of reserve cell generation based on double Pax7/Ki-67 staining is required in order to test this hypothesis. This strongly supports the idea that HS-mediated signalling events regulate satellite cell fate in a complex manner, simultaneously affecting multiple signalling pathways. Furthermore, it lends strength to the argument that the structure-function activity of HS is not solely reliant on the level of charge since there is no simple correlation between the level of sulfation (and thus charge) of the HS mimetic treatment and the levels of reserve-cell generation. This implies that there is some structure-function redundancy of HS. Indeed, previous findings have shown that non-HS or glycosaminoglycan analogues can promote FGF2 signalling, but do not support FGF2 stabilisation (Rudd et al., 2010), highlighting that HS-mediated promotion of FGF2 signalling is dependent on mechanisms other than protein stabilisation.

One explanation for the sustained FGF2 signalling with HS mimetic 2 compared to cells treated with FGF2 alone, could be that HS mimetic 2 binds FGF2 in a way that prevents its proteolytic degradation by extracellular proteinases (Saksela et al., 1988) which may be in turn due to differences in the stabilising interaction between the HS mimetic and FGF2. However, previous investigations into the stabilising effects of the HS mimetics on FGF2, reported that heparin has the largest stabilising effect on FGF2 followed by oversulfated heparin (HS mimetic 1) (Uniewicz et al., 2012). This is further supported by highly sulfated fractions of heparin, which bind FGF2 more strongly than less sulfated fractions of heparin (Naimy et al., 2011). Furthermore, the relative stabilising effect of HS mimetic 2 was four times lower than that of oversulfated heparin yet had the most significant effect on increasing myoblast proliferation compared to non-treated cells (Uniewicz et al., 2010). This suggests that there is not a direct correlation between HS-mediated stabilization of FGF2 and FGF2 induced myoblast proliferation. Therefore, the level of FGF2 stabilization by the HS mimetics does not predict HS-mediated FGF2 activity alone. Instead, HS mediated FGF2 activity is

reliant on a combination of interactions involving FGF2, HS and the FGF receptor (Schlessinger et al., 2000). For example, HS mimetic 2 contains 2- and 6-O-sulfation, which is important for supporting FGF2 signalling (Pye et al., 1998) and thus may support sustained FGF2 induced Erk1/2 phosphorylation. Indeed, HS mimetic 2 has been reported to support FGF2/FGFR1 BaF3 mitogenic activity (Guimond et al., 2006) and thus our data further support this finding that HS mimetic 2 promotes FGF2 signalling. In contrast, the large number of sulfate groups on HS mimetic 1, which binds strongly to FGF2 may sequester FGF2 away from the FGF receptor leading to reduced FGF2 signalling. Alternatively, the more highly sulfated heparin derivative may compete with endogenous HS for FGF2 signalling in which the sulfation pattern does not support formation of the HS-FGF2-FGFR1 ternary complex. A similar phenomenon has previously been reported with a highly sulfated heparin mimicking polymer poly(sodium-4-styrenesulfonate) (PSS) (Sangaj et al., 2010). Here, the authors report that PSS binds strongly to FGF2 and in turn blocks Erk1/2 activation in the C2C12 myoblast cell line promoting myogenic differentiation (Sangaj et al., 2010). Since myoblast fusion is heavily influenced by the level of myoblast differentiation, it is not surprising that the HS mimetics affect myoblast fusion in a similar pattern to that presented in myogenic differentiation. This suggests that HS mediated signalling events have a direct role on myogenic differentiation but a less pronounced effect on regulating myoblast fusion. However, further work may involve investigating specific HS-mediated signalling pathways that could modulate myoblast fusion independent on myoblast differentiation. Furthermore, from the phenotypes displayed through the treatment with HS mimetics, effects on other HS-mediated signalling pathways on myogenesis cannot be excluded. However, there is no correlation between the biological activity and the charge density alone. Instead, these observations suggest that it is the overall structural consequences of a combination of; a) the level of sulfation, b) the position of sulfation and c) the conformation of HS structures that are critical for interactions and biological activity.

Chapter 6

6 Effect of Fully Synthetic HS Mimetic Clusters on Myogenesis

6.1 General Introduction

6.1.1 HS mimetics as therapeutics

In the previous chapter, it was demonstrated that chemically modified heparins differentially affect muscle stem cell homeostasis depending on the pattern and level of sulfation. Therefore, HS mimetics may represent novel therapeutic entities for muscle wasting conditions, where muscle stem cell homeostasis is dysregulated. However, heparin itself is a heterogeneous mixture containing polysaccharides of different lengths and structures; although modified heparins can have less heterogeneity in sulfation, they are still mixtures containing polysaccharides of different lengths. Thus, although modified heparins provide an important indication of the structural requirements for a particular HS-mediated function, it could be beneficial to produce fully synthetic HS mimetics that maintain the same potency of HS or modified heparins as potential therapeutic molecules.

6.1.2 Carbohydrate Chemistry

The synthesis of oligosaccharide-based HS mimetics requires a multifaceted, complex process. Since particular techniques are consistently required in the handling of sugars, carbohydrate chemistry in itself is a specialised branch of organic chemistry. Oligosaccharide synthetic complexity arises from the large numbers of hydroxyl functional groups around a sugar, which must be differentiated to attain chemoselectivity and regioselectivity. Importantly, the large numbers of hydroxyl groups give rise to a highly hydrophilic macromolecule and thus solvent choice can be limited during synthesis, adding to the synthetic complexity.

Most monosaccharides, such as glucose and galactose, are readily obtained from natural sources, which are commonly the starting point for oligosaccharide synthesis. Monosaccharides are linked together by the glycosylation reaction (**Figure 6.1**), leading to the formation of a mixture of anomers connected by either 1,2-*cis* or 1,2-*trans* linkages. It is these linkages that determine the stereochemistry of the oligosaccharide, which is an important factor for determining the conformation of a sugar and thus their chemical properties. Firstly, one monosaccharide is termed the 'glycosyl donor x', which contains a leaving group X, at the anomeric position. The lone pair of electrons on the ring oxygen aids the departure of X and stabilises the planar intermediate **2**. The second monosaccharide is termed the glycosyl acceptor **3**, which bears a free hydroxyl group that can attack either face of the planar intermediate, allowing for the formation of both the equatorial anomer **4** and the axial anomer **5**. The axial anomer is the more thermodynamically favourable product due to hyperconjugation, known as the anomeric effect and hence axial anomers are formed preferentially over equatorial anomers. Achieving the correct glycosidic bond stereoselectivity is crucial in HS oligosaccharide synthesis but this remains a significant challenge. Functional groups adjacent to the anomeric carbon (the site of glycosylation) can be employed to direct the stereoselectivity of the glycoside bond. This is termed 'neighbouring group participation' and is a strategy frequently used in HS oligosaccharide synthesis.
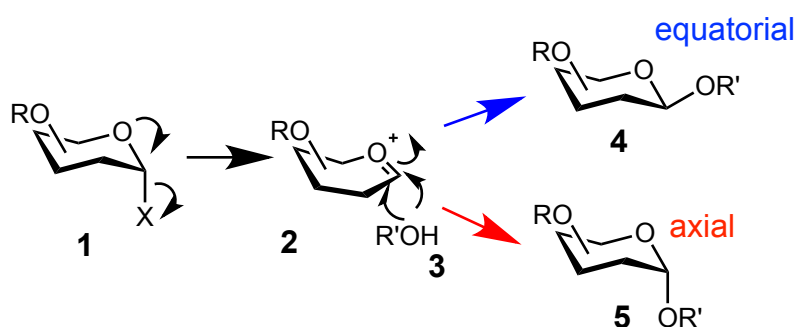
Figure 6.1 Schematic of glycosylation reactions. General scheme for the glycosylation reaction of glycosyl donor 1 and glycosyl acceptor 3 forming a mixture of (compound 4) equatorial and axial (compound 5) anomers. The formation of anomers is due to the intermediate 2, which is a planar molecule and can be attacked from either side.

In addition to achieving stereoselectivity, regioselectivity is also crucial in oligosaccharide synthesis. Depending on the position around the ring, and thus the surrounding chemical environment, the hydroxyl groups can have different chemical properties. When hydroxyl groups have similar chemical properties, the glycosylation reaction can involve multiple hydroxyl groups on the glycosyl acceptor. Likewise, in a desired reaction, for example in a sulfation reaction, hydroxyl groups can interfere by reacting instead of the functional group (FG) required. To overcome this, hydroxyl groups can be chemically shielded with a non-reactive, protecting group (PG) (**Figure 6.2**). The desired reaction can then take place at the

functional group, without the competing hydroxyl groups. Once the chemical reaction has taken place, the protecting group can be removed. In the majority of cases in oligosaccharide synthesis, the protection of more than one hydroxyl group is necessary. The use of orthogonal protecting groups with different chemical properties allows for selective de-protection. For HS synthesis, the use of protecting groups is crucial for regioselectivity enabling the production of libraries of HS sequences containing different positions of sulfation of the multiple hydroxyl groups. Five of the most commonly used protecting groups in oligosaccharide synthesis are listed in **Table 6.1**.
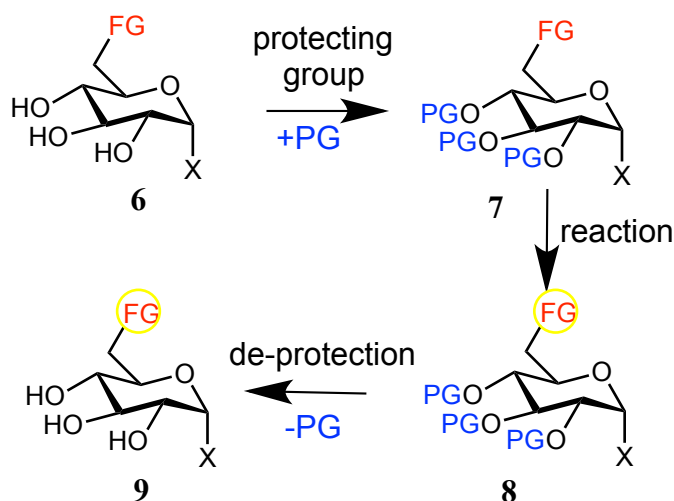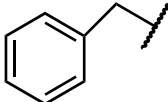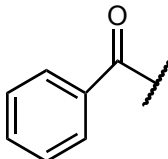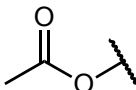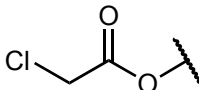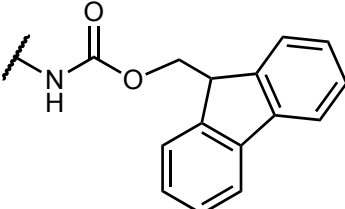
Figure 6.2 Schematic showing hydroxyl group protection. Compound 6 contains one functional group (FG) for a chemical reaction in which the three free hydroxyl groups are competing. Therefore, the remaining three hydroxyl groups are protected with protecting groups (PG) in 7 prior to the chemical reaction producing 8. Compound 8 then undergoes chemical de-protection to produce compound 9 with free hydroxyl groups.

6.1.3   HS synthesis

Although there has been significant progress in the development of strategies for HS oligosaccharide synthesis, the synthesis of longer chains of HS sequences remains a multi-step (more than 50 steps for the synthetic pentasaccharide drug, Arixtra), arduous and costly process (Arungundram et al., 2009; Cole et al., 2010; Hung et al., 2012; Lee et al., 2004; Noti and Seeberger, 2005; Polat and Wong, 2007; Schwörer et al., 2013). To overcome this, chemoenzymatic approaches have been developed (Liu et al., 2010; Xu et al., 2011), which use multiple HS biosynthetic enzymes for the synthesis of low molecular weight heparin oligosaccharides. However, it is difficult to regulate enzyme activity and specificity in chemoenzymatic reactions (Xu et al., 2011) and thus the production of specific and pure HS oligosaccharide sequences using chemoenzymatic approaches remains a challenge.

Table 6.1 Structures of 5 common protecting groups employed in HS oligosaccharide synthesis with their corresponding selective removal conditions.

Protecting Groups	Removal Conditions
Benzyl (Bn)	Pd/C/H$_2$
Benzoyl (BzO)	NaOH/MeOH
Acetate (AcO)	DCM/MeOH/AcCl
Chloroacetate (ClAcO)	DABCO
NHFMoc	piperidine

6.1.4   HS Dendrimer Clusters

Recently, a greatly simplified synthetic procedure has been developed for producing a library of HS mimetics, which have been found to retain the bioactivity of long chained HS oligosaccharide structures. These HS mimetics, termed HS dendrimers, consist of a single entity tetravalent glycomimetic containing a core which has been end capped with short specific HS sequences. A wide range of dendrimer structures have been readily synthesised utilising the same dendritic core and disaccharide-building block, with few steps (Tyler et al 2015). Owing to the long, flexible dendritic core, bioactivity can be maintained with end-capped HS sequences as short as disaccharides, which individually would not retain bioactivity. All the dendrimers synthesised so far lack anticoagulant activity, making them promising therapeutic molecules with potentially few off-target effects (Tyler et al., 2015).

6.2   Hypothesis

Since: *a)* different structures of modified heparins affect myogenesis differently and *b)* HS dendrimers are able retain the bioactivity of longer HS oligosaccharides, it was hypothesised that HS-mimicking dendrimers (HS dendritic clusters) would affect myogenesis in a structure-dependent manner.

In this chapter it is shown that:

1. The synthesis of a new HS mimetic cluster containing N-sulfation.
2. Biological activities of the dendrimers produced is only observed at relatively high concentrations in bioassays testing myoblast differentiation or Pax7 expression.

6.3   Results

6.3.1   *Preliminary Screen of HS dendrimers on Satellite Cell-Derived Primary Myoblasts*

6.3.1.1   HS Mimetic Cluster Selection

As a preliminary screen, to test the hypothesis that HS dendritic clusters would affect myogenesis, primary satellite cell-derived myoblasts were treated, concomitant with induction to differentiation, with a selection of HS dendritic clusters, which had been previously synthesised and kindly donated by Dr Olga Zubkova and Prof Peter Tyler (Victoria University of Wellington, New Zealand). The synthesis of some of these compounds had previously been published (Tyler et al., 2015). Six tetramer dendrimers were selected (dendrimers 3, 4, 5, 6, 7 and 8) in which the end-capped saccharide contained at least 6-*O*-sulfation since these dendrimers had been found to mimic much longer poly- and oligo-saccharide chains of natural HS in their inhibition of BACE-1. All 6 dendrimers tested consisted of the 'long-armed' dendritic core since previous studies had confirmed these to be more potent than the corresponding 'short-armed' dendritic cores. Three disaccharide and three tetrasaccharide end-capped dendrimers including L-iduronic or D-glucuronic acid residues were tested (**Figure 6.3** and **Table 6.2**).
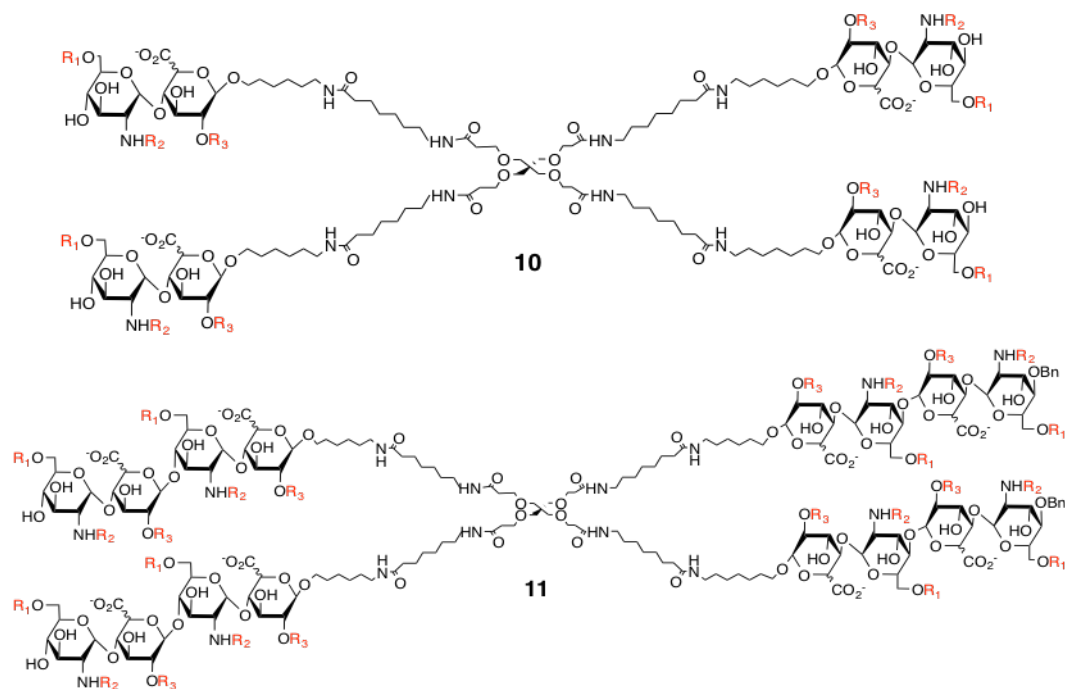
Figure 6.3 General structures of HS dendritic clusters tested on myoblast differentiation.
Tetramer **10** contains iduronic acid (dendrimer 3 and dendrimer 5) or glucuronic acid (dendrimer 4). **11** contains iduronic acid (dendrimer 6) or glucuronic acid (dendrimer 7 and dendrimer 8). The pattern of sulfation of the dendrimers tested is shown in Table 2 where R_1/R_2 = H or SO_3^- and R_3 = Ac or SO_3^-.

Table 6.2. The pattern of sulfation of the HS dendritic clusters tested on myoblast differentiation. The structural componenets of dendrimer 3, 4, 5, 6, 7 and 8 based on the teteramer HS clusters 10 and 11 shown in Figure 6.3.

Dendrimer	HS Cluster	R_1	R_2	R_3	Position of Sulfation	Uronic Acid
den 3	**10**	SO_3^-	Ac	H	6S	L–iduronic
den 4	**10**	SO_3^-	Ac	SO_3^-	2S, 6S	D–glucuronic
den 5	**10**	SO_3^-	Ac	SO_3^-	2S, 6S	L–iduronic
den 6	**11**	SO_3^-	SO_3^-	SO_3^-	2S, 6S, NS	L–iduronic
den 7	**11**	SO_3^-	Ac	H	6S	D–glucuronic
den 8	**11**	SO_3^-	Ac	SO_3^-	2S, 6S	D–glucuronic

6.3.1.2   Preliminary Screen Differentiation Assay

The differentiation index was measured in satellite cell-derived primary myoblasts that had been treated with the dendritic clusters at 0.1, 1 and 10 µg/ml for 72 hours concomitant with induction to differentiation. As seen with the modified heparin HS mimetics from the previous chapter, there was a general trend for a reduction in differentiation of myoblasts treated with the HS dendritic clusters. From the preliminary screen, the dendritic clusters that appeared to have the largest effects on reducing myogenic differentiation were the disaccharide-capped clusters: dendrimer 3, dendrimer 4 and dendrimer 5 (**Figure 6.4**). The uronic acid residue (L-iduronic acid or D-glucuronic acid) did not appear to have a significant effect on myogenesis, since both dendrimer 4 and 5 (which consist of the same disaccharide unit with exception of the uronic acid residue) had comparable effects on myogenesis. There did, however, appear to be a more significant effect of HS fragment size, since disaccharide-capped dendrimer 4, produced a reduction in differentiation whereas the same concentration of tetrasaccharide-capped dendrimer 5 (1 µg/ml), produced an increase in differentiation compared to non-treated cells.
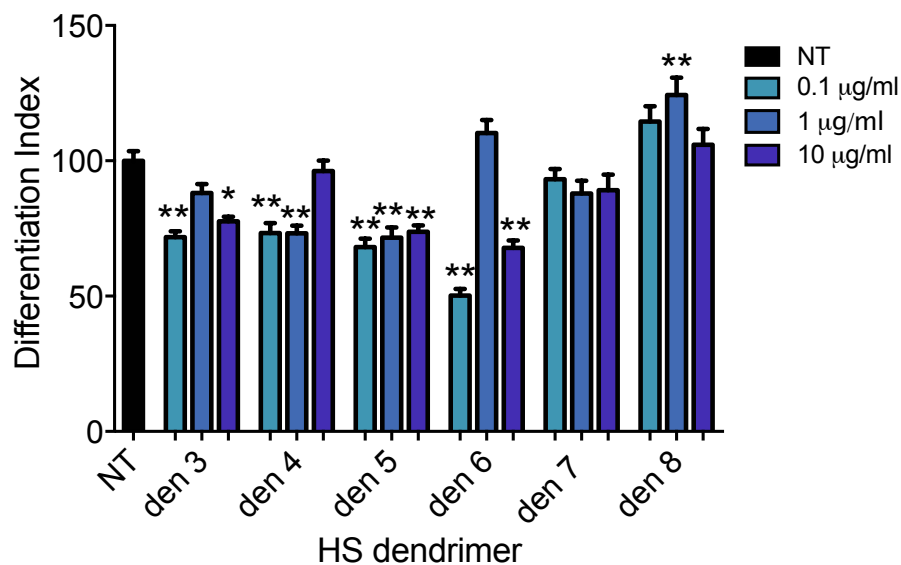
Figure 6.4 Preliminary screen of a selection of HS dendritic clusters for their effects on myoblast differentiation. Primary SC-derived myoblasts were cultured for 2 days in growth medium and then induced to differentiate for a further 3 days. The differentiation index was calculated as the percentage of nuclei in MyHC+ cells (both mono- and multi-nucleated) over the total number of nuclei (DAPI+). The average of ten images across two technical replicates ± S.E.M. was calculated and plotted normalised to the non-treated cells.

From the preliminary screen of the HS dendritic clusters, there appeared to be a general trend for a reduction in myoblast differentiation in satellite cell-derived myoblasts treated with the HS dendritic clusters. Therefore, it was hypothesised that the reduction in myoblast differentiation could be accompanied by an increase in myoblast expansion. Thus, the number of cells present after 72 hours in differentiating conditions was analysed. Dendrimer

6 had the most significant effect on increasing cell numbers in differentiating conditions at 0.1, 1 and 10 µg/ml (**Figure 6.5**). Dendrimer 3, which also reduced myogenic differentiation, produced a significant increase in myoblast cell numbers at 0.1 and 1 µg/ml, although the results were not as pronounced. Myoblasts treated with dendrimers 5, 7 or 8 presented no differences in myoblast numbers compared with non-treated cells. The most significant difference in phenotype appeared to arise from the pattern and level of sulfation, since the addition of N-sulfation, in dendrimer 6, appeared to have a marked effect on increasing myoblast numbers.
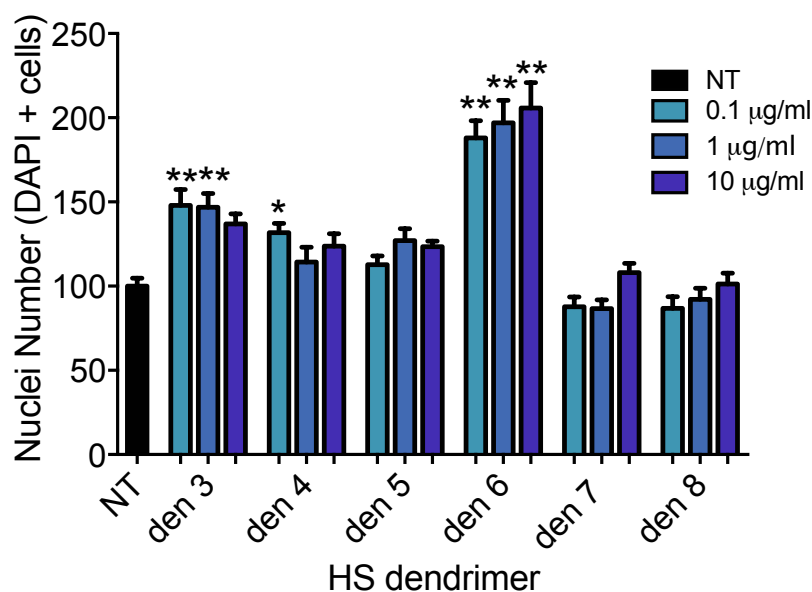
Figure 6.5 Preliminary screen of a selection of HS dendritic clusters for their effects on myoblast differentiation. Primary SC-derived myoblasts were cultured for 2 days in growth medium and then induced to differentiate for a further 3 days. The differentiation index was calculated as the percentage of nuclei in MyHC+ cells (both mono- and multi-nucleated) over the total number of nuclei (DAPI+). The average of ten images across two technical replicates ± S.E.M. was calculated and plotted normalised to the non-treated cells.

6.3.2 The Development of an N-sulfated HS Disaccharide Dendrimer Cluster

From the preliminary screen of the HS dendritic clusters tested on myogenic differentiation and myoblast cell expansion, dendrimer 6 appeared to have the most significant effects on myogenesis. Dendrimer 6 consists of a tetrasaccharide-capped-tetramer made up of iduronic acid and glucosamine disaccharide unit containing, *N*-sulfation, 6-*O*- and 2-*O*-sulfation; this represents the main disaccharide unit of heparin. From the preliminary screen, the disaccharide-capped HS clusters appeared to have the most significant effects on reducing myogenic differentiation. A dendrimer consisting of *disaccharide* tetramer is synthetically less challenging than a dendrimer consisting of a *tetrasaccharide* tetramer. Thus, we reasoned it would be useful to investigate the properties of a dendrimer consisting

of a disaccharide tetramer, with an iduronic acid residue and glucosamine containing *N*-sulfation, 6-*O*- and 2-*O*-sulfation. Furthermore, we sought to explore the effects of using a HS mimetic cluster containing a short arm dendritic core. Such a construct may produce similar effects on myogenesis as dendrimer 6, being made up of the same disaccharide unit but in disaccharide form and with the shorter-armed dendritic core. Therefore, we aimed to synthesise the appropriate target compound designated Den T (**Figure 6.6**).

Target Dendrimer
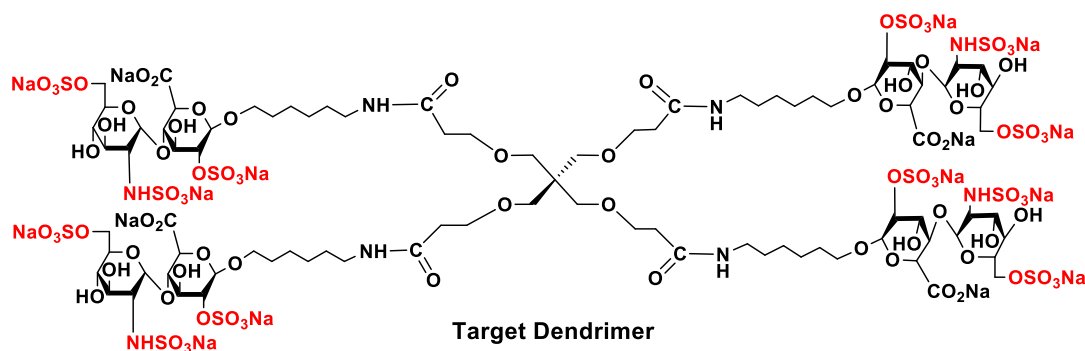
Figure 6.6 Structure of the target compound, Den T. The structure of the desired target compound based on a long-armed dendritic core end capped with HS disaccharides consisting of glucosamine and iduornic acid containing sulfation at position 2, position 6 and position N (highlighted in red).

6.3.2.1   Disaccharide Building Block

The synthesis of a wide range of the HS structural units can be achieved through just one disaccharide building block, designed to contain orthogonal protecting groups on the key structural positions (position 2, position 6 and position N), which can be selectively de-protected and sulfated. The details of the synthesis of a disaccharide building block has been previously synthesised and published (Schwörer et al., 2013). *β*-disaccharide **12** (**Figure 6.7**) contains a linker region, which is protected with an Fmoc group and can be selectively removed before coupling the disaccharide building block to the dendritic core. The disaccharide building block **12** had been previously synthesised (Tyler et al., 2015) and was kindly donated to us by Professor Tyler.

12
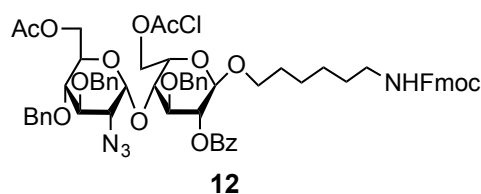
Figure 6.7 Structure of the disaccharide building block. Disaccharide building block 12 for synthesising the target dendrimer   which had been previously synthesised (Dr Olga Zubkova).

6.3.2.2   Dendritic Core

The target compound was designed based on the use of the short-armed dendritic core **13** (**Figure 6.8**). This dendritic core had been previously synthesised (Tyler et al 2015) and kindly donated to us by Professor Tyler.
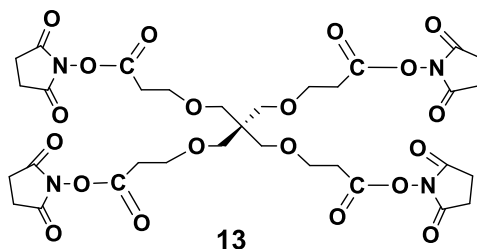
Figure 6.8 Structure of the short-armed dendritic core. The short-armed dendritic core 13 consists of a 4 armed structure which can be end-capped with HS seqeunces via the linker region. 13 had been previously synthesised and donated to us.

6.3.2.3   Partial Processing of the Disaccharide

The synthetic process for synthesising a wide range of HS dendrimers has been previously published (Tyler et al., 2015). Thus it was hypothesised that the target compound could be synthesised following a similar synthetic procedure. Prior to coupling the disaccharide to the dendritic core, the disaccharide was partially processed (**Figure 6.9**). Firstly, the chloroacetate group was selectivity removed from the disaccharide building block **12,** to expose a free hydroxyl group. The disaccharide containing a free hydroxyl group and the N-Fmoc protected linker region was then isolated as compound **13** at 78% yield. The free hydroxyl group was then oxidised to the corresponding carboxylic acid **14**, forming the basis of the iduronic acid residue. The carboxylic acid group was then re-protected as a methyl ester **15** at 66% yield, prior to coupling with the dendritic core. The methyl ester was detected by the singlet peak on the ^{1}H NMR spectra at 3.82 ppm representing 3 protons (appendix). *N*-Fmoc was then selectively removed to furnish amine **16** at 80% yield. Fmoc benzylic protons were no longer present at 7.76 and 7.59 ppm on the ^{1}H NMR spectra (appendix) in amine **16**.

120
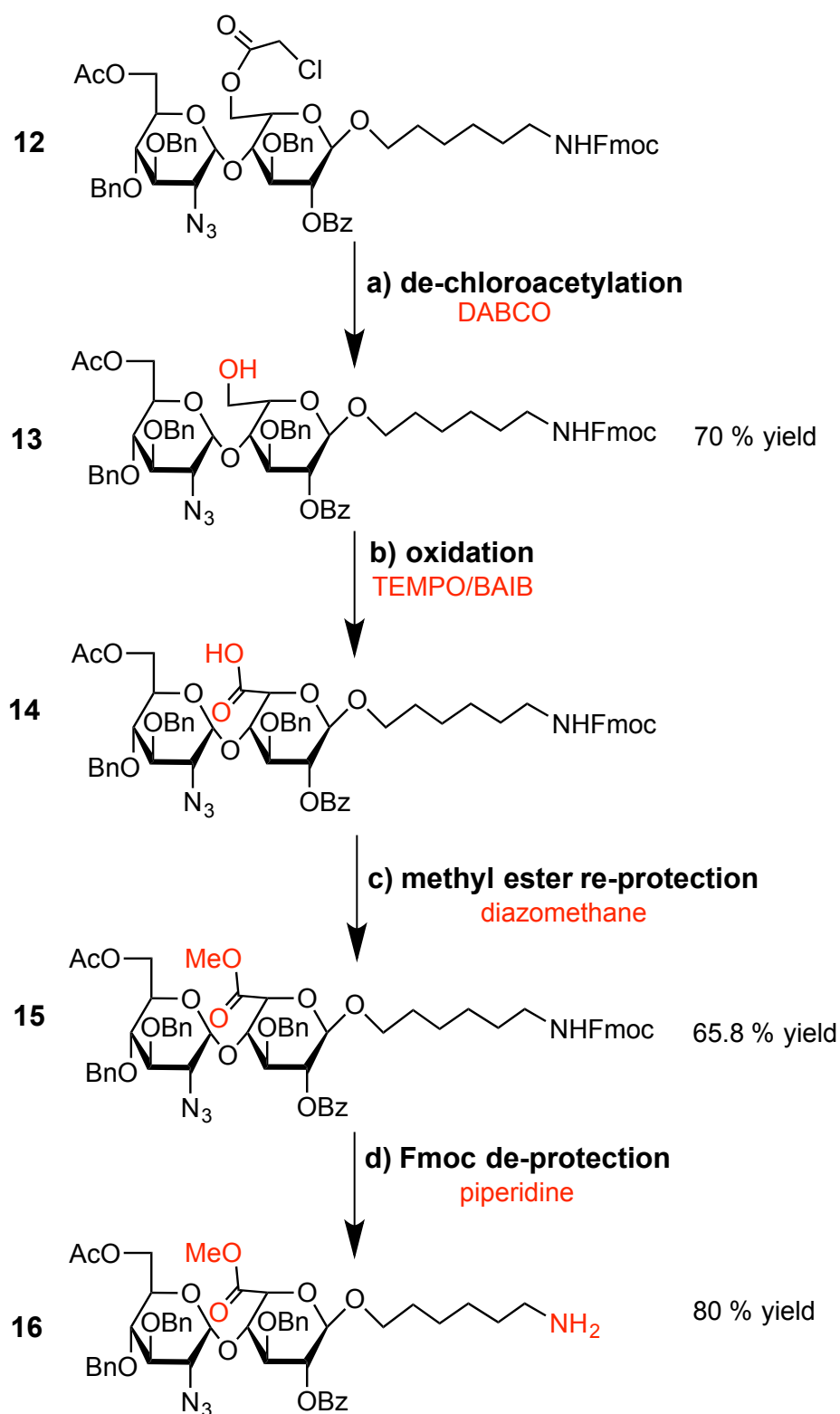
Figure 6.9 Scheme showing partial processing of disaccharide building block. a) Selective de-chloracetylation with DABCO, MeCN/EtOH, 70 °C (Appendix 2.2.1); b) Oxidation of the hydroxyl group to a carboxylic acid functional group with TEMPO, BAIB aq MeCN, RT, then c) methyl ester re-protection of the carboxylic acid with CH_2N_2, 0 °C to room temperature (Appendix 2.2.2) and finally d) *N*-Fmoc de-protection with piperidine to afford the amine (Appendix 2.2.3).

6.3.2.4   Coupling Reaction

After the disaccharide had been partially processed to afford amine **16**, it was coupled to the dendritic core **13** (**Figure 6.10**). Since the dendritic core is a tetravalent compound, four equivalents of the HS disaccharide **16** were coupled with the dendritic core **13** to afford the tetramer clusters after purification chromatography to afford the tetramer cluster **17** at 81 % yield which was confirmed by the production of the ion for $[C_{213}H_{252}N_{16}O_{60}]^{+}3H$ *m/z* 3996.72 found 3996.8 (**Appendix 2.2.4**).
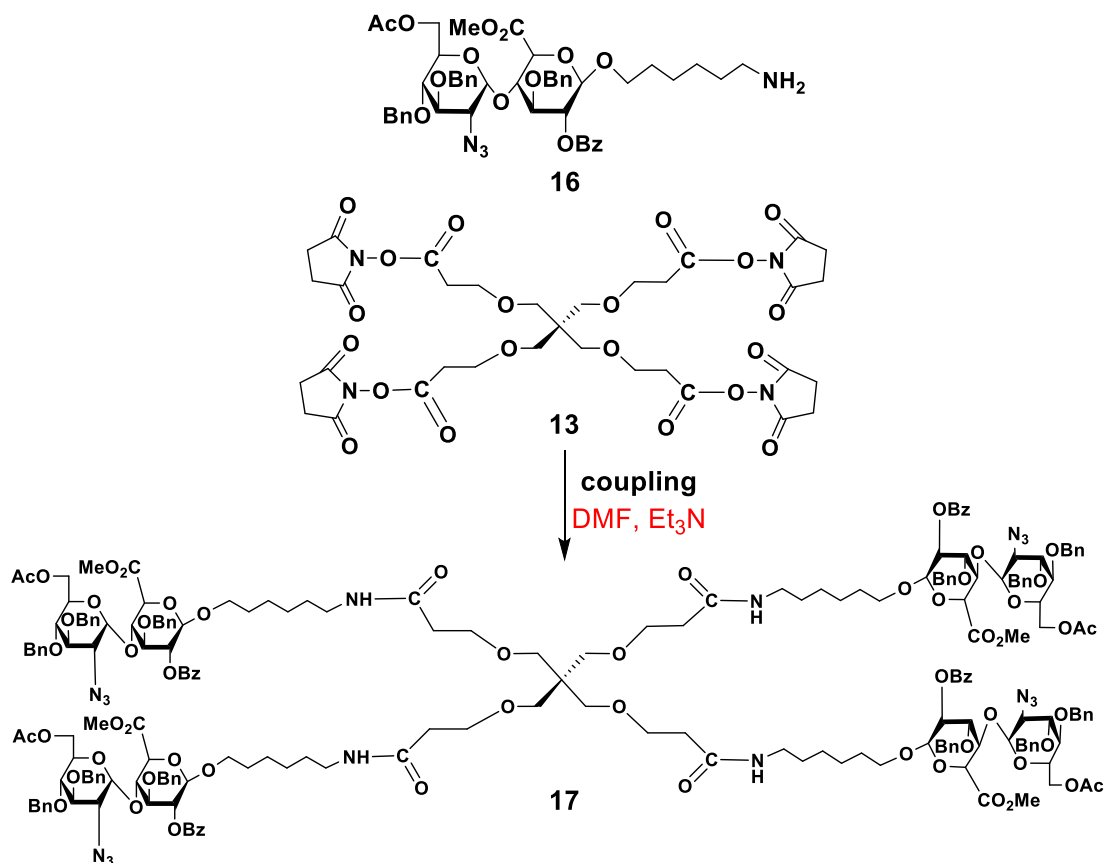
Figure 6.10 Scheme showing the formation of the disaccharide tetramer. Coupling of compound 16 to the dendritic core 13 was achieved with DMF, Et$_3$N at room temperature at 81.4 % yield (Appendix 2.2.4).

6.3.2.5   Selective Sulfation

After successfully coupling the disaccharide to the dendritic core, tetramer cluster **17** was then subjected to a series of de-protecting reactions to reveal free hydroxyl groups for subsequent sulfation steps. Sulfation reactions are repeatedly used in HS oligosaccharide synthesis. Since sulfate groups are highly negatively charged, the presence of multiple

sulfate groups produces a highly polar compound. As the compound becomes more polar, solvent choices for further chemical reactions become overly limited. Thus, it is easier synthetically to sulfate groups as the last synthetic stage in a step-wise manner; this also reduces the risk of partial-sulfation reactions. As mentioned previously, the orthogonal protecting groups present on the disaccharide unit allow for the selective de-protection and sulfation on the key positions: position 6, position 2 and position N (**Figure 6.11**) on the HS disaccharide unit.
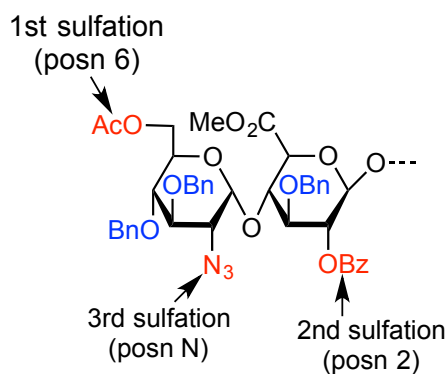
Figure 6.11 Orthogonally protected disaccharide unit. Diagram depicting the protected disaccharide unit (protecting groups highlighted in red) with the corresponding order of sulfation. The acetate group at position 6 of glucosamine is removed first, followed by removal of the benzoate group at position 2 of iduronic acid and finally the azide group at the N-position of glucosamine. The benzoylated groups (highlighted in blue) are removed to afford three free hydroxyl groups.

Tetramer cluster **17** was first subjected to acid hydrolysis to selectively remove the *O*-acetates to afford the free primary hydroxyl group (position 6) tetramer cluster **18** (59% yield), which was then subjected to the initial sulfation of the primary hydroxyl group to produce the mono-sulfated disaccharide-capped tetramer **19** (93% yield), revealing 6-*O*-sulfation on the glucosamine residue. Tetramer cluster **19** was then subjected to saponification, to simultaneously remove i) the methyl ester-protecting group (chemical shift at 3.82 ppm) to reveal the carboxylic acid and ii) the benzoate-protecting group to reveal a free hydroxyl group at position 2, furnishing **20** (95% yield). The free hydroxyl group was then sulfated at position 2 of the iduronic acid residue, to form the di-sulfated disaccharide-capped tetramer **21 (Figure 6.12)**.
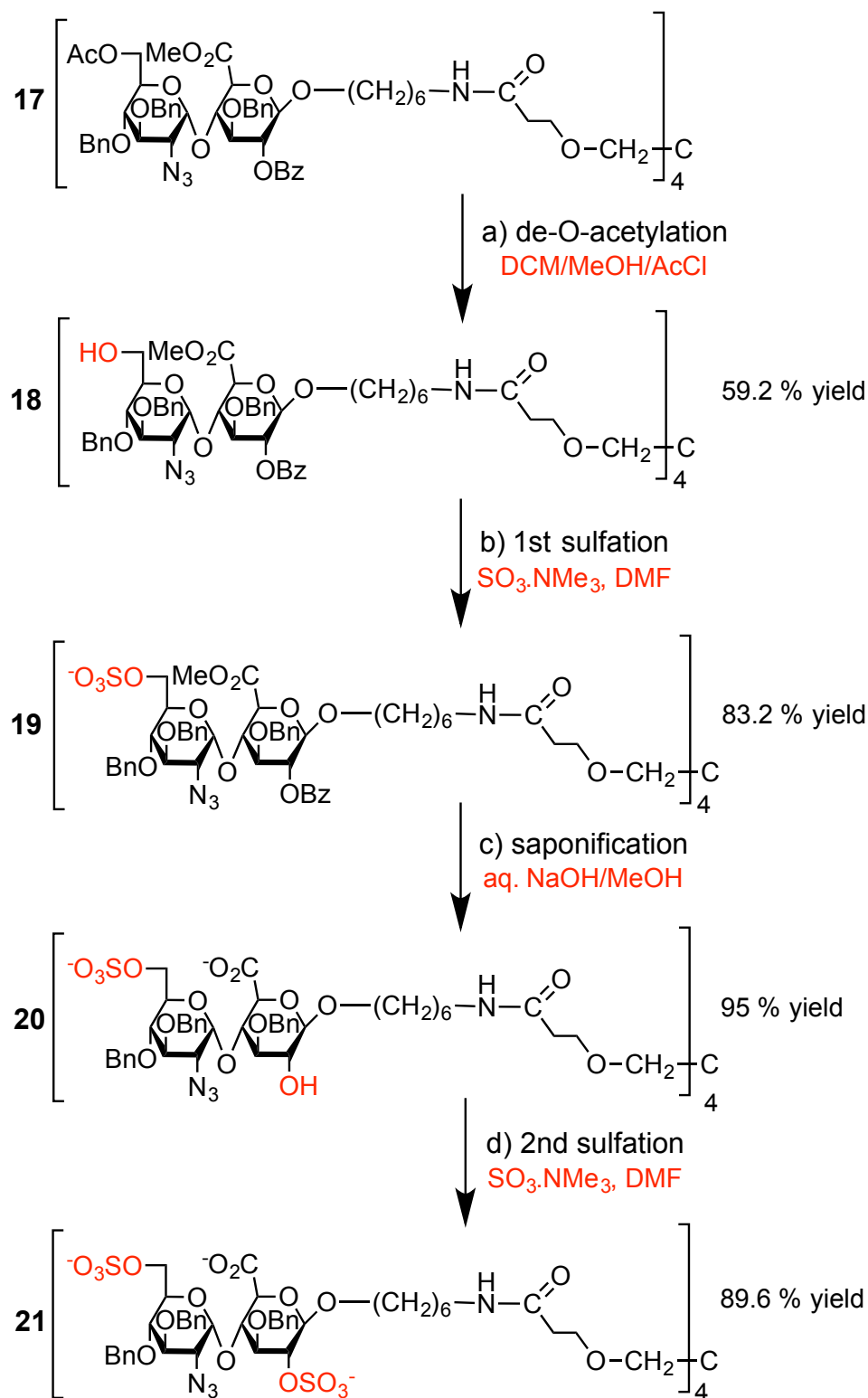
Figure 6.12 Scheme showing selective de-protection and sulfation of the disaccharide endcapped tetramer. a) Selective de-O-acetylation with DCM/MeOH/AcCl to afford free primary hydroxyl groups (Appendix 2.2.5) b) sulfation of the hydroxyl groups (at posn 6) with $SO_3.NMe_3$, DMF, H_2O, 0 °C to room temperature (Appendix 2.2.7). c) saponification to remove the benzoate group and the methyl ester protecting group with NaOH, aq. MeOH, 0 °C to room temperature (Appendix 2.2.8). d) sulfation of the hydroxyl groups (position 2) with $SO_3.NMe_3$, DMF, 0 °C to room temperature (Appendix 2.2.9). Scheme depicts one arm of the tetramer cluster.

124

Hydrogenolysis of **21**, furnished the fully de-benzylated amine **22** (80% yield)**.** Finally, **22** was subjected to selective *N*-sulfation to yield the desired target dendrimer (Den T); the tri-sulfated disaccharide capped tetramer (**Figure 6.13**).
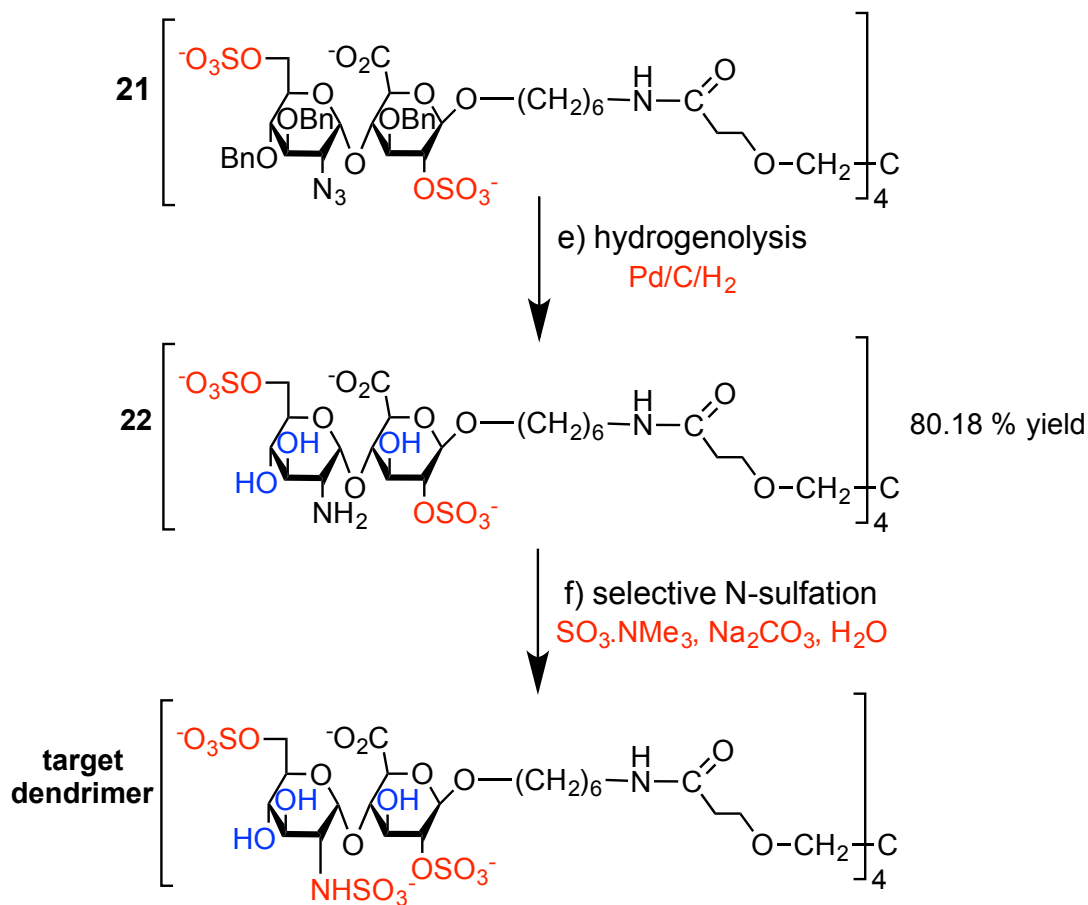
Figure 6.13 Scheme showing de-benzylation and selective *N*-sulfation of the end-capped disaccharide. e) Hydrogenolysis of the disaccharide to remove the benzyl groups and reduce the azide group to a free amine group with Pd/C/H$_2$ (Appendix 2.2.10) f) Selective *N*-sulfation was achieved with SO$_3$.NMe$_3$, H$_2$O at 0 °C to room temperature to afford the target dendrimer. Scheme depicts one arm of the tetramer cluster (Appendix 2.2.11).

However, after the initial purification, the NMR presented two distinct anomeric carbons suggesting some impurity was present after chromatography (**Figure 6.14**). From the ^{1}H NMR 65 % of the anomeric proton was identified as the *N*-sulfated product **Den T.** Therefore the target dendrimer, Den T was subjected to further purification after flash column chromatography, which finally afforded 4 mg of the target dendrimer as its sodium salt, of sufficient purity (79 %) suitable for testing in biological assays (**Figure 6.6**).
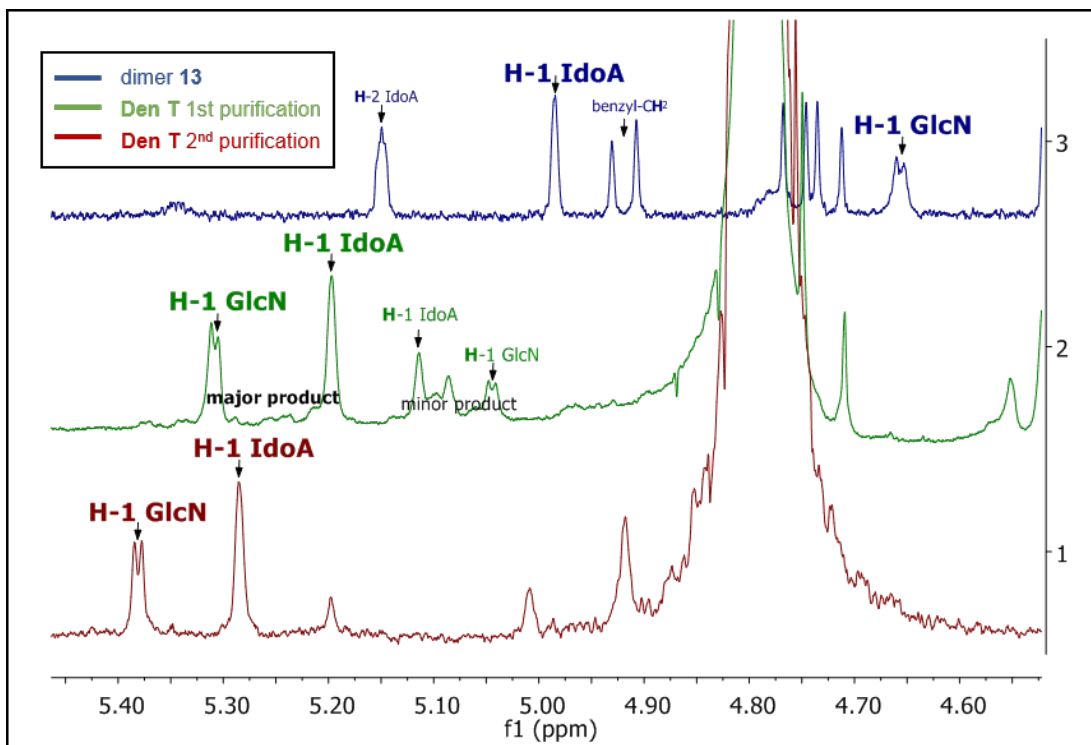
Figure 6.14 Proton NMR of anomeric regions of disaccharide 13 and Den T. (Proton NMR) shows chemical shift of anomeric protons of the glucosamine residue (H1 GlcN) and the chemical shifts of the anomeric protons of the iduronic acid residue (H1 Ido) for compound **13** (blue), for Den T after 1st purification (green) and Den T after the 2nd purification (red). The major anomeric product represents 65 % of the total material after the first purification (green). After a second purification the major anomeric product of Den T represents 79 % of the total material.

6.3.3   Effects of Dendrimer Den T on Myogenesis

To investigate the effects of the target dendrimer on myogenesis, primary satellite cell-derived myoblasts were treated with the target dendrimer (Den T), concomitant with induction to differentiation. From the preliminary screen, the largest effects on myogenesis appeared at the higher concentrations tested and thus, myoblasts were treated with the target dendrimer at 1 μg/ml, 10 μg/ml and 100 μg/ml to first investigate the effects on myoblast differentiation and cell expansion (**Figure 6.16**). At the lowest concentration tested (1 μg/ml) there were no statistically significant differences in the level of differentiation or cell number in treated myoblasts compared to non-treated cells (**Figure 6.17**). However, myoblasts treated with the target dendrimer at 10 μg/ml showed a statistically significant increase in cell number, although the level of differentiation remained unchanged. These results thus contrast with those observed with den 6 treatment (**Figure 6.4 and 6.5**). At 100 μg/ml however, there was no statistically significant differences in cell number compared to non-treated cells but a statistically significant reduction in myoblast differentiation.
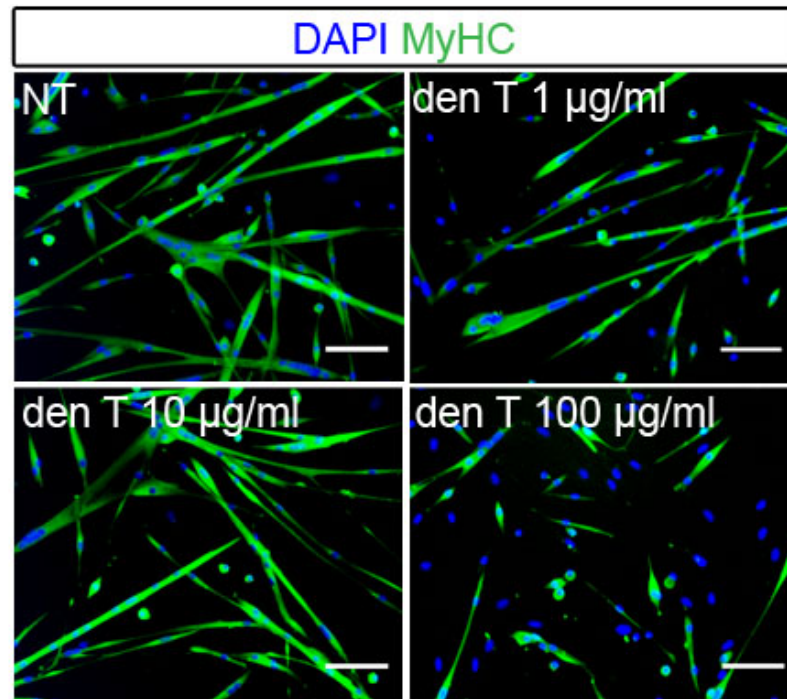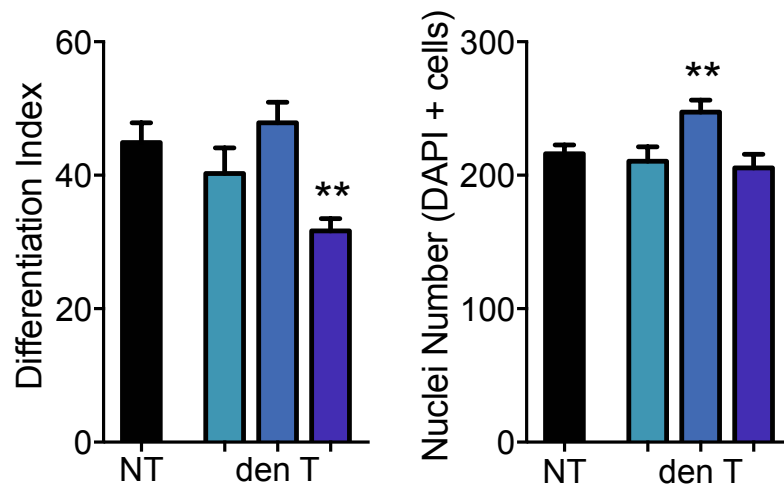
Figure 6.16 Representative images showing the concentration dependent effect of the target dendrimer on myoblast differentiation. Primary SC-derived myoblasts were cultured for 48 h and then induced to differentiate for an additional 72 h. Differentiated cells, both mono- and multi-nucleated, were identified via immuno-staining to detect myosin heavy chain (MyHC, green). Nuclei are detected with DAPI (blue). The differentiation index was calculated as the percentage of nuclei in MyHC+ cells (both mono- and multi-nucleated) over the total number of nuclei (DAPI+). The average of ten images across two technical replicates for three independent experiments ± S.E.M. is calculated and plotted. Asterisks are p-values for each condition compared to non-treated (NT) cells. ** = $p < 0.01$. Scale bar = 100 µm across all images.

Since Den T affected cell numbers and differentiation at the highest concentrations tested (10 µg/ml and 100 µg/ml) without affecting cell numbers, it was hypothesised that the level of Pax7 expression may also be affected. Satellite cell-derived myoblasts were treated with the Den T at 10 µg/ml and 100 µg/ml to test the effects on Pax7 expression (**Figure 6.18**). At 10 µg/ml there were no statistically significant differences in the level of non-differentiated cells compared to non-treated cells. However, at 100 µg/ml there was a statistically significant increase in the proportion of cells expressing Pax7 (**Figure 6.18**).
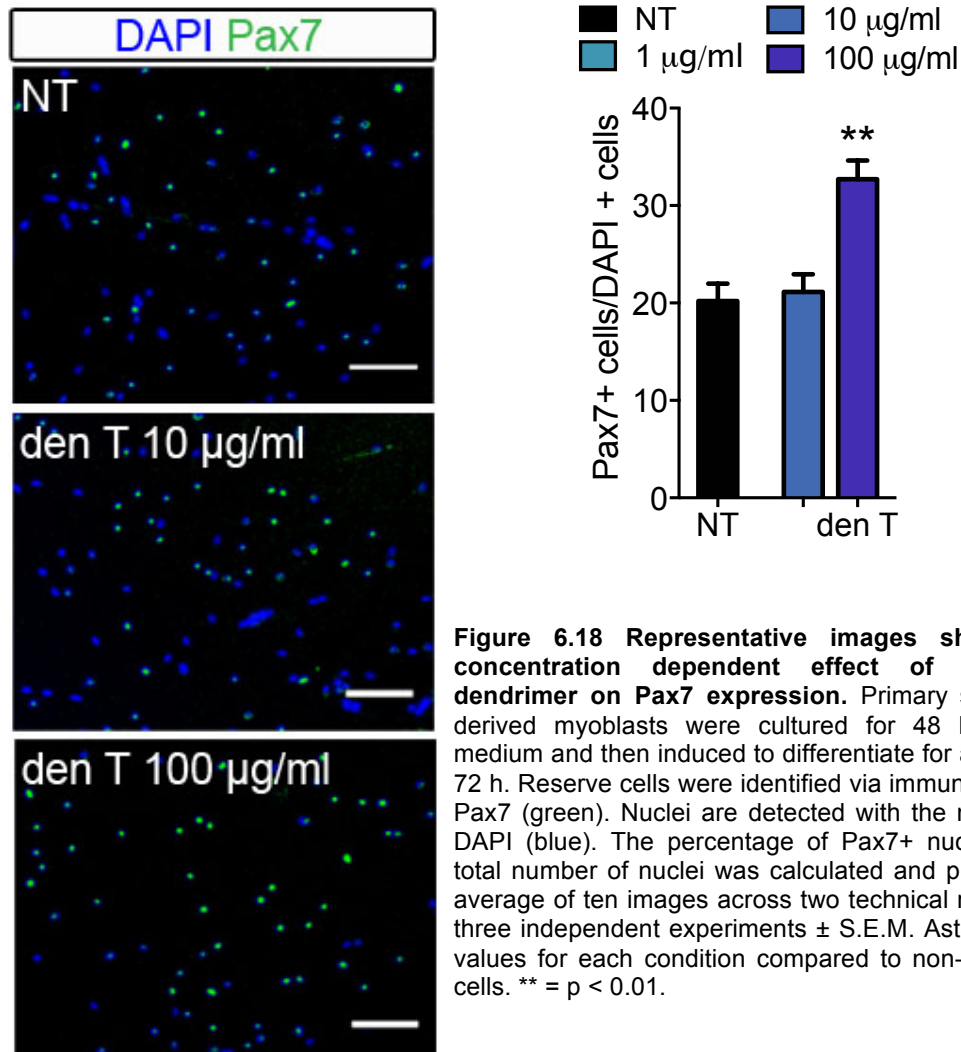
Figure 6.18 Representative images showing the concentration dependent effect of the target dendrimer on Pax7 expression. Primary satellite cell-derived myoblasts were cultured for 48 h in growth medium and then induced to differentiate for an additional 72 h. Reserve cells were identified via immunostaining for Pax7 (green). Nuclei are detected with the nuclear stain DAPI (blue). The percentage of Pax7+ nuclei over the total number of nuclei was calculated and plotted as the average of ten images across two technical replicates for three independent experiments ± S.E.M. Asterisks are p-values for each condition compared to non-treated (NT) cells. ** = $p < 0.01$.

6.4 Discussion

In this chapter, a small library of HS mimetic dendritic clusters, with differing levels and patterns of sulfation, were tested on primary myoblasts for their effects on differentiation and myoblast expansion. The ability of the HS mimetic clusters to inhibit the BACE-1 protease has been reported (Tyler et al., 2015), but thus far, the HS mimetic clusters have not been widely investigated in further HS-mediated biological processes. Tetrasaccharide end capped-HS mimetic clusters have displayed a similar potency in their ability to inhibit BACE-1, to the most potent longer saccharide sequences (up to dodecasaccharides) of a similar structural sequence (Tyler et al., 2015), suggesting that they could be useful therapeutic approaches in other HS-mediated signalling events. Since I have shown in the previous chapter (Chapter 5) that HS mimetics differentially affect myogenesis, it was hypothesised that HS mimetic clusters might also affect myogenesis depending on their structure. Out of the six HS mimetic clusters tested, four appeared to have significant effects on myogenesis. Notably, dendrimer 6, consisting of the most common disaccharide unit of heparin, had the greatest effect on increasing myoblast cell numbers and also led to a reduction in differentiation which corresponds to the same phenotype as myoblasts treated with heparin. Dendrimer 3 and dendrimer 5, which are made up of the same disaccharide units of HS mimetic 5 and HS mimetic 2 respectively, led to comparable phenotypes on myogenesis suggesting that the HS mimetic clusters are able to mimic the longer HS mimetic equivalents.

A new HS mimetic cluster, Den T, was synthesised, consisting of the most common disaccharide unit of heparin, in which the 'long-armed' dendritic core was replaced with a 'short-armed' dendritic core (Tyler et al., 2015) to explore the effects of the dendritic core size and its affect on myogenesis. Overall, Den T had less of an effect on both myogenic differentiation and myoblast numbers compared to dendrimer 6, suggesting that the tetrasaccharide-capped 'long-armed' tetramer displays a higher level of potency than the disaccharide capped 'short-armed' equivalent. It has previously been reported that the HS mimetic clusters with the 'long-armed' dendritic cores displayed higher potencies than HS mimetic clusters with the 'short-armed' dendritic core in their ability to inhibit BACE-1 (Tyler et al., 2015). Our results support these findings that the size of dendritic core is an important factor in determining the biological potency of the HS mimetic cluster, since significant effects of Den T on myogenesis were only observed at high concentrations (100 µg/ml). At this concentration, the level of myoblast differentiation was reduced, cell number was unaffected and there were a significantly higher proportion of cells expressing Pax7.

During ageing, the numbers of quiescent satellite cells expressing Pax7 decrease leading to reduced regenerative potential (Brack et al., 2005; Dedkov et al., 2003; Gibson and Schultz, 1983; Shefer et al., 2006). Thus, it is interesting to speculate that a compound, such as Den

T, which leads to an increase in reserve-cell generation, might prove useful as a potential therapeutic strategy for muscle wasting during ageing. However, the mechanisms by which they function remain unknown. From the previous chapter it was shown that HS mimetics modulate myogenesis partly by their ability to support or repress FGF2 signalling affecting myoblast proliferation and differentiation. In contrast, it has previously been reported that HS mimetic clusters do not support FGF signalling by FGF-1 or FGF-2 via the FGF receptor 1 at concentrations up to 10 µg/ml (Tyler et al., 2015). Thus, Den T might be inhibiting FGF signalling or alternatively be affecting an alternative-signalling pathway other than FGF2 signalling, which inhibits differentiation. Den T has not been tested for its effects on FGF2 signalling and thus cannot yet be ruled out as a target. Therefore, future directions may involve studying the signalling pathways that are affected by the HS mimetic clusters during myogenesis.

Previous investigations into GAG mimetics, known as regenerating agents (RGTAs), as therapeutic targets for muscle injury were undertaken; they were developed to 're-model' the extracellular satellite-cell niche and provide a matrix for increased growth factor signalling by preventing their proteolysis and promoting angiogenesis, allowing for prolonged muscle regeneration (Meddahi et al., 2002b; Rouet et al., 2005). Furthermore, they significantly alter the GAG species produced during myogenesis of C2C12 myoblasts (Barbosa et al., 2005), suggesting there may be further indirect effects on HS-mediated signalling events. Although this has not been explicitly investigated here, it may represent an additional mechanism behind the effects observed with dendrimer treatments. However, in an ageing environment, increased growth factor signalling may lead to an increase in the number of satellite cells breaking quiescence, accelerating satellite-cell depletion and thus reducing their regenerative potential further. Moreover, increasing the level of multiple heparin-binding growth factor signalling events might lead to many off-target effects. Thus, the HS mimetic clusters may present themselves as potential new therapeutic agents with fewer off-target effects, since have been found not to support FGF2 signalling, and they do not exhibit anticoagulant activity. An additional benefit to the HS mimetic clusters is that their synthesis is greatly simplified compared to longer oligosaccharide syntheses. Thus many different structures can be synthesised from the same starting materials allowing for easy optimisation of highly defined and controllable structures.

Chapter 7

7   General Discussion

Heparan sulfate is a dynamic, structurally complex biomolecule that regulates multiple biological processes due to its ability to bind numerous proteins and facilitate many growth factor signalling pathways (Turnbull et al., 2001). Heparan sulfate proteoglycans constitute a key component of the satellite cell niche (Brandan and Gutierrez, 2013; Cornelison et al., 2001; Cornelison et al., 2004; Pisconti et al., 2010). In skeletal muscle, interactions between the satellite cell and the extracellular environment are a critical factor for determining satellite cell fate (Barberi et al., 2013; Conboy and Rando, 2002; Le Grand et al., 2009; Shea et al., 2010; Urciuolo et al., 2013). Satellite cell dysregulation and depletion during ageing is largely attributed to the alterations in the extracellular environment, including changes in growth factor signalling (Chakkalakal et al., 2012; Yousef et al., 2015). However, the role of the HS structural component of the satellite cell niche during myogenesis in the absence of injury or during ageing in muscle has been largely unexplored. In this study, we aimed to advance our understanding of the HS structural component of the satellite cell niche and its role in regulating myogenesis.

We have found that the structure of HS changes during myogenic differentiation and during ageing in skeletal muscle, and these changes are associated with altered FGF2 signalling. Others have also reported more recently, that the structure of HS is altered during muscle regeneration and is associated with altered growth factor signalling (Chevalier et al., 2015), further supporting our findings that the structure of HS is a critical signalling component of the satellite cell niche in the regulation of myogenesis. This study demonstrates that there is an overall increase in the level of HS sulfation during myoblast differentiation, which fails to promote FGF2-induced mitogenic activity. One explanation for this could be that the more highly sulfated HS sequesters FGF2 away from the cell surface FGF receptor. A further explanation is that the increased sulfation is present in patterns not compatible with promoting FGF2 signalling. Since FGF2 signalling is a potent inhibitor of myoblast differentiation, it is possible to speculate that the more highly sulfated HS from differentiating myoblasts indirectly permits myogenic differentiation by preventing FGF2 signalling (**Figure 7.1**). In contrast, HS from proliferating myoblasts is associated with an increase in HS-dependent FGF2 induced mitogenic activity, suggesting that the HS supports formation of

the quaternary FGF2-FGFR-HS complex, and thus supports myogenic proliferation whilst inhibiting myogenic differentiation (**Figure 7.1**).
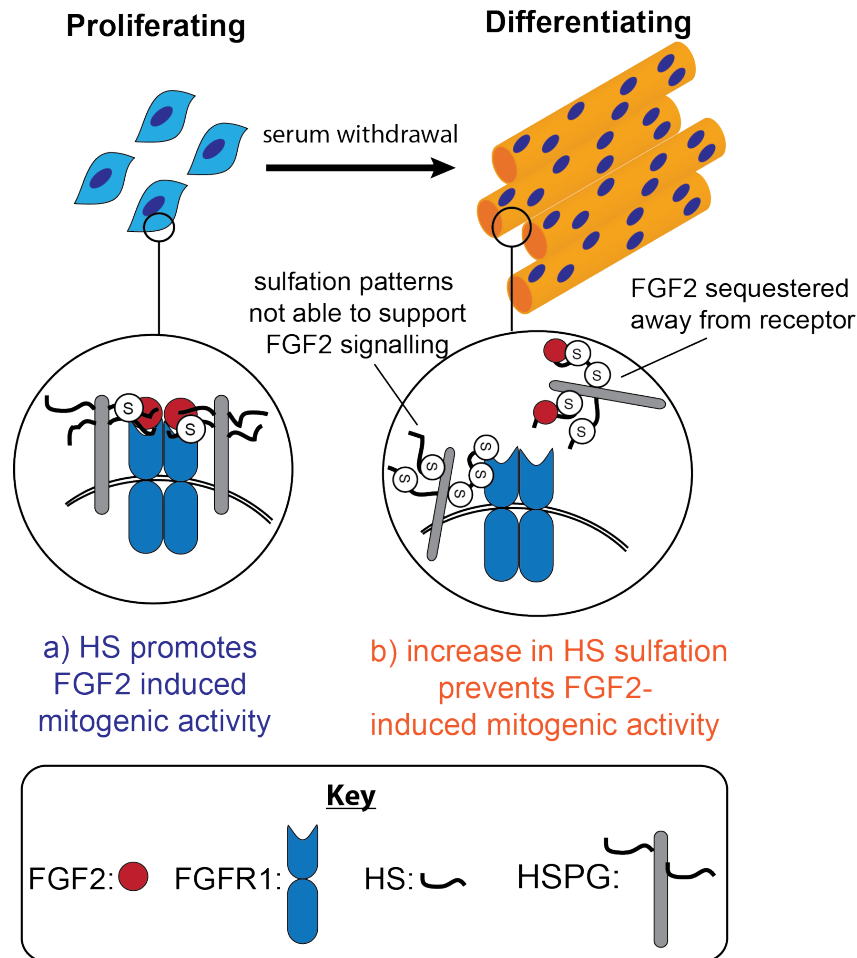
Figure 7.1 Structural Changes in HS During Myoblast Differentiation. a) HS extracted from proliferating myoblasts in culture promotes FGF2-induced mitogenic activity thus inhibiting myoblast differentiation b) Serum reduction leads to induction of myoblast differentiation. HS extracted from differentiated myoblast cultures shows a higher level of sulfation, which does not promote FGF2 signalling, thus supporting myoblast differentiation, likely via a number of potential mechanisms.

Interestingly, the HS present in uninjured ageing muscle is associated with an increase in FGF2 induced mitogenic activity compared to the HS from younger muscle, yet the level of HS sulfation in muscle during ageing does not change. Instead, in ageing muscle, there is an overall increase in the level of HS 6-*O*-sulfation compared to the HS from younger muscle. It is established that HS 6-*O*-sulfation is important for supporting FGF2 signalling (Pye et al., 1998). This study suggests that HS with higher levels of 6-*O*-sulfation from the ageing muscle promotes FGF2-induced mitogenic activity more than HS from younger muscle, which partly inhibits FGF2-induced mitogenic activity. A reduction in C2C12 myoblast HS 6-*O*-sulfation was also associated with reduced levels of myoblast proliferation further supporting our findings that an increase in 6-*O*-sulfation leads to increased levels of satellite cell proliferation. Thus, we speculate that the HS from young muscle, with lower levels of 6-

O-sulfation, is a contributory factor to maintaining satellite cells in a non-proliferative state and thus conserving the quiescent satellite cell pool available for muscle growth and regeneration (**Figure 7.2**). Our findings also support those that demonstrate that 6-*O*-sulfation is an important regulator of FGF2 signalling in many biological processes (Ferreras et al., 2012; Higginson et al., 2012; Huynh et al., 2012a; Lamanna et al., 2008; Seffouh et al., 2013; Sugaya et al., 2008).

A notable result obtained in this study is that FGF2 signalling can be similarly affected with distinct structural changes in HS. This supports the case that there is some structural redundancy in the ability of HS to support a specific type of growth factor interaction (Catlow et al., 2003; Guimond et al., 2009b; Rudd et al., 2010). In this example, our data indicate that there is more than one type of structural modification of HS that affects HS-dependent FGF2 signalling. Structural redundancies in HS likely permit combinations of a wider range of HS-interactions adding to its structural complexity and functional possibilities. This may be of significance in the regulation of muscle stem cell homeostasis where a number of other heparin-binding growth factor signalling pathways are involved (Gill et al., 2010; Sheehan and Allen, 1999; Shefer and Benayahu, 2012), and thus the difference in HS structural composition is likely a reflection of the different functional requirements of HS. In the first instance described, the HS analysed was extracted from a largely pure population of myoblasts, whereas in the second instance, the HS analysed was extracted from whole muscle, which is made up of multiple cell types. The number of muscle-resident fibroblasts significantly increase during ageing (Brack et al., 2007). Since the structure of HS is cell-type specific, it is possible that an increase in the number of resident fibroblasts leads to an altered structure of HS present in the whole muscle. However, the increase in HS 6-*O*-sulfation is already apparent in muscles of 1 year-old mice and is comparable to the HS from muscles of 2 year-old mice, yet there are significantly more fibroblasts (Brack et al., 2005). This suggests that the structure of HS is altered in myoblasts during ageing, since there is an increase in HS 6-*O*-sulfation when there is not considerable fibrosis (Brack et al., 2005). It has recently been demonstrated that myogenic progenitor cells (activated satellite cells) present in the extracellular matrix surrounding myofibres, inhibit ECM deposition by fibrogenic cells (Fry et al., 2017). Thus, it is possible that an altered HS structure in ageing myoblasts might also play a role in their interaction with interstitial fibrogenic cells and ECM production. It has previously been reported that high levels of HS 6-*O*-sulfation are present in idiopathic pulmonary fibrosis, which is associated with high levels of fibrosis in the lungs (Lu et al., 2014). Silencing of HS6ST1 in primary lung fibroblasts *in vitro* leads to a decrease in ECM deposition in response to TGF-β stimulation (Lu et al., 2014). TGF-β is well known to promote muscle fibrosis (Border and Noble, 1994; Li et al., 2004) and thus the increase in 6-*O*-sulfation in the muscle of aged mice might also contribute to the increase in muscle fibrosis ECM deposition that is associated with ageing muscle. However, further studies would be required to investigate the precise cell type origin of the structural changes of HS

during ageing in skeletal muscle and the effects on neighbouring cells present in the satellite cell niche.
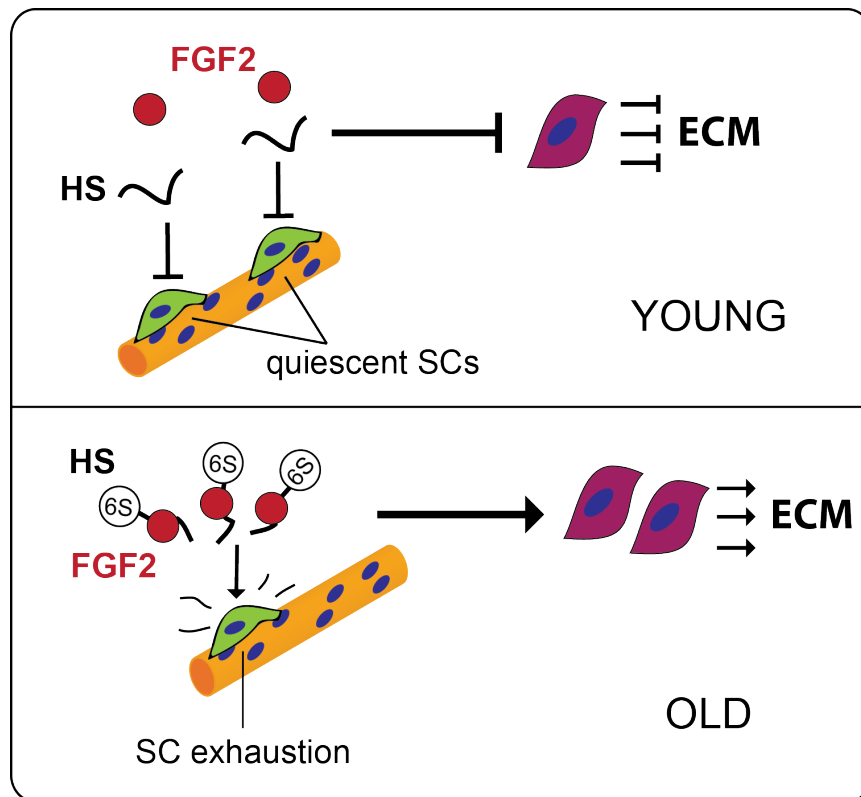
Figure 7.2 The effects of an increase in 6-*O*-sulfation on myogenesis during ageing. Schematic representing the potential effects of an increase in muscle HS 6-*O*-sulfation during ageing; a) the increase in HS 6-*O*-sulfation in ageing muscle leads to an increase in FGF2 myoblast proliferation which in turn might contribute to the reduction in SC self-renewal in ageing muscle b) an increase in 6-*O*-sulfation has also been related to increased levels of fibrosis (Lu et al., 2014) and thus may play a part in skeletal muscle leading to increased ECM deposition by fibrogenic cells (purple cells in Fig 7.2)

Furthermore, we have shown that different structures of both chemically modified heparin HS mimetics and fully synthetic HS mimetic clusters are capable of modulating myogenesis. We have demonstrated that modified heparin HS mimetics differentially affect myogenesis in part by differences in their abilities to support FGF2 signalling. Specifically, an increase in the level of sulfation using HS mimetic 1 (oversulfated heparin) treatment is associated with reduced FGF2 induced myoblast proliferation associated with inhibition of Erk1/2 activation. This is consistent with our previous observation that the more highly sulfated HS from differentiating myoblasts exhibits reduced FGF2 signalling inhibiting myogenic differentiation whilst permitting proliferation. Since it has previously been reported that oversulfated heparin binds FGF2 (Uniewicz et al., 2010), we propose that HS mimetic 1 prevents endogenous HS-dependent FGF2 signalling by binding to FGF2 and sequestering it away from the cell surface FGF receptor (**Figure 7.3**). HS mimetic 2 (with reduced sulfation; 2S, 6S and NS)

treatment, on the other hand, is associated with increased FGF2 induced myoblast proliferation associated with sustained Erk1/2 activation (**Figure 7.3**). Thus we propose that HS mimetic 2 supports the formation of the FGF2-FGFR1 quaternary complex, and thus exceeds the amount of endogenous HS-dependent FGF2 signalling. In contrast, the HS mimetic clusters do not support FGF2 signalling; yet can differentially effect myoblast differentiation, expansion and the number of Pax7+ undifferentiated cells (*bona fide* reserve cells) (**Figure 7.3)**. This suggests that the HS mimetic clusters affect myogenesis via alternative signalling pathways, which provides avenues for future experiments.

A problem for many cell therapies involving myoblast transplantation to promoted muscle repair, is that the majority proliferate whilst a small sub-population of cells divide slowly, which contribute more extensively to muscle repair (Beauchamp et al., 1999; Ono et al., 2012). Thus, it is interesting to consider the use of HS mimetic clusters in cell-based therapies for myoblast transplantations. A compound that inhibits differentiation whilst not greatly affecting proliferative capacity could be highly beneficial for maintaining satellite cells in a resting state prior to transplantation (Briggs and Morgan, 2013). Overall, HS mimetic clusters are synthetically accessible and a wide range of structures can be synthesised from the same starting materials. They can be produced at a high level of purity and display no anticoagulant activity. HS mimetic clusters are thus potential candidates in clinical applications because of their ability to mimic longer chains of HS whilst potentially presenting fewer off-target effects.

a) HS mimetic 2 promotes FGF2 induced myoblast proliferation

differentiation

b) Oversulfated HS mimetic 1 inhibits FGF2 induced myoblast proliferation

proliferation

c) HS mimetic cluster Den T reduces myoblast differentiaion

Erk

MYOBLAST

?

differentiation

Key

FGF2:   FGFR1:   HS: HSPG:

HS tetramer cluster: phospho Erk1/2:
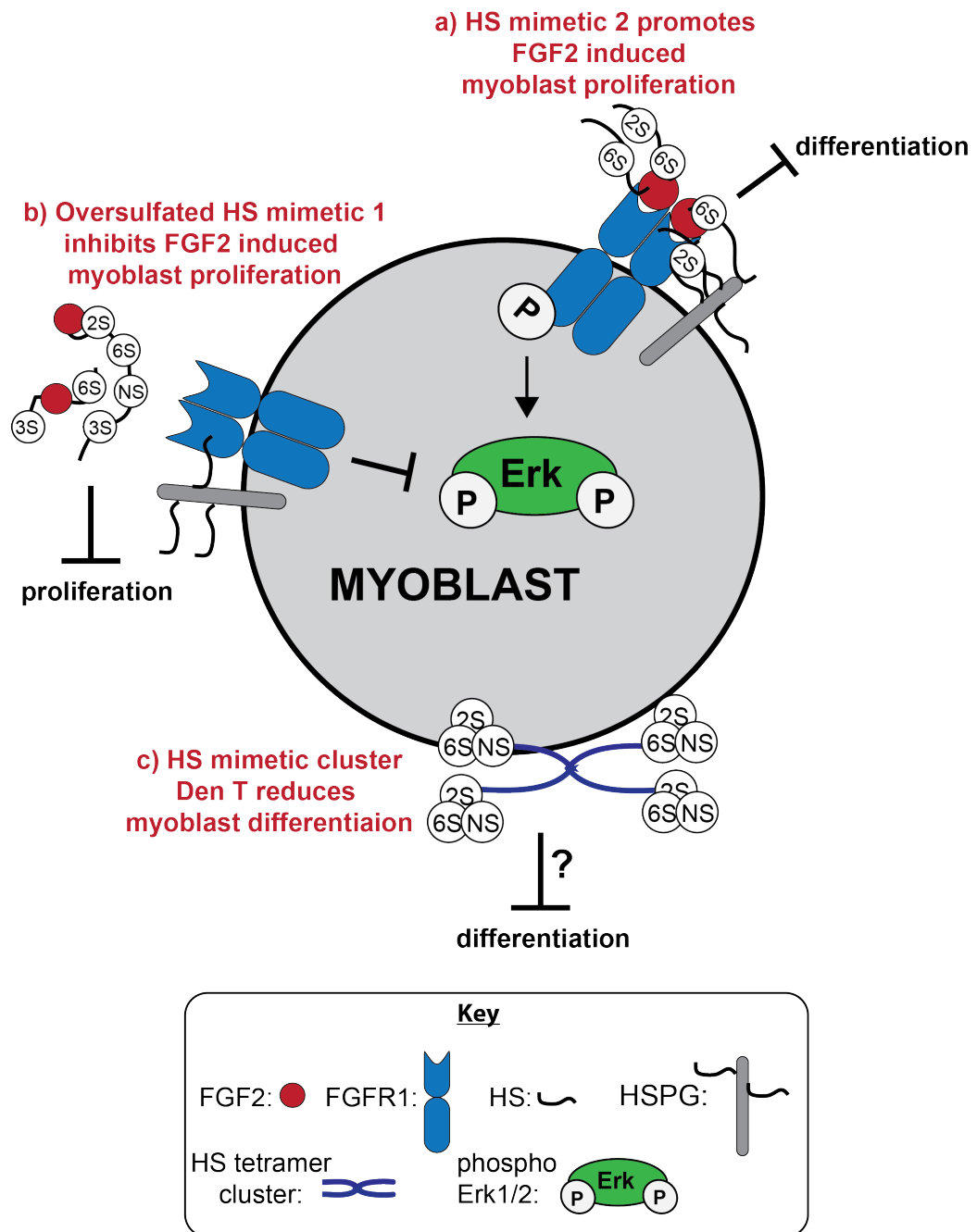
Figure 7.3 Summary of effects of HS mimetics on myogenesis. Schematic summarising the effects of HS mimetics on myogenesis. a) N-acetylated heparin, (HS mimetic 2), leads to prolonged FGF2 induced Erk1/2 activation and increased proliferation b) oversulfated heparin (HS mimetic 1) represses FGF2 induced Erk1/2 activation and decreased proliferation and c) a newly synthesised tetramer cluster, Den T, leads to a reduction in myoblast differentiation at high concentrations although the mechanisms by which it acts, remain unknown.

7.1   Future Directions

Overall this study provides a bridge between the satellite cell field and the HS field by highlighting the importance of the structure of the HS component in satellite cell regulation and in muscle during ageing. This study has also provided an indication of potential novel therapeutic strategies for muscle ageing and further implicates HS clusters as easily accessible, synthetic HS mimetics. However, this project has also opened up avenues for further research questions such as: what regulates the structural changes of HS during ageing in muscle? What other signalling pathways are affected by the change in HS during myogenesis and in ageing? Can the ageing muscle phenotype be rescued with HS from young muscle or HS mimetics?

Understanding how and why the structure of HS is regulated remains a significant challenge in the HS field. In this project, we investigated the transcript expression levels of the HS biosynthetic and remodelling enzymes in an attempt to elucidate the origin of the structural changes in HS observed during ageing. However, the increase in HS 6-*O*-sulfation in ageing muscle did not correspond to the expression levels of the 6-*O*-sulfation modifying enzymes. Therefore, further experiments to evaluate their protein levels and to better understand the activity of HS biosynthesis enzymes, and their regulation, is required. Moreover, future experiments might involve investigating the effects of increased FGF2 signalling on the structure of HS in skeletal muscle. Transgenic mice either overexpressing or with conditional knockouts of the HS biosynthetic enzymes might provide further information into the effects of specific HS structural modifications on muscle during ageing.

Considering the structural impact of HS sulfation, it has previously been demonstrated that an increase in 6-*O*-sulfation has the least dramatic effect on the structural conformation of HS chains. Thus it is interesting that we and others have found that changes in the level of 6-O-sulfation have a significant biological outcome, suggesting that direct interactions of 6-*O*-sulfate groups with protein targets may be crucial. Therefore, future experiments may be designed to better understand the structural importance of HS 6-*O*-modifications on its functional activity. Moreover, further investigations would be required to unravel other HS-dependent signalling pathways that might be affected by the change in structure of HS during ageing. For example, investigating the effects of 6-*O*-sulfation on TGF- β signalling in fibrosis in muscle would be important.

Since previous findings have demonstrated that the ageing muscle phenotype can be rescued by engrafting old muscle in a young muscle environment (Carlson and Faulkner, 1989), it is interesting to speculate that HS from young muscle might improve the phenotype in ageing muscle. Thus, future experiments could involve *in vivo* assays treating young mice with HS from old muscle and *vice versa*. In this way we could better elucidate the effects of

the structural changes of HS during ageing on the skeletal muscle phenotype. *In vitro* assays could further investigate this by culturing myoblasts lacking endogenous HS in the presence of HS from young and aged muscle. To further investigate the effects of the increase in HS 6-*O*-sulfation during ageing in muscle, reserve-cell generation assays could be employed to explore the effects of structural changes of HS observed during ageing in muscle on satellite cell self-renewal. Finally, to validate the hypothesis that a compound that leads to an increase in the level of reserve-cell generation could improve the muscle phenotype during ageing, Den T could be used *in vivo* on ageing mice.

7.2   Concluding Remarks

The studies in this thesis have demonstrated that:

- myogenic differentiation is associated with an increase in the level of HS sulfation in primary myoblasts isolated from young muscles and in the C2C12 myoblast cell line
- there is a specific increase in HS 6-*O*-sulfation in skeletal muscle during ageing and that this might be a significant contributory factor to satellite cell depletion during ageing
- the HS component of the satellite cell niche is able to modulate myogenesis partly through its ability to support HS-dependent FGF2 signalling.
- successful synthesis of a new HS mimetic cluster, Den T, which may have application as a novel therapeutic agent to enhance satellite cell self-renewal

References

Aamiri, A., Mobarek, A., Carpentier, G., Barritault, D., Gautron, J., 1995. [Effects of substituted dextran on reinnervation of a skeletal muscle in adult rats during regeneration]. C R Acad Sci III 318, 1037-1043.

Ai, X., Do, A.T., Kusche-Gullberg, M., Lindahl, U., Lu, K., Emerson, C.P., 2006. Substrate specificity and domain functions of extracellular heparan sulfate 6-O-endosulfatases, QSulf1 and QSulf2. J Biol Chem 281, 4969-4976.

Aikawa, J., Esko, J.D., 1999. Molecular cloning and expression of a third member of the heparan sulfate/heparin GlcNAc N-deacetylase/ N-sulfotransferase family. J Biol Chem 274, 2690-2695.

Aizawa, S., Mitsui, Y., Kurimoto, F., Matsuoka, K., 1980. Cell-surface changes accompanying aging in human diploid fibroblasts: effects of tissue, donor age and genotype. Mech Ageing Dev 13, 297-307.

Allbrook, D.B., Han, M.F., Hellmuth, A.E., 1971. Population of muscle satellite cells in relation to age and mitotic activity. Pathology 3, 223-243.

Allen, B.L., Rapraeger, A.C., 2003. Spatial and temporal expression of heparan sulfate in mouse development regulates FGF and FGF receptor assembly. The Journal of cell biology 163, 637-648.

Alsharidah, M., Lazarus, N.R., George, T.E., Agley, C.C., Velloso, C.P., Harridge, S.D., 2013. Primary human muscle precursor cells obtained from young and old donors produce similar proliferative, differentiation and senescent profiles in culture. Aging Cell 12, 333-344.

Alvarez, K., Fadic, R., Brandan, E., 2002. Augmented synthesis and differential localization of heparan sulfate proteoglycans in Duchenne muscular dystrophy. J Cell Biochem 85, 703-713.

Arrington, C.B., Yost, H.J., 2009. Extra-embryonic syndecan 2 regulates organ primordia migration and fibrillogenesis throughout the zebrafish embryo. Development 136, 3143-3152.

Arungundram, S., Al-Mafraji, K., Asong, J., Leach, F.E., Amster, I.J., Venot, A., Turnbull, J.E., Boons, G.J., 2009. Modular synthesis of heparan sulfate oligosaccharides for structure-activity relationship studies. J Am Chem Soc 131, 17394-17405.

Ashikari-Hada, S., Habuchi, H., Kariya, Y., Itoh, N., Reddi, A.H., Kimata, K., 2004. Characterization of growth factor-binding structures in heparin/heparan sulfate using an octasaccharide library. J Biol Chem 279, 12346-12354.

Asundi, V.K., Keister, B.F., Stahl, R.C., Carey, D.J., 1997. Developmental and cell-type-specific expression of cell surface heparan sulfate proteoglycans in the rat heart. Exp Cell Res 230, 145-153.

Baldwin, R.J., ten Dam, G.B., van Kuppevelt, T.H., Lacaud, G., Gallagher, J.T., Kouskoff, V., Merry, C.L., 2008. A developmentally regulated heparan sulfate epitope defines a subpopulation with increased blood potential during mesodermal differentiation. Stem Cells 26, 3108-3118.

Barberi, L., Scicchitano, B.M., De Rossi, M., Bigot, A., Duguez, S., Wielgosik, A., Stewart, C., McPhee, J., Conte, M., Narici, M., Franceschi, C., Mouly, V., Butler-Browne, G., Musarò, A., 2013. Age-dependent alteration in muscle regeneration: the critical role of tissue niche. Biogerontology 14, 273-292.

Barbosa, I., Garcia, S., Barbier-Chassefiere, V., Caruelle, J.P., Martelly, I., Papy-Garcia, D., 2003. Improved and simple micro assay for sulfated glycosaminoglycans quantification in biological extracts and its use in skin and muscle tissue studies. Glycobiology 13, 647-653.

Barbosa, I., Morin, C., Garcia, S., Duchesnay, A., Oudghir, M., Jenniskens, G., Miao, H.Q., Guimond, S., Carpentier, G., Cebrian, J., Caruelle, J.P., van Kuppevelt, T., Turnbull, J., Martelly, I., Papy-Garcia, D., 2005. A synthetic glycosaminoglycan mimetic (RGTA) modifies natural glycosaminoglycan species during myogenesis. J Cell Sci 118, 253-264.

Baumann, K., 2012. Stem cells: An ageing decline. Nat Rev Mol Cell Biol 13, 681.

Beauchamp, J.R., Morgan, J.E., Pagel, C.N., Partridge, T.A., 1999. Dynamics of myoblast transplantation reveal a discrete minority of precursors with stem cell-like properties as the myogenic source. The Journal of cell biology 144, 1113-1122.

Bentzinger, C.F., Wang, Y.X., Rudnicki, M.A., 2012. Building muscle: molecular regulation of myogenesis. Cold Spring Harbor perspectives in biology 4.

Bernet, J.D., Doles, J.D., Hall, J.K., Kelly Tanaka, K., Carter, T.A., Olwin, B.B., 2014. p38 MAPK signaling underlies a cell-autonomous loss of stem cell self-renewal in skeletal muscle of aged mice. Nat Med 20, 265-271.

Bernfield, M., Götte, M., Park, P.W., Reizes, O., Fitzgerald, M.L., Lincecum, J., Zako, M., 1999. Functions of cell surface heparan sulfate proteoglycans. Annu Rev Biochem 68, 729-777.

Bink, R.J., Habuchi, H., Lele, Z., Dolk, E., Joore, J., Rauch, G.J., Geisler, R., Wilson, S.W., den Hertog, J., Kimata, K., Zivkovic, D., 2003. Heparan sulfate 6-o-sulfotransferase is essential for muscle development in zebrafish. J Biol Chem 278, 31118-31127.

Bishop, J.R., Schuksz, M., Esko, J.D., 2007. Heparan sulphate proteoglycans fine-tune mammalian physiology. Nature 446, 1030-1037.

Björk, I., Olson, S.T., 1997. Antithrombin. A bloody important serpin. Adv Exp Med Biol 425, 17-33.

Blanquaert, F., Saffar, J.L., Colombier, M.L., Carpentier, G., Barritault, D., Caruelle, J.P., 1995. Heparan-like molecules induce the repair of skull defects. Bone 17, 499-506.

Blau, H.M., Chiu, C.P., Webster, C., 1983a. Cytoplasmic activation of human nuclear genes in stable heterocaryons. Cell 32, 1171-1180.

Blau, H.M., Webster, C., Chiu, C.P., Guttman, S., Chandler, F., 1983b. Differentiation properties of pure populations of human dystrophic muscle cells. Exp Cell Res 144, 495-503.

Boldrin, L., Neal, A., Zammit, P.S., Muntoni, F., Morgan, J.E., 2012. Donor satellite cell engraftment is significantly augmented when the host niche is preserved and endogenous satellite cells are incapacitated. Stem Cells 30, 1971-1984.

Border, W.A., Noble, N.A., 1994. Transforming growth factor beta in tissue fibrosis. N Engl J Med 331, 1286-1292.

Brack, A.S., Bildsoe, H., Hughes, S.M., 2005. Evidence that satellite cell decrement contributes to preferential decline in nuclear number from large fibres during murine age-related muscle atrophy. J Cell Sci 118, 4813-4821.

Brack, A.S., Conboy, M.J., Roy, S., Lee, M., Kuo, C.J., Keller, C., Rando, T.A., 2007. Increased Wnt signaling during aging alters muscle stem cell fate and increases fibrosis. Science 317, 807-810.

Brack, A.S., Muñoz-Cánoves, P., 2016. The ins and outs of muscle stem cell aging. Skelet Muscle 6, 1.

Brack, A.S., Rando, T.A., 2007. Intrinsic changes and extrinsic influences of myogenic stem cell function during aging. Stem Cell Rev 3, 226-237.

Brandan, E., Carey, D.J., Larraín, J., Melo, F., Campos, A., 1996. Synthesis and processing of glypican during differentiation of skeletal muscle cells. Eur J Cell Biol 71, 170-176.

Brandan, E., Gutierrez, J., 2013. Role of skeletal muscle proteoglycans during myogenesis. Matrix Biol 32, 289-297.

Braun, T., Buschhausen-Denker, G., Bober, E., Tannich, E., Arnold, H.H., 1989. A novel human muscle factor related to but distinct from MyoD1 induces myogenic conversion in 10T1/2 fibroblasts. EMBO J 8, 701-709.

Brickman, Y.G., Ford, M.D., Gallagher, J.T., Nurcombe, V., Bartlett, P.F., Turnbull, J.E., 1998a. Structural modification of fibroblast growth factor-binding heparan sulfate at a determinative stage of neural development. J Biol Chem 273, 4350-4359.

Brickman, Y.G., Nurcombe, V., Ford, M.D., Gallagher, J.T., Bartlett, P.F., Turnbull, J.E., 1998b. Structural comparison of fibroblast growth factor-specific heparan sulfates derived from a growing or differentiating neuroepithelial cell line. Glycobiology 8, 463-471.

Briggs, D., Morgan, J.E., 2013. Recent progress in satellite cell/myoblast engraftment -- relevance for therapy. FEBS J 280, 4281-4293.

Burgess, W.H., Maciag, T., 1989. The heparin-binding (fibroblast) growth factor family of proteins. Annu Rev Biochem 58, 575-606.

Campbell, J.S., Wenderoth, M.P., Hauschka, S.D., Krebs, E.G., 1995. Differential activation of mitogen-activated protein kinase in response to basic fibroblast growth factor in skeletal muscle cells. Proc Natl Acad Sci U S A 92, 870-874.

Canales, A., Angulo, J., Ojeda, R., Bruix, M., Fayos, R., Lozano, R., Giménez-Gallego, G., Martín-Lomas, M., Nieto, P.M., Jiménez-Barbero, J., 2005. Conformational flexibility of a synthetic glycosylaminoglycan bound to a fibroblast growth factor. FGF-1 recognizes both the (1)C(4) and (2)S(O) conformations of a bioactive heparin-like hexasaccharide. J Am Chem Soc 127, 5778-5779.

Carlson, B.M., Faulkner, J.A., 1989. Muscle transplantation between young and old rats: age of host determines recovery. Am J Physiol 256, C1262-1266.

Carlson, R.E., Kirby, B.S., Voyles, W.F., Dinenno, F.A., 2008. Evidence for impaired skeletal muscle contraction-induced rapid vasodilation in aging humans. Am J Physiol Heart Circ Physiol 294, H1963-1970.

Catlow, K., Deakin, J.A., Delehedde, M., Fernig, D.G., Gallagher, J.T., Pavão, M.S., Lyon, M., 2003. Hepatocyte growth factor/scatter factor and its interaction with heparan sulphate and dermatan sulphate. Biochem Soc Trans 31, 352-353.

Chakkalakal, J.V., Jones, K.M., Basson, M.A., Brack, A.S., 2012. The aged niche disrupts muscle stem cell quiescence. Nature 490, 355-360.

Charge, S.B., Rudnicki, M.A., 2004. Cellular and molecular regulation of muscle regeneration. Physiol Rev 84, 209-238.

Chen, R.L., Lander, A.D., 2001. Mechanisms underlying preferential assembly of heparan sulfate on glypican-1. J Biol Chem 276, 7507-7517.

Chevalier, F., Arnaud, D., Henault, E., Guillevic, O., Siñeriz, F., Ponsen, A.C., Papy-Garcia, D., Barritault, D., Letourneur, D., Uzan, G., Meddahi-Pellé, A., Hlawaty, H., Albanese, P., 2015. A fine structural modification of glycosaminoglycans is correlated with the progression of muscle regeneration after ischaemia: towards a matrix-based therapy? Eur Cell Mater 30, 51-68.

Christman, K.L., Vázquez-Dorbatt, V., Schopf, E., Kolodziej, C.M., Li, R.C., Broyer, R.M., Chen, Y., Maynard, H.D., 2008. Nanoscale growth factor patterns by immobilization on a heparin-mimicking polymer. J Am Chem Soc 130, 16585-16591.

Chua, C.C., Rahimi, N., Forsten-Williams, K., Nugent, M.A., 2004. Heparan sulfate proteoglycans function as receptors for fibroblast growth factor-2 activation of extracellular signal-regulated kinases 1 and 2. Circ Res 94, 316-323.

Clegg, C.H., Linkhart, T.A., Olwin, B.B., Hauschka, S.D., 1987. Growth factor control of skeletal muscle differentiation: commitment to terminal differentiation occurs in G1 phase and is repressed by fibroblast growth factor. J Cell Biol 105, 949-956.

Cole, C.L., Hansen, S.U., Baráth, M., Rushton, G., Gardiner, J.M., Avizienyte, E., Jayson, G.C., 2010. Synthetic heparan sulfate oligosaccharides inhibit endothelial cell functions essential for angiogenesis. PLoS One 5, e11644.

Collins, C.A., Zammit, P.S., Ruiz, A.P., Morgan, J.E., Partridge, T.A., 2007. A population of myogenic stem cells that survives skeletal muscle aging. Stem Cells 25, 885-894.

Conboy, I.M., Conboy, M.J., Smythe, G.M., Rando, T.A., 2003. Notch-mediated restoration of regenerative potential to aged muscle. Science 302, 1575-1577.

Conboy, I.M., Conboy, M.J., Wagers, A.J., Girma, E.R., Weissman, I.L., Rando, T.A., 2005. Rejuvenation of aged progenitor cells by exposure to a young systemic environment. Nature 433, 760-764.
Conboy, I.M., Rando, T.A., 2002. The regulation of Notch signaling controls satellite cell activation and cell fate determination in postnatal myogenesis. Dev Cell 3, 397-409.

Connell, B.J., Lortat-Jacob, H., 2013. Human immunodeficiency virus and heparan sulfate: from attachment to entry inhibition. Front Immunol 4, 385.

Conrad, H.E., 2001. Degradation of heparan sulfate by nitrous acid. Methods Mol Biol 171, 347-351.

Cooper, R.N., Tajbakhsh, S., Mouly, V., Cossu, G., Buckingham, M., Butler-Browne, G.S., 1999. In vivo satellite cell activation via Myf5 and MyoD in regenerating mouse skeletal muscle. Journal of cell science 112 (Pt 17), 2895-2901.

Cornelison, D.D., 2008. Context matters: in vivo and in vitro influences on muscle satellite cell activity. J Cell Biochem 105, 663-669.

Cornelison, D.D., Filla, M.S., Stanley, H.M., Rapraeger, A.C., Olwin, B.B., 2001. Syndecan-3 and syndecan-4 specifically mark skeletal muscle satellite cells and are implicated in satellite cell maintenance and muscle regeneration. Dev Biol 239, 79-94.

Cornelison, D.D., Wilcox-Adelman, S.A., Goetinck, P.F., Rauvala, H., Rapraeger, A.C., Olwin, B.B., 2004. Essential and separable roles for Syndecan-3 and Syndecan-4 in skeletal muscle development and regeneration. Genes Dev 18, 2231-2236.

Cosgrove, B.D., Gilbert, P.M., Porpiglia, E., Mourkioti, F., Lee, S.P., Corbel, S.Y., Llewellyn, M.E., Delp, S.L., Blau, H.M., 2014. Rejuvenation of the muscle stem cell population restores strength to injured aged muscles. Nat Med 20, 255-264.

Coutu, D.L., Galipeau, J., 2011. Roles of FGF signaling in stem cell self-renewal, senescence and aging. Aging (Albany NY) 3, 920-933.

Crisona, N.J., Allen, K.D., Strohman, R.C., 1998. Muscle satellite cells from dystrophic (mdx) mice have elevated levels of heparan sulphate proteoglycan receptors for fibroblast growth factor. J Muscle Res Cell Motil 19, 43-51.

Crist, C.G., Montarras, D., Buckingham, M., 2012. Muscle satellite cells are primed for myogenesis but maintain quiescence with sequestration of Myf5 mRNA targeted by microRNA-31 in mRNP granules. Cell Stem Cell 11, 118-126.

David, G., Bai, X.M., Van der Schueren, B., Cassiman, J.J., Van den Berghe, H., 1992. Developmental changes in heparan sulfate expression: in situ detection with mAbs. The Journal of cell biology 119, 961-975.

David, G., Bai, X.M., Van der Schueren, B., Marynen, P., Cassiman, J.J., Van den Berghe, H., 1993. Spatial and temporal changes in the expression of fibroglycan (syndecan-2) during mouse embryonic development. Development 119, 841-854.

Davis, R.L., Weintraub, H., Lassar, A.B., 1987. Expression of a single transfected cDNA converts fibroblasts to myoblasts. Cell 51, 987-1000.

Day, K., Shefer, G., Shearer, A., Yablonka-Reuveni, Z., 2010. The depletion of skeletal muscle satellite cells with age is concomitant with reduced capacity of single progenitors to produce reserve progeny. Dev Biol 340, 330-343.

de Paz, J.L., Angulo, J., Lassaletta, J.M., Nieto, P.M., Redondo-Horcajo, M., Lozano, R.M., Giménez-Gallego, G., Martín-Lomas, M., 2001. The activation of fibroblast growth factors by heparin: synthesis, structure, and biological activity of heparin-like oligosaccharides. Chembiochem 2, 673-685.

Deakin, J.A., Lyon, M., 2008. A simplified and sensitive fluorescent method for disaccharide analysis of both heparan sulfate and chondroitin/dermatan sulfates from biological samples. Glycobiology 18, 483-491.

Dedkov, E.I., Borisov, A.B., Wernig, A., Carlson, B.M., 2003. Aging of skeletal muscle does not affect the response of satellite cells to denervation. J Histochem Cytochem 51, 853-863.

Delehedde, M., Seve, M., Sergeant, N., Wartelle, I., Lyon, M., Rudland, P.S., Fernig, D.G., 2000. Fibroblast growth factor-2 stimulation of p42/44MAPK phosphorylation and IkappaB degradation is regulated by heparan sulfate/heparin in rat mammary fibroblasts. J Biol Chem 275, 33905-33910.

Desai, U.R., Wang, H.M., Linhardt, R.J., 1993. Substrate specificity of the heparin lyases from Flavobacterium heparinum. Arch Biochem Biophys 306, 461-468.

Desgranges, P., Barbaud, C., Caruelle, J.P., Barritault, D., Gautron, J., 1999. A substituted dextran enhances muscle fiber survival and regeneration in ischemic and denervated rat EDL muscle. FASEB J 13, 761-766.

DiMicco, M.A., Patwari, P., Siparsky, P.N., Kumar, S., Pratta, M.A., Lark, M.W., Kim, Y.J., Grodzinsky, A.J., 2004. Mechanisms and kinetics of glycosaminoglycan release following in vitro cartilage injury. Arthritis Rheum 50, 840-848.

Dombrowski, C., Song, S.J., Chuan, P., Lim, X., Susanto, E., Sawyer, A.A., Woodruff, M.A., Hutmacher, D.W., Nurcombe, V., Cool, S.M., 2009. Heparan sulfate mediates the proliferation and differentiation of rat mesenchymal stem cells. Stem Cells Dev 18, 661-670.

Drummond, K.J., Yates, E.A., Turnbull, J.E., 2001. Electrophoretic sequencing of heparin/heparan sulfate oligosaccharides using a highly sensitive fluorescent end label. Proteomics 1, 304-310.

Edmondson, D.G., Olson, E.N., 1990. A gene with homology to the myc similarity region of MyoD1 is expressed during myogenesis and is sufficient to activate the muscle differentiation program. Genes & development 4, 1450.

Emery, A.E., 2002. The muscular dystrophies. Lancet 359, 687-695.

Ervasti, J.M., 2003. Costameres: the Achilles' heel of Herculean muscle. J Biol Chem 278, 13591-13594.

Ervasti, J.M., Campbell, K.P., 1993. A role for the dystrophin-glycoprotein complex as a transmembrane linker between laminin and actin. The Journal of cell biology 122, 809-823.

Esko, J.D., Zhang, L., 1996. Influence of core protein sequence on glycosaminoglycan assembly. Curr Opin Struct Biol 6, 663-670.

Eswarakumar, V.P., Lax, I., Schlessinger, J., 2005. Cellular signaling by fibroblast growth factor receptors. Cytokine Growth Factor Rev 16, 139-149.

Evinger-Hodges, M.J., Ewton, D.Z., Seifert, S.C., Florini, J.R., 1982. Inhibition of myoblast differentiation in vitro by a protein isolated from liver cell medium. The Journal of cell biology 93, 395-401.

Faham, S., Hileman, R.E., Fromm, J.R., Linhardt, R.J., Rees, D.C., 1996. Heparin structure and interactions with basic fibroblast growth factor. Science 271, 1116-1120.

Farndale, R.W., Buttle, D.J., Barrett, A.J., 1986. Improved quantitation and discrimination of sulphated glycosaminoglycans by use of dimethylmethylene blue. Biochim Biophys Acta 883, 173-177.

Farndale, R.W., Sayers, C.A., Barrett, A.J., 1982. A direct spectrophotometric microassay for sulfated glycosaminoglycans in cartilage cultures. Connect Tissue Res 9, 247-248.

Fedorov, Y.V., Jones, N.C., Olwin, B.B., 1998. Regulation of myogenesis by fibroblast growth factors requires beta-gamma subunits of pertussis toxin-sensitive G proteins. Mol Cell Biol 18, 5780-5787.

Ferreras, C., Rushton, G., Cole, C.L., Babur, M., Telfer, B.A., van Kuppevelt, T.H., Gardiner, J.M., Williams, K.J., Jayson, G.C., Avizienyte, E., 2012. Endothelial heparan sulfate 6-O-sulfation levels regulate angiogenic responses of endothelial cells to fibroblast growth factor 2 and vascular endothelial growth factor. J Biol Chem 287, 36132-36146.

Ferro, D.R., Provasoli, A., Ragazzi, M., Casu, B., Torri, G., Bossennec, V., Perly, B., Sinaÿ, P., Petitou, M., Choay, J., 1990. Conformer populations of L-iduronic acid residues in glycosaminoglycan sequences. Carbohydr Res 195, 157-167.

Feyzi, E., Saldeen, T., Larsson, E., Lindahl, U., Salmivirta, M., 1998. Age-dependent modulation of heparan sulfate structure and function. J Biol Chem 273, 13395-13398.

Fire, A., Xu, S., Montgomery, M.K., Kostas, S.A., Driver, S.E., Mello, C.C., 1998. Potent and specific genetic interference by double-stranded RNA in Caenorhabditis elegans. Nature 391, 806-811.

Forsberg, M., Holmborn, K., Kundu, S., Dagälv, A., Kjellén, L., Forsberg-Nilsson, K., 2012. Undersulfation of heparan sulfate restricts differentiation potential of mouse embryonic stem cells. J Biol Chem 287, 10853-10862.

Fry, C.S., Kirby, T.J., Kosmac, K., McCarthy, J.J., Peterson, C.A., 2017. Myogenic Progenitor Cells Control Extracellular Matrix Production by Fibroblasts during Skeletal Muscle Hypertrophy. Cell Stem Cell 20, 56-69.

Fry, C.S., Lee, J.D., Mula, J., Kirby, T.J., Jackson, J.R., Liu, F., Yang, L., Mendias, C.L., Dupont-Versteegden, E.E., McCarthy, J.J., Peterson, C.A., 2015. Inducible depletion of satellite cells in adult, sedentary mice impairs muscle regenerative capacity without affecting sarcopenia. Nat Med 21, 76-80.

Fuentealba, L., Carey, D.J., Brandan, E., 1999. Antisense inhibition of syndecan-3 expression during skeletal muscle differentiation accelerates myogenesis through a basic fibroblast growth factor-dependent mechanism. J Biol Chem 274, 37876-37884.

Gao, Q., Chen, C.Y., Zong, C., Wang, S., Ramiah, A., Prabhakar, P., Morris, L.C., Boons, G.J., Moremen, K.W., Prestegard, J.H., 2016. Structural Aspects of Heparan Sulfate Binding to Robo1-Ig1-2. ACS Chem Biol 11, 3106-3113.

García-Prat, L., Sousa-Victor, P., Muñoz-Cánoves, P., 2013. Functional dysregulation of stem cells during aging: a focus on skeletal muscle stem cells. FEBS J 280, 4051-4062.

Gautron, J., Kedzia, C., Husmann, I., Barritault, D., 1995. [Acceleration of the regeneration of skeletal muscles in adult rats by dextran derivatives]. C R Acad Sci III 318, 671-676.

George, T., Velloso, C.P., Alsharidah, M., Lazarus, N.R., Harridge, S.D., 2010. Sera from young and older humans equally sustain proliferation and differentiation of human myoblasts. Exp Gerontol 45, 875-881.

Gerdes, J., Schwab, U., Lemke, H., Stein, H., 1983. Production of a mouse monoclonal antibody reactive with a human nuclear antigen associated with cell proliferation. Int J Cancer 31, 13-20.

Ghadiali, R.S., Guimond, S.E., Turnbull, J.E., Pisconti, A., 2016. Dynamic changes in heparan sulfate during muscle differentiation and ageing regulate myoblast cell fate and FGF2 signalling. Matrix Biol.

Ghatak, S., Maytin, E.V., Mack, J.A., Hascall, V.C., Atanelishvili, I., Moreno Rodriguez, R., Markwald, R.R., Misra, S., 2015. Roles of Proteoglycans and Glycosaminoglycans in Wound Healing and Fibrosis. Int J Cell Biol 2015, 834893.

Gibson, M.C., Schultz, E., 1983. Age-related differences in absolute numbers of skeletal muscle satellite cells. Muscle Nerve 6, 574-580.

Gill, R., Hitchins, L., Fletcher, F., Dhoot, G.K., 2010. Sulf1A and HGF regulate satellite-cell growth. J Cell Sci 123, 1873-1883.

Goetsch, K.P., Snyman, C., Myburgh, K.H., Niesler, C.U., 2015. Simultaneous isolation of enriched myoblasts and fibroblasts for migration analysis within a novel co-culture assay. Biotechniques 58, 25-32.

Gong, F., Jemth, P., Escobar Galvis, M.L., Vlodavsky, I., Horner, A., Lindahl, U., Li, J.P., 2003. Processing of macromolecular heparin by heparanase. J Biol Chem 278, 35152-35158.

Gospodarowicz, D., Cheng, J., 1986. Heparin protects basic and acidic FGF from inactivation. J Cell Physiol 128, 475-484.

Gottlieb, H.E., Kotlyar, V., Nudelman, A., 1997. NMR Chemical Shifts of Common Laboratory Solvents as Trace Impurities. J Org Chem 62, 7512-7515.

Grounds, M.D., Sorokin, L., White, J., 2005. Strength at the extracellular matrix-muscle interface. Scand J Med Sci Sports 15, 381-391.

Grzesik, W.J., Frazier, C.R., Shapiro, J.R., Sponseller, P.D., Robey, P.G., Fedarko, N.S., 2002. Age-related changes in human bone proteoglycan structure. Impact of osteogenesis imperfecta. J Biol Chem 277, 43638-43647.

Guimond, S., Maccarana, M., Olwin, B.B., Lindahl, U., Rapraeger, A.C., 1993. Activating and inhibitory heparin sequences for FGF-2 (basic FGF). Distinct requirements for FGF-1, FGF-2, and FGF-4. J Biol Chem 268, 23906-23914.

Guimond, S.E., Puvirajesinghe, T.M., Skidmore, M.A., Kalus, I., Dierks, T., Yates, E.A., Turnbull, J.E., 2009a. Rapid purification and high sensitivity analysis of heparan sulfate from cells and tissues: toward glycomics profiling. J Biol Chem 284, 25714-25722.

Guimond, S.E., Rudd, T.R., Skidmore, M.A., Ori, A., Gaudesi, D., Cosentino, C., Guerrini, M., Edge, R., Collison, D., McInnes, E., Torri, G., Turnbull, J.E., Fernig, D.G., Yates, E.A., 2009b. Cations modulate polysaccharide structure to determine FGF-FGFR signaling: a comparison of signaling and inhibitory polysaccharide interactions with FGF-1 in solution. Biochemistry 48, 4772-4779.

Guimond, S.E., Turnbull, J.E., 1999. Fibroblast growth factor receptor signalling is dictated by specific heparan sulphate saccharides. Curr Biol 9, 1343-1346.

Guimond, S.E., Turnbull, J.E., Yates, E.A., 2006. Engineered bio-active polysaccharides from heparin. Macromol Biosci 6, 681-686.

Gutiérrez, J., Brandan, E., 2010. A novel mechanism of sequestering fibroblast growth factor 2 by glypican in lipid rafts, allowing skeletal muscle differentiation. Mol Cell Biol 30, 1634-1649.

Gutierrez, J., Osses, N., Brandan, E., 2006. Changes in secreted and cell associated proteoglycan synthesis during conversion of myoblasts to osteoblasts in response to bone morphogenetic protein-2: role of decorin in cell response to BMP-2. J Cell Physiol 206, 58-67.

Habuchi, H., Miyake, G., Nogami, K., Kuroiwa, A., Matsuda, Y., Kusche-Gullberg, M., Habuchi, O., Tanaka, M., Kimata, K., 2003. Biosynthesis of heparan sulphate with diverse structures and functions: two alternatively spliced forms of human heparan sulphate 6-O-sulphotransferase-2 having different expression patterns and properties. Biochem J 371, 131-142.

Habuchi, H., Tanaka, M., Habuchi, O., Yoshida, K., Suzuki, H., Ban, K., Kimata, K., 2000. The occurrence of three isoforms of heparan sulfate 6-O-sulfotransferase having different specificities for hexuronic acid adjacent to the targeted N-sulfoglucosamine. J Biol Chem 275, 2859-2868.

Hannon, K., Kudla, A.J., McAvoy, M.J., Clase, K.L., Olwin, B.B., 1996. Differentially expressed fibroblast growth factors regulate skeletal muscle development through autocrine and paracrine mechanisms. The Journal of cell biology 132, 1151-1159.

Hausburg, M.A., Doles, J.D., Clement, S.L., Cadwallader, A.B., Hall, M.N., Blackshear, P.J., Lykke-Andersen, J., Olwin, B.B., 2015. Post-transcriptional regulation of satellite cell quiescence by TTP-mediated mRNA decay. Elife 4, e03390.

Higginson, J.R., Thompson, S.M., Santos-Silva, A., Guimond, S.E., Turnbull, J.E., Barnett, S.C., 2012. Differential sulfation remodelling of heparan sulfate by extracellular 6-O-sulfatases regulates fibroblast growth factor-induced boundary formation by glial cells: implications for glial cell transplantation. J Neurosci 32, 15902-15912.

Hileman, R.E., Fromm, J.R., Weiler, J.M., Linhardt, R.J., 1998. Glycosaminoglycan-protein interactions: definition of consensus sites in glycosaminoglycan binding proteins. Bioessays 20, 156-167.

Hirano, K., Sasaki, N., Ichimiya, T., Miura, T., Van Kuppevelt, T.H., Nishihara, S., 2012. 3-O-sulfated heparan sulfate recognized by the antibody HS4C3 contributes [corrected] to the differentiation of mouse embryonic stem cells via fas signaling. PLoS One 7, e43440.

Höök, M., Lindahl, U., Iverius, P.H., 1974. Distribution of sulphate and iduronic acid residues in heparin and heparan sulphate. Biochem J 137, 33-43.

Hsieh, P.H., Thieker, D.F., Guerrini, M., Woods, R.J., Liu, J., 2016. Uncovering the Relationship between Sulphation Patterns and Conformation of Iduronic Acid in Heparan Sulphate. Sci Rep 6, 29602.

Hsieh, P.H., Xu, Y., Keire, D.A., Liu, J., 2014. Chemoenzymatic synthesis and structural characterization of 2-O-sulfated glucuronic acid-containing heparan sulfate hexasaccharides. Glycobiology 24, 681-692.

Hung, S.C., Lu, X.A., Lee, J.C., Chang, M.D., Fang, S.L., Fan, T.C., Zulueta, M.M., Zhong, Y.Q., 2012. Synthesis of heparin oligosaccharides and their interaction with eosinophil-derived neurotoxin. Org Biomol Chem 10, 760-772.

Huynh, M.B., Morin, C., Carpentier, G., Garcia-Filipe, S., Talhas-Perret, S., Barbier-Chassefière, V., van Kuppevelt, T.H., Martelly, I., Albanese, P., Papy-Garcia, D., 2012a. Age-related changes in rat myocardium involve altered capacities of glycosaminoglycans to potentiate growth factor functions and heparan sulfate-altered sulfation. J Biol Chem 287, 11363-11373.

Huynh, M.B., Villares, J., Díaz, J.E., Christiaans, S., Carpentier, G., Ouidja, M.O., Sissoeff, L., Raisman-Vozari, R., Papy-Garcia, D., 2012b. Glycosaminoglycans from aged human hippocampus have altered capacities to regulate trophic factors activities but not Aβ42 peptide toxicity. Neurobiol Aging 33, 1005.e1011-1022.

Ikeda, Y., Charef, S., Ouidja, M.O., Barbier-Chassefière, V., Sineriz, F., Duchesnay, A., Narasimprakash, H., Martelly, I., Kern, P., Barritault, D., Petit, E., Papy-Garcia, D., 2011. Synthesis and biological activities of a library of glycosaminoglycans mimetic oligosaccharides. Biomaterials 32, 769-776.

Inoue, Y., Nagasawa, K., 1976. Selective N-desulfation of heparin with dimethyl sulfoxide containing water or methanol. Carbohydr Res 46, 87-95.

Jakobsson, L., Kreuger, J., Holmborn, K., Lundin, L., Eriksson, I., Kjellén, L., Claesson-Welsh, L., 2006. Heparan sulfate in trans potentiates VEGFR-mediated angiogenesis. Dev Cell 10, 625-634.

Jastrebova, N., Vanwildemeersch, M., Rapraeger, A.C., Giménez-Gallego, G., Lindahl, U., Spillmann, D., 2006. Heparan sulfate-related oligosaccharides in ternary complex formation with fibroblast growth factors 1 and 2 and their receptors. J Biol Chem 281, 26884-26892.

Jen, Y.H., Musacchio, M., Lander, A.D., 2009. Glypican-1 controls brain size through regulation of fibroblast growth factor signaling in early neurogenesis. Neural Dev 4, 33.

Jennische, E., Hansson, H.A., 1987. Regenerating skeletal muscle cells express insulin-like growth factor I. Acta Physiol Scand 130, 327-332.

Jenniskens, G.J., Hafmans, T., Veerkamp, J.H., van Kuppevelt, T.H., 2002. Spatiotemporal distribution of heparan sulfate epitopes during myogenesis and synaptogenesis: a study in developing mouse intercostal muscle. Dev Dyn 225, 70-79.

Jenniskens, G.J., Oosterhof, A., Brandwijk, R., Veerkamp, J.H., van Kuppevelt, T.H., 2000. Heparan sulfate heterogeneity in skeletal muscle basal lamina: demonstration by phage display-derived antibodies. The Journal of neuroscience : the official journal of the Society for Neuroscience 20, 4099-4111.

Jin, L., Abrahams, J.P., Skinner, R., Petitou, M., Pike, R.N., Carrell, R.W., 1997. The anticoagulant activation of antithrombin by heparin. Proc Natl Acad Sci U S A 94, 14683-14688.

Johnson, C.E., Crawford, B.E., Stavridis, M., Ten Dam, G., Wat, A.L., Rushton, G., Ward, C.M., Wilson, V., van Kuppevelt, T.H., Esko, J.D., Smith, A., Gallagher, J.T., Merry, C.L., 2007. Essential alterations of heparan sulfate during the differentiation of embryonic stem cells to Sox1-enhanced green fluorescent protein-expressing neural progenitor cells. Stem Cells 25, 1913-1923.

Kalus, I., Rohn, S., Puvirajesinghe, T.M., Guimond, S.E., Eyckerman-Kölln, P.J., Ten Dam, G., van Kuppevelt, T.H., Turnbull, J.E., Dierks, T., 2015. Sulf1 and Sulf2 Differentially Modulate Heparan Sulfate Proteoglycan Sulfation during Postnatal Cerebellum Development: Evidence for Neuroprotective and Neurite Outgrowth Promoting Functions. PLoS One 10, e0139853.

Keenan, T.D., Pickford, C.E., Holley, R.J., Clark, S.J., Lin, W., Dowsey, A.W., Merry, C.L., Day, A.J., Bishop, P.N., 2014. Age-dependent changes in heparan sulfate in human Bruch's membrane: implications for age-related macular degeneration. Invest Ophthalmol Vis Sci 55, 5370-5379.

Kim, B.T., Kitagawa, H., Tamura, J., Saito, T., Kusche-Gullberg, M., Lindahl, U., Sugahara, K., 2001. Human tumor suppressor EXT gene family members EXTL1 and EXTL3 encode alpha 1,4- N-acetylglucosaminyltransferases that likely are involved in heparan sulfate/ heparin biosynthesis. Proc Natl Acad Sci U S A 98, 7176-7181.

Kinoshita, A., Sugahara, K., 1999. Microanalysis of glycosaminoglycan-derived oligosaccharides labeled with a fluorophore 2-aminobenzamide by high-performance liquid chromatography: application to disaccharide composition analysis and exosequencing of oligosaccharides. Anal Biochem 269, 367-378.

Kitagawa, H., Kinoshita, A., Sugahara, K., 1995. Microanalysis of glycosaminoglycan-derived disaccharides labeled with the fluorophore 2-aminoacridone by capillary electrophoresis and high-performance liquid chromatography. Anal Biochem 232, 114-121.

Knelson, E.H., Nee, J.C., Blobe, G.C., 2014. Heparan sulfate signaling in cancer. Trends Biochem Sci 39, 277-288.

Kobayashi, M., Habuchi, H., Yoneda, M., Habuchi, O., Kimata, K., 1997. Molecular cloning and expression of Chinese hamster ovary cell heparan-sulfate 2-sulfotransferase. J Biol Chem 272, 13980-13985.

Kovanen, V., 2002. Intramuscular extracellular matrix: complex environment of muscle cells. Exerc Sport Sci Rev 30, 20-25.

Kraushaar, D.C., Yamaguchi, Y., Wang, L., 2010. Heparan sulfate is required for embryonic stem cells to exit from self-renewal. J Biol Chem 285, 5907-5916.

Kreuger, J., Kjellén, L., 2012. Heparan sulfate biosynthesis: regulation and variability. J Histochem Cytochem 60, 898-907.

Kreuger, J., Prydz, K., Pettersson, R.F., Lindahl, U., Salmivirta, M., 1999. Characterization of fibroblast growth factor 1 binding heparan sulfate domain. Glycobiology 9, 723-729.

Kreuger, J., Salmivirta, M., Sturiale, L., Giménez-Gallego, G., Lindahl, U., 2001. Sequence analysis of heparan sulfate epitopes with graded affinities for fibroblast growth factors 1 and 2. J Biol Chem 276, 30744-30752.

Kudla, A.J., Jones, N.C., Rosenthal, R.S., Arthur, K., Clase, K.L., Olwin, B.B., 1998. The FGF receptor-1 tyrosine kinase domain regulates myogenesis but is not sufficient to stimulate proliferation. The Journal of cell biology 142, 241-250.

Kurima, K., Warman, M.L., Krishnan, S., Domowicz, M., Krueger, R.C., Deyrup, A., Schwartz, N.B., 1998. A member of a family of sulfate-activating enzymes causes murine brachymorphism. Proc Natl Acad Sci U S A 95, 8681-8685.

Lamanna, W.C., Frese, M.A., Balleininger, M., Dierks, T., 2008. Sulf loss influences N-, 2-O-, and 6-O-sulfation of multiple heparan sulfate proteoglycans and modulates fibroblast growth factor signaling. J Biol Chem 283, 27724-27735.

Lander, A.D., Selleck, S.B., 2000. The elusive functions of proteoglycans: in vivo veritas. The Journal of cell biology 148, 227-232.

Langsdorf, A., Do, A.T., Kusche-Gullberg, M., Emerson, C.P., Jr., Ai, X., 2007. Sulfs are regulators of growth factor signaling for satellite cell differentiation and muscle regeneration. Developmental biology 311, 464-477.

Lanner, F., Lee, K.L., Sohl, M., Holmborn, K., Yang, H., Wilbertz, J., Poellinger, L., Rossant, J., Farnebo, F., 2010. Heparan sulfation-dependent fibroblast growth factor signaling maintains embryonic stem cells primed for differentiation in a heterogeneous state. Stem Cells 28, 191-200.

Larraín, J., Alvarez, J., Hassell, J.R., Brandan, E., 1997a. Expression of perlecan, a proteoglycan that binds myogenic inhibitory basic fibroblast growth factor, is down regulated during skeletal muscle differentiation. Exp Cell Res 234, 405-412.
Larraín, J., Carey, D.J., Brandan, E., 1998. Syndecan-1 expression inhibits myoblast differentiation through a basic fibroblast growth factor-dependent mechanism. J Biol Chem 273, 32288-32296.

Larraín, J., Cizmeci-Smith, G., Troncoso, V., Stahl, R.C., Carey, D.J., Brandan, E., 1997b. Syndecan-1 expression is down-regulated during myoblast terminal differentiation. Modulation by growth factors and retinoic acid. J Biol Chem 272, 18418-18424.

Lawrence, R., Olson, S.K., Steele, R.E., Wang, L., Warrior, R., Cummings, R.D., Esko, J.D., 2008. Evolutionary differences in glycosaminoglycan fine structure detected by quantitative glycan reductive isotope labeling. J Biol Chem 283, 33674-33684.

Le Grand, F., Jones, A.E., Seale, V., Scimè, A., Rudnicki, M.A., 2009. Wnt7a activates the planar cell polarity pathway to drive the symmetric expansion of satellite stem cells. Cell Stem Cell 4, 535-547.

Leary, J.A., Miller, R.L., Wei, W., Schwörer, R., Zubkova, O.V., Tyler, P.C., Turnbull, J.E., 2015. Composition, sequencing and ion mobility mass spectrometry of heparan sulfate-like octasaccharide isomers differing in glucuronic and iduronic acid content. Eur J Mass Spectrom (Chichester) 21, 245-254.

Ledin, J., Staatz, W., Li, J.P., Götte, M., Selleck, S., Kjellén, L., Spillmann, D., 2004. Heparan sulfate structure in mice with genetically modified heparan sulfate production. J Biol Chem 279, 42732-42741.

Lee, J.C., Lu, X.A., Kulkarni, S.S., Wen, Y.S., Hung, S.C., 2004. Synthesis of heparin oligosaccharides. J Am Chem Soc 126, 476-477.

Lee, S.G., Brown, J.M., Rogers, C.J., Matson, J.B., Krishnamurthy, C., Rawat, M., Hsieh-Wilson, L.C., 2010. End-functionalized glycopolymers as mimetics of chondroitin sulfate proteoglycans. Chem Sci 1, 322-325.

Lepper, C., Partridge, T.A., Fan, C.M., 2011. An absolute requirement for Pax7-positive satellite cells in acute injury-induced skeletal muscle regeneration. Development 138, 3639-3646.

Li, J., Hagner-McWhirter, A., Kjellén, L., Palgi, J., Jalkanen, M., Lindahl, U., 1997. Biosynthesis of heparin/heparan sulfate. cDNA cloning and expression of D-glucuronyl C5-epimerase from bovine lung. J Biol Chem 272, 28158-28163.

Li, Y., Foster, W., Deasy, B.M., Chan, Y., Prisk, V., Tang, Y., Cummins, J., Huard, J., 2004. Transforming growth factor-beta1 induces the differentiation of myogenic cells into fibrotic cells in injured skeletal muscle: a key event in muscle fibrogenesis. Am J Pathol 164, 1007-1019.

Lim, R.W., Hauschka, S.D., 1984. EGF responsiveness and receptor regulation in normal and differentiation-defective mouse myoblasts. Dev Biol 105, 48-58.

Lin, X., 2004. Functions of heparan sulfate proteoglycans in cell signaling during development. Development 131, 6009-6021.

Lind, T., Tufaro, F., McCormick, C., Lindahl, U., Lidholt, K., 1998. The putative tumor suppressors EXT1 and EXT2 are glycosyltransferases required for the biosynthesis of heparan sulfate. J Biol Chem 273, 26265-26268.

Lindahl, U., Kusche, M., Lidholt, K., Oscarsson, L.G., 1989. Biosynthesis of heparin and heparan sulfate. Ann N Y Acad Sci 556, 36-50.

Lindahl, U., Kusche-Gullberg, M., Kjellén, L., 1998. Regulated diversity of heparan sulfate. J Biol Chem 273, 24979-24982.

Linhardt, R.J., Rice, K.G., Kim, Y.S., Lohse, D.L., Wang, H.M., Loganathan, D., 1988. Mapping and quantification of the major oligosaccharide components of heparin. Biochem J 254, 781-787.

Linhardt, R.J., Turnbull, J.E., Wang, H.M., Loganathan, D., Gallagher, J.T., 1990. Examination of the substrate specificity of heparin and heparan sulfate lyases. Biochemistry 29, 2611-2617.

Linkhart, T.A., Clegg, C.H., Hauschka, S.D., 1980. Control of mouse myoblast commitment to terminal differentiation by mitogens. J Supramol Struct 14, 483-498.

Liu, J., Linhardt, R.J., 2014. Chemoenzymatic synthesis of heparan sulfate and heparin. Nat Prod Rep 31, 1676-1685.

Liu, J., Pedersen, L.C., 2007. Anticoagulant heparan sulfate: structural specificity and biosynthesis. Appl Microbiol Biotechnol 74, 263-272.

Liu, J., Shworak, N.W., Sinaÿ, P., Schwartz, J.J., Zhang, L., Fritze, L.M., Rosenberg, R.D., 1999. Expression of heparan sulfate D-glucosaminyl 3-O-sulfotransferase isoforms reveals novel substrate specificities. J Biol Chem 274, 5185-5192.

Liu, L., Cheung, T.H., Charville, G.W., Rando, T.A., 2015. Isolation of skeletal muscle stem cells by fluorescence-activated cell sorting. Nat Protoc 10, 1612-1624.

Liu, R., Xu, Y., Chen, M., Weïwer, M., Zhou, X., Bridges, A.S., DeAngelis, P.L., Zhang, Q., Linhardt, R.J., Liu, J., 2010. Chemoenzymatic design of heparan sulfate oligosaccharides. J Biol Chem 285, 34240-34249.

Liu, X., McFarland, D.C., Nestor, K.E., Velleman, S.G., 2004. Developmental regulated expression of syndecan-1 and glypican in pectoralis major muscle in turkeys with different growth rates. Dev Growth Differ 46, 37-51.

Liu, X., Nestor, K.E., McFarland, D.C., Velleman, S.G., 2002. Developmental expression of skeletal muscle heparan sulfate proteoglycans in turkeys with different growth rates. Poult Sci 81, 1621-1628.

Lohse, D.L., Linhardt, R.J., 1992. Purification and characterization of heparin lyases from Flavobacterium heparinum. J Biol Chem 267, 24347-24355.

Londhe, P., Davie, J.K., 2011. Sequential association of myogenic regulatory factors and E proteins at muscle-specific genes. Skeletal muscle 1, 14.

Lu, J., Auduong, L., White, E.S., Yue, X., 2014. Up-regulation of heparan sulfate 6-O-sulfation in idiopathic pulmonary fibrosis. Am J Respir Cell Mol Biol 50, 106-114.
Lundin, L., Larsson, H., Kreuger, J., Kanda, S., Lindahl, U., Salmivirta, M., Claesson-Welsh, L., 2000. Selectively desulfated heparin inhibits fibroblast growth factor-induced mitogenicity and angiogenesis. J Biol Chem 275, 24653-24660.

Maccarana, M., Casu, B., Lindahl, U., 1993. Minimal sequence in heparin/heparan sulfate required for binding of basic fibroblast growth factor. J Biol Chem 268, 23898-23905.

Maccarana, M., Sakura, Y., Tawada, A., Yoshida, K., Lindahl, U., 1996. Domain structure of heparan sulfates from bovine organs. J Biol Chem 271, 17804-17810.

Manon-Jensen, T., Itoh, Y., Couchman, J.R., 2010. Proteoglycans in health and disease: the multiple roles of syndecan shedding. FEBS J 277, 3876-3889.

Mathew, S.J., Hansen, J.M., Merrell, A.J., Murphy, M.M., Lawson, J.A., Hutcheson, D.A., Hansen, M.S., Angus-Hill, M., Kardon, G., 2011. Connective tissue fibroblasts and Tcf4 regulate myogenesis. Development 138, 371-384.

Mauro, A., 1961. Satellite cell of skeletal muscle fibers. J Biophys Biochem Cytol 9, 493-495.

McKeehan, W.L., Wu, X., Kan, M., 1999. Requirement for anticoagulant heparan sulfate in the fibroblast growth factor receptor complex. J Biol Chem 274, 21511-21514.

Meddahi, A., Alexakis, C., Papy, D., Caruelle, J.P., Barritault, D., 2002a. Heparin-like polymer improved healing of gastric and colic ulceration. J Biomed Mater Res 60, 497-501.

Meddahi, A., Benoit, J., Ayoub, N., Sézeur, A., Barritault, D., 1996a. Heparin-like polymers derived from dextran enhance colonic anastomosis resistance to leakage. J Biomed Mater Res 31, 293-297.

Meddahi, A., Brée, F., Papy-Garcia, D., Gautron, J., Barritault, D., Caruelle, J.P., 2002b. Pharmacological studies of RGTA(11), a heparan sulfate mimetic polymer, efficient on muscle regeneration. J Biomed Mater Res 62, 525-531.

Meddahi, A., Lemdjabar, H., Caruelle, J.P., Barritault, D., Hornebeck, W., 1995. Inhibition by dextran derivatives of FGF-2 plasmin-mediated degradation. Biochimie 77, 703-706.

Meddahi, A., Lemdjabar, H., Caruelle, J.P., Barritault, D., Hornebeck, W., 1996b. FGF protection and inhibition of human neutrophil elastase by carboxymethyl benzylamide sulfonate dextran derivatives. Int J Biol Macromol 18, 141-145.

Meneghetti, M.C., Hughes, A.J., Rudd, T.R., Nader, H.B., Powell, A.K., Yates, E.A., Lima, M.A., 2015. Heparan sulfate and heparin interactions with proteins. J R Soc Interface 12, 0589.

Milasincic, D.J., Calera, M.R., Farmer, S.R., Pilch, P.F., 1996. Stimulation of C2C12 myoblast growth by basic fibroblast growth factor and insulin-like growth factor 1 can occur via mitogen-activated protein kinase-dependent and -independent pathways. Mol Cell Biol 16, 5964-5973.

Miller, R.L., Dykstra, A.B., Wei, W., Holsclaw, C., Turnbull, J.E., Leary, J.A., 2016a. Enrichment of Two Isomeric Heparin Oligosaccharides Exhibiting Different Affinities toward Monocyte Chemoattractant Protein-1. Anal Chem 88, 11551-11558.

Miller, R.L., Guimond, S.E., Shivkumar, M., Blocksidge, J., Austin, J.A., Leary, J.A., Turnbull, J.E., 2016b. Heparin Isomeric Oligosaccharide Separation Using Volatile Salt Strong Anion Exchange Chromatography. Anal Chem 88, 11542-11550.

Mitsi, M., Hong, Z., Costello, C.E., Nugent, M.A., 2006. Heparin-mediated conformational changes in fibronectin expose vascular endothelial growth factor binding sites. Biochemistry 45, 10319-10328.

Mollet, M., Godoy-Silva, R., Berdugo, C., Chalmers, J.J., 2007. Acute hydrodynamic forces and apoptosis: a complex question. Biotechnol Bioeng 98, 772-788.

Montarras, D., L'Honore, A., Buckingham, M., 2013. Lying low but ready for action: the quiescent muscle satellite cell. FEBS J 280, 4036-4050.

Morgan, J.E., Beauchamp, J.R., Pagel, C.N., Peckham, M., Ataliotis, P., Jat, P.S., Noble, M.D., Farmer, K., Partridge, T.A., 1994. Myogenic cell lines derived from transgenic mice carrying a thermolabile T antigen: a model system for the derivation of tissue-specific and mutation-specific cell lines. Dev Biol 162, 486-498.

Morgan, J.E., Partridge, T.A., 2003. Muscle satellite cells. Int J Biochem Cell Biol 35, 1151-1156.

Morgan, J.E., Zammit, P.S., 2010. Direct effects of the pathogenic mutation on satellite cell function in muscular dystrophy. Exp Cell Res 316, 3100-3108.

Morley, J.E., Baumgartner, R.N., Roubenoff, R., Mayer, J., Nair, K.S., 2001. Sarcopenia. J Lab Clin Med 137, 231-243.

Motohashi, N., Asakura, Y., Asakura, A., 2014. Isolation, culture, and transplantation of muscle satellite cells. J Vis Exp.

Mourey, R.J., Vega, Q.C., Campbell, J.S., Wenderoth, M.P., Hauschka, S.D., Krebs, E.G., Dixon, J.E., 1996. A novel cytoplasmic dual specificity protein tyrosine phosphatase implicated in muscle and neuronal differentiation. J Biol Chem 271, 3795-3802.

Mulloy, B., 2005. The specificity of interactions between proteins and sulfated polysaccharides. An Acad Bras Cienc 77, 651-664.

Mulloy, B., Johnson, E.A., 1987. Assignment of the 1H-n.m.r. spectra of heparin and heparan sulphate. Carbohydr Res 170, 151-165.

Murphy, M.M., Lawson, J.A., Mathew, S.J., Hutcheson, D.A., Kardon, G., 2011. Satellite cells, connective tissue fibroblasts and their interactions are crucial for muscle regeneration. Development 138, 3625-3637.

Nader, H.B., Kobayashi, E.Y., Chavante, S.F., Tersariol, I.L., Castro, R.A., Shinjo, S.K., Naggi, A., Torri, G., Casu, B., Dietrich, C.P., 1999. New insights on the specificity of heparin and heparan sulfate lyases from Flavobacterium heparinum revealed by the use of synthetic derivatives of K5 polysaccharide from E. coli and 2-O-desulfated heparin. Glycoconj J 16, 265-270.

Naimy, H., Buczek-Thomas, J.A., Nugent, M.A., Leymarie, N., Zaia, J., 2011. Highly sulfated nonreducing end-derived heparan sulfate domains bind fibroblast growth factor-2 with high affinity and are enriched in biologically active fractions. J Biol Chem 286, 19311-19319.

Nairn, A.V., Kinoshita-Toyoda, A., Toyoda, H., Xie, J., Harris, K., Dalton, S., Kulik, M., Pierce, J.M., Toida, T., Moremen, K.W., Linhardt, R.J., 2007. Glycomics of proteoglycan biosynthesis in murine embryonic stem cell differentiation. J Proteome Res 6, 4374-4387.

Neal, A., Boldrin, L., Morgan, J.E., 2012. The satellite cell in male and female, developing and adult mouse muscle: distinct stem cells for growth and regeneration. PLoS One 7, e37950.

Negroni, E., Henault, E., Chevalier, F., Gilbert-Sirieix, M., Van Kuppevelt, T.H., Papy-Garcia, D., Uzan, G., Albanese, P., 2014. Glycosaminoglycan modifications in Duchenne muscular dystrophy: specific remodeling of chondroitin sulfate/dermatan sulfate. J Neuropathol Exp Neurol 73, 789-797.

Nnodim, J.O., 2000. Satellite cell numbers in senile rat levator ani muscle. Mech Ageing Dev 112, 99-111.

Noti, C., Seeberger, P.H., 2005. Chemical approaches to define the structure-activity relationship of heparin-like glycosaminoglycans. Chem Biol 12, 731-756.
Oh, E.S., Couchman, J.R., 2004. Syndecans-2 and -4; close cousins, but not identical twins. Mol Cells 17, 181-187.

Oh, J., Lee, Y.D., Wagers, A.J., 2014. Stem cell aging: mechanisms, regulators and therapeutic opportunities. Nat Med 20, 870-880.

Okada, Y., Yamada, S., Toyoshima, M., Dong, J., Nakajima, M., Sugahara, K., 2002. Structural recognition by recombinant human heparanase that plays critical roles in tumor metastasis. Hierarchical sulfate groups with different effects and the essential target disulfated trisaccharide sequence. J Biol Chem 277, 42488-42495.

Olguin, H., Brandan, E., 2001. Expression and localization of proteoglycans during limb myogenic activation. Dev Dyn 221, 106-115.

Olguín, H.C., Pisconti, A., 2012. Marking the tempo for myogenesis: Pax7 and the regulation of muscle stem cell fate decisions. J Cell Mol Med 16, 1013-1025.

Olson, S.T., Björk, I., Sheffer, R., Craig, P.A., Shore, J.D., Choay, J., 1992. Role of the antithrombin-binding pentasaccharide in heparin acceleration of antithrombin-proteinase reactions. Resolution of the antithrombin conformational change contribution to heparin rate enhancement. J Biol Chem 267, 12528-12538.

Olwin, B.B., 1989. Heparin-binding growth factors and their receptors. Cytotechnology 2, 351-365.

Olwin, B.B., Arthur, K., Hannon, K., Hein, P., McFall, A., Riley, B., Szebenyi, G., Zhou, Z., Zuber, M.E., Rapraeger, A.C., 1994. Role of FGFs in skeletal muscle and limb development. Mol Reprod Dev 39, 90-100; discussion 100-101.

Ono, Y., Masuda, S., Nam, H.S., Benezra, R., Miyagoe-Suzuki, Y., Takeda, S., 2012. Slow-dividing satellite cells retain long-term self-renewal ability in adult muscle. J Cell Sci 125, 1309-1317.

Ori, A., Wilkinson, M.C., Fernig, D.G., 2008. The heparanome and regulation of cell function: structures, functions and challenges. Front Biosci 13, 4309-4338.

Ori, A., Wilkinson, M.C., Fernig, D.G., 2011. A systems biology approach for the investigation of the heparin/heparan sulfate interactome. J Biol Chem 286, 19892-19904.

Ornitz, D.M., Xu, J., Colvin, J.S., McEwen, D.G., MacArthur, C.A., Coulier, F., Gao, G., Goldfarb, M., 1996. Receptor specificity of the fibroblast growth factor family. J Biol Chem 271, 15292-15297.

Paliwal, P., Pishesha, N., Wijaya, D., Conboy, I.M., 2012. Age dependent increase in the levels of osteopontin inhibits skeletal muscle regeneration. Aging (Albany NY) 4, 553-566.

Papakonstantinou, E., Karakiulakis, G., 2009. The 'sweet' and 'bitter' involvement of glycosaminoglycans in lung diseases: pharmacotherapeutic relevance. Br J Pharmacol 157, 1111-1127.

Papy-Garcia, D., Barbosa, I., Duchesnay, A., Saadi, S., Caruelle, J.P., Barritault, D., Martelly, I., 2002. Glycosaminoglycan mimetics (RGTA) modulate adult skeletal muscle satellite cell proliferation in vitro. J Biomed Mater Res 62, 46-55.

Pasut, A., Oleynik, P., Rudnicki, M.A., 2012. Isolation of muscle stem cells by fluorescence activated cell sorting cytometry. Methods Mol Biol 798, 53-64.

Patel, M., Yanagishita, M., Roderiquez, G., Bou-Habib, D.C., Oravecz, T., Hascall, V.C., Norcross, M.A., 1993. Cell-surface heparan sulfate proteoglycan mediates HIV-1 infection of T-cell lines. AIDS Res Hum Retroviruses 9, 167-174.

Patel, V.N., Lombaert, I.M., Cowherd, S.N., Shworak, N.W., Xu, Y., Liu, J., Hoffman, M.P., 2014. Hs3st3-modified heparan sulfate controls KIT+ progenitor expansion by regulating 3-O-sulfotransferases. Dev Cell 29, 662-673.

Patey, S.J., Edwards, E.A., Yates, E.A., Turnbull, J.E., 2006. Heparin derivatives as inhibitors of BACE-1, the Alzheimer's beta-secretase, with reduced activity against factor Xa and other proteases. J Med Chem 49, 6129-6132.

Perrimon, N., Bernfield, M., 2000. Specificities of heparan sulphate proteoglycans in developmental processes. Nature 404, 725-728.

Peterson, S.B., Liu, J., 2010. Unraveling the specificity of heparanase utilizing synthetic substrates. J Biol Chem 285, 14504-14513.

Pinhal, M.A., Smith, B., Olson, S., Aikawa, J., Kimata, K., Esko, J.D., 2001. Enzyme interactions in heparan sulfate biosynthesis: uronosyl 5-epimerase and 2-O-sulfotransferase interact in vivo. Proc Natl Acad Sci U S A 98, 12984-12989.

Pisconti, A., Banks, G.B., Babaeijandaghi, F., Betta, N.D., Rossi, F.M., Chamberlain, J.S., Olwin, B.B., 2016. Loss of niche-satellite cell interactions in syndecan-3 null mice alters muscle progenitor cell homeostasis improving muscle regeneration. Skelet Muscle 6, 34.

Pisconti, A., Bernet, J.D., Olwin, B.B., 2012. Syndecans in skeletal muscle development, regeneration and homeostasis. Muscles Ligaments Tendons J 2, 1-9.

Pisconti, A., Cornelison, D.D., Olguin, H.C., Antwine, T.L., Olwin, B.B., 2010. Syndecan-3 and Notch cooperate in regulating adult myogenesis. The Journal of cell biology 190, 427-441.

Polat, T., Wong, C.H., 2007. Anomeric reactivity-based one-pot synthesis of heparin-like oligosaccharides. J Am Chem Soc 129, 12795-12800.

Poulain, F.E., Yost, H.J., 2015. Heparan sulfate proteoglycans: a sugar code for vertebrate development? Development 142, 3456-3467.

Powell, A.K., Ahmed, Y.A., Yates, E.A., Turnbull, J.E., 2010. Generating heparan sulfate saccharide libraries for glycomics applications. Nat Protoc 5, 821-833.

Powell, A.K., Fernig, D.G., Turnbull, J.E., 2002. Fibroblast growth factor receptors 1 and 2 interact differently with heparin/heparan sulfate. Implications for dynamic assembly of a ternary signaling complex. J Biol Chem 277, 28554-28563.

Price, F.D., von Maltzahn, J., Bentzinger, C.F., Dumont, N.A., Yin, H., Chang, N.C., Wilson, D.H., Frenette, J., Rudnicki, M.A., 2014. Inhibition of JAK-STAT signaling stimulates adult satellite cell function. Nat Med 20, 1174-1181.

Pye, D.A., Vives, R.R., Turnbull, J.E., Hyde, P., Gallagher, J.T., 1998. Heparan sulfate oligosaccharides require 6-O-sulfation for promotion of basic fibroblast growth factor mitogenic activity. J Biol Chem 273, 22936-22942.

Qu-Petersen, Z., Deasy, B., Jankowski, R., Ikezawa, M., Cummins, J., Pruchnic, R., Mytinger, J., Cao, B., Gates, C., Wernig, A., Huard, J., 2002. Identification of a novel population of muscle stem cells in mice: potential for muscle regeneration. The Journal of cell biology 157, 851-864.

Rando, T.A., Blau, H.M., 1994. Primary mouse myoblast purification, characterization, and transplantation for cell-mediated gene therapy. The Journal of cell biology 125, 1275-1287.

Rao, C.N., Margulies, I.M., Liotta, L.A., 1985. Binding domain for laminin on type IV collagen. Biochem Biophys Res Commun 128, 45-52.

Rapraeger, A.C., Krufka, A., Olwin, B.B., 1991. Requirement of heparan sulfate for bFGF-mediated fibroblast growth and myoblast differentiation. Science 252, 1705-1708.

Reznik, M., 1969. Thymidine-3H uptake by satellite cells of regenerating skeletal muscle. The Journal of cell biology 40, 568-571.

Rhodes, S.J., Konieczny, S.F., 1989. Identification of MRF4: a new member of the muscle regulatory factor gene family. Genes & development 3, 2050-2061.

Richler, C., Yaffe, D., 1970. The in vitro cultivation and differentiation capacities of myogenic cell lines. Dev Biol 23, 1-22.
Roubenoff, R., 2001. Origins and clinical relevance of sarcopenia. Can J Appl Physiol 26, 78-89.

Rouet, V., Hamma-Kourbali, Y., Petit, E., Panagopoulou, P., Katsoris, P., Barritault, D., Caruelle, J.P., Courty, J., 2005. A synthetic glycosaminoglycan mimetic binds vascular endothelial growth factor and modulates angiogenesis. J Biol Chem 280, 32792-32800.

Roy, S., El Hadri, A., Richard, S., Denis, F., Holte, K., Duffner, J., Yu, F., Galcheva-Gargova, Z., Capila, I., Schultes, B., Petitou, M., Kaundinya, G.V., 2014. Synthesis and biological evaluation of a unique heparin mimetic hexasaccharide for structure-activity relationship studies. J Med Chem 57, 4511-4520.

Rudd, T.R., Gaudesi, D., Skidmore, M.A., Ferro, M., Guerrini, M., Mulloy, B., Torri, G., Yates, E.A., 2011. Construction and use of a library of bona fide heparins employing 1H NMR and multivariate analysis. Analyst 136, 1380-1389.

Rudd, T.R., Uniewicz, K.A., Ori, A., Guimond, S.E., Skidmore, M.A., Gaudesi, D., Xu, R., Turnbull, J.E., Guerrini, M., Torri, G., Siligardi, G., Wilkinson, M.C., Fernig, D.G., Yates, E.A., 2010. Comparable stabilisation, structural changes and activities can be induced in FGF by a variety of HS and non-GAG analogues: implications for sequence-activity relationships. Org Biomol Chem 8, 5390-5397.

Rudd, T.R., Yates, E.A., 2010. Conformational degeneracy restricts the effective information content of heparan sulfate. Mol Biosyst 6, 902-908.

Rudd, T.R., Yates, E.A., 2012. A highly efficient tree structure for the biosynthesis of heparan sulfate accounts for the commonly observed disaccharides and suggests a mechanism for domain synthesis. Mol Biosyst 8, 1499-1506.

Sabourin, L.A., Rudnicki, M.A., 2000. The molecular regulation of myogenesis. Clin Genet 57, 16-25.

Saksela, O., Moscatelli, D., Sommer, A., Rifkin, D.B., 1988. Endothelial cell-derived heparan sulfate binds basic fibroblast growth factor and protects it from proteolytic degradation. The Journal of cell biology 107, 743-751.

Sambasivan, R., Yao, R., Kissenpfennig, A., Van Wittenberghe, L., Paldi, A., Gayraud-Morel, B., Guenou, H., Malissen, B., Tajbakhsh, S., Galy, A., 2011. Pax7-expressing satellite cells are indispensable for adult skeletal muscle regeneration. Development 138, 3647-3656.

Sanes, J.R., 2003. The basement membrane/basal lamina of skeletal muscle. J Biol Chem 278, 12601-12604.

Sangaj, N., Kyriakakis, P., Yang, D., Chang, C.W., Arya, G., Varghese, S., 2010. Heparin mimicking polymer promotes myogenic differentiation of muscle progenitor cells. Biomacromolecules 11, 3294-3300.

Saoncella, S., Echtermeyer, F., Denhez, F., Nowlen, J.K., Mosher, D.F., Robinson, S.D., Hynes, R.O., Goetinck, P.F., 1999. Syndecan-4 signals cooperatively with integrins in a Rho-dependent manner in the assembly of focal adhesions and actin stress fibers. Proc Natl Acad Sci U S A 96, 2805-2810.

Sarrazin, S., Lamanna, W.C., Esko, J.D., 2011. Heparan sulfate proteoglycans. Cold Spring Harb Perspect Biol 3.

Sattelle, B.M., Hansen, S.U., Gardiner, J., Almond, A., 2010. Free energy landscapes of iduronic acid and related monosaccharides. J Am Chem Soc 132, 13132-13134.

Schabort, E.J., van der Merwe, M., Loos, B., Moore, F.P., Niesler, C.U., 2009. TGF-beta's delay skeletal muscle progenitor cell differentiation in an isoform-independent manner. Exp Cell Res 315, 373-384.

Schäfer, R., Zweyer, M., Knauf, U., Mundegar, R.R., Wernig, A., 2005. The ontogeny of soleus muscles in mdx and wild type mice. Neuromuscul Disord 15, 57-64.

Schlessinger, J., Plotnikov, A.N., Ibrahimi, O.A., Eliseenkova, A.V., Yeh, B.K., Yayon, A., Linhardt, R.J., Mohammadi, M., 2000. Crystal structure of a ternary FGF-FGFR-heparin complex reveals a dual role for heparin in FGFR binding and dimerization. Mol Cell 6, 743-750.

Scholefield, Z., Yates, E.A., Wayne, G., Amour, A., McDowell, W., Turnbull, J.E., 2003. Heparan sulfate regulates amyloid precursor protein processing by BACE1, the Alzheimer's beta-secretase. The Journal of cell biology 163, 97-107.

Schwörer, R., Zubkova, O.V., Turnbull, J.E., Tyler, P.C., 2013. Synthesis of a targeted library of heparan sulfate hexa- to dodecasaccharides as inhibitors of β-secretase: potential therapeutics for Alzheimer's disease. Chemistry 19, 6817-6823.

Seed, J., Hauschka, S.D., 1988. Clonal analysis of vertebrate myogenesis. VIII. Fibroblasts growth factor (FGF)-dependent and FGF-independent muscle colony types during chick wing development. Dev Biol 128, 40-49.

Seffouh, A., Milz, F., Przybylski, C., Laguri, C., Oosterhof, A., Bourcier, S., Sadir, R., Dutkowski, E., Daniel, R., van Kuppevelt, T.H., Dierks, T., Lortat-Jacob, H., Vivès, R.R.,

2013. HSulf sulfatases catalyze processive and oriented 6-O-desulfation of heparan sulfate that differentially regulates fibroblast growth factor activity. FASEB J 27, 2431-2439.

Selleck, S.B., 2000. Proteoglycans and pattern formation: sugar biochemistry meets developmental genetics. Trends Genet 16, 206-212.

Shavlakadze, T., McGeachie, J., Grounds, M.D., 2010. Delayed but excellent myogenic stem cell response of regenerating geriatric skeletal muscles in mice. Biogerontology 11, 363-376.

Shea, K.L., Xiang, W., LaPorta, V.S., Licht, J.D., Keller, C., Basson, M.A., Brack, A.S., 2010. Sprouty1 regulates reversible quiescence of a self-renewing adult muscle stem cell pool during regeneration. Cell Stem Cell 6, 117-129.

Sheehan, S.M., Allen, R.E., 1999. Skeletal muscle satellite cell proliferation in response to members of the fibroblast growth factor family and hepatocyte growth factor. J Cell Physiol 181, 499-506.

Shefer, G., Benayahu, D., 2012. The effect of exercise on IGF-I on muscle fibers and satellite cells. Front Biosci (Elite Ed) 4, 230-239.

Shefer, G., Van de Mark, D.P., Richardson, J.B., Yablonka-Reuveni, Z., 2006. Satellite-cell pool size does matter: defining the myogenic potency of aging skeletal muscle. Dev Biol 294, 50-66.

Shriver, Z., Capila, I., Venkataraman, G., Sasisekharan, R., 2012. Heparin and heparan sulfate: analyzing structure and microheterogeneity. Handb Exp Pharmacol, 159-176.

Shworak, N.W., Liu, J., Petros, L.M., Zhang, L., Kobayashi, M., Copeland, N.G., Jenkins, N.A., Rosenberg, R.D., 1999. Multiple isoforms of heparan sulfate D-glucosaminyl 3-O-sulfotransferase. Isolation, characterization, and expression of human cdnas and identification of distinct genomic loci. J Biol Chem 274, 5170-5184.

Shworak, N.W., Shirakawa, M., Colliec-Jouault, S., Liu, J., Mulligan, R.C., Birinyi, L.K., Rosenberg, R.D., 1994. Pathway-specific regulation of the synthesis of anticoagulantly active heparan sulfate. J Biol Chem 269, 24941-24952.

Siegel, A.L., Atchison, K., Fisher, K.E., Davis, G.E., Cornelison, D.D., 2009. 3D timelapse analysis of muscle satellite cell motility. Stem Cells 27, 2527-2538.

Skidmore, M.A., Guimond, S.E., Dumax-Vorzet, A.F., Atrih, A., Yates, E.A., Turnbull, J.E., 2006. High sensitivity separation and detection of heparan sulfate disaccharides. J Chromatogr A 1135, 52-56.

Skidmore, M.A., Guimond, S.E., Dumax-Vorzet, A.F., Yates, E.A., Turnbull, J.E., 2010. Disaccharide compositional analysis of heparan sulfate and heparin polysaccharides using UV or high-sensitivity fluorescence (BODIPY) detection. Nat Protoc 5, 1983-1992.

Smith, E.M., Mitsi, M., Nugent, M.A., Symes, K., 2009. PDGF-A interactions with fibronectin reveal a critical role for heparan sulfate in directed cell migration during Xenopus gastrulation. Proc Natl Acad Sci U S A 106, 21683-21688.

Smith, R.A., Meade, K., Pickford, C.E., Holley, R.J., Merry, C.L., 2011. Glycosaminoglycans as regulators of stem cell differentiation. Biochem Soc Trans 39, 383-387.

Smythe, G.M., Shavlakadze, T., Roberts, P., Davies, M.J., McGeachie, J.K., Grounds, M.D., 2008. Age influences the early events of skeletal muscle regeneration: studies of whole muscle grafts transplanted between young (8 weeks) and old (13-21 months) mice. Exp Gerontol 43, 550-562.

Sogos, V., Balaci, L., Ennas, M.G., Dell'era, P., Presta, M., Gremo, F., 1998. Developmentally regulated expression and localization of fibroblast growth factor receptors in the human muscle. Dev Dyn 211, 362-373.

Solari, V., Rudd, T.R., Guimond, S.E., Powell, A.K., Turnbull, J.E., Yates, E.A., 2015. Heparan sulfate phage display antibodies recognise epitopes defined by a combination of sugar sequence and cation binding. Org Biomol Chem 13, 6066-6072.

Sousa-Victor, P., Gutarra, S., García-Prat, L., Rodriguez-Ubreva, J., Ortet, L., Ruiz-Bonilla, V., Jardí, M., Ballestar, E., González, S., Serrano, A.L., Perdiguero, E., Muñoz-Cánoves, P., 2014a. Geriatric muscle stem cells switch reversible quiescence into senescence. Nature 506, 316-321.

Sousa-Victor, P., Perdiguero, E., Muñoz-Cánoves, P., 2014b. Geroconversion of aged muscle stem cells under regenerative pressure. Cell Cycle 13, 3183-3190.

Sugaya, N., Habuchi, H., Nagai, N., Ashikari-Hada, S., Kimata, K., 2008. 6-O-sulfation of heparan sulfate differentially regulates various fibroblast growth factor-dependent signalings in culture. J Biol Chem 283, 10366-10376.

Suzuki, K., Yamamoto, K., Kariya, Y., Maeda, H., Ishimaru, T., Miyaura, S., Fujii, M., Yusa, A., Joo, E.J., Kimata, K., Kannagi, R., Kim, Y.S., Kyogashima, M., 2008. Generation and characterization of a series of monoclonal antibodies that specifically recognize [HexA(+/-2S)-GlcNAc]n epitopes in heparan sulfate. Glycoconj J 25, 703-712.

Takemura, M., Nakato, H., 2017. Drosophila Sulf1 is required for the termination of intestinal stem cell division during regeneration. J Cell Sci 130, 332-343.

Tatsumi, R., Allen, R.E., 2004. Active hepatocyte growth factor is present in skeletal muscle extracellular matrix. Muscle & nerve 30, 654-658.

Templeton, D.M., 1988. The basis and applicability of the dimethylmethylene blue binding assay for sulfated glycosaminoglycans. Connect Tissue Res 17, 23-32.

Templeton, T.J., Hauschka, S.D., 1992. FGF-mediated aspects of skeletal muscle growth and differentiation are controlled by a high affinity receptor, FGFR1. Dev Biol 154, 169-181.

Thacker, B.E., Seamen, E., Lawrence, R., Parker, M.W., Xu, Y., Liu, J., Vander Kooi, C.W., Esko, J.D., 2016. Expanding the 3-O-Sulfate Proteome--Enhanced Binding of Neuropilin-1 to 3-O-Sulfated Heparan Sulfate Modulates Its Activity. ACS Chem Biol 11, 971-980.

Thacker, B.E., Xu, D., Lawrence, R., Esko, J.D., 2014. Heparan sulfate 3-O-sulfation: a rare modification in search of a function. Matrix Biol 35, 60-72.

Thompson, S.M., Fernig, D.G., Jesudason, E.C., Losty, P.D., van de Westerlo, E.M., van Kuppevelt, T.H., Turnbull, J.E., 2009. Heparan sulfate phage display antibodies identify distinct epitopes with complex binding characteristics: insights into protein binding specificities. J Biol Chem 284, 35621-35631.

Toyoda, H., Nagashima, T., Hirata, R., Toida, T., Imanari, T., 1997. Sensitive high-performance liquid chromatographic method with fluorometric detection for the determination of heparin and heparan sulfate in biological samples: application to human urinary heparan sulfate. J Chromatogr B Biomed Sci Appl 704, 19-24.

Tran, T.H., Shi, X., Zaia, J., Ai, X., 2012. Heparan sulfate 6-O-endosulfatases (Sulfs) coordinate the Wnt signaling pathways to regulate myoblast fusion during skeletal muscle regeneration. J Biol Chem 287, 32651-32664.

Turnbull, J., Powell, A., Guimond, S., 2001. Heparan sulfate: decoding a dynamic multifunctional cell regulator. Trends Cell Biol 11, 75-82.

Turnbull, J.E., 2001. Analytical and preparative strong anion-exchange HPLC of heparan sulfate and heparin saccharides. Methods Mol Biol 171, 141-147.

Turnbull, J.E., Fernig, D.G., Ke, Y., Wilkinson, M.C., Gallagher, J.T., 1992. Identification of the basic fibroblast growth factor binding sequence in fibroblast heparan sulfate. J Biol Chem 267, 10337-10341.

Tyler, P.C., Guimond, S.E., Turnbull, J.E., Zubkova, O.V., 2015. Single-entity heparan sulfate glycomimetic clusters for therapeutic applications. Angew Chem Int Ed Engl 54, 2718-2723.

Uniewicz, K.A., Ori, A., Rudd, T.R., Guerrini, M., Wilkinson, M.C., Fernig, D.G., Yates, E.A., 2012. Following protein-glycosaminoglycan polysaccharide interactions with differential scanning fluorimetry. Methods Mol Biol 836, 171-182.

Uniewicz, K.A., Ori, A., Xu, R., Ahmed, Y., Wilkinson, M.C., Fernig, D.G., Yates, E.A., 2010. Differential scanning fluorimetry measurement of protein stability changes upon binding to glycosaminoglycans: a screening test for binding specificity. Anal Chem 82, 3796-3802.

Urciuolo, A., Quarta, M., Morbidoni, V., Gattazzo, F., Molon, S., Grumati, P., Montemurro, F., Tedesco, F.S., Blaauw, B., Cossu, G., Vozzi, G., Rando, T.A., Bonaldo, P., 2013. Collagen VI regulates satellite cell self-renewal and muscle regeneration. Nat Commun 4, 1964.

van den Born, J., Salmivirta, K., Henttinen, T., Ostman, N., Ishimaru, T., Miyaura, S., Yoshida, K., Salmivirta, M., 2005. Novel heparan sulfate structures revealed by monoclonal antibodies. J Biol Chem 280, 20516-20523.

van Kuppevelt, T.H., Dennissen, M.A., van Venrooij, W.J., Hoet, R.M., Veerkamp, J.H., 1998. Generation and application of type-specific anti-heparan sulfate antibodies using phage display technology. Further evidence for heparan sulfate heterogeneity in the kidney. J Biol Chem 273, 12960-12966.

Venkataraman, G., Shriver, Z., Raman, R., Sasisekharan, R., 1999. Sequencing complex polysaccharides. Science 286, 537-542.

Verdijk, L.B., Snijders, T., Drost, M., Delhaas, T., Kadi, F., van Loon, L.J., 2014. Satellite cells in human skeletal muscle; from birth to old age. Age (Dordr) 36, 545-547.

Victor, X.V., Nguyen, T.K., Ethirajan, M., Tran, V.M., Nguyen, K.V., Kuberan, B., 2009. Investigating the elusive mechanism of glycosaminoglycan biosynthesis. J Biol Chem 284, 25842-25853.

Vlodavsky, I., Bar-Shavit, R., Ishai-Michaeli, R., Bashkin, P., Fuks, Z., 1991. Extracellular sequestration and release of fibroblast growth factor: a regulatory mechanism? Trends Biochem Sci 16, 268-271.

Vlodavsky, I., Miao, H.Q., Medalion, B., Danagher, P., Ron, D., 1996. Involvement of heparan sulfate and related molecules in sequestration and growth promoting activity of fibroblast growth factor. Cancer Metastasis Rev 15, 177-186.

von der Mark, H., Dürr, J., Sonnenberg, A., von der Mark, K., Deutzmann, R., Goodman, S.L., 1991. Skeletal myoblasts utilize a novel beta 1-series integrin and not alpha 6 beta 1 for binding to the E8 and T8 fragments of laminin. J Biol Chem 266, 23593-23601.

Wang, S., Ai, X., Freeman, S.D., Pownall, M.E., Lu, Q., Kessler, D.S., Emerson, C.P., 2004. QSulf1, a heparan sulfate 6-O-endosulfatase, inhibits fibroblast growth factor signaling in mesoderm induction and angiogenesis. Proc Natl Acad Sci U S A 101, 4833-4838.

Woods, A., Longley, R.L., Tumova, S., Couchman, J.R., 2000. Syndecan-4 binding to the high affinity heparin-binding domain of fibronectin drives focal adhesion formation in fibroblasts. Arch Biochem Biophys 374, 66-72.

Wu, L., Viola, C.M., Brzozowski, A.M., Davies, G.J., 2016. Corrigendum: Structural characterization of human heparanase reveals insights into substrate recognition. Nat Struct Mol Biol 23, 91.

Xia, G., Chen, J., Tiwari, V., Ju, W., Li, J.P., Malmstrom, A., Shukla, D., Liu, J., 2002. Heparan sulfate 3-O-sulfotransferase isoform 5 generates both an antithrombin-binding site and an entry receptor for herpes simplex virus, type 1. J Biol Chem 277, 37912-37919.

Xu, Y., Masuko, S., Takieddin, M., Xu, H., Liu, R., Jing, J., Mousa, S.A., Linhardt, R.J., Liu, J., 2011. Chemoenzymatic synthesis of homogeneous ultralow molecular weight heparins. Science 334, 498-501.

Xu, Y., Pempe, E.H., Liu, J., 2012. Chemoenzymatic synthesis of heparin oligosaccharides with both anti-factor Xa and anti-factor IIa activities. J Biol Chem 287, 29054-29061.

Yablonka-Reuveni, Z., Danoviz, M.E., Phelps, M., Stuelsatz, P., 2015. Myogenic-specific ablation of Fgfr1 impairs FGF2-mediated proliferation of satellite cells at the myofiber niche but does not abolish the capacity for muscle regeneration. Front Aging Neurosci 7, 85.

Yablonka-Reuveni, Z., Rivera, A.J., 1997. Proliferative Dynamics and the Role of FGF2 During Myogenesis of Rat Satellite Cells on Isolated Fibers. Basic Appl Myol 7, 189-202.

Yablonka-Reuveni, Z., Seger, R., Rivera, A.J., 1999. Fibroblast growth factor promotes recruitment of skeletal muscle satellite cells in young and old rats. J Histochem Cytochem 47, 23-42.

Yaffe, D., Saxel, O., 1977. Serial passaging and differentiation of myogenic cells isolated from dystrophic mouse muscle. Nature 270, 725-727.

Yamauchi, H., Desgranges, P., Lecerf, L., Papy-Garcia, D., Tournaire, M.C., Moczar, M., Loisance, D., Barritault, D., 2000. New agents for the treatment of infarcted myocardium. FASEB J 14, 2133-2134.

Yates, E.A., Santini, F., Guerrini, M., Naggi, A., Torri, G., Casu, B., 1996. 1H and 13C NMR spectral assignments of the major sequences of twelve systematically modified heparin derivatives. Carbohydr Res 294, 15-27.

Yayon, A., Klagsbrun, M., Esko, J.D., Leder, P., Ornitz, D.M., 1991. Cell surface, heparin-like molecules are required for binding of basic fibroblast growth factor to its high affinity receptor. Cell 64, 841-848.

Ye, S., Luo, Y., Lu, W., Jones, R.B., Linhardt, R.J., Capila, I., Toida, T., Kan, M., Pelletier, H., McKeehan, W.L., 2001. Structural basis for interaction of FGF-1, FGF-2, and FGF-7 with different heparan sulfate motifs. Biochemistry 40, 14429-14439.

Yin, H., Price, F., Rudnicki, M.A., 2013. Satellite cells and the muscle stem cell niche. Physiol Rev 93, 23-67.

Yoshida, N., Yoshida, S., Koishi, K., Masuda, K., Nabeshima, Y., 1998. Cell heterogeneity upon myogenic differentiation: down-regulation of MyoD and Myf-5 generates 'reserve cells'. J Cell Sci 111 (Pt 6), 769-779.

Yousef, H., Conboy, M.J., Morgenthaler, A., Schlesinger, C., Bugaj, L., Paliwal, P., Greer, C., Conboy, I.M., Schaffer, D., 2015. Systemic attenuation of the TGF-beta pathway by a single drug simultaneously rejuvenates hippocampal neurogenesis and myogenesis in the same old mammal. Oncotarget 6, 11959-11978.

Zacks, S.I., Sheff, M.F., 1982. Age-related impeded regeneration of mouse minced anterior tibial muscle. Muscle Nerve 5, 152-161.

Zammit, P.S., Carvajal, J.J., Golding, J.P., Morgan, J.E., Summerbell, D., Zolnerciks, J., Partridge, T.A., Rigby, P.W., Beauchamp, J.R., 2004. Myf5 expression in satellite cells and spindles in adult muscle is controlled by separate genetic elements. Dev Biol 273, 454-465.

Zhang, G.L., Zhang, X., Wang, X.M., Li, J.P., 2014. Towards understanding the roles of heparan sulfate proteoglycans in Alzheimer's disease. Biomed Res Int 2014, 516028.

Zhang, L., 2010. Glycosaminoglycan (GAG) biosynthesis and GAG-binding proteins. Prog Mol Biol Transl Sci 93, 1-17.

Zhang, L., David, G., Esko, J.D., 1995. Repetitive Ser-Gly sequences enhance heparan sulfate assembly in proteoglycans. J Biol Chem 270, 27127-27135.

Zhao, S., Deng, C., Wang, Z., Teng, L., Chen, J., 2015. Heparan sulfate 6-O-sulfotransferase 3 is involved in bone marrow mesenchymal stromal cell osteogenic differentiation. Biochemistry (Mosc) 80, 379-389.

Ziebell, M.R., Zhao, Z.G., Luo, B., Luo, Y., Turley, E.A., Prestwich, G.D., 2001. Peptides that mimic glycosaminoglycans: high-affinity ligands for a hyaluronan binding domain. Chem Biol 8, 1081-1094.

Zimowska, M., Constantin, B., Papy-Garcia, D., Raymond, G., Cognard, C., Caruelle, J.P., Moraczewski, J., Martelly, I., 2005. Novel glycosaminoglycan mimetic (RGTA, RGD120) contributes to enhance skeletal muscle satellite cell fusion by increasing intracellular Ca2+ and calpain activity. J Cell Physiol 205, 237-245.

Zimowska, M., Duchesnay, A., Dragun, P., Oberbek, A., Moraczewski, J., Martelly, I., 2009. Immunoneutralization of TGFbeta1 Improves Skeletal Muscle Regeneration: Effects on Myoblast Differentiation and Glycosaminoglycan Content. International journal of cell biology 2009, 659372.

Zimowska, M., Szczepankowska, D., Streminska, W., Papy, D., Tournaire, M.C., Gautron, J., Barritault, D., Moraczewski, J., Martelly, I., 2001. Heparan sulfate mimetics modulate calpain activity during rat Soleus muscle regeneration. J Cell Physiol 188, 178-187.

Zou, Y., Zhang, R.Z., Sabatelli, P., Chu, M.L., Bönnemann, C.G., 2008. Muscle interstitial fibroblasts are the main source of collagen VI synthesis in skeletal muscle: implications for congenital muscular dystrophy types Ullrich and Bethlem. J Neuropathol Exp Neurol 67, 144-154.

Appendix

Appendix 1: RT PCR For SiRNA Knockdown
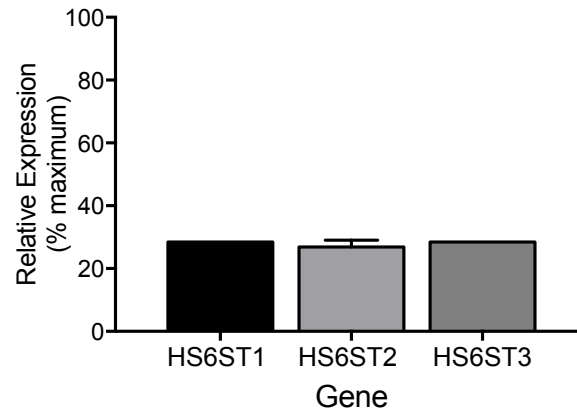
Appendix 1 Extent of knockdown Transfection of siRNA against HS6ST1, HS6ST2 and HS6ST3 results in knock-down of HS6ST expression by approximately 75%. C2C12 cells were transfected with either 60 nM universal control siRNA or with a combined treatment of 20 nM of siRNA directed to each one of the three HS6STs (HS6ST1, HS6ST2 and HS6ST3). GAPDH was used as a house-keeping gene and the mRNA levels of the three HS6STs and of GAPDH measured by qPCR in both transfection conditions. The ΔΔCt method was used to quantify and normalise the results which are expressed as percentage of each HS6ST/GAPDH mRNA in the 3xHS6ST siRNA-transfected cells over the amount of each HS6ST/GAPDH mRNA in the cells transfected with control siRNA. One representative of two independent experiments is shown where the results from two technical replicates are averaged and plotted ± standard deviation (Ghadiali et al., 2016).

Appendix 2: Effects of HS mimetics on proliferation in high serum conditions
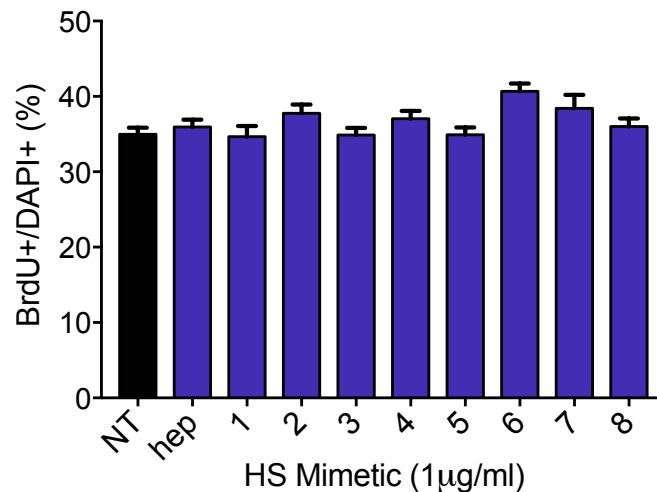
Appendix 2: Effects of HS mimetics on myoblast proliferation in high serum conditions. HS mimetics differentially effect myoblast cell number. Primary SC-derived myoblasts were cultured for 2 days in growth medium and then treated with the HS mimetics snd grown for a further 24 hours followed by a BrdU proliferation assay. For each condition shown, the proortion of BrdU+ nuclei was measured and the average of ten images across two technical replicates for three independent experiments ± S.E.M. plotted.

A 2.1 General Chemistry Methods

Air sensitive reactions were performed under argon. Organic solutions were dried over anhydrous $MgSO_4$ and the solvents were evaporated under reduced pressure. Anhydrous and chromatography solvents were obtained commercially and used without any further purification.

A 2.1.2 NMR Spectroscopy

Proton magnetic resonance spectra were recorded on 500 MHz spectrometers at ambient temperatures. Chemical shifts (δ_H) are reported in parts per million (ppm) and are referenced to the residual solvent peak (Gottlieb et al., 1997). ^{1}H NMR spectra were measured in $CDCl_3$, CD_3OD or D_2O (HOD, δ 4.79). Carbon magnetic resonance spectra were recorded on 500 MHz spectrometers at ambient temperatures. Chemical shits (δ_C) are reported in parts per million (ppm) and are referenced to the residual solvent peak. ^{13}C NMR spectra in $CDCl_3$ (centre line, δ 77.0), CD_3OD (centre line, δ 49.0), D_2O (no internal reference, δ1.47 where stated). Assignments of ^{1}H and ^{13}C resonances were based on 2D (1H-1H COSY, 1H-13C HSQC) experiments. Coupling constants (*J*) are recorded to the nearest 0.5Hz. Multiplicities are abbreviated as s (singlet), d (doublet), t (triplet) or m (multiplet).

A 2.1.3 Analytical Thin Layer Chromatograph (TLC)

Thin layer chromatography was performed on aluminium sheets coated with 60 F254 silica gel. Organic compounds were visualized under UV light or use of a dip of ammonium molybdate (5 wt%) and cerium(IV) sulfate 4 H_2O (0.2 wt%) in aq. H_2SO_4 (2M), or 0.1% ninhydrin in ethanol.

A 2.1.4 Column Chromatography

Chromatography (flash column, or an automated system with continuous gradient facility) was performed on silica gel (40-63 μm). The crude material was applied to the column by pre-adsorption onto silica, as appropriate.

A 2.1.4 Mass Spectrometry

High resolution electrospray mass spectra (ESIHRMS) were recorded on a Q-TOF Tandem Mass Spectrometer.

A 2.2 Chemical Procedures and Compound Characterisations

A 2.2.1 De-chloroacetylation
Synthesis of Compound 13

Compound **13** was prepared from dimer **12:** DABCO (6 equiv. per chloroacetyl group) was added to the starting material in dry ethanol/acetonitrile, 5:1 (5 mL for 40 µmol) at room temperature. The mixture was heated at 60-70 $^{\circ}$C under argon for 2hoursAfter TLC (ethyl acetate:petroleum ether, 1:1) indicated the completion of the reaction the reaction was diluted with ethyl acetate and washed with 1M aq. HCL and extracted. The organic layer was washed with sodium hydrogen carbonate, extracted and then washed with brine and dried over $MgSO_4$. Concentrated in vacuo. Hivac o/n. To ensure the *N*-Fmoc group had not been removed, the crude reaction mixture was dissolved in methanol and triethylamine (1.1 equiv.) was added followed by FmocCl (1 equiv) at 0 $^{\circ}$C. The reaction mixture was stirred for 2 hours at RT until completion. The reaction was diluted with chloroform, washed with 1M aq HCL, sodium hydrogen carbonate, extracted. The organic layer was then washed with brine and dried over $MgSO_4$. Concentrated in vacuo. Chromatography (ethyl acetate:petroleum ether, 1:1) afforded product **13** with an unblocked primary hydroxyl group (**13**, 0.95g, 0.44mmol, 78% yield). TLC (ethyl acetate: petroleum ether, 1:9 → 1:1) Rf = 0.52. **^{1}H NMR** (500 MHz, $CDCl_3$) δ 8.16-8.13 (m, 2H, Ar H), 7.77-7.74 (m, 2H, Ar H), 7.42-7.24 (m, 22H, Ar H), 7.17-7.14 (m, 2H, Ar H), 5.15 (bs, 1H, i*H*2), 4.98 (s, 1H, i*H*1), 4.92 (d, *J* = 11.7 Hz, 1H, Bn-C*H*), 4.78-4.71 (m, 2H, Bn-C*H*), 4.64 (d, *J* = 1H,) g*H*1), 4.51 (d, *J* = 10.9 Hz, 1H, Bn-C*H*), 4.43-4.36 (m, 3H, C*H*Fmoc + Bn-C*H*), 4.32-4.26 (m, 2H, i*H*5 + g*H*6), 4.24-4.19 (m, 1H, C*H*Fmoc), 4.16-4.08 (m, g*H*6), 4.00-3.95 (m, 1H, g*H*5), 3.92-3.87 (m, 1H, CH2), 3.80-3,71 (m, 3H, i*H*4) 3.68 – 3.63 (m, 1H, g*H*3), 3.50-3.45 (m, 1H, linker), 3.38 – 3.32 (m, 1H, g*H*4), 3.29 (dd, *J* = 10.2, 3.7 Hz, 1H, g*H*2), 3.17-3.11 (m, 1H, linker), 2.02 (s, 3H, OAc), 1.67-1.59 (m, 1H), 1.47-1.22 (11 H). **^{13}C NMR:** (126 MHz, $CDCl_3$) δ ^{13}C NMR (126 MHz, $CDCl_3$) δ 133.15, 129.81, 128.55, 128.40, 128.27, 128.00, 127.64, 127.03, 125.02, 98.59 (gC1), 98.43 (iC1), 80.78 (gC3), 77.93 (gC4), 75.10 (iC4), 72.68 (iC3), 72.15, 70.29 (gC5), 68.87 (iC2), 67.88, 67.25 (iC4), 63.86 (gC2), 63.07, 61.78, 47.35 (Fmoc).

A 2.2.2 TEMPO/BAIB Oxidation and Esterification with TMS-diazomethane

Synthesis of Compound 15

A solution of **13** in acetonitrile (5 mL for 32 µmol) and water (0.9 mL) was treated with TEMPO (0.2 equiv.) and BAIB (2.5 equiv. per hydroxyl group) at room temperature for 4-24 hours. After TLC (ethyl acetate: petroleum ether, 3:2) indicated the completion of the reaction chloroform and water were added. The solution was acidified with diluted HCl, back-extracted with chloroform, dried and concentrated. Residue **14**, was dissolved in diethyl ether/methanol (3:2) and a 2M solution of TMS-diazomethane in hexane (1.5 eq per carboxylate) was added drop-wise at 0 °C. After completion TLC (toluene : ethyl acetate, 3:2), 0.5 mL acetic acid was added to quench the reaction. Solvents were evaporated *in vacuo* and the residues were purified by silica gel chromatography (ethyl acetate : petroleum ether, 1:9 → 2:3) gradient to furnish the ester **15** (**15,** 0.64g, 0.56mmol, 65.8%). TLC (ethyl acetate: petroleum ether, 1:1). Rf = 0.7. **^{1}H NMR** (500 MHz, CDCl$_3$) δ 8.11 (d, *J* = 7.2 Hz, 2H, Ar H), 7.76 (d, *J* = 7.5 Hz, 2H, Ar H), 7.59 (d, *J* = 7.5 Hz, 2H, Ar H), 7.42 – 7.22 (m, 20H, Ar H), 7.16 – 7.12 (m, 2H, Ar H), 5.29 (s, 1H), 5.17 (s, 1H, i*H*1), 5.15 (bs, i*H*2), 4.93 (d, *J* = 11.5 Hz, 1H, Bn-C*H*), 4.84 (d, *J* = 2.2 Hz, 1H, i*H*5), 4.80 (d, *J* = 3.4 Hz, 1H, g*H*1), 4.76-4.71 (m, 2H, Bn-C*H$_2$*), 4.54 (d, *J* = 10.9, 1H, Bn-C*H*), 4.41-4.38 (m, 2H, C*H*Fmoc + g*H*6), (dd, *J* = 3.2 Hz, 9.1, 1H, g*H*6), 4.21 (t, *J* = 6.7 Hz, 1H, C*H*Fmoc), 4.17-4.15 (m, 2H, iH3 + Bn-C*H*), 4.10 (m, 1H, i*H*4), 4.05 (d, *J* = 10.6 Hz, 1H, Bn-C*H*), 4.01 (d, *J* = 10.0 Hz, 1H, g*H*5), 3.80 (s, 4H, OMe, linker), 3.57 (dd, *J* = 18.1, 8.1 Hz, 1H, g*H*3), 3.55-3.50 (m, 1H, linker), 3.46 (t, *J* = 9.1, g*H*4), 3.20 (dd, *J* = 3.42, 10.22, 1H, gH2), 3.14-3.12 (m, 2H, linker), 2.01 (s, 3H, OAc), 1.62-1.58 (m, 2H), 1.46-1.26 (m 10 H). **^{13}C NMR:** (126 MHz, CDCl$_3$) δ 165.58, 156.43, 144.09, 141.37, 137.86, 137.72, 133.27, 130.00, 129.71, 129.06, 128.76, 128.46, 128.41, 128.35, 128.25, 128.00, 127.91, 127.87, 127.82, 127.68, 127.05, 125.33, 125.06 (Bn), 119.98 (Bn), 99.57 (gC1), 99.20 (iC1), 80.16 (gC3), 77.47 (gC4), 77.42, 77.16, 76.91, 76.08 (iC4), 74.91 (Bn-C), 74.76 (Bn-C), 73.45 (iC3), 72.35 (Bn-C), 70.18 (gC5), 68.71, 68.06 (iC2), 67.47 (iC5), 66.47 (CHFmoc), 63.81 (gC2), 62.41 (gC6), 52.38 (OMe), 47.39, 40.98, 29.86, 29.72, 29.30, 26.47, 25.83, 21.47, 20.84 (OAc). MS (ESI, positive mode) calculated for [C$_{64}$H$_{68}$N$_4$O$_{15}$]$^{+}$Na *m/z* 1132.47, found 1132.52.

A 2.2.3 Removal of *N*-Fmoc

15 → **16**
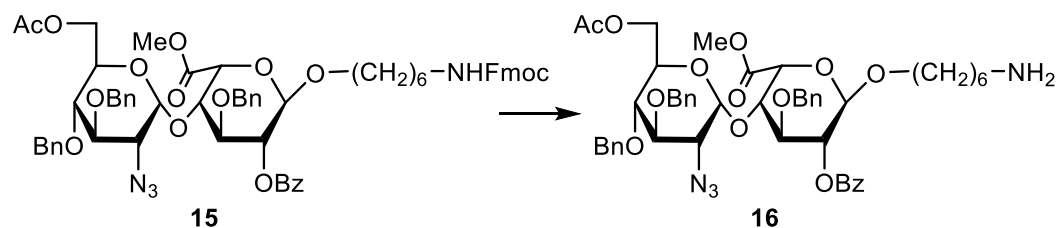
Fmoc protected **15** (638 mg, 0.563mmol) was dissolved in dry DMF (15 mL). Piperidine (5 mL) was added and stirred at RT for 1.5 hours. The solvents were removed *in vacuo* and the residue was purified by chromatography (ethyl acetate : methanol: aq. ammonia, 4:1:0.05) to furnish **16** (**16**, 0.41g, 0.452mmol, 80%). TLC (ethyl acetate : ethanol : water, 3:1:1) Rf = 0.23. **^{1}H NMR** (500 MHz, CDCl$_3$) δ 8.10 (d, *J* = 7.2 Hz, 2H, Ar H), 7.39- 7.24 (m, 16, Ar H), 7.14 (d, J = 6.3 Hz, 2H, Ar H), 5.17 (s, 1H, i*H*1), 5.12 (s, 1H, i*H*2), 4.91 (d, *J* = 11.5 Hz, 1H, Bn-C*H*), 4.82 (d, *J* = 2.1 Hz, 1H, i*H*5), 4.79 (d, *J* = 3.5 Hz, 1H, g*H*1), 4.76 – 4.70 (m, 2H, Bn-C*H*$_2$), 4.53 (d, *J* = 10.9 Hz, 1H, Bn-C*H*), 4.43-4.38 (m, 1H, g*H*6), 4.25 (dd, *J* = 12.3, 3.1 Hz, 1H, g*H*6), 4.18 – 3.97 (m, 5H, Bn-C*H*$_2$, i*H*3, i*H*4, g*H*5), 3.79-3.75 (m, 4H, linker, O$_2$C*H*$_3$), 3.59-3.44 (m, 4H, linker, g*H*3, g*H*4), 3.19 (dd, *J* = 10.2, 3.5 Hz, 1H, g*H*2), 2.94 – 2.88 (m, 1H, linker). **^{13}C NMR:** (126 MHz, CDCl$_3$) δ 167.95, 167.27, 167.16, 162.98, 135.18, 130.66, 127.42, 127.15, 126.17, 125.87, 125.82, 125.76, 125.41, 125.31, 125.24, 97.02 (gC1), 96.63 (iC1), 77.58 (gC3), 74.90 (gC4), 74.81 (iC4), 74.55 (Bn-C), 74.30 (Bn-C), 73.58 (iC3), 72.31 (Bn-C), 72.15, 70.84 (gC5), 69.72 (linker), 67.59 (iC2), 66.20 (iC5), 65.40 (gC2), 64.81 (gC6), 61.25, 59.82, 50.88 (OMe), 49.77, 48.89, 39.49 (linker), 30.89, 28.22, 26.84, 24.83, 24.07, 23.41, 18.26 (OAc).

### A 2.2.4 Coupling with tetra-*N*-hydroxysuccinimide activated ester

Synthesis of Compound 17

16 + **13**

↓

17
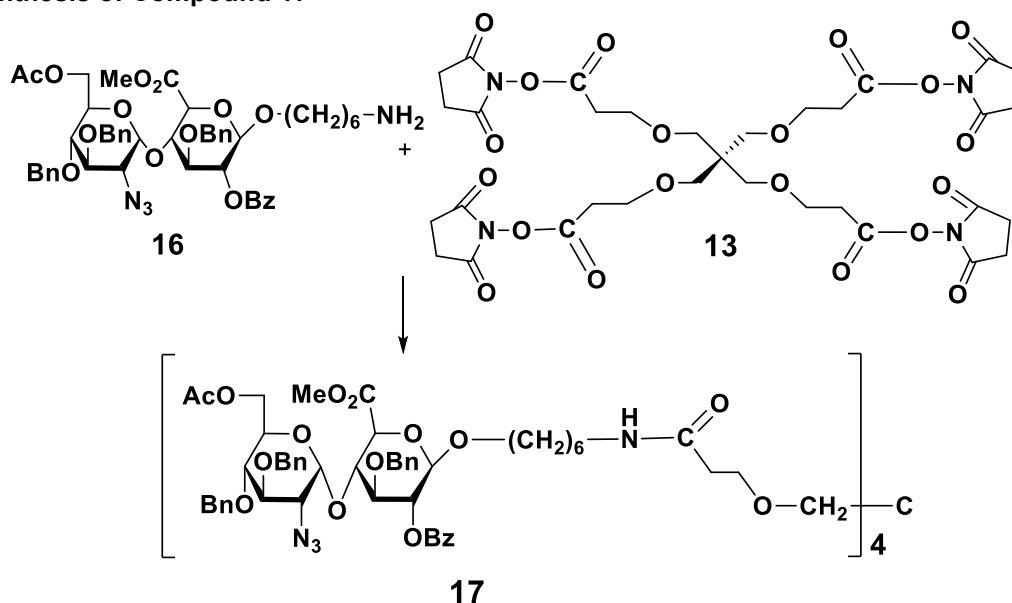
A solution of tetra-*N*-hydroxysuccinimide activated ester **13** (1 eq) in dry DMF (40 mg per 1 mL of DMF) was added to the solution of glycoside **16** (4-6 eq.) in dry DMF (100 mg per 1 mL of DMF) at room temperature. The reaction mixture was treated with triethylamine (8 eq) and stirred at RT for 24 hrs. DMF was removed *in vacuo* and the residue was purified by flash chromatography on silica gel eluting with ethyl acetate followed by ethyl acetate: methanol, 9:1→3:2 to give tetramer **17** (**17,** 0.4mg, 0.10mmol, 81.4%). TLC (ethyl acetate : methanol, 9:1). Rf = 0.52. ^{1}**H NMR** (500 MHz, CDCl$_3$) δ 8.11-8.09 (m, 8H, Ar H), 7.39-7.23 (m, 64 H, Ar H), 7.15-7.13 (m, 8H, Ar H), 5.16 (s, 4H, i*H*1), 5.13 (s, 4H, i*H*2), 4.91 (d, *J* = 11.6 Hz, 4H, Bn-C*H*), 4.83 (d, *J* = 2.2 Hz, 4H, i*H*5), 4.78 (d, *J* = 3.5 Hz, 4H, g*H*1), 4.76 – 4.70 (m, 8H, Bn-C*H*), 4.53 (d, *J* = 10.9 Hz, 4H, Bn-C*H*), 4.39 (dd, *J* = 12.3, 1.9 Hz, 4H, g*H*6), 4.26 (dd, *J* = 12.3, 3.1 Hz, 4H, g*H*6), 4.17 – 4.03 (m, 20H, i*H*4, i*H*3, Bn-C*H*, core), 4.02-3.98 (m, 4H, g*H*5) 3.81 – 3.74 (m, 16H, OMe, linker), 3.63- 3.55 (m, 12 H, g*H*3, linker, core), 3.52-3.45 (m, 8H, g*H*4 + linker), 3.28 (s, 4H), 3.21-3.16 (m, 12 H, g*H*2 + linker), 2.04 (s, 4H), 2.01 (s, 12 H, OAc), 1.61-1.59 (m, 10 H), 1.46-1.41 (m, 9 H), 1.33-1.24 (m, 48 H). ^{13}**C NMR (126 MHz, CDCl$_3$)** δ 171.25, 170.53, 169.71, 165.55, 137.68, 133.25, 129.96, 128.73, 128.43, 128.38, 128.33, 127.97, 127.88, 127.80, 99.56 (gC1), 99.15 (iC1), 80.13 (gC3), 77.42 (gC4), 76.08 (iC4), 74.87 (Bn-C), 74.73 (Bn-C), 73.36 (iC3), 72.31 (Bn-C), 70.13 (gC5), 69.04 (core), 68.72 (linker), 68.03 (iC2), 67.40 (iC5), 63.78 (gC2), 62.36 (gC6), 60.38 (core), 52.35 (OMe), 39.49 (linker), 39.42, 36.86, 29.70, 29.63, 29.34, 26.78, 25.82, 20.82 (OAc). MS (ESI, positive mode) calculated for [C$_{213}$H$_{252}$N$_{16}$O$_{60}$]$^+$3H *m/z* 3996.72, found 3996.8.

## A 2.2.5 Selective De-*O*-acetylation
Synthesis of Compound 18
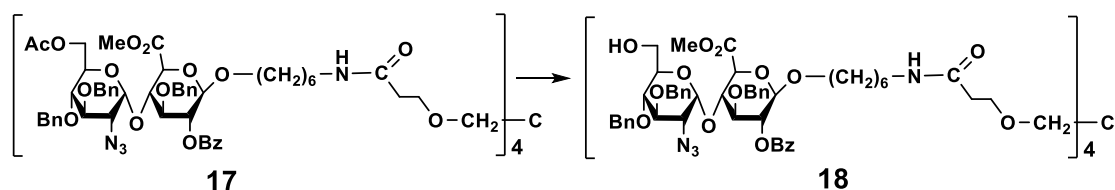
Starting material was dissolved in dry dichloromethane (2 mL for 9 μmol) at 0 °C and treated with a solution of cold dry methanol (4 mL) containing 80 μL of acetyl chloride. The reaction mixture was stirred for 30 min at 0° and then at RT for 24 hours. After TLC (ethyl acetate) indicated completion of the reaction dichloromethane was added and the solution was washed with water and sodium hydrogen carbonate solution (sat., aq.), dried and concentrated. The residue was purified by silica gel chromatography (ethyl acetate : methanol, 9:1) to give fully de-*O*-acetylated product **18** (**18**, 0.23 g, 0.05 mmol, 59.2 % yield). TLC (DCM : methanol : aq ammonia, 7:2:0.25) Rf = 0.85. ^{1}**H NMR** (500 MHz, CDCl$_3$) δ 8.10-8.09 (m, 8H, Ar H), 7.39-7.23 (m, 64 H, Ar H), 7.15 – 7.11 (m, 8H, Ar H), 5.17 (s, 4H, i*H*1), 5.12 (s, 4H, i*H*2), 4.91 (d, J = 10.0Hz, 4H, Bn-C*H*), 4.84 (d, *J* = 2.0 Hz, 4H, i*H*5), 4.79 (d, *J* = 3.5 Hz, 1H, g*H*1), 4.75-4.72 (m,

8H, Bn-C*H*), 4.61 (d, *J* = 11.0 Hz, 4H, Bn-C*H*), 4.21 (d, *J* = 10.8 Hz, 4H, Bn-C*H*), 4.14-4.09 (m, 12H, i*H*3, i*H*4), 4.06 (d, *J* = 10.8 Hz, 4H, Bn-C*H*), 3.94-3.91 (m, 4H, g*H*5), 3.86 (d, *J* = 12.0 Hz, 4H, g*H*6), 3.80 (s, OMe), 3.78 – 3.75 (m, 4H, linker), 3.71 – 3.66 (m, 4H, g*H*6), 3.63-3.61 (m, 8H, core), 3.59 – 3.54 (m, 4H, g*H*3), 3.53-3.48 (m, 4H, linker), 3.44-3.40 (m, 4H, g*H*4), 3.20-3.14 (m, 12H, linker, g*H*2), 2.04 (s, 7H), 1.64-1.57 (m, 8H), 1.47-1.41 (m, 8H), 1.34-1.24 (m, 32H). ^{13}C NMR (126 MHz, CDCl$_3$) δ 171.32, 170.08, 165.57, 138.01, 137.79, 137.67, 133.24, 129.93, 129.62, 128.74, 128.43, 128.33, 127.94, 127.85, 127.74, 99.42 (gC1), 99.25 (iC1), 79.84 (gC3), 77.86 (gC4), 75.77 (iC4), 74.99 (Bn-C), 74.74 (Bn-C), 73.61(iC3), 72.95 (gC5), 72.39 (Bn-C), 69.05 (core), 68.72 (linker), 68.26 (iC2), 67.40 (iC5), 63.69 (gC2), 61.62 (gC6), 60.37, 52.37 (OMe), 39.49 (linker), 36.84, 29.58, 29.31, 26.74, 25.80, 21.01, 14.19.

A 2.2.6 General Sulfation Procedure

Sulfur trioxide trimethylamine complex (5 equivalents. per hydroxyl group) was added to the starting materials in dry DMF (3 mL for 50 mg). The mixture was heated at 50-60 ºC under argon for 48-72 hours. Methanol (1 mL) was added and the mixture stirred for 15 minutes and concentrated *in vacuo*. Chromatography (DCM : methanol : aq. ammonia, 7:2:0.5) afforded *O*-sulfated products.

### A 2.2.7 Synthesis of Compound 19
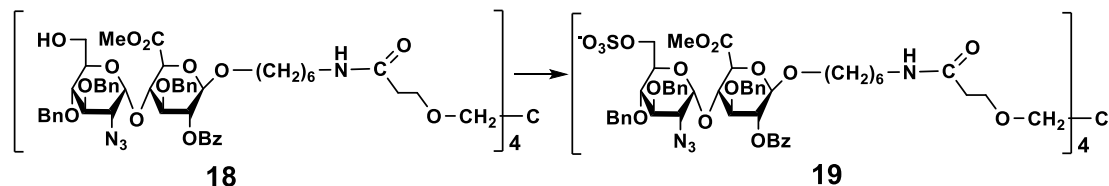
Compound **19** was synthesised from starting material **18** following the general sulfation procedure. Chromatography (DCM: methanol: aq. ammonia, 7:2:0.5) afforded the singly *O*-sulfated product **19** (**19**, 120mg, 0.025 mmol, 83.2 % yield). TLC (DCM : methanol : aq ammonia, 7:2:0.25) Rf = 0.69. ^{1}H NMR (500 MHz, MeOD) δ 8.05 (d, *J* = 7.3 Hz, 8H, Ar H), 7.39-7.20 (m, 64 H, Ar H), 7.11-7.10 (m, 8H, Ar H), 5.13 (s, 4H, i*H*1), 5.05 (s, 4H, i*H*2), 4.87-4.82 (m, 16H, g*H*1, i*H*5 , Bn-C*H*), 4.63 (d, *J* = 10.3 Hz, 4H, Bn-C*H*), 4.38 (dd, *J* = 10.8, 2.2 Hz, 4H, g*H*6), 4.30 (d, *J* = 9.6 Hz, 4H, g*H*6), 4.22-4.10 (m, 12, BnCH2, i*H*3, i*H*4), 4.02-3,91 (m, 8H, g*H*5 + Ar H), 3.82 (s, 12 H, OMe), 3.76-3.72 (m, 4H, linker), 3.74 (H$_2$O), 3.62-3.49 (m, 20 H, g*H*4, g*H*3, linker, core), 3.32-3.30 (m, 12 H, core), 3.21 (dd, *J* = 10.2, 3.4 Hz, 4H, g*H*2), 3.13-3.10 (m, 8H, linker), 1.59-1.27 (m, 38 H). ^{13}C NMR (126 MHz, MeOD) δ 172.42, 170.17, 165.48, 138.37, 138.09, 137.80, 133.14, 129.62, 128.69, 128.14, 128.06, 128.01, 127.88, 127.76, 127.59, 127.54, 127.22, 127.16, 99.69 (gC1), 99.07 (iC1), 79.75 (gC3), 77.50 (gC4), 75.87 (iC4), 74.63 (Bn-C), 74.19 (Bn-C), 73.52 (iC3), 71.98 (Bn-C), 70.75 (gC5), 69.31 (core), 68.35 (iC2), 67.36 (iC5), 65.42 (gC6), 63.56 (gC2), 51.92 (OMe), 39.08 (linker), 36.35, 29.13, 29.08, 26.43, 25.63.

A 2.2.8 Saponification

Synthesis of 20
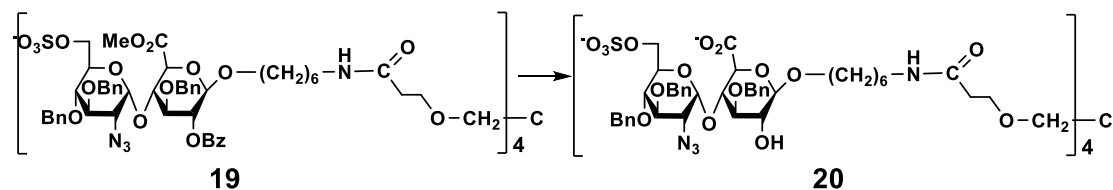
Starting material **19** was dissolved in methanol and water (4/1, v/v, 1.25 mL for 20 mg - 100 mg therefore **5ml**) containing 2M solution of sodium hydroxyl (50 L per 1.25 mL of reaction mixture) at 0 °C. The reaction mixture was stirred at room temperature for 48-72 hours. After TLC (ethyl acetate: ethanol : water, 3:1:1) indicated the completion of the reaction, the volume of the solvents was reduced *in vacuo*. The solution was applied to a column of silica for flash chromatography (DCM : methanol : aq. ammonia, 7:2:0.5 → 5:4:1) to furnish the product **20** (**20**, 80 mg, 0.02 mmol, 95 % yield). TLC (DCM : methanol : aq. ammonia, 7:2:0.25) Rf = 0.23. **^{1}H NMR** (500 MHz, MeOD) δ 7.97 (s, 8H), 7.39-7.26 (m, 52 H), 5.11 (s, 4 H), 4.94 (s, 4 H), 4.75-4.63 (m, 20 H), 4.31 (bs, 4H), 4.26-4.24 (m, 4 H), 4.19 (bs, 4H), 3.95-3.86 (m, 16 H), 3.74 (bs, 8H), 3.67-3.58 (m, 20 H), 3.50 (bs, 4H), 3.15-3.12 (m, 12 H), 2.42-2.38 (10 H), 2.01 (s, 8H), 1.94 (s, 4H), 1.59-1.29 (m, 53H). **^{13}C NMR** (126 MHz, MeOD) δ 174.78, 172.61, 171.59, 163.47, 138.11, 128.02, 127.98, 127.87, 127.48, 127.43, 127.33, 101.38 (gC1), 95.65 (iC1), 80.61 (gC3), 77.70 (gC4), 74.99 (iC4), 74.61 (Bn-C), 73.54 (Bn-C), 72.81 (iC3), 71.67 (Bn-C), 70.46 (gC5), 69.24 (core), 68.01 (iC2), 67.35 (iC5), 66.92, 65.69 (gC6), 63.85 (gC2), 60.13, 53.71, 39.16 (linker), 36.39, 35.56, 30.27, 29.24, 29.09, 26.38, 25.65

### A 2.2.9 2nd Sulfation

Synthesis of Compound 21
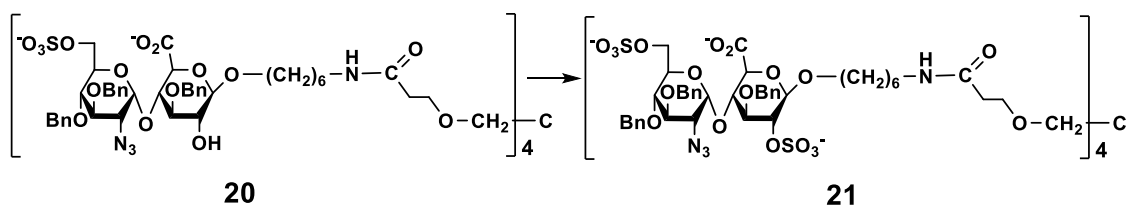
Compound **21** was synthesised from starting material **20** following the general sulfation procedure. Chromatography (DCM: methanol: aq. ammonia, 7:2:0.5) afforded the di-sulfated product **21**. TLC (ethyl acetate, ethanol: water, 3:1:1) Rf = 0.18. **^{1}H NMR** (500 MHz, MeOD) δ 7.41 – 7.28 (m, 60H), 5.18 (d, *J* = 3.4 Hz, 4H, g*H*1), 5.14 (s, 4H, i*H*1), 4.89 (m, 20 H), 4.66-4.64 (m, 16 H), 4.48 (bs, 4H), 4.34 (dd, *J* = 10.7, 2.6 Hz, 4H), 4.25-4.21 (m, 8H), 4.15 (bs, 4H), 3.98 (d, *J* = 10.0 Hz, 4H), 3.85-3.81 (m, 4H), 3.61-3.59 (m, 12 H), 3.50-3.45 (m, 8H), 3.35 (s, 3H), 3.32-3.30 (m, 18H), 3.28 (9H), 3.14-3.11 (m, 8H), 3.02 (s, 1H), 2.88 (304 H), 2.73 (s, 1H), 2.70 (3H), 2.64 (s, 7H), 2.41-3.37 (m, 10H), 1.66-1.49 (m, 12H), 1.47-1.27 (m, 40 H). **^{13}C NMR** (126 MHz, MeOD) δ 175.64, 173.94, 173.87, 139.83, 139.52, 129.86, 129.48, 129.08, 128.84,

100.46 (gC1), 95.80 (iC1), 81.83 (gC3), 79.10 (gC4), 76.17 (iC4), 72.78, 71.80, 71.50, 71.33, 70.64 (gC5), 69.28, 68.79 (iC2), 68.5, 67.08 (iC5), 65.47 (gC6), 55.24, 52.34, 40.52, 39.76, 37.80, 30.67, 30.51, 27.93, 27.15.

A 2.2.10 Hydrogenolysis

Synthesis of Compound 22
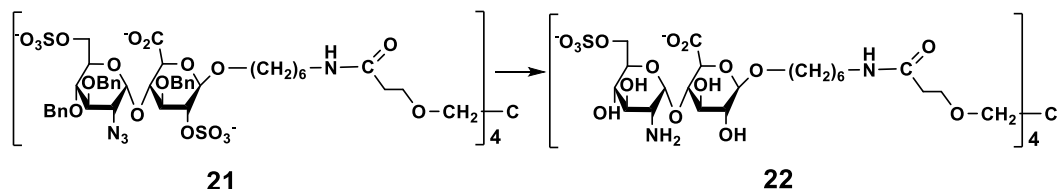
Starting material **21** was dissolved in THF and water (1/1, v/v, 3 mL for 10 mg) containing aqueous ammonia solution (10% of reaction mixture) and treated with palladium hydroxide on carbon (20% Pd, 5 times the weight of **21**). The reaction mixture was stirred for 24-48 hours under hydrogen at ambient temperature and pressure. After TLC (ethyl acetate : ethanol : water, 2:1:1) indicated the completion of the reaction, the catalyst was filtered off and washed with 50% aqueous THF. The solution was concentrated to dryness and chromatography of the residue (DCM : methanol : aq. ammonia, 5:4:1) gave the final products as ammonium salts. The resulting materials were dissolved in water, passed through a Dowex 50WX8-200 (Na+) resin column (8 x 1 cm) and eluted with water. Fractions containing the products were evaporated and dried *in vacuo* to furnish sodium salts of final product **22** (**22**, 55 mg, 0.0136 mmol, 80.18 % yield). TLC (DCM : methanol : aq. ammonia, 7:2:0.25) Rf = 0.1. **¹H NMR** (500 MHz, D_2O) δ 5.48 (d, J = 3.7 Hz, 4H, gH1), 5.20 (s, 4H, iH5), 4.71 (s, 4H), 4.66 (s, 4H), 4.42-4.39 (m, 10H), 4.32 – 4.23 (m, 12H), 4.22 (bs, 4H), 4.05-3.99 (m, 8H), 3.99-3.92 (8H), 3.82-3.77 (m, 16H), 3.65-3.6 (m, 12 H), 3.50 (bs, 2H), 3.46- 3.38 (m, 16H), 3.32 (s, 3H), 3.27-3.20 (m, 54H), 3.15-3.08 (182 H), 2.93 (bs, 23 H), 2.57-2.48 (m, 16H), 1.79 (solvent), 1.68 (solvent), 1.61 – 1.52 (m, 22 H), 1.48 – 1.3 (m, 40H). **¹³C NMR** (126 MHz, D_2O) 175.18, 174.01, 97.99 (gC1), 92.20 (iC1), 72.84, 70.78, 70.26, 70.01, 69.27, 68.76, 68.64, 67.61, 66.40, 66.28, 62.93, 54.24, 39.47, 36.40, 28.46, 28.35, 25.91, 25.02.

A 2.2.11 Selective *N*-Sulfation

Synthesis of Target Dendrimer (Den T)

$$\mathbf{22} \qquad\qquad \mathbf{Den\ T}$$
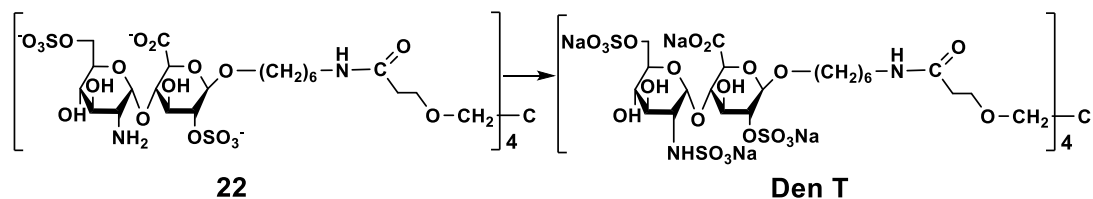
Starting material **22** was dissolved in 2.5ml H_2O. Treated with sodium carbonate (0.0346 g, 0.326 mmol) and sulfur trioxide-triethylamine complex (0.0346 g, 0.181 mmol). The reaction mixture was stirred at RT over night. The volume was then reduced volume and poured on top of Silica Column and purified with acetonitrile : water : ammonia , 8:1→ 6:2:1. NMR showed mixture of 2 products in anomeric region. All fractions were re-collected and subjected to the reaction again over night using 7 equivalents per amine group. TLC (acetonitrile:water: aq ammonia, 4:2:1.2) Rf = 0.62. **^{1}H NMR** (500 MHz, D_2O) δ 5.31 (d, *J* = 3.2 Hz, 4H, g*H*1, 65%), 5.20 (s, 4H, i*H*1, 65 %), 5.11 (2.6, i*H*1, 35 %), 5.04 (d, 2 H), 4.52 (t, *J* = 14.8 Hz, 3H, i*H*5), 4.37 (t, *J* = 9.6 Hz, 4H), 4.27-4.10 (m, 32H, i*H*2, i*H*3), 4.04 (bs, 8H, i*H*4), 3.78-3.56 (m, 20H, g*H*3, g*H*4, g*H*5, g*H*6), 3.42-3.31 (m, 4H), 3.29-3.23 (g*H*1), 3.19 (bs, 8H), 3.07 – 3.03 (m, 4H,), 2.98 (t, *J* = 6.8 Hz, 4H), 2.70 (s, 8H), 2.51 – 2.41 (m, 4H), 1.66 – 1.48 (m, 24H), 1.40 – 1.30 (m, 9H). **^{13}C NMR** (126 MHz, D_2O) δ 175.00, 174.07, 98.21 (iC1), 97.31 (gC1), 97.009 (*g2*), 75.39 (iC4), 74.40 (iC2), 69.96 (gC3), 69.89 (gC6), 69.57 (gC4), 69.29 (gC5), *68.79 (CH2), 68.57, 67.64*, 67.42 (iC3), 67.15 (iC5), 66.64, 66.46, 61.54, 61.42, 57.84, 55.71 (gC2), 55.38, 52.36, 51.12, 49.33, 48.68, 45.31, 45.02, 43.33, 39.48, 36.46, 29.01, 28.90, 28.50, 28.44, 25.96, 25.30, 25.04, 24.07.

^{1}H
500MHz NMR

1.84
1.81
1.78
14.13
0.90
1.69
0.95
1.00
1.12
2.87
1.00
1.08
2.89
1.96
1.16
3.75
1.22
1.21
3.03
1.30
1.24
1.12
1.03
1.79
2.61
2.41
5.75
2.33

^{13}C
500MHz NMR

133.15
129.81
128.55
128.40
128.27
128.00
127.64
127.03
125.02

98.59
98.43

80.78
77.93
75.10
72.68
70.29
68.87
67.25
63.86

47.35

1H NMR integration labels:
2.06 18.73 2.09 0.97 1.02 1.02 1.07 0.98 2.15 1.02 1.00 1.02 6.03 1.55 2.84 1.09 2.14 1.44 2.90 1.40 1.05 3.36 2.67 2.34 12.19

13C NMR peak labels:
171.25 170.53 169.71 165.55
137.68 133.25 129.96 128.73 128.43 128.38 128.33 127.97 127.88 127.80
99.56 99.15
80.13 77.42 76.08 74.87 74.73 73.36 72.31 70.13 69.04 68.72 68.03 67.40 63.78 62.36 60.38 52.35
39.49 39.42 36.86 29.70 29.63 29.34 26.78 25.82 20.82 14.19

13C
500MHz NMR

175